Investigative Urology 2

Edited by
G. H. Jacobi · H. Rübben
R. Harzmann

With 169 Figures, Some in Color,
and 47 Tables

Springer-Verlag
Berlin Heidelberg New York
London Paris Tokyo

Volume 1 of the series "Investigative Urology" is "Experimentelle Urologie"
edited by R. Harzmann, G. H. Jacobi, L. Weißbach, 1985

Professor Dr. Günther H. Jacobi
Urologische Klinik und Poliklinik
im Klinikum der Johannes-Gutenberg-Universität
Langenbeckstraße 1, D-6500 Mainz

Professor Dr. Herbert Rübben
Knappschaftskrankenhaus Bardenberg
Abteilung Urologie
Dr.-Hans-Böckler-Platz 1, D-5102 Würselen 1

Professor Dr. Rolf Harzmann
Zentralklinikum, Urologische Klinik
Stenglinstraße, D-8900 Augsburg

ISBN-13:978-3-642-72737-5 e-ISBN-13:978-3-642-72735-1
DOI: 10.1007/978-3-642-72735-1

Library of Congress Cataloging-in-Publication Data. Investigative urology 2. Includes bibliographies and index. 1. Urinary organs – Diseases. 2. Urinary organs – Cancer. 3. Calculi, Urinary. I. Jacobi, Günther H. II. Rübben, Herbert, 1949– . III. Harzmann, Rolf. IV. Title: Investigative urology two. [DNLM: 1. Urologic Diseases. WJ 100 I635] RC872.I57 1987 616.6 87-16557
ISBN-13:978-3-642-72737-5 (U.S.)

Softcover reprint of the hardcover 1st edition 1987

2122/3130-543210

List of Contributors

The addresses are given at the beginning of each contribution

Preface

In the last 15 years the working group Experimental Urology, a part of the German Society of Urology, has developed from its relatively modest beginnings into a forum whose seven symposia have demonstrated its strength and vitality. Its primary task was to create a platform for the open discussion of all scientific ideas concerning new diagnostic and therapeutic approaches in innovative urology.

This second volume within the series *Investigative Urology* is not only a collection of the proceedings of the last biennial symposium of the working group, but moreover a summary of the recent experimental developments in the field of urology around the world. It is divided into four sections: Urological Oncology, Neurophysiology, Urolithiasis, and Various Innovations in Urological Research. This classification correctly reflects the current aims of many active urologists and researchers; their common goal is to advance clinical urology experimentally.

This second volume in *Investigative Urology* is intended to set a sign for permanent development and to encourage all our colleagues engaged in experimental urology to undertake increased international cooperation.

Finally, we hope that this series gets the attention it deserves.

Mainz — G. H. Jacobi
Aachen — H. Rübben
Augsburg — R. Harzmann

Contents

I. Urological Oncology

II. Neurophysiology

III. Urolithiasis

IV. Various Innovations in Urological Research

I. Urological Oncology

Expression of Transforming Growth Factor Receptors in Human Bladder Cancer Cells

W. Heckl[1], J. Täuber[2], K. Jocham[2], and H. W. Vohr[2]

Introduction

Transforming growth factors (TGFs) are polypeptides that reversibly induce the anchorage independent growth of nontransformed cells (De Larco et al. 1978). The ability of cells to grow in soft agar (anchorage independence) has a high correlation with neoplastic growth in vivo (Khan and Shin 1979). Two classes of TGFs, TGF-alpha and TGF-beta, have been purified from the conditioned medium of transformed cells, from embryonic tissue, embryo-derived cell lines and from tumor tissues (Roberts et al. 1983; Anzano et al. 1983; Nickell et al. 1983; Marquardt et al. 1983). Both types of TGF induce the anchorage independent growth of nontransformed indicator cells, such as NRK-cells (clone 49F) or AKR-2B cells (Anzano et al. 1982). TGF-alpha competes with the epidermal growth factor (EGF) for binding to the EGF receptor, and EGF can substitute for TGF-alpha, inducing anchorage-independent growth of the indicator cells in the presence of TGF-beta (Anzano et al. 1982; Roberts et al. 1983; Marquardt et al. 1983).

TGF-beta binds to another cell surface receptor (Frolik et al. 1984; Massague and Like 1985; Tucker et al. 1984), is a bifunctional regulator of cellular growth (Assoian et al. 1985; Roberts et al. 1985; Moses et al. 1985), and has an important role in cells of the immune system (Rook et al. 1986) and connective tissue (Roberts et al. 1986), as well as in epithelia (Shipley et al. 1986; Masui et al. 1986).

The discovery of TGFs suggests that some types of transformation may be mediated in part, through the action of overproduced or oversecreted growth factors. De Larco and Todaro (1978) have proposed that TGFs secreted by transformed cells reach sufficient concentrations to autostimulate the secreting cells, thus constituting an autocrine system which serves to initiate or aid in the maintenance of the transformed state. Moreover, Sporn and Todaro (1980) and later on Sporn and Roberts (1985) proposed that any loss of regulation at any levels, i.e., concentration of the growth factor itself and its half-life, the display of the cell surface receptors for the growth factors, and the ability of the responding cell to "internalize" and "downregulate" the receptor in the presence of its ligand, the status of the intracellular signalling pathways, can result in transformation and acquisition of the growth factor autonomy that characterizes many malignant cells. This has been demonstrated by characterization of oncogenes representative on each of these functional control levels: the *sis* oncogene product is homologous to the growth factor PDGF; the *erb-B* oncogene product is homologous to the EGF receptor; the cytoplasmic

[1]Department of Urology, Medical School, University of Würzburg, Josef-Schneider-Str. 2, D-8700 Würzburg
[2]Institute of Virology and Immunobiology, University of Würzburg, D-8700 Würzburg

Investigative Urology 2
Edited by G. H. Jacobi et al.

p21 product of the *Ha-ras* gene is a putative intermediate in intracellular signalling pathways.

The finding of elevated levels of TGFs in the urine of patients with neoplastic disease, the fact that a human bladder cancer cell line can stimulate its own growth (Messing et al. 1984), and the isolation of the *ras* oncogene product in human bladder cancer cell lines T-24 and EJ prompted us to demonstrate TGFs in the bladder cancer cell line EJ and to demonstrate a possible endocrine regulation.

Material and Methods

Cell Culture. The EJ cell line, a poorly differentiated human bladder carcinoma (Heaney et al. 1978), was cultured in DMEM containing 10% FCS (v/v). Nontransformed cells NRK (clone 49F), and AKR-2B (clone 84A), and A431 human epidermoid carcinoma cell line were a generous gift from Dr. Moses, Rochester, USA. These cells were routinely cultured as described elsewhere (Moses et al. 1985; Roberts et al. 1985). All cell lines were used for the experiments within 10 passages of the frozen stock. They were routinely examined for, and found free of, mycoplasma.

Preparation of Cell Extracts. The intracellular material was obtained from EJ cells by the acid-ethanol extraction procedure as described by Roberts et al. (1980). The resulting precipitate was collected by centrifugation, resuspended in 1 *M* acetic acid, dialyzed extensively against 1% acetic acid (5 changes of 50 volumes) in Spectrapor 3 dialysis tubing with a cutoff of M 3500, lyophilized and stored at −70°C until further processed. The lyophilized dialysates were dissolved in 1 *M* acetic acid and centrifuged. The supernatant was applied along with molecular weight markers to Bio Gel P30 column equilibrated in 1 *M* acetic acid. The chromatography was performed at 4°C with approximately 3 ml fractions being collected. The absorption of each fraction was determined at 280 nm and aliquots of fractions were lyophilized for determination of soft agar stimulating activity and physical and chemical treatment as well. Fractions with a stimulating activity were collected, lyophilized and further purified by HPLC (Bruker-Franzen Analytic) using a C18 column (J.T. Baker) according to the method of Matrisian et al. (1982). The fractions were used for the ^{125}J-labeled EGF and ^{125}J-labeled TGF-beta-assays.

Soft Agar Colony Stimulation Assay. Soft agar assays were performed using normal indicator cells NRK-49F, AKR-2B (clone 84A) and EJ cells. Varying concentrations of these cells were suspended in 24 wells Falcon plates in 0.3 ml of 0.3% DIFCO agar supplemented with DMEM or McCoy's 5A/10% FCS (v/v) in the absence or presence of aliquots of the cell extracts with or without the addition of 2 ng/ml EGF, and layered over 0.3 ml of a 0.6% agar-medium base layer. All cultures were incubated at 37°C in a 95% air − 5% CO_2 atmosphere. Colonies greater than 30 μm in diameter (approximately 30 cells) were read unfixed and unstained at 10 days. The data represent the average of results abtained from at least triplicate cultures.

EGF-Radioreceptor Assay. The ^{125}J-labeled EGF radioreceptor assay was performed using the A431 human sqamous cell carcinoma line. EGF, purified from mouse sub-

maxillary glands were purchased from SIGMA, ^{125}J-labeled EGF were purchased from New England Nuclear. The A431 cells were subcultured into 6 wells (35 mm diameter) costar plates at a density of 2.5×10^4 cells/well in McCoy's 5A/10% FCS (v/v). After incubation for 24 h at 37°C the medium was removed and the cells were washed three times with a binding buffer (McCoy's 5A, 50 m*M* BIS, 0.14% BSA) at ph = 6.8. Aliquots of the cell extracts were dissolved in 1.0 ml binding buffer and added to the A431 cells along with 1 ng of ^{125}J-labeled EGF (163 μCi/μg). The incubation was carried out for 60 min at room temperatur (22°C). Nonspecific binding was assessed by addition of 1 μg EGF/ml. After removing the incubation mixture the cells were rinsed with cold TRIS (50 m*M*, pH = 7.5) 3 times and dissolved in 1 ml of 0.2 *N* NaOH before counting in a gamma-counter.

TGF-Beta Radioreceptor Assay. The ^{125}J-labeled TGF-beta radioreceptor assay was performed using AKR-2B (clone 84A) cells. TGF-beta from human platelets was purified by the method of Assoian et al. (1983) and modified as per Tucker et al. (1984). Purified TGF-beta was radioiodinated with ^{125}J-labeled Bolton and Hunter reagent as described by Tucker et al. (1984). The AKR-2B (clone 84A) cells were plated in 6 well culture plates at a density of 1×10^5 cells/well in DMEM/10% FCS (v/v). After incubation for 24 h the medium was removed and the cells washed with binding buffer essentially as described above. 1 ml of binding buffer containing 0.2 ng of ^{125}J-labeled TGF-beta was added to each well along with or without different aliquots of the cell extracts. Nonspecific binding of ^{125}J-TGF-beta was determined in the presence of 1 μg of unlabeled TGF-beta. After incubation for 2 h and washing the cells three times with binding buffer, the cells were removed by scraping with a rubber policeman before counting in a gamma counter.

The ratio of bound to free EGF or TGF-beta was plotted as a function of the nanograms bound to generate the scatchard plots (Scatchard, 1949).

Comparative Binding Assays. The binding of ^{125}J-labeled TGF-beta and ^{125}J-EGF to the EJ cells were compared with their binding to AKR-2B and AKR-2B (clone 84A) by using the conditions of the TGF-beta/EGF radioreceptor assays. The relative binding was expressed as a ratio of the bound ^{125}J-TGF-beta/^{125}J-EGF per 10^6 EJ cells and the bound ^{125}J-TGF-beta/^{125}J-EGF per 10^6 cells for AKR-2B (clone 84A)/AKR-2B cells.

Effect of the Cell Extract on the Tumor Cells Compared with Exogeneous EGF and TGF-Beta. The partial purified cell extracts were added in varying concentrations to the EJ cells plated at a density of $1–2 \times 10^3$ cells/well in 0.3% soft agar and DMEM/10% FCS (v/v). Concurrently exogeneous EGF or TGF-beta were added at increasing concentrations to the tumor cells cultured in 0.3% agar. The colonies were counted after 5 and 10 days and compared with untreated EJ-control cells.

Characterization by Chemical and Physical Treatment. The partial purified cell extracts were tested for their sensitity to heat, acid, sulfhydryl reagent and proteases. One aliquot was treated with trypsin (50 μg/ml) for 2 h at 37°C. The reaction was stopped by the addition of soybean trypsin inhibitor (100 μg/ml). A control sample

was treated concurrently with 50 µg/ml trypsin and 100 µg/ml soybean trypsin inhibitor (preincubated for 30 min) for 2 h at 37°C. One aliquot was subjected to 0.065 *M* dithiothreitol in PBS and 0.1 *M* NH_4 HCO_3 at ph 7.2 for 1 h at 20°C. Other samples were treated by heating in a water bath for 30 min at 56°C and 3 min in boiling water. After these treatments the samples were dialyzed for 48 h against 1% acetic acid, lyophilized, dissolved in DMEM/10% FCS (v/v) and tested in the soft agar assay.

The protein content was measured using a dye binding assay (Bradford 1979).

Results

Colony-Stimulating Activity. Fractions from the Bio-Gel P30 chromatography of the EJ cell extract were tested for the stimulation of colony formation in soft agar using the untransformed cells NRK-49F and AKR-2B cells. Fig. 1A shows that NRK-49F

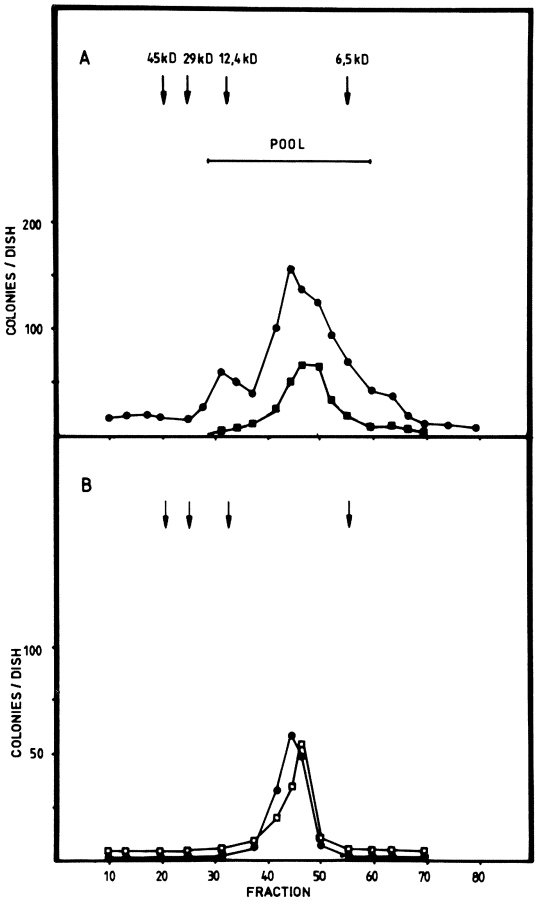

Fig. 1A, B. BioGel P-30 chromatography of acid soluble acid-ethanol extract of the EJ cells. An aliquot of every third fraction was tested for stimulation of NRK-49F cells in the absence (—■—) or presence (—●—) of 2 ng/ml EGF. 30 cells/colony were scored as positive. The colony formation of AKR-2B was not enhanced upon addition of EGF. The pooled fraction were further purified by HPLC

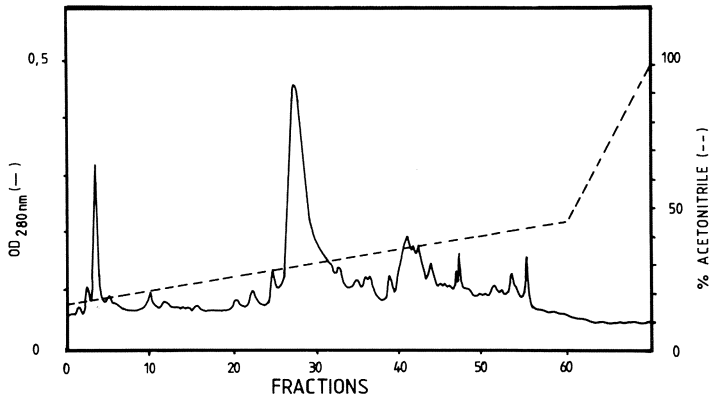

Fig. 2. HPLC-purification of the EJ cell extracts. The major TGF-alpha/EGF competing activity was at 36% acetonnitrile

cells respond to a TGF-activity that elutes in a MW-range between 27 kD and 6 kD. The peak of the normal rat cell formation was 4 times potentiated upon addition of 2 ng/ml EGF to the soft agar. In Fig. 1B there is also stimulation of the AKR-2B cells, but the numbers of colonies were apparently smaller than in Fig. 1A. Addition of EGF showed no further stimulation of the normal cells. The fractions with a stimulation activity were pooled and further purified by HPLC (Fig. 2). These fractions were used for further characterization of the TGF-activity in the cell extracts.

EGF and TGF-Beta Radioreceptor Assays of EJ-Cell Extracts. To examine the presence of specific growth factors in the cell extracts of the human bladder cancer cell line EJ, EGF and TGF-beta radioreceptor assays were used. The EJ cells contained a competing activity of the EGF. The EJ cells produced a TGF-alpha like activity with maximal 52% inhibition of the EGF at the EGF-receptors of the A-431 cells. In the TGF-beta radioreceptor assay the partial purified cell extracts showed the greatest amount of TGF-beta like competing activity with 81% compared to the inhibition of AKR-2B (clone 84A). These findings, i.e., the presence of TGF-beta competing activity were also seen in all experiments with unprocessed cell extracts and maintained when dialyzed, lyophilized cell extract supernatants were examined. The effect was enhanced by changing the pH to 3.

TGF-Receptors on the EJ Cell Line. Todaro et al. (1980) has shown previously that cells that produce significant amounts of alpha-TGF lack demonstrable EGF-receptors. The reason for this is thought to be a result of the downregulation of the EGF-receptors or receptors saturation by endogenous TGF-alpha. Therefore, we examined the ability of the bladder cancer cell line EJ to bind EGF and/or TGF-beta (Fig. 3/4). The EJ cells had high-affinity binding sites for EGF. Scatchard plots of the specific binding of ^{125}J-EGF to EJ cells generated a straight line (correl. coeff. = 0.92) indicating a single class of binding site with an apparent KD of 4 m*M*. The theoretical maximum number of binding sites determined from x-intercept of the Scatchard plot was 82/mol/mg of protein EJ cells with 9000 ^{125}J-EGF molecules bound specifically per cell

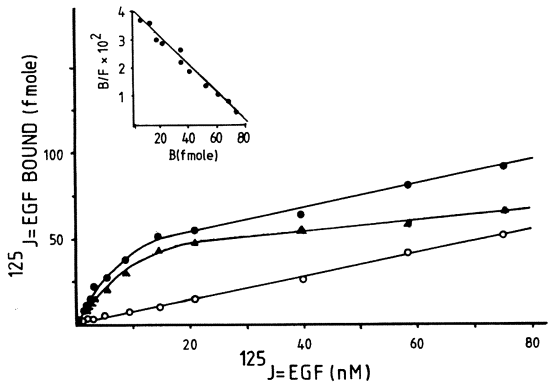

Fig. 3. Analysis of ^{125}J-EGF binding at various concentrations. The specific binding (▲) was calculated by subtracting the nonspecific binding (○) from the mean of duplicate total binding values (●). *Inset,* Scatchard plot of the specific binding

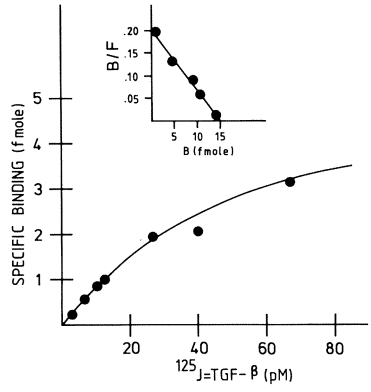

Fig. 4. Radioreceptor ^{125}J-TGF-beta binding study in the EJ cells. The specific binding was estimated as in the ^{125}J-EGF binding study. *Inset,* Scatchard plot of the specific binding

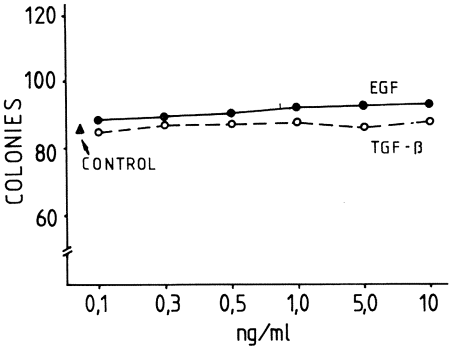

Fig. 5. Effect of exogeneous EGF and TGF-beta on soft agar growth of EJ. EGF and TGF-beta were added in varying concentrations to the EJ-cells. Control represent untreated EJ cells

(Fig. 3). The Scatchard analysis of the binding of ^{125}J-TGF-beta to the EJ cells shows a KD of 27 and 18000 receptors per cell (Fig. 4). The EJ cells contain amounts of EGF-receptors and TGF-beta receptors on their cell surface.

Effect of Exogeneous EGF and TGF-Beta on Cells from the Bladder Cancer Cell Line. For the examination of any possibility of a autocrine stimulation by TGF-alpha and TGF-beta as well, the effect of exogeneous EGF and platelet-derived TGF-beta on the growth of the EJ cell line in soft agar was determined (Fig. 5). In the presence of 10% fetal calf serum there was no significant stimulatory or inhibitory effect detected after the addition of EGF and TGF-beta at concentrations between 0.1 and 10 ng/ml. The combined addition of both factors had also no stimulatory effect on the colony formation of EJ cells in soft agar.

Influence of Chemical and Physical Treatment on Growth Promoting Activity. The cell extract of EJ cells was subjected to various treatments. The growth promoting

Table 1. Characteristics of TGF colony-stimulating activity as revealed by various treatments

Treatment	Colonies/ dish[a]	% of control
Control[b]	62 ± 8	100
Trypsin (50 μg/ml for 2 h at 37°C)	6 ± 2	9.6
Trypsin (50 μg/ml) plus soybean Trypsin inhibitor (100 μg/ml) for 2 h at 37°C	54 ± 12	87.1
Dithiothreitol (0.065 *M* in 0.1 *M* NH_4HCO_3, 1 h at 20°C)	8 ± 3	12.9
Heat (56°C for 30 min)	58 ± 6	93.5
Heat (100°C for 3 min)	56 ± 4	90.3

[a] Mean ± SD derived from triplate experiments
[b] Treated with 1 *M* acetic acid

activity was stable to acid and heat (56°C for 30 min, 100°C for 3 min), but was destroyed by trypsin. As revealed by the unchanged colony formation the trypsin inactivation was partially prevented by preincubation with soybean trypsin inhibitor prior to adding the sample. The growth promoting activity was completely destroyed by dithiothreitol (Table 1).

Discussion

The results of this study demonstrate the occurrence of transforming activity in human bladder cancer cells. The EJ cell line produces substances with TGF-alpha-like and TGF-beta-like activities, carries specific receptors for these peptides on the cell surface, but does not respond to exogeneous EGF or TGF-beta in soft agar even in the presence of fetal calf serum (Childs et al. 1982). Its molecular weights are within the range of the well characterized TGF-alpha (6400 daltons) and TGF-beta (25000 daltons). Like the TGF-alpha and TGF-beta the partially purified substances are heat and acid stable and are destroyed by dithiothreitol and trypsin, i.e., in their active form they contain sulfide bonds. To our knowledge this is the first report of the production of TGF beta-like substances and expression of their receptors by human bladder cancer cells, although it is known that TGF-beta is found in the urine of cancer patients. The existence of this growth factor is not surprising because of its ubiquous existence. Like TGF-alpha from other sources the normal rat cells were stimulated to form colonies. This colony formation was enhanced upon addition of EGF. The competition of their receptors on the cell surface of the target cells had a maximum at the acetonnitrile gradient of 36%. In this region in the TGF-beta radioreceptor assay a competition was not detected. As noted earlier the competition activities of the TGF beta-like substances were enhanced by the acidification of the partial purified cell extracts. However, the mechanism of this activation is not clear yet (Pircher et al. 1984; Coffey et al. 1986).

It is not surprising that the TGF-alpha and TGF-beta-like substances had no stimulatory or inhibitory effect on the tumor cell in soft agar. This is in agreement with the report of Coffey et al. (1986) who found similar results. As mentioned ear-

lier the autocrine growth control has been a major interest in studying the TGF-mechanism (Sporn and Todaro 1980; Sporn and Roberts 1985). The inability to detect any effect on the EJ cells upon addition of the cell extracts or exogeneous EGF and/or TGF beta does not disprove an autocrine mechanism for these cells. The lack of any growth inhibition of the EJ cells in soft agar by TGF-beta is in agreement with the findings by Roberts et al. (1985) and Coffey et al. (1986). As reported for colon carcinoma cell lines the TGF-beta did not induce any inhibitory effect on human bladder cancer cells.

References

Anzano MA, Roberts AB, Meyers CA, Komoriya A, Lamb LC, Smith JM, Sporn MB (1982) Synergistic interaction of two classes of transforming growth factors from murine sarcoma cells. Cancer Res 42:4776–4778

Anzano MA, Roberts AB, Smith JM, Sporn MB, DeLarco JE (1983) Sarcoma growth factor from conditioned medium of virally transformed cells is composed of both type alpha and type beta transforming growth factors. Proc Natl Acad Sci USA 80:6264–6268

Assoian RK, Komoriya A, Meyers CA, Miller DM, Sporn MB (1983) Transforming growth factor-beta in human platelets. J Biol Chem 258:7155–7160

Assoian RK (1985) Biphasic effects of type beta transforming growth factor on epidermal growth factor receptors in NRK fibroblasts. J Biol Chem 260:9613–9617

Bolton AE, Hunter WM (1973) The labelling of proteins to high specific radioactivities by coniugation to a ^{125}J-containing acylating agent. Biochem J 133:529–539

Bradford MM (1976) A rapid and sensitive method for the quantitation of microgram quantities of protein utilizing the principle of protein-dye binding. Analyt Biochem 72:248–254

Childs CB, Proper JA, Tucker RF, Moses HL (1982) Serum contains a plateled-derived transforming growth factor. Proc Natl Acad Sci USA 79:5312–5316

Coffey RF, Shipley GD, Moses HL (1986) Production of transforming growth factors by human colon cancer lines. Cancer Res 46:1164–1169

Frolik CA, Waterfield LM, Smith DM, Sporn MB (1984) Characterization of a membrane receptor for transforming growth factor-beta in normal rat kidney fibroblasts. J Biol Chem 259:10995–11000

Heaney JA, Ornellas EP, Daly JJ, Lin JC, Prout GR (1978) In vivo growth of human bladder cancer cell lines. Invest Urol 15:380–384

Kahn P, Shin S (1979) Cellular tumorgenicity in nude mice. Tests of associations among loss of cellsurface fibronetin, anchorage-independence, and tumor-forming ability. J Cell Biol 82:1–16

DeLarco JE, Todaro GJ (1978) Growth factors from murine sarcoma virus-transformed cells. Proc Natl Acad Sci USA 75:4001–4005

Marquardt H, Hunkapiller MW, Hood LE, Twardzik DR, De Larco JE, Stephenson JR, Todaro GJ (1983) Transforming growth factors produced by retrovirus-transformed rodent fibroblasts and human melanoma cells: amino acid sequence homology with epidermal growth factor. Proc Natl Acad Sci USA 80:4684–4688

Massague J, Like B (1985) Cellular receptors for type-beta transforming growth factor. Ligand binding and affinity-labeling in human and rodent cell lines. J Biol Chem 260:2636–2645

Masui T, Wakefield LM, Lechner JF, Laveck MA, Sporn MB, Harris CC (1986) Type beta transforming growth factor is the primary differentiation inducing serum factor for normal human bronchial epithelial cells. Proc Natl Acad Sci USA 83:2438–2442

Matrisian LM, Larsen BR, Finch JS, Magun BE (1982) Further purification of epidermal growth factor by high-performance liquid chromatography. Anal Biochem 125:339–351

Messing EM, Bubbers JE, De Kernion JB, Fahey JL (1984) Growth stimulating activity produced by human bladder cancer cells. J Urol 132:1230–1234

Moses HL, Tucker RF, Leof EB, Coffey RJ, Halper J, Shipley GD (1985) Type-beta transforming growth factor is a stimulator and a growth inhibitor Cancer cells 3. In: Feramisco J, Ozanne B, Stiles C (eds) Growth factors and transformation. Cold Spring Harbor Laboratory, pp 65–71

Nickell KA, Halper J, Moses HL (1983) Transforming growth factors in solid human malignant neoplasms. Cancer Res 43:1966–1971

Pircher R, Lawrence DA, Jullien P (1984) Latent beta-transforming growth factor in nontransformed and Kirsten sarcoma virus-transformed normal rat kidney cells, clone 49F. Cancer Res 44:5538–5543

Roberts AB, Lamb LC, Newton DL, Sporn MB, DeLarco JE, Todaro GJ (1980) Transforming growth factors: Isolation of polypeptides from virally and chemically transformed cells by acid/ethanol extraction. Proc Natl Acad Sci USA 77:3494–3498

Roberts AB, Lamb CC, Newton DL, Sporn MB, DeLarco JE, Todaro GJ (1983) Transforming growth factors from neoplastic and non-neoplastic tissues. Fed Proc 42:2621–2626

Roberts AB, Anzano MA, Wakefield LM, Roche NS, Stern DF, Sporn MB (1985) Type-beta transforming growth factor: A bifunctional regulator of cellular growth. Proc Natl Acad Sci USA 82: 119–223

Roberts AB, Sporn MB, Assoian RK, Smith JM, Roche NS, Wakefield LM, Heine UI, Liotta LA, Falanga K, Kehrl JH, Fauci AS (1986) Transforming growth factor type-beta: Rapid induction of fibrosis and angiogenesis in vivo and stimulation of collagen formation in vitro. Proc Natl Acad Sci USA 83:4167–4171

Rook AH, Kehrl JH, Wakefield LM, Roberts AB, Sporn MB, Burlington DB, Lane HC, Fauci AS (1986) Effects of transforming growth factor beta on the functions of natural killer cells: Depressed cytolytic activity and blunting of interferon responsiveness. J Immunol 136:3916–3920

Scatchard G (1949) The attractions of proteins for small molecules and ions. Ann NY Acad Sci 51: 660–672

Shipley GD, Pittelkow MR, Wille JJ, Scott RE, Moses HL (1986) Reversible inhibitor of normal human prokeratinocyte proliferation by type β transforming growth factor – growth inhibitor in serum free medium. Cancer Res 46:2068–2071

Sporn MB, Todaro GJ (1980) Autocrine secretion and malignant transformation of cells. N Engl J Med 303:878–880

Sporn MB, Roberts AB (1985) Autocrine growth factors and cancer. Nature 313:237–239

Todaro GJ, Fryling C, DeLarco JE (1980) Transforming growth factors produced by certain human tumor cells: Polypeptides that interact with epidermal growth factor receptors. Proc Natl Acad Sci USA 77:5258–5262

Tucker RF, Branum EL, Shipley GD, Ryan RJ, Moses HL (1984) Specific binding to cultured cells of ^{125}J-labeled type beta transforming growth factor from human platelets. Proc Natl Acad Sci USA 81:6757–6761

Serum Antibodies Against Cell Membrane Extracts of Human Bladder Carcinomas

J. W. Grups[1], W. Hock[1], and M. P. Wirth[1]

Introduction

Circulating specific antibodies have been demonstrated in a variety of human malignancies (Ackermann 1975; Hellström et al. 1968; Wolf et al. 1980). In bladder cancer patients tumor-associated membrane antigens and circulating antibodies against these structures have been described (Schneider et al. 1980).

These antibodies are a result of immunological reactions of the immune system of the host against tumor associated antigens on the tumor cell membrane. In 1985, Studer et al. reported preliminary results on the successful use of this humoral immune response as a serum marker in patients with bladder tumors (Studer et al. 1985). A human bladder cancer tissue culture cell line was used as antigenic material in a modified avidin-biotin-complex (ABC) peroxidase test. In this study it was reported that all examined serum samples of patients with the presence of bladder tumor had values above the cut-off line when compared with those from two control groups.

In one recently published experiment it was not possible to confirm these results reported previously by Studer et al. (Grups and Wirth 1985).

It was the purpose of our study to improve the sensitivity and specifity of this test system by using isolated cell membranes from bladder cancer cell lines as the antigenic material in the ABC method described by Studer et al. instead of testing on complete cells.

Material and Methods

Blood samples from patients with histologically proven bladder cancer, adenoma of the prostate, healthy volunteers, and other tumor patients were collected and the serum stored at −18°C.

The ABC peroxidase technique was performed against the isolated cell membranes of cells of the long term cultures J82 and 639V according to the technique published by Hsu 1981 (Hsu et al. 1981).

The cell membrane isolation was performed as published by Howard et al. All procedures were performed at 0–4°C. The cells were harvested from monolayer cultures by scratching them from tissue culture plates (Howard et al. 1980). The plastic tubes used in the course of isolation were soaked overnight in 1 m*M* EDTA, pH 7.0, and then rinsed 10 times with distilled water. 15 ml homogenization buffer (PBS,

[1]Department of Urology, University of Würzburg, Medical School, Josef-Schneider-Str. 2, D-8700 Würzburg

Investigative Urology 2
Edited by G. H. Jacobi et al.

pH 7.4 containing 1 m*M* MgCl, 30 m*M* NaCl, 5 μ*M* phenylmethylsulfonyl fluoride, 1.5 μ*M* aprotinin and 5 μ*M* pepstatin) was added to the tumor cells. The cell suspension was homogenized using a Polytron homogenizer. The cell breakage was monitored by light microscopy.

The homogenate (28–30 ml) was layered over 10 ml of 41% sucrose in homogenization buffer and ultracentrifuged at 95000 × g for 2 h. The membranes, forming a white band at the interface of the homogenate and sucrose solution, were aspirated. Homogenization buffer was added to dilute the sucrose, and the membranes were pelleted by centrifugation for 20 min. The membranes were then washed 3 times by resuspension in PBS. Membrane protein was measured with an Assay of Bio Rad, and the membranes were stored at −70°C. For the membrane binding on microtiter plates, the membranes were diluted with a coating buffer 10 μg protein/ml and 50 μg of the suspension was added to each well of the microtiter plates. The plates were kept overnight at 4°C and then 50 μl 0.5% glutaraldehyd solution was added for 10 min at 20°C. The plates were then washed 3 times with PBS and the vectastain ABC assay was performed.

Normal goat serum was added to each well and the plates were incubated for 60 min at 37°C and washed three times with PBS. The patient serum, 1:24 diluted, was then added and the plates were incubated for 30 min and washed once again with PBS. Then an incubation with rabbit anti-human-IgG was performed and ABC reagent (Vectastain) was added. After washing 5 times with PBS 100 μl ABTS-Peroxidase substrate was given to each well. The supernatant was aspirated, and the optical density (OD) was measured by a spectrophotometer.

For each test a control serum from one single healthy donor was used as the standard value and the other results were adjusted accordingly by subtraction of this OD value.

Table 1. Presence of serum antibodies against the membrane extracts of bladder carcinoma cell line 639 V

Diagnoses	Patients	Relative optical density	
		Mean value ± SD	95% Confidence limit
Bladder cancer	61	810.0 ± 164.5	481.9–1139.9
No cancer	43	768.4 ± 119.8	528.8–1008.0
Other cancers	27	856.4 ± 182.6	491.2–1221.6

Table 2. Presence of serum antibodies against the membrane extracts of bladder carcinoma cell line J82

Diagnoses	Patients	Relative optical density	
		Mean value ± SD	95% Confidence limit
Bladder cancer	63	114.2 ± 24.4	65.5–163.1
No cancer	46	107.7 ± 22.1	63.5–151.9
Other cancers	29	123.2 ± 23.6	75.6–170.8

Results

The frozen serum samples of 63 patients with histologically proven bladder cancer, 29 patients with various other malignant tumors, 9 patients with adenoma of the prostate, and 37 healthy volunteers were tested by the technique described above.

Using the cell membrane extract of the cell line 639V, the mean value of the OD measured by using the serum of patients with histologically proven bladder carcinoma was 810.0. In healthy donors this value was 768.4, and in patients with various other carcinomas (all were histologically proven) – the OD value was 856.4.

The standard deviation (SD) was however so high that there was no significant difference between the groups tested (Table 1). Similar results were obtained by using the cell membrane extract of the cell line J82 (Table 2).

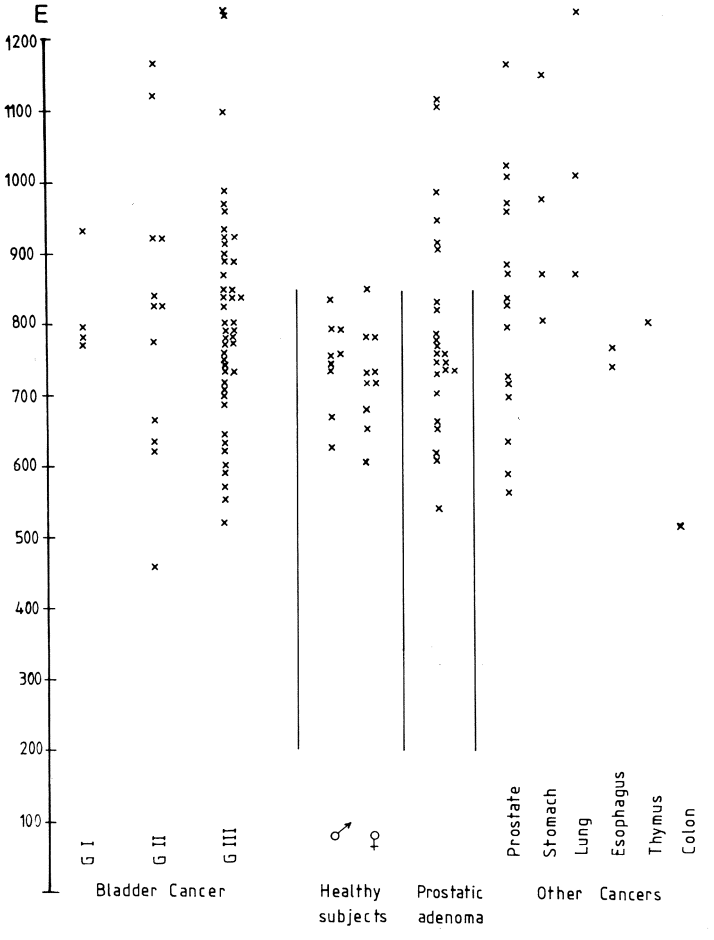

Fig. 1. Presence of individual serum antibodies against the antigenic material of the membranes of the cell line 639V

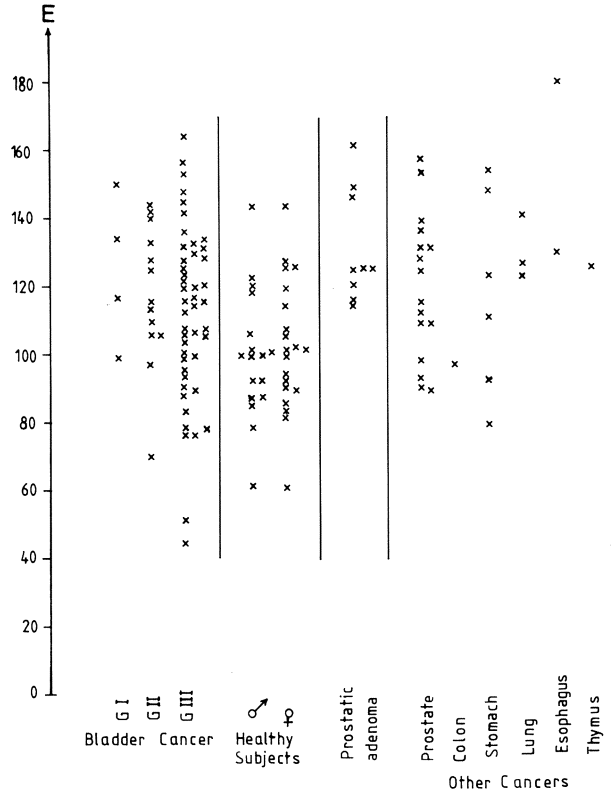

Fig. 2. Presence of individual serum antibodies against the antigenic material of the membranes of the cell line J82

The OD values of single patients using the cell membrane extract of the cells 639V and J82 are demonstrated in Figs. 1 and 2.

Comparing the test results of the various investigated groups it was not possible to find any statistically significant differences in the serum antibody level. It was, however, possible to detect serum antibodies binding on the cell membrane extracts which were used as antigen. These seem to be unspecific antibodies and therefore not usable as tumor markers.

These results confirmed our previously published findings using complete bladder tumor cells as antigenic material (Grups and Wirth 1985).

Discussion

In this study isolated cell membranes were used as the antigenic source for testing the binding of serum antibodies from patients with bladder cancer. It could be clearly indicated that with this modified ABC technique no significant differences in the serum were detectable when compared with the data of healthy volunteers or other cancer patients. There were even no differences between the patients with grade 1 and grade 3 tumors.

Small differences, however, are identifiable in the sensitivity of the tumor cell line 639 V and J 82 which were used as antigenic material in this study when compared to the control group of healthy volunteers. There were, however, no differences measurable when compared to the antibody level in patients with prostatic adenoma.

These results suggest that even with the modified ABC method it is not possible to differentiate on the basis of a serum test between bladder cancer patients and other individuals.

References

Ackermann R (1975) Tumor-associated antibodies against renal cell carcinomas detected by immunofluorescence. Eur Urol 1:154

Grups JW, Wirth M (1985) Nachweis von Serumantikörpern gegen Blasen-Carcinome. In: Verhandlungsbericht der DGU, 37. Tagung. Thieme, Stuttgart New York, pp 568–569

Hellström J, Hellström KE, Pierce GE, Yang JP (1968) Cellular and humoral immunity to different types of human neoplasms. Nature 220:1352–1356

Howard FD, Ledbetter JA, Mehdi SQ, Herzenberg LA (1980) A rapid method for the detection of antibodies to cell surface antigens: A solid phase radioimmunoassay using cell membranes. J Immunol Meth 38:75–84

Hsu SM, Raine L, Fanger H (1981) The use of avidin-biotin-peroxidase-complex (ABC) in immunperoxidase techniques: A comparison between ABC and unlabelled antibody (PAP) procedures. J Histochem Cytochem 29:577–580

Schneider MU, Troye M, Paulie S, Perlmann P (1980) Membrane-associated antigens on tumor cells from transitional cell carcinoma of the human urinary bladder. I. Immunological characterization by xenogenetic antisera. Int J Cancer 26:185

Studer UE, de Kernion JB, Lovrekovich L (1985) Preliminary results on the use of the humoral immune response as a serum marker in patients with bladder tumors. Urol Res 13:117–121

Wolf H, Hyden H, Langvad E (1980) Extracorporal immunoadsorption of circulating specific serum factors in renal carcinoma. In: Nieburgs HE (ed) Prevention and detection of cancer, Part 2. Dekker, New York, pp 2237–2249

Determination of Elements in Normal Urothelium and Bladder Carcinoma by X-Ray Microanalysis*

R. Friedrichs[1], W.-G. Burchard[2], H. Rübben[1], and W. Lutzeyer[1]

X-ray microanalysis (also called electron probe microanalysis, energy-dispersive microanalysis, and EDX) combines the possibility of a very sensitive elemental analysis with the localization of elements by the electron microscope. It is based on a finely focused electron probe over a sample surface to excite a characteristic X-ray emission. Measurements of the total amounts of elements can detect concentrations as small as 10^{-18} to 10^{-19} g (Baker 1985; Hall and Gupta 1984; Roomans 1983).

X-ray microanalysis is based on interacting of electron beams with the specimen. Under the impact of the electron beam, electrons from the inner shells of the atoms in the specimen may be knocked out of their orbits. An electron from an outer orbit will immediately fall into this gap. Since electrons in an outer orbit are in a higher energy state, energy will be liberated in this process: an X-ray photon of a certain energy is emitted. The energy of the X-ray photon is equal to the potential energy difference between the two shells. If an electron is knocked out from the K-shell, and the gap is filled by an electron from the L-shell, an X-ray photon will be emitted with an energy $E = E_L - E_K$. Since this energy is characteristic for the element from which it originates and for the shells between which the electron transition occurs, these photons are called characteristic X-rays (Roomans 1983). The gap in the L-shell will be filled immediately by an electron from a higher shell, for instance the M-shell, and another X-ray photon with a different energy $E' = E_M - E_L$ is emitted. The radiation resulting from the filling of a gap in the K-shell is called K-radiation. If this gap is filled by an electron from the L-shell, it is spoken about K_α-radiation. The gap may also be filled by an electron from the M-shell (K_β-radiation). Since the energy difference between the M- and K-shell is greater than between L- and K-shell, K_β-radiation has a higher energy than K_α-radiation (Fig. 1).

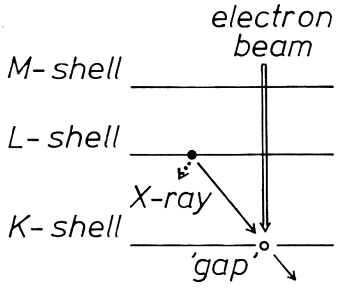

Fig. 1. An electron is knocked out of the K-shell. The gap is filled by an electron from the L-shell. The energy difference between K- and L-shell is liberated in the form of an X-ray (Roomans 1983)

* Partly supported by a grant from the Minister für Wissenschaft und Forschung des Landes Nordrhein-Westfalen, Düsseldorf, FRG

[1] Department of Urology, RWTH Aachen, Pauwelsstr., D-5100 Aachen
[2] Central Electron Microscopy Laboratory, RWTH Aachen, D-5100 Aachen

Investigative Urology 2
Edited by G. H. Jacobi et al.

Table 1

Element	Atomic number	Principal emission line	Energy (kV)
C	6	K_{α}	0.28
Na	11	K_{α}	1.04
Mg	12	K_{α}	1.25
Si	14	$K_{\alpha 1,2}$	1.74
P	15	$K_{\alpha 1,2}$	2.02
S	16	$K_{\alpha 1,2}$	2.31
Cl	17	$K_{\alpha 1,2}$	2.62
		K_{β}	2.82
K	19	$K_{\alpha 1,2}$	3.31
		K_{β}	3.59
Ca	20	$K_{\alpha 1,2}$	3.69
		K_{β}	4.01
Fe	26	$K_{\alpha 1,2}$	6.40
		K_{β}	7.06
Cu	29	$K_{\alpha 1,2}$	8.05
		K_{β}	8.90
		L_{α}	0.93
Zn	30	$K_{\alpha 1,2}$	8.64
		K_{β}	9.57
		L_{α}	1.01
As	33	$K_{\alpha 1,2}$	10.54
		K_{β}	11.73
		L_{α}	1.28

Elements with atomic numbers $Z \geq 11$ can be determined by X-ray microanalysis. The energy of X-ray radiation increases with increasing atomic numbers. The energies of X-ray radiation for a selected number of elements can be found in Table 1.

The instrumentation for energy-dispersive X-ray microanalysis consists of two main parts: the electron microscope and the detector system (a solid state semiconductor detector, preamplifier, amplifier, multichannel analyzer and data display). The electron microscope is producing an electron beam that can be focused into a small probe and is providing an image of the specimen. Thus the results of X-ray microanalysis can be correlated with the morphological structure. X-rays come into the detector (a lithium-drifted silicon solid state detector) and the resulting currents are amplified. The voltage pulses are stored in the multichannel analyzer so that characteristic elemental spectra are obtained. These spectra can be displayed or written out. The acceleration voltage ideal for the tissue examined should fulfill the following requirements: optimal peak-to-background-ratio, minimal specimen damage and good image quality (Roomans 1983).

X-ray microanalysis has given many informations about the physiology and pathology of inorganic constituents in the human body. The elemental concentration of normal urothelium and bladder carcinoma however is hardly known. The purpose

of this study is to present X-ray microanalysis as a method of element determination in biopsies of normal urothelium and bladder carcinoma. A method for specimen preparation and preliminary data are presented.

Material and Methods

Specimens of normal urothelium and bladder carcinoma obtained at TUR are immediately fixed in glutaraldehyde 2.5% (solved in cacodylate buffer) at 4°C for 2 h. Dehydration is carried out in alcohol (70% for 10 min), absolute alcohol (2×10 min) and xylene (10 min). The specimens are then embedded in paraffin. Fifteen-micron sections are cut from the paraffin blocks, floated out in a water bath and mounted on carbon blocks. The carbon blocks are deparaffinized with xylene (2×10 min), absolute alcohol (3×20 min) and dried at 60°C for 30 min. The blocks are now coated in vacuo with carbon. The blocks are processed through a scanning electron microscope JSM 35 CF^R (equipped with an X-ray system ORTEC-EEDS II) and a back-scattered-electron-detector Robinson. The determination of elements is performed by point analysis. The acceleration voltage has a value of 15 kV (LaB_6-cathode). Characteristic spectra of simultaneously determined elements are obtained. The number of counts in the peak is proportional to the quantity of the element at the analyzed point.

Results

Scanning electron micrographs of sections of normal urothelium and a poorly differentiated bladder carcinoma (T3b) are shown in Figs. 2 and 3. Elemental determination is performed by X-ray microanalysis at a variety of casually selected points. Figures 4 and 5 show X-ray microanalysis spectrographs of normal urothelium and bladder carcinoma. The elements detected in normal urothelium and bladder carcinoma are sulphur, phosphorus, chlorine, calcium and potassium. The silicium peak of normal urothelium (Fig. 4) is an artifact caused by the detector unit. The point analyses repeated at different sites and in specimens of other patients show similiar results: Different from normal urothelium phosphorus is detected in bladder carcinoma only. A statistical evaluation as well as a correlation of element content to stage and grade was not yet performed because of the small number of specimens analyzed.

Discussion

Elements are involved in the regulation of many physiologic and pathologic processes of the body (e.g., the regulation of enzymatic activity). They seem to be also involved in the pathogenesis of carcinomas. It is demonstrated that the prostate contains a high concentration of zinc. An increasing amount of zinc is found in benign prostatic hyperplasia, but a decrease in prostatic cancer (Feustel 1982; Okada 1983). With increasing age the cadmium content of the kidney increases, and an association

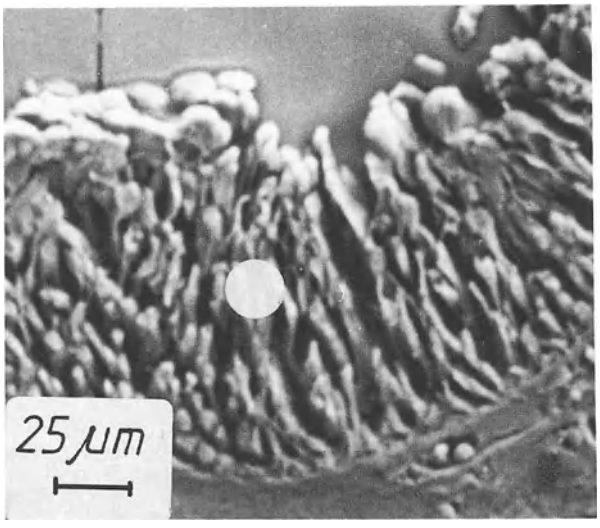

Fig. 2. Scanning electron micrograph of normal urothelium. The area where X-ray microanalysis (point analysis) is performed is indicated by the white point

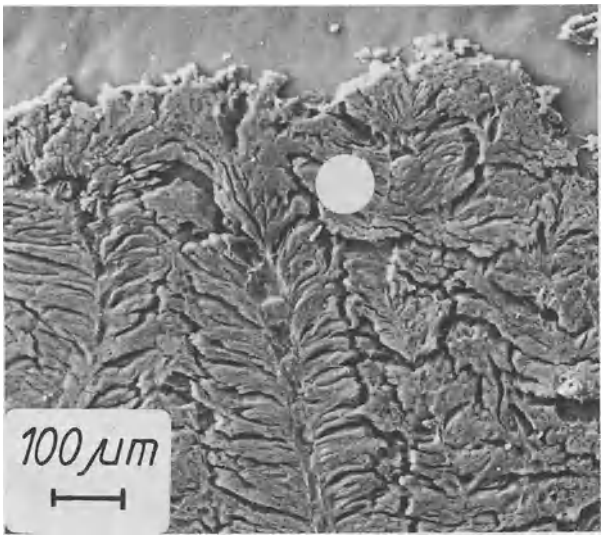

Fig. 3. Scanning electron micrograph of a transitional cell carcinoma (T3b, G3). The area where X-ray microanalysis is performed is indicated by the white point (point analysis)

of cadmium and renal cancer is discussed (Scott 1983). In cell cultures it is found that cells of different origin need a different calcium concentration for growing. Proliferation in low calcium concentration is typical of most tumorigenic cell lines (Swierenga 1983). In cultivated bladder carcinoma cells calcium is involved in the uptake of cytostatic drugs. After adding the calcium antagonist verapamil to the medium the uptake of doxorubicin hydrochloride and vincristine is increased (Simpson 1984).

The element content in normal human bladder and in bladder carcinoma is hardly known. Cadmium, selenium and zinc are found in human bladders by determination with atomic absorption spectrophotometry. Differences between normal

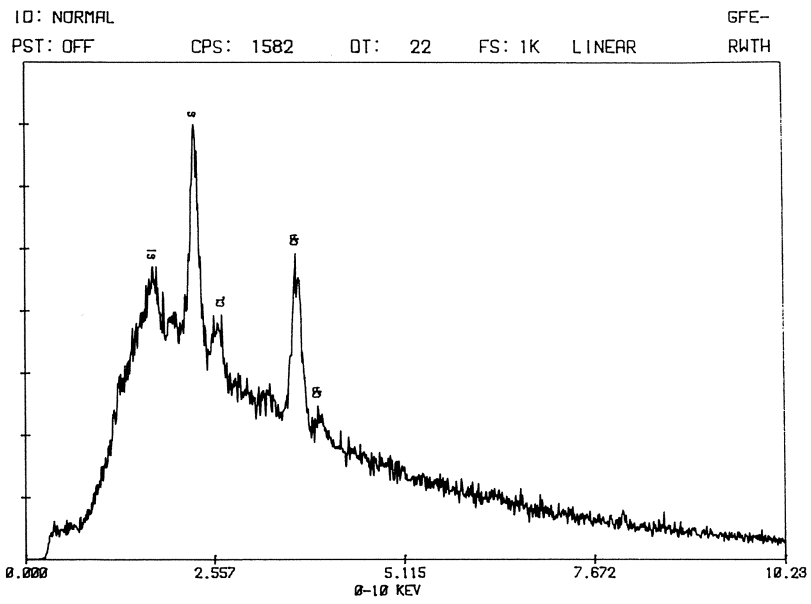

Fig. 4. X-ray microanalysis spectrograph of normal urothelium. The first peak *(Si)* indicates silicium which is an artifact from the detector unit. The elements detected are sulphur *(S)*, chlorine *(Cl)* and calcium *(Ca)*. The full scale of the axis of X represents 1000 counts, the elements are found at the points of their specific energy

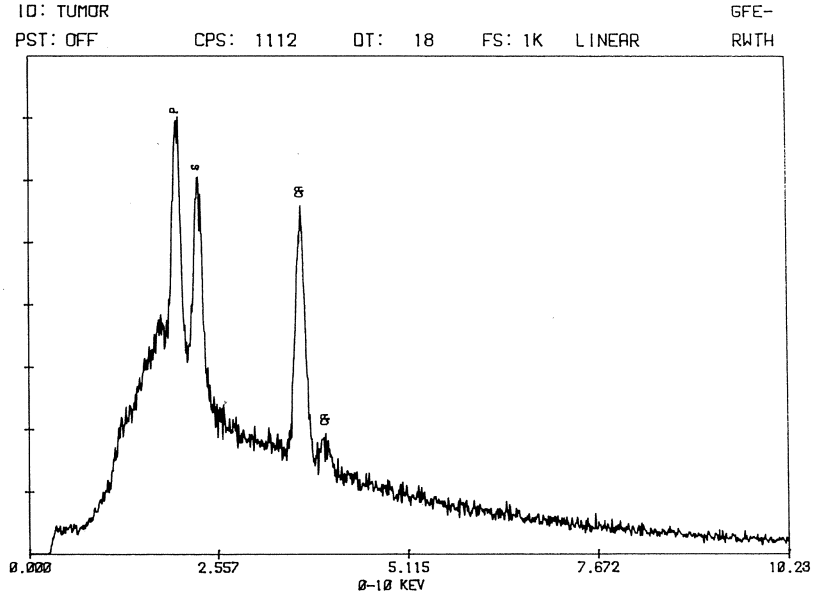

Fig. 5. X-ray microanalysis spectrograph of a bladder carcinoma (T3b, G3). The full scale of the axis of X represents 1000 counts. The elements are found at the points of their specific energy. Phosphorus *(P)*, sulphur *(S)* and calcium *(Ca)* are found

urothelium and bladder carcinomas occur (Feustel 1986). X-ray microanalysis is used for determination of the concanavalin A binding sites in urothelium and bladder carcinoma, because the reaction complexes contain iron (Takayama 1984). The distribution pattern of elements has been determined in normal urothelium and in bladder granulomata after bladder surgery by X-ray microanalysis. Beside a prominent sulphur peak calcium and iron are found in granulomata (Spagnolo 1986). Our own results demonstrate sulphur, phosphorus, chlorine, calcium and potassium in normal urothelium and in bladder carcinoma. The spectrum taken from the urothelium shows no peak of phosphorus, whereas a peak of phosphorus is seen in the elemental histogram taken over from the bladder carcinomas (Friedrichs 1986). The ubiquitous distribution of elements makes the interpretation of the preliminary results difficult.

Prominent sulphur-containing molecules in tissues are sulfated proteoglycans and glycoproteins (Friedrichs 1984), and sulphur-containing amino acids (e.g., cysteine). The content of phosphorus may be due to inorganic phosphate, nucleoside triphosphates, nucleic acids, phosphocreatine, phosphorylcholine, and phosphorylethanolamine. It is known that the higher the levels of inorganic phosphorus the lower ist the metabolism of the tissue. There is evidence from results based on ^{31}P magnetic resonance spectroscopy in tumors that changes in phosphocreatine/inorganic phosphate and adenosine triphosphate/inorganic phosphate-ratios occur between treated and untreated tumors (Bhujwalla 1986).

The urothelium is exposed to a concentration of sulphate and phosphate ions in the urine which is thirty times the concentration compared to blood plasma (Melicow 1978). The asymmetric unit membrane of the urothelium is replaced by a non-specific membrane in bladder carcinoma. Therefore, a passive influx of elements in the cells might be observed.

It has to be considered that element concentration in human tissues may sometimes be modified by artifacts due to fixation and not represent the true in vivo state (Saubermann 1986).

Our own results and the results from the literature also encourage chemical studies. Chemical studies, however, require much more material than X-ray microanalysis, therefore, data based on examinations in normal urothelium are difficult to obtain.

It is suggested from our preliminary data that there may be a specific distribution pattern of elements in tumors of different stage and grade. Therefore, further work will include a quantitative, statistically evaluated determination of elements in dependence of stage and grade. Combined investigations of transmission and scanning electron microscopy which are in progress may also answer open questions.

Acknowledgements. The authors wish to thank Mrs. H. Lange, Mrs. A. Lentzen and Mrs. M. Nitritz for their excellent technical assistance.

References

Baker D, Kupke KG, Ingram P, Roggli VL, Shelburne JD (1985) Microprobe analysis in human pathology. Scan Electron Microsc (Pt II): 659

Bhujwalla Z, Maxwell RJ, Tozer GM, Griffiths JR (1986) 31P MRS monitoring of radiotherapy in mouse tumors. Abstracts of the Fifth Annual Meeting of the Society of Magnetic Resonance in Medicine, Montreal, Quebec, Canada, p 161

Feustel A, Wennrich R, Steininger D, Klauss P (1982) Zinc and cadmium concentration in prostatic carcinoma of different histological grading in comparison to normal prostate tissue and adenomyomatosis. Urol Res 10:301

Feustel A, Wennrich R, Vorberg B (1986) Schwermetallgehalte menschlicher Harnblasentumoren und normaler Harnblase. 8. Symposium für Experimentelle Urologie. Demeter, Gräfelfing, p 28

Friedrichs R, Rübben H, Stuhlsatz HW, Lutzeyer W (1984) Biochemical determination of glycosaminoglycans in patients with benign prostatic hyperplasia and prostatic carcinoma. In: Bracci U, di Silverio F (eds) Advances in urological oncology and endocrinology. Rome, pp 197–210

Friedrichs R, Burchard WG (1986) Mikroanalytischer Vergleich der Elementverteilung in normaler menschlicher Blasenschleimhaut und in Blasenkarzinomen. Beitr Elektronenmikroskop Direktabb Oberfl 19:413

Hall TA, Gupta BL (1984) The application of EDXS to the biological sciences. J Microsc 136:193

Melicow MM (1978) The urothelium: a battleground for oncogenesis. J Urol 120:43

Okada K, Morita H, Arai R, Kishimoto T (1983) Ultrastructural localization of zinc in the hyperplastic prostate. The Prostate 4:631

Roomans GM (1983) Energy-dispersive X-ray microanalysis. In: Electron microscopy in human medicine, vol 11b: Special techniques and applications. McGraw-Hill, New York, p 91

Saubermann AJ, Dobyan DC, Scheid VL, Bulger RE (1986) Rat renal papilla: comparison of two techniques for X-ray analysis. Kidney Int 29:675

Scott R, Aughey E, Reilly M, Cunningham C, McClelland A, Fell GSF (1983) Renal cadmium content in the west of Scotland. Urol Res 11:285

Simpson WG, Tseng MT, Anderson KC, Harty JI (1984) Verapamil enhancement of chemotherapeutic efficacy in human bladder cancer cells. J Urol 132:574

Spagnolo DV, Waring PM (1986) Bladder granulomata after bladder surgery. Am J Clin Pathol 86:430

Swierenga SHH, Auersperg N, Wong KS (1983) Effect of calcium deprivation on the proliferation and ultrastructure of cultured human carcinoma cells. Cancer Res 43:6012

Takayama H (1984) Distribution of concanavalin A binding sites on normal human urinary bladder mucosa and bladder tumors by transmission and scanning electron microscopy and X-ray microanalysis. Urol Res 12:135

Analysis of Cell Cycle Distribution of Human Bladder Cancer Cells by BrdU-Hoechst Flowcytometry

W. Heckl[1], R. Friedl[2], and M. Kubbies[2]

Introduction

The natural history and therapy of bladder tumors are dictated primarily by the stage and histopathology of the disease. Nevertheless, among this tumor type there is a broad spectrum of biological behavior, and its response to a particular treatment regimen is highly variable. One reason for this heterogeneous biological behavior could arise from differences in cell cycle kinetics. Traditionally, in vitro growth and cell cycle kinetics of bladder tumors have been investigated by mitotic chromosome labelling techniques, such as radioactive thymidine uptake (Morimoto et al. 1980) or BrdU-incorporation (Hefton et al. 1980). Except for an accurate but time-consuming double-labelling technique (Schultze 1981) these standard methods do not provide exact estimates of the growth fractions. Moreover, the identification of kinetically divergent subpopulations within the heterogenic bladder tumor cell culture has not been possible. The introduction of monoclonal BrdU antibodies have improved the estimates of S-phase cell fractions, but there is no evidence that this new technique can differentiate between phase fractions which belong to successive cell cycle generations. Here, we introduce an alternative technique which likewise uses the principle of BrdU-incorporation, but which detects BrdU-substitution by its quenching effect on Hoechst-dye fluorescence (Latt et al. 1977). This method allows the flow cytometric discrimination between cycling and non-cycling cells (Böhmer 1979; Nüsse 1981). In conjunction with a proposed modification of the Smith and Martin model of exponential compartment exit (Smith and Martin 1973; Rabinovitch 1983) the BrdU-Hoechst flow-histograms presented in this report provide the most comprehensive information to date about the cell cycle, i.e., exact estimates of the growth fraction, compartment durations, cell cycle arrest, and transition probabilities; the potential of this new cell kinetic assay has been demonstrated with human fibroblasts and lymphocytes (Kubbies et al. 1983; 1985). The aim of the present study is to demonstrate the applicability of the BrdU/Hoechst technique to cultivated human bladder cancer cells.

Material and Methods

Cell Culture and Sample Preparation. The RT-4 cell line, a well differentiated transitional cell carcinoma, was obtained from L.M.Franks, London, U.K. The tumor cells were routinely cultured in DMEM containing 10% FCS. The cell line was used

[1]Department of Urology, Medical School, University of Würzburg, Josef-Schneider-Str. 2, D-8700 Würzburg
[2]Department of Human Genetics, University of Würzburg, D-8700 Würzburg

Investigative Urology 2
Edited by G. H. Jacobi et al.

within 10 passages after thawing from frozen stock vials. The cultures were routinely examined for, and found free of, mycoplasma.

The RT-4 cells were seeded at a density of 2×10^5 cells/25 cm^2 flask in DMEM/10% FCS for 24 h. Thereafter, the medium was changed, the monolayers were washed three times with PBS, and the cells were offered serum-free DMEM in order to accumulate most the cells in the G_0/G_1 phase. After 48 h, the RT-4 cells were stimulated with DMEM containing 10% FCS, and the desired concentrations of BrdU were added to the culture medium (Sigma). For some experiments the RT-4 cells were treated with 100 ng/ml Doxorubicin (ADM) along with 5×10^5 *M* BrdU. The monolayers were harvested at the desired intervals by rinsing twice with PBS and adding trypsin (Gibco). After centrifugation the cells were resuspended in 1 ml DMEM containing 10% FCS and 10% DMSO for storage at −20°C. (Histograms from frozen samples were identical to that of unfrozen cells.) During all stages of handling after BrdU incorporating care was taken to avoid exposure to short wave length light (Severin et al. 1982).

Flow Cytometric Analysis. For flow cytometric analysis, the samples were thawed, pelleted and resuspended in 4°C staining solution consisting of 100 m*M* TRIS, ph 7.4, 0.9% NaCl, 1 m*M* $CaCl_2$, 0.5 m*M* $MgCl_2$, 0.2% BSA, 0.1% Non-idet P 40 and 0.8 µg/ml Hoechst 33258. The fluorescence intensity was measured with an epi-ilumination flow system ICP22 (Phywe AG, now Ortho Instruments) equipped with a model 2103 multichannel analyzer (Ortho) interfaced to a PDP/11 series microcomputer (Digital Equipment). The fluorescence of approximately $3–5 \times 10^4$ cells was recorded in each measurement. The individual cell cycle compartment sizes were determined by automated curve fitting of uni- or multi-modal BrdU-Hoechst fluorescence histograms (Rabinovitch 1983). Histograms representing overlapping cell maturity distributions were deconvoluted by non-linear least squares fitting of the respective G_1, S and G_2 phases (Dean and Jett 1974). The number of parameters in the fitting process was reduced by use of first order S phase polynomials, constraints on the G_1/G_2 peak ratios, and uniformity of coefficients of variation. Standard errors of the fitted parameters were calculated by use of the error and curvature matrices of the analytical least squares fitting technique (Bevington 1969). Data on compartment size were plotted on a semilogarithmic scale as a function of time after stimulation. These plots were fitted according to a modified Smith/Martin modell (Smith and Martin 1973) of exponential compartment exit and as modified by Rabinovitch (1983). Compartment specific cell cycle arrest was calculated from these plots as difference in the computed plateau phase levels between successive exit curves (Kubbies et al. 1985).

Results

By optimization of multiple parameters, the flow cytometric histograms obtained by the BrdU/Hoechst quench technique display a series of fluorescence peaks which correspond to cycling and noncycling cells in the first and second cell cycles after stimulation. Figure 1 illustrates a representative sequence of flow histograms after stimulation of the serum deprived human bladder cancer cell line RT-4. At 8 h after stimulation, the first cells begin to cycle as their decreasing fluorescence indicates

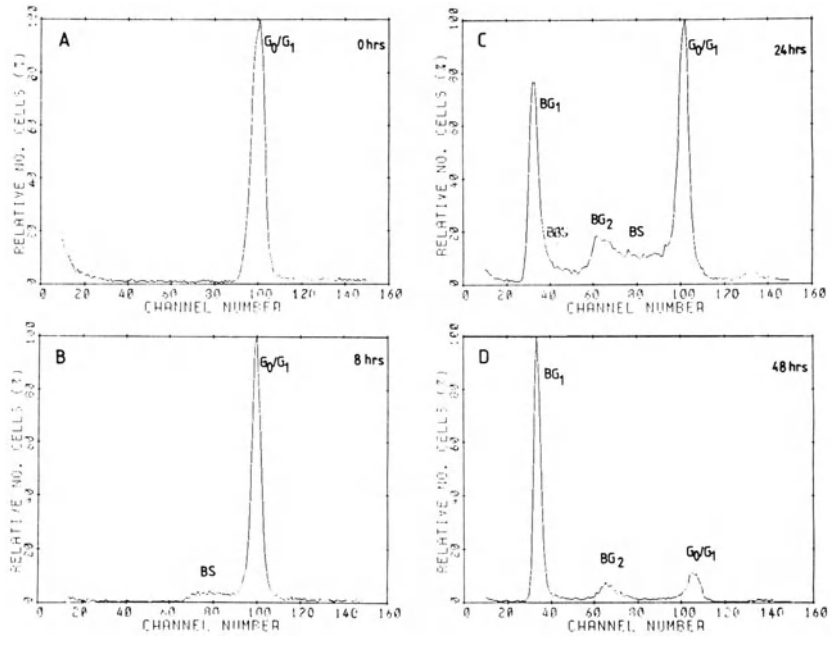

Fig. 1A–D. BrdU-Hoechst fluorescence histograms of RT-4 cells at various times after growth stimulation. 5×10^5 cells were grown in 5×10^{-5} *M* BrdU. Fluorescence analyses correspond to the following times after stimulation: **A** 0 h, **B** 8 h, **C** 24 h, **D** 48 h

BrdU-substitution during semi-conservative replication (BS-phase in panel B). After 24 h (panel C) a sizeable portion of cells have left the first cell cycle and entered the second G_1-phase (denoted BG_1) after stimulation. Because of the increase of BrdU substitution during replication S- and G_2-phase cells display less Hoechst fluorescence than the non cycling G_0/G_1 cells. The mitotic division of such BrdU-substituted cells yields daughter cells with half of the value of the BG_2-fluorescence. These cells are designated as "BG_1" 24 h and 48 h after stimulation (panel C, D in Fig. 1). The prefix "B" in all panels denotes the fact that the cells have replicated their DNA once in the presence of BrdU and thus appear left of the G_0G_1 peak. By conventional flow cytometry the DNA histograms show newly divided populations indistinguishable from the noncycling G_0/G_1 cells due to identical DNA content. In contrast the BrdU/Hoechst histograms clearly distinguish between cells which have remained in the G_0G_1 stage and those which have completed one round of replication in the presence of BrdU. Also at the 48 h timepoint 79% of the initial cell population have left the G_0G_1 compartment and less than 5% of the cells continue to synthesize DNA (decreased amplitudes of the G_0G_1, BS and BG_2 cell fractions). At this point there might be a block, because we never could observe any complete third cell cycle, as revealed in repeated experiments. The addition of 100 ng/ml doxorubicin along with BrdU led to reduced cell exit from the G_0G_1 compartment (Fig. 2). Compared with the untreated cells, more than 60% of treated cells have failed to divide by 48 h; only 24.0% have arrived in the second G_1-phase, whereas the cycling cell fraction of the untreated culture amounts close to 80% of the original population (Table 1).

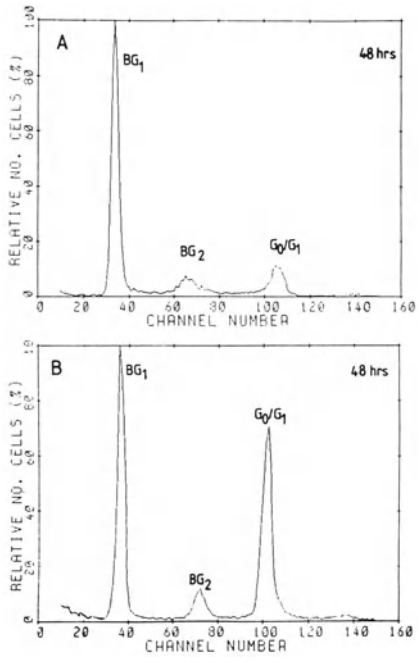

Fig. 2A, B. BrdU-Hoechst fluorescence histograms of RT-4 cells at 48 h after stimulation with 10% FCS and exposure to $5 \times 10^{-5} M$ BrdU. **B** shows a parallel culture treated with 100 ng/ml doxorubicin

Table 1. Distribution of individual cell cycle compartments of the RT-4 cell cultures after stimulation with 10% FCS with and without exposure to 100 ng/ml doxorubicin

	Cell cycle compartments (%)			
	G_0G_1	BS[a]	BG_2[a]	BG_1[a]
Time (h)				
0	100	–	–	–
8	84.3	15.6	0.1	–
24	45.2	32.0	3.4	7.3
48 control	21.5	12.2	8.8	51.3
48 (ADM)	58.5	6.1	8.4	24.0

[a] The prefix "B" denotes one round of replication in the presence of BrdU. Deviations of the sum total from 100% is due to variable background signals (cellular debris)

Discussion

In accordance with the findings of Kubbies et al. (1983, 1985) and the observations of Latt et al. (1977) our studies confirm a BrdU-concentration dependence of the quenching effect. The highest concentration $1 \times 10^{-3} M$ gave a bimodal distribution

with a blocking effect at BG_1, whereas the lowest BrdU-concentration yielded trimodal peaks with insufficient quenching. A BrdU-concentration of $5 \times 10^{-5} M$ yields excellent histograms. The Hoechst fluorescence of the nearly divided cells decreased to less than 50% of the original G_0/G_1 value. With a Hoechst 33258 dye concentration ranging from between 0.6 and 1 μg/ml (usually 0.8 μg/ml) and the above mentioned BrdU-concentration, the BrdU-Hoechst analysis yields well separated peaks which denote noncycling and cycling cells. This degree of resolution permits the detailed analysis of the cell cycle kinetics of a variety of cultured cells (Rabinovitch 1983). We here demonstrate that human bladder carcinoma cells are likewise amenable to this type of analysis. It should be noted, however, that with the BrdU-concentrations required to achieve an optimum quench effect, cell cycle transit times might be disturbed owing to BrdU-induced cell cycle blockage (Böhmer 1979; Latt et al. 1977). This potential problem may be dissolved by employing bivariate Ethidiumbromide/Hoechst analysis which permits the use of reduced BrdU-concentrations. As we have demonstrated with one example, BrdU-Hoechst technique may allow a more accurate and sophisticated assessment of the effects of cell cycle active agents. The exploration of the specific cell cycle effects of potential chemotherapeutic agents may, therefore, benefit from the application of this novel technique.

References

Bevington PR (1969) Data reduction and error analysis for the physical sciences. McGraw-Hill, New York

Böhmer RM (1979) Flow cytometric cell cycle analysis using quenching of 33258 Hoechst fluorescence by bromodeoxyuridine incorporation. Cell Tissue Kinet 12:101–110

Dean PN, Jett JH (1974) Mathematical analysis of DNA distributions derived from flow microfluorometry. J Cell Biol 60:523–527

Hefton JM, Darlington GI, Casazza BA, Weksler ME (1980) Impaired proliferation of PHA responsive human lymphocytes in culture. J Immunol 125:1007–1010

Kubbies M, Rabinovitch PS (1983) Flow cytometric analysis of factors which influence the BrdU-Hoechst quenching effect in cultivated human fibroblasts and lymphocytes. Cytometry 3:276–281

Kubbies M, Schindler D, Hoehn H, Rabinovitch PS (1985) Cell cycle kinetics by BrdU-Hoechst flow cytometry: an alternative to the differential metaphase labelling technique. Cell Tissue Kinet 18:551–562

Latt SA, George YS, Gray JW (1977) Flow cytometric analysis of BrdU substituted cells stained with 33258 Hoechst. J Histochem Cytochem 25:927–934

Morimoto K, Wolff S (1980) Cell cycle kinetics in human lymphocyte cultures. Nature 288:604–606

Nüsse M (1981) Cell cycle kinetics of irradiated synchronous and asynchronous tumor cells with DNA distribution analysis and BrdU 33258 technique. Cytometry 2:70–79

Rabinovitch PS (1983) Regulation of human fibroblast growth rate both by non-cycling cell fraction and transition probality is shown by growth in 5-bromodeoxyuridine followed by Hoechst 33258 flow cytometry. Proc Natl Acad Sci USA 80:2951–2955

Schultze B (1981) Cell kinetic studies with H-3 and C-14-Thymidine. J Histochem Cytochem 29:109–112

Severin E, Ohnemus B (1982) UV-dose dependent increase in the Hoechst fluorescence intensity of both normal and BrdU-DNA. Histochemistry 74:279–291

Smith JA, Martin L (1973) Do cells cycle? Proc Natl Acad Sci USA 70:1263–1267

Development of Bladder Carcinoma Following Portacaval Shunt in Rats

U. Engelmann[1], P. Schramek[1], M. Grün[2], H. P. Baum[3], B. Wertmann[1], and G. H. Jacobi[1]

Portacaval anastomosis (PCA) was first introduced by Eck (1877) and was investigated in a number of different animals. Lee et al. (1961; 1974) published a reliable method with low mortality in rats. The occurrence of urolithiasis in rats following portacaval anastomosis happened to be noticed by chance. It was published by Herz et al. (1972a, 1972b, 1973), who defined the portacaval shunt rat as an experimental model. Heine et al. (1979) described dysplastic and neoplastic changes of the bladder mucosa following portacaval anastomosis. His findings were confirmed by Duy et al. (1981); Grün et al. (1982), and Dubuisson et al. (1984). However, Wallace et al. (1984) found papillary hyperplasia, not neoplastic changes, always in the presence of urolithiasis. The results obtained so far regarding the development of bladder carcinoma following PCA differ, and our investigation intends to address the following questions:

1. Does a portocaval shunt in rats lead to neoplastic changes of the urinary bladder?
2. What is the sex distribution?
3. Do bladder neoplasms develop independently from urolithiasis, or can they be seen only in rats with bladder stones?
4. If the malignant changes are not caused by urolithiasis but are the result of excretion of a carcinogen as proposed by some – can then carcinogen concentration and tumor induction in the upper urinary tract be increased by unilateral nephrectomy?

Mostly male rats were used in the investigations reported so far: in our investigations, care was taken to include female rats as well as a sham operated control group and a group with implantation of a sterile bladder stone (without PCA in order to answer question 3).

Material and Methods

111 Chbb Thom- and 13 Sprague Dawley rats (67 males and 57 females) were operated under general anesthesia using ketamine. According to the technique reported by Lee and Fisher (1961), the portacaval shunts were done in an end-to-side fashion under an operating microscope with 10/0 ethilon or under magnifying loops with 8/0 ethilon running sutures. The V. pancreatic-duodenalis was included in the shunt.

The distribution of control and treatment groups is shown in Table 1. Sham operated animals (SOP) underwent a median laporotomy, during which the V. cava and por-

[1]Department of Urology, Medical School, Johannes Gutenberg University, Langenbeckstr. 1, D-6500 Mainz
[2]St. Vincenz and Elisabeth Hospital, D-6500 Mainz
[3]Institute of Pathology, Medical School, Johannes Gutenberg University, D-6500 Mainz

Investigative Urology 2
Edited by G. H. Jacobi et al.

Table 1. Treatment and control groups, number of operated and evaluable animals

	Male	Female	
PCA	27[a]/41	23[a]/44	
PCA+N	4[a]/ 5	0[a]/ 0	
SOP	11[a]/11	2[a]/ 3	
St.I	10[a]/10	9[a]/10	
Total	52[a]/67	34[a]/57	86[a]/124

PCA, Portacaval anastomosis; PCA+N, portacaval anastomosis + nephrectomy; SOP, sham operated animals; St.I, implantation of a bladder stone

[a] Available for histological evaluation

tae were clamped for 10 min. In order to investigate the influence of chronic urothelial irritation, a sterile stone (quarzit) was implanted into the bladder (group St.I), and the rats were checked daily and weighed weekly. Animals were sacrificed in intervals, and median follow up was 49.7 weeks (min. 3, max. 69 weeks). 13 rats died of postoperative complications, and in 25 rats the bladder histological evaluation was unavailable or unsatisfactory owing to early autolytic changes or postmortem cannibalism. The following results are, therefore, based on the remaining 86 rats (52 male and 34 females). During autopsy, the liver, spleen and complete urinary tract were removed and inspected under the microscope. Bladder urine was taken under sterile conditions for microscopy and cultures. The removed bladders were cut open, attached to cardboard and fixated in 10% formalin solution. 1 mm^3 sized tissue specimen were fixated in a 2.5% glutaraldehyde solution for scanning electron microscopy (SEM). Sections were stained H&E for light microscopy.

Results

At the time of autopsy, all portacaval anastomoses were patent and the liver was atrophic. Changes in the upper urinary tract – nephrolithiasis, pyelonephritis, stone formation in renal tubuli, ureteral stones – and the observed histological changes will be reported separately.

Body Weight. At the time of operation, the average body weight was 300–350 g (males) or 250–300 g (females). Postoperative weight loss averaged at 25% with a maximum 4 weeks postop. By 8 to 10 weeks postop, the rats had regained their preop weight; at the time of autopsy, the average body weight was 320 (females) and 350 g (males).

Development of Bladder Carcinoma. 35 out of 86 animals developed a urothelial carcinoma of the bladder, and 51 rats did not show a bladder tumor. The distribution of tumors in the various groups is shown in Table 2. 34 of these rats also had bladder stones. Only one rat had a bladder carcinoma without bladder stones; however, it

Table 2. Development of urothelial carcinoma (related to the number of evaluable animals)

	Male	Female	
PCA	16/27	1/23	
PCA+N	2/ 4	0/ 0	
SOP	2/11	0/ 2	
St.I	9/10	5/ 9	
Total	29/52 (55.7%)	6/34 (17.6%)	35/86 (40.7%)

Table 3. Histological differentiation of the described malign changes of the bladder mucosa

Papillomatosis (G0)	1
Urothelial carcinoma (GI)	24
Urothelial carcinoma (GI–GII)	1
Urothelial carcinoma (GII)	9
Total	35

(no. 397, male, PCA, follow up 64 weeks) had developed kidney stones. At the time of autopsy, neither stones nor sand could be found in the bladder.

Sex Difference. Predominantly male rats developed bladder stones and bladder tumors. In the PCA group, 59% of the male rats and only 4% of the female rats developed a carcinoma. Male rats with an implanted bladder stone – but without a PCA – had a very high incidence (90%) of bladder carcinoma, whereas only 55% of the female rats developed a carcinoma. Spontaneous growth of bladder carcinoma was seen in 2/11 male controls, in both cases accompanied by bladder stones.

Histology. 15 animals showed chronic inflammation of the bladder mucosa, always connected with positive urine cultures, large stone masses or multiple stones. 6 rats had a lymphoplasmocellular infiltration of the lamina propria, and hyperplasia or dysplasia of the bladder urothelium was seen in 8 rats.

All tumors were urothelial carcinomas, accompanied in 20 cases by squamous cell metaplasia. 2 animals had developed squamous cell metaplasia without carcinoma. The tumors were graded as GI-GIII (Table 3). One animal showed a papillomatosis (G0), 24 rats developed a papillary urothelial carcinoma (GI), in one case a urothelial carcinoma GI-GII was seen, and the remaining 9 rats had a moderately differentiation of Carcinoma (GII). Undifferentiated tumors (GIII) were not found. The islets of squamous cell metaplasia (keratinizing and non-keratinizing) mostly were confined to the level of the urothelium; sometimes, however, they protruded into the bladder lumen or bulged deeply into the lamina propria (Fig. 1). The

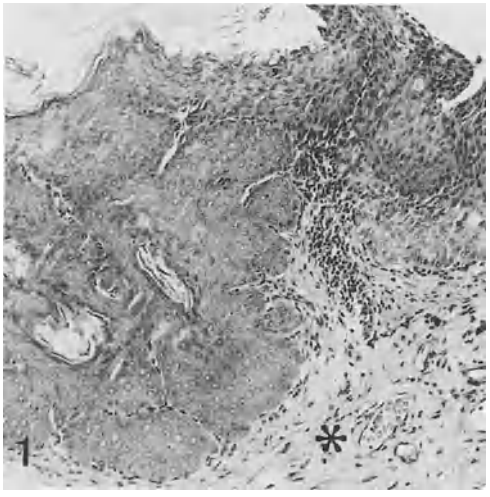
1
*

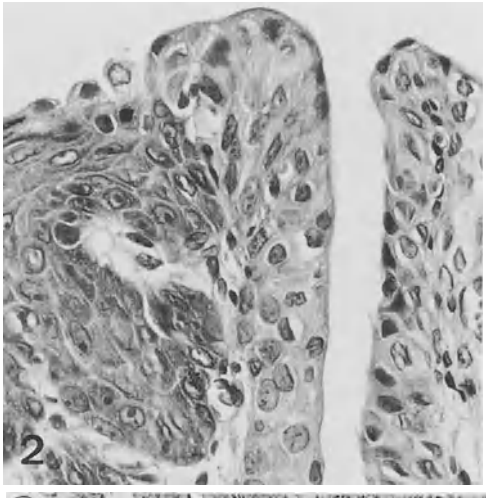
2

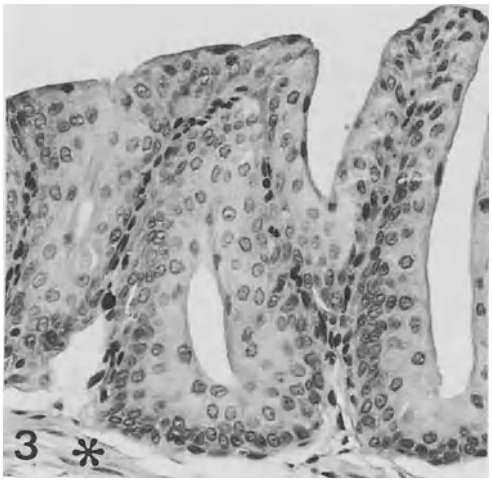
3
*

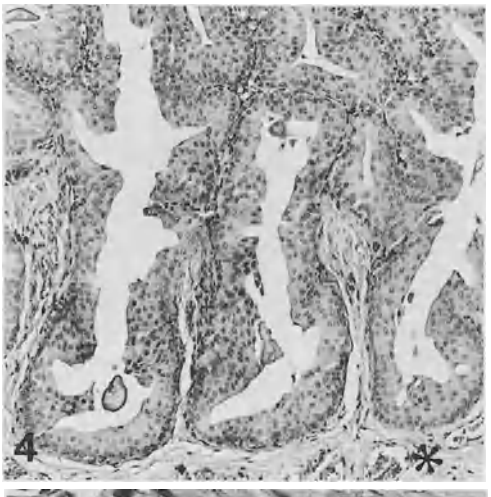
4
*

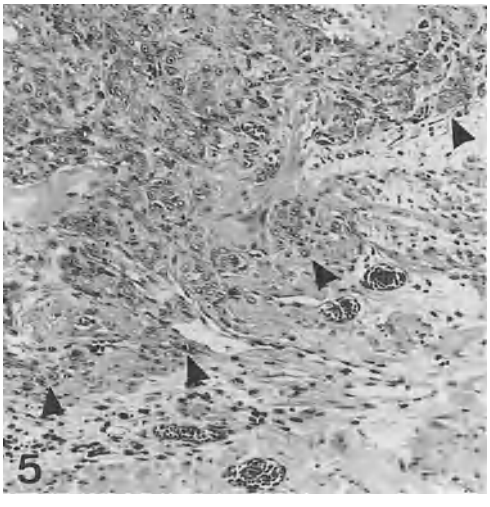
5

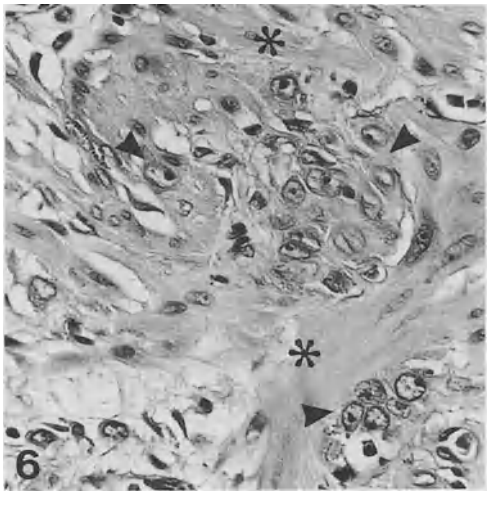
6
*
*

neighboring parts of the urothelium showed hyperplasia (Fig. 1) as well as dysplasia (Fig. 2). Transformation of squamous cell metaplasia into a squamous cell carcinoma was not seen. The papillomatosis (G0) displayed multiple flat papillary folds of the urothelium without dysplastic changes or increase of the cellular layers (Fig. 3). Well-differentiated carcinomas were seen as solitary or multifocal tumors forming partly flat, partly markedly papillary structures. The number of urothelial cell layers was sometimes smaller, sometimes larger than 7. The nuclei showed mild irregularities in size, and the nucleoli were more prominent than normal. The polarity of the nuclei was not disturbed (Fig. 4). Well differentiated carcinomas (GI) did not invade the deeper layers of the bladder wall; they only showed displacement of normal mucosa while growing towards the lamina propria. Moderately differentiated carcinomas (GII), however, showed focal invasion of underlying structures. In comparison with GI tumors, irregularities of nuclei (variation in size, prominence of nucleoli, basophily) were more marked, with the nuclei partly losing their polarity. GII tumors not only showed papillary structures with 10–20 cell layers, but also grew as solid tumors forming small basal cell nests and invading the lamina propria of the bladder wall (Figs. 5, 6). Tumor invasion of blood and lymph vessel was not seen.

Discussion

Reports concerning the development of urothelial carcinoma following portacaval shunts are conflicting. Wallace et al. (1984) found only hyperplasia without any dysplastic or carcinomatous changes in Sprague-Dawley rats with PCA after a follow up of up to 46 weeks. They felt that the urothelial reactions were only caused by chronic irritation due to bladder stones, which they found in all these cases. In female rats, neither bladder stones nor urothelial hyperplasia could be detected.

Heine et al. (1979) described urothelial hyperplasia in all their rats. The reactions were most severe in the bladder, but could also be seen in the ureter and kidney

Fig. 1. Islet of metaplastic keratinizing squamous epithelium *(left side)* bulging into the lamina propria *(asterisk)* of the urinary bladder wall. There is hyperplastic urothelium to the right of the metaplastic squamous epithelium. Chronic inflammation in the lamina propria. HE, × 340

Fig. 2. Borderline between metaplastic squamous epithelium *(left side)* and urothelium *(right side)* showing mildly dysplastic changes. HE, × 1260

Fig. 3. Papillomatosis (G0) of the urothelium displaying a flat folding with 3–4 layers of normally differentiated urothelial cells. The lamina propria is marked by an *asterisk*. HE, × 725

Fig. 4. Basal portion of a papillary urothelial carcinoma (GI). The papillae are tall and are made up of a thin central branch of connective tissue bearing 4–6 layers of urothelium with mild nuclear irregularities. The carcinomatous urothelium impinges upon the lamina propria *(asterisk)* but does not invade it. HE, × 300

Fig. 5. Basal portion of a urothelial carcinoma (GII) invading the muscle layer of the urinary bladder from top left. The front of invasion is indicated by *arrowheads*. HE, × 330

Fig. 6. Urothelial carcinoma (GII), detail from Fig. 5. Small nests of carcinoma cells *(arrowheads)* infiltrate the smooth muscle layer *(asterisks)* of the urinary bladder. The carcinoma cells display enlarged and partly vesicular nuclei with prominent nucleoli. HE, × 1200

pelvis. In cases with a sufficiently long follow up, they reported proliferate changes, including invasive urothelial carcinomas.

Grün et al. (1982) investigated 38 male Chbb Thom rats with a PCA and confirmed the finding of preneoplastic and neoplastic changes of the bladder mucosa. An increase of bile acid excretion acting as a carcinogen on the urothelium could not be found.

Duy et al. (1981) saw urothelial tumors in rats as soon as 4–5 months after PCA. At the same time, they noticed an increased incidence of bladder stones. After a follow up of 52 weeks, Dubuisson et al. (1984) found bladder tumors in 8/8 Chbb-Thom rats, 6 of these also with bladder stones.

In our investigations, the following results were significant: the incidence of stone formation in female rats in considerably lower than in males, which will be reported by Schramek et al. (p. 220). Not only the rate of stone formation, but also the development of urothelial tumors showed themselves sex-related: i.e., male animals showed a much higher rate of carcinomas (55.7%) than female rats (17.6%). We saw only one rat out of 35 with a vesical tumor in a bladder which was free of stones at the time of necropsy. However, this animal had kidney stones. Interestingly enough, a high rate of bladder tumors (14/19) was found in animals with an implanted bladder stone, and no PCA; even more striking was the occurance of tumors in 2 sham operated male rats – in both cases accompanied by stones.

We not only found hyperplastic changes like Wallace et al. (1984), but also true urothelial carcinomas with all signs of malignancy, including invasiveness.

Various reasons for the urothelial reactions – hyperplasia and development of tumors in PCA rats have been discussed. The portacaval shunt leads to liver atrophy, and this could result in renal excretion of carcinogenic substances. These could be produced endogenously like bile acids, but they might also be absorbed from food (Dubuisson et al. 1984; Grün et al. 1982).

Investigators who discuss such a mechanism have either used only male rat that have a high rate of stone formation (Dubuisson et al. 1984; Grün et al. 1982) or the sex is not specified in their publications (Heine et al. 1979; Duy et al. 1981).

Others feel that the urothelial reactions are only caused by chronic irritation due to bladder stones (Wallace et al. 1984). It is well known that chronic urinary tract infections connected with mechanical irritation by steel wire implants can cause hyperplasia and urothelial carcinoma in rats (Davis et al. 1984). The development of bladder stones following repeated injection of 0.9% saline solution has been described in rats. In all cases, a diffuse papillomatosis of the urothelium and invasion of the tunica muscularis could be seen after only 9 weeks (Oyashu et al. 1984).

Conclusion

Urothelial reactions following portacaval shunts vary from benign hyperplasia and squamous cell metaplasias to infiltrating, moderately differentiated urothelial carcinomas. Up to now, metabolic changes leading to renal excretion of endogenous or exogenous carcinogenic substances have been predominantly discussed. In the investigations presented here, the epithelial changes are always accompanied by urolithiasis. Chronic irritation and inflammation thus caused can be held responsible

for the tumor induction, even more so since a high rate of tumors was seen in rats without a portacaval shunt but with bladder stones.

The possibility can not be excluded that a portacaval shunt may result in the renal excretion of substances which are normally detoxified in the liver; however, we feel that this did not cause induction of bladder tumors in our investigations, as is nicely illustrated by the development of bladder tumors in 2 sham operated animals, which spontaneously developed bladder stones. Further investigations should mainly address the question of urolithiasis caused by portacaval shunts.

References

Davis CP, Cohen MS, Gruber MB, Anderson MD, Warren MM (1984) Urothelial hyperplasia and neoplasia: A response to chronic urinary tract infections in rats. J Urol 132:1025–1031

Dubuisson L, Vonnahme FJ, Balabaud CH, Grün M (1984) Neoplastic surface changes in urothelium of rats after portocaval anastomosis. A combined light and scanning electron microscopic study. Exp Pathol 26:49–58

Duy N, Yamaguchi Y, Prabhudessi M, Babb J, Gans H (1981) Cancer of the bladder in the portacaval shunted rat. Gastroenterology 80:1331

Grün M, Richter E, Heine WD (1982) Renal bile acid excretion as a cause of neoplastic lesions in the urinary tract after total portacaval shunt in the normal rat? Hepat-gastroenterol 29:232–235

Heine WD, Grün M, Rasenack U, Liehr H (1979) Präneoplastische und neoplastische Urothelveränderungen nach portocavaler Anastomose der Ratte. Histologische und autoradiographische Befunde. Verh Dtsch Ges Pathol 63:517

Herz R, Sautter V, Bircher J (1972a) Fortuitous discovery of urate nephrolithiasis in rats subjected to portacaval anastomosis. Experientia 28:27–28

Herz R, Sautter V, Robert F, Bircher J (1972b) The Eck fistula rat: Definition of an experimental model. Eur J Clin Invest 2:390–397

Herz R, Sautter V, Lauterburg B, Bircher J (1973) Urolithiasis, eine unvorhergesehene Folge der portokavalen Anastomose. Z Gastroenterologie 11:117–120

Lee SH, Fisher B (1961) Portacaval shunt in the rat. Surgery 50:668–672

Lee S, Chandler JF, Broelsch CE, Flamant YM, Orloff MJ (1974) Portal systemic anastomosis in the rat. J Surg Res 17:53–73

Oyashu R, Iwasaki T, Ozono S (1984) Diffuse papillomatosis of rat urinary bladder occurring in association with vesical calculi. J Urol 132:1012–1015

Wallace DMA, Ackermann D, Davis B, Hartmann WH (1984) Uric acid lithiasis and proliferative changes in the rat urinary bladder after portacaval anastomosis. In: Harzmann R, Jacobi GH, Weißbach L (eds) Experimentelle Urologie. Springer, Berlin Heidelberg New York, pp 430–433

Fluorescence Imaging of Porphyrin-Sensitized Bladder Tumors

D. Jocham[1], R. Baumgartner[1,2], N. Fuchs[1,2], H. Stepp[1,2], and E. Unsöld[2]

Introduction

Many organic substances emit characteristic fluorescence radiation after excitation with light in the visible or near UV region of the electromagnetic spectrum. Tissues with low innate fluorescence (autofluorescence) may be stained with socalled fluorochromes to induce secondary fluorescence. This technique plays an increasing role in (micro-)biological investigations and medical diagnosis. Already in 1924 (Policard 1924) the observation of a red fluorescence of tumors has been reported and attributed to endogenic porphyrins after an infection with hemolytic bacteria. Further investigations on tumorspecific fluorescence and especially the development of fluorochromes with high affinity to tumor tissue, opened up new possibilities for tumor detection. New techniques for tumor diagnosis due to specific properties of hematoporphyrin derivative (Hpd), a tumorselective fluorochrome for diagnosis of tumors in vivo as well as a photosensitizer of tissue for photodynamic therapy, have been developed since 1961 (Lipson 1961). After a certain clearance time for normal tissue, tumor detection occurs by observation of Hpd-fluorescence (Profio 1983; Aizawa 1983; Baumgartner et al. 1986). This paper deals with the use of newly developed electrooptical devices necessary for imaging of Hpd-fluorescence at low light levels gathering even small amounts of Hpd-fluorescence in mouse and rat tissue at different times following Hpd i.v. application. In addition the correlation between Hpd-fluorescence intensity and the histologically described type of tissue was examined.

Material and Methods

Fluorescence of Hpd (Photofrin II delivered by Photomedica, Raritan, USA) was excited by light of appropriate wave lengths, preferentially the violet lines of a Krypton ion laser (406.7, 413.1 and 415.5 nm). Using these wave lengths but also further UV, bluegreen and green lines of the same laser (350.7, 356.4, 468.0, 476.2, 482.5, 520.8, 530.9 and 568.2 nm) the excitation of Hpd in muscle tissue of mice ($n = 5$) was measured in vivo. Using constant excitation power densities the fluorescence emission was monitored at a wave length of 630 nm, which is a typical emission peak of Hpd in tissue.

Since tumor diagnosis is based on a higher storage and probably longer retention of Hpd in the tumor compared with normal tissue which – after a certain delay –

[1] Urologische Klinik und Poliklinik der Ludwig-Maximilians-Universität, Klinikum Großhadern, Marchionini-Str. 15, D-8000 München 70
[2] Gesellschaft für Strahlen- und Umweltforschung mbH, Zentrales Laserlabor, D-8042 Neuherberg

Investigative Urology 2
Edited by G. H. Jacobi et al.

results in a brighter fluorescence image of the tumor we have studied uptake and release of Hpd (Photofrin II) quantitatively in vivo in an animal test model. For that purpose a fluorescence detection device has been developed, which allows for measurements at constant experimental conditions over a time period up to 4 weeks. For our experiments we used rats with normal bladder tissue ($n = 48$) and those with a chemically induced bladder tumor ($n = 33$). The bladder tissue was irradiated with violet light at a wavelength of 406.7 nm from a Krypton ion laser guided in a single fused quartz light fiber. The power density of the excitation light was limited to 10 mW/cm^2, to avoid photobleaching of Hpd in tissue (Schneckenburger et al. 1984). Additionally the autofluorescence level was monitored under equal experimental conditions on rats not treated with Hpd. For cases of high autofluorescence levels at simultaneously low Hpd content in tissue we developed a new method of Hpd contrast enhancement based on fluorescence imaging at two different excitation wave lengths (Baumgartner et al. 1985). The light source was a high pressure mercury arc lamp combined with the corresponding optical filters selecting strong Hg emission lines at 405 nm and 550 nm, respectively. If the light intensities at both wave lengths were adjusted to equal autofluorescence levels (Fig. 1, upper part), Hpd excitation was more than 5 times stronger at excitation with violet light than with green light (Fig. 1, medium part). By subtracting the image obtained at green excitation from that obtained at violet excitation the contrast-impairing autofluorescence was eliminated, and only fluorescence of tissue remained, owing to Hpd (Fig. 1, lower part). The low quantum efficiency of Hpd in tissue of about 2% requires highly sensitive camera systems including intensifier tubes for fluorescence imaging of tumors. The head of the video intensified camera was directly attached to the endoscope. Fluorescence observation occurs through optical filters which select light of various band widths within the Hpd-fluorescence spectrum and serve additionally for blocking of the strong laser excitation light. The sensitivity of the experimental equipment has been examined on chemically induced tumors in the rat bladder in vivo. For that purpose the bladder was dissected and pinned on a thin cork plate with a black foil to avoid background fluorescence from the intestines. Hpd (Photofrin II) was injected into the tail vein at a dose of 5 mg/kg at 6 to 350 h before diagnostic examination.

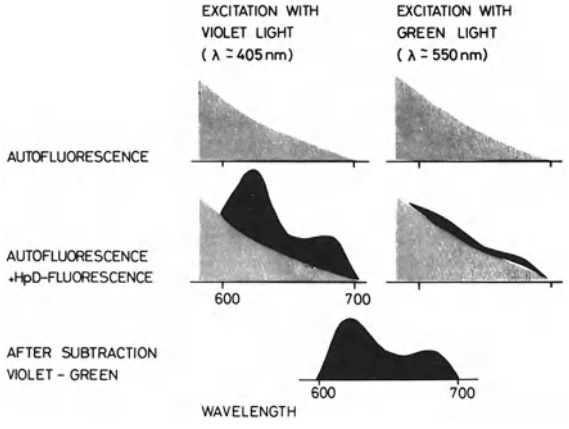

Fig. 1. Method of 2 wave length excitation for suppression of tissue autofluorescence

Results

In Fig. 2 the spectrally resolved dependence of fluorescence excitation is shown for Hpd (Photofrin II) determined at the observation wave length of 630 nm in the muscle of mice in vivo. We found maximum fluorescence intensity after excitation with violet laser lines and significantly lower excitation strength at blue-green and green laser lines. Our data are in good agreement with the excitation spectrum obtained from transplanted tumors in rats (Gijsbers et al. 1984) (Fig. 2, solid line). The fluorescence spectrum of Hpd in tissue (Fig. 2, dotted line) shows the wellknown fluorescence bands at 630 nm and 690 nm. Additionally, we observe two fluorescence bands at 590 and 660 nm, possibly due to metalloporphyrins or other Hpd species in tissue.

Using the violet line (406.7 nm) of a Krypton ion laser guided in a single fused quartz fiber, excitation of Hpd in multifocal growing tumors inside a dissected rat bladder was performed. The bladder itself and the corresponding fluorescence image is shown in Fig. 3. The monitor display shows a bright fluorescing exophytic tumor of about 3 mm in diameter in the upper part of the bladder. Besides that tiny fluorescent

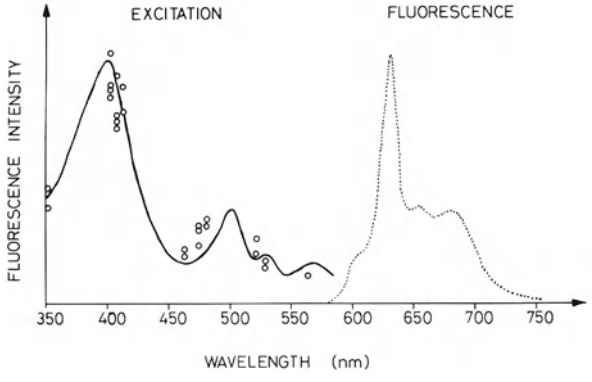

Fig. 2. Excitation strength of Hpd (Photofrin II) in the muscle of mice at different excitation wave lengths of a krypton ion laser *(dots)* compared with the Hpd-excitation spectrum in experimental rat tumors (*solid line*, Gijsbers et al. 1984) and fluorescence spectrum of Hpd in tissue after excitation with the violet krypton ion laser line at 406.7 nm *(dotted line)*

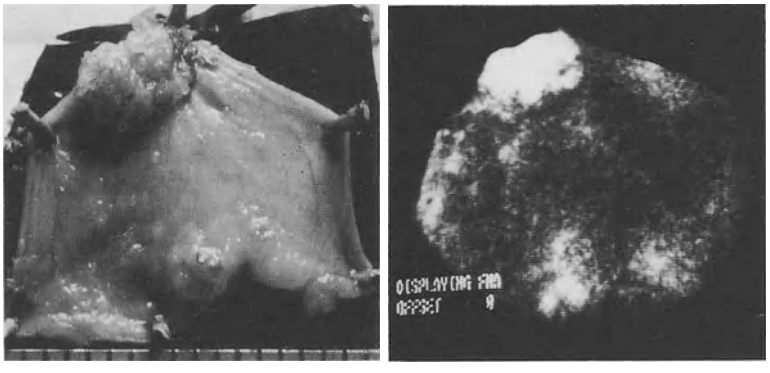

Fig. 3. Chemically induced tumors in a rat bladder *(left)* and fluorescence image of the same bladder *(right)*

spots were detected coinciding with tumor sites well below few tenth of millimeters in diameter.

For the case of a high autofluorescence level at simultaneously low Hpd content in tissue we made use of our newly developed method of Hpd contrast enhancement. An example is shown in Fig. 4. Pictures are arranged in the series: fluorescence image of tumorous tissue at violet excitation, followed by image at green excitation and at last the image after subtraction (violet minus green). It can easily be seen that part of the tissue fluoresce equally bright, at violet and green excitation, respectively. Although fluorescence emission occurs from tissue it is not caused by Hpd. After image subtraction this area appears dark.

For the performance of fluorescence diagnosis of tumors it is important to know uptake and release of the fluorescent component of Hpd (Gomer 1979). In Fig. 5 the result of the fluorometrically determined content of Hpd in tumorous and normal rat bladder tissue is shown different times after systemic application of Hpd. In normal tissue we observe a maximum in Hpd fluorescence intensity 3 h after Hpd-application (solid line in Fig. 5). The intensity decreases strongly within 2 days followed by a slow decrease up to 2 weeks. It should be stressed, that the mean values of the autofluorescence intensities were significantly lower at identical experimental conditions (dotted line in Fig. 5). In comparison with normal regions within the rat bladder

Fig. 4. Fluorescence image of a tumorous region in a rat bladder at violet light excitation. Same region at green light excitation *(medium)*. Image after subtraction (violet minus green). Fluorescing areas not caused by Hpd-excitation appear dark *(right)*

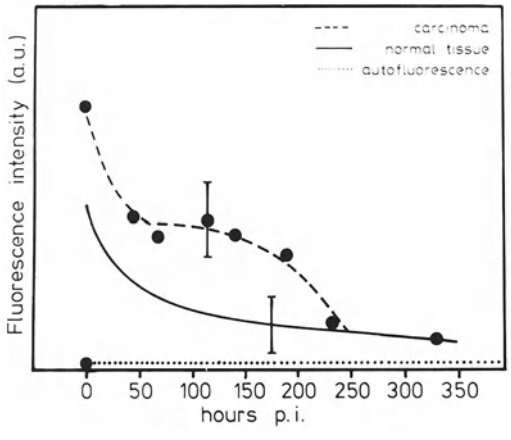

Fig. 5. Uptake and release of the fluorescing component of Hpd in tumorous and normal tissue

we found, that the fluorescence intensity in tumorous tissue (dashed line in Fig. 5) is more than two times higher, indicating selective storage of Hpd in malignant tissue. Hpd was found to be stored preferentially in severe dysplasia as well as carcinoma in situ and tumors of different histological grades in comparison to normal tissue as well as mild atypia.

Summary

In our experiments we have found that fluorescence diagnosis of tumors with use of the fluorochrome Hpd can be successfully applied under following conditions:

a) Installation of a technical equipment suitable for endoscopic detection of low light levels. The system includes a Krypton ion laser for Hpd excitation via single fused quartz fibers, highly sensitive TV cameras and image processing units for real time image subtraction to suppress tissue autofluorescence.
b) Performance of the diagnostic session at times, where fluorescence contrast between malignant and normal tissue is high, e.g., 2 to 8 days after systemic application of Hpd.
c) High excitation light levels should be avoided in order to minimize photobleaching of Hpd in tissue.
d) Choice of a dose of Hpd, necessary for fluorescence detection. We have experimental evidence that Hpd can be applied in a lower dose compared to concentrations used for therapeutic treatment of tumors (2–5 mg/kg body weight). This would be advantageous since side effects from photosensitization of the skin could be reduced.

Finally we want to note that our method of fluorescence imaging of Hpd is not only limited to diagnosis of bladder tumors but also suited for detection of superficial as well as all endoscopic attainable tumors.

Acknowledgements. The authors thank H. Fisslinger for her helpful assistance, Karl Storz KG, Tuttlingen, for placing endoscopic equipment at our disposal and the Bundesministerium für Forschung und Technologie (BMFT), Bonn, for supporting our work under grant no. MMT 51.

References

Aizawa K (1983) Endoscopic detection of hematoporphyrin derivative fluorescence in tumor. In: Lasers and Hpd in cancer. Igaku-Shoin, Tokyo, pp 21–24

Baumgartner R, Stepp H, Ruprecht L, Unsöld E, Jocham D (1985) Experimental study on fluorescence diagnosis of bladder cancer. In: Jori G, Perria C (eds) Photodynamic therapy of tumors and other diseases. Libreria Progetto, Padova, pp 259–262

Baumgartner R, Feyh J, Götz A, Jocham D, Schneckenburger H, Stepp H, Unsöld E (1986) Experimental study on laser-induced fluorescence of hematoporphyrin derivative (hpd) in tumor cells and animal tissue. Laser in Medicine and Surgery 1:4–10

Gijsbers GHM, van Gemert MJC, Breederveld D, Langelaar J, Boon TA (1984) In vivo fluorescence excitation spectra of hematoporphyrin derivative (hpd). In: Andreoni A, Cubeddu R (eds) Porphyrins in tumor phototherapy. Plenum Press, New York London, pp 339–345

Gomer CJ, Dougherty TJ (1979) Determination of ^{3}H- and ^{14}C hematoporphyrin derivative distribution in malignant and normal tissue. Canc Res 39:146–151

Lipson RL (1961) Hematoporphyrin derivative: a new aid for endoscopic detection of tumors. J Thorac Cardiovasc Surg 42:623–629

Policard A (1924) Etudes sur les aspects offerts par des tumeurs expérimentales examinée à la lumière de Woods. CR Soc Biol 91:1423–1424

Profio AE (1983) Fluorescence bronchoscopy for localization of carcinoma in situ. Med Phys 10: 83–87

Schneckenburger H, Unsöld E, Weinsheimer W, Jocham D (1984) Time resolved laser fluorescence and photobleaching of single cells after photosensitization with hematoporphyrin derivative. In: Andreoni A, Cubeddu R (eds) Porphyrins in tumor phototherapy. Plenum Press, New York London, pp 137–141

Trace Elements in Cellular Fractions of Normal and Carcinogenic Tissues from Human Urinary Bladder

A. Feustel[1], R. Wennrich[2], and B. Vorberg[2]

Introduction

In the past few years there have been intensive investigations to find specific causative agents in human carcinogenesis. Since Rehn had studied carcinoma of different urinary bladder agents, like aromatic amines – especially 2-aminonaphthalene (Rehn 1895), tryptophane-metabolites, phenacitine and oncogene are held responsible for the etiology of these tumors. It seems that these organic chemicals induce multifactorially a multistage carcinogenesis in the epithelial tissue of the urinary bladder together with urinary infections (Kunze 1984; Rice 1983), the consumption of tobacco as well as the waste of saccharine.

The importance of the role played by trace elements on the biochemistry of humans as well as in the carcinogenesis was discerned in the past few years, coupled with continual improvements in the instrumentation for trace element analysis.

Several authors have studied the concentration of trace elements, especially Zn, Cu, Se, Mn and Cd, in body fluids hoping to find new markers for the diagnosis of urological and internal diseases (Versieck and Cornelis 1980; Habib et al. 1980; Feustel and Wennrich 1986).

In our recent investigations with tissues of human kidney (Feustel et al. 1986), of human testes (Feustel et al. 1985) and prostatic tissues (Feustel et al. 1982; Feustel and Wennrich 1984) we could show that the concentration of several trace elements is changed in malignant tissues compared with normal ones. We could not find any paper dealing with trace elements, which are important in both the bio-synthesis of enzymes and the metabolism of protein, inside the bladder tissue. Therefore, it was interesting for us to compare the concentration of Cd, Cr, Mn, Pb, Se and Zn in the cellular fractions of normal human bladder tissue with the values in the cellular fractions of solid cancer of the same patients.

Materials and Methods

Tissue samples were obtained from 13 patients with urinary bladder cancer. Sections of carcinogenic bladder and surrounding normal bladder tissues were used. One part of each sample was examined histologically. The other part was stored in acid-washed polyethylene containers at −35°C.

The cellular fractions were prepared in the following manner. Sliced tissues were transfered into a Potter homogenizer made from PTFE. A few millilitres of Tris-

[1] Urologische Abteilung, Krankenhaus Markkleeberg/Leipzig, Pfarrgasse 15, DDR-7113 Markkleeberg
[2] Sektion Chemie, KMU Leipzig, Leipzig (DDR)

Investigative Urology 2
Edited by G. H. Jacobi et al.

HCI-buffer were added. The homogenate was filtered through a nylon gauze with a pore width of 150 µm, which had been cleaned in 0.1 *M* HCI (suprapure, Merck).

The homogenate was then sedimented in a refrigerated centrifuge at 1,000 × g for 10 min. The supernatant was decanted from the nuclear fraction. The solution was centrifuged at 100,000 × g for 1 h to isolate the mitochondrial fraction together with microsomes from the cytosol.

All fractions were transferred into small acid washed silica beakers to be heated at 180°C until a constant weight was obtained. Then the samples were wet ashed with suprapure nitric acid. The solutions were transferred into polyethylene containers.

All sample solutions (1 *M* HNO_3) were analyzed by flameless atomic absorption spectrometry. The standard addition technique was used for the determination of Cd, Zn, Pb, Cr, Mn, Se. Selenium values were measured with the hydride generation a.a.s. (AAS-1, VEB Carl Zeiss, Jena, with a home-made hydride generation system) using the 196.0 nm wave length. Cadmium (228.8 nm), zinc (307.6 nm) and lead (283.3 nm) were analyzed with a Jarrell-Ash 811-device and a Beckman 1268 graphite furnace. Chromium (357.9 nm) and manganese (279.5 nm) were analyzed with the AAS-3/EA-3 spectrometer (VEB Carl Zeiss, Jena). The concentration values were based on the weight of the dried samples for both the nuclear and mitochondrial fractions. The concentration in the cytosol fraction was based on the mass of the nucleus of the separated sample – 100 mg (dried nucleus) were taken for comparison.

The relative standard deviation obtained for all elements varied between 4% and 9% in each sample.

Results

Table 1 summarizes the results obtained (Table 1). The variance of the concentration values of all elements analyzed both in tumor and normal tissues was very high in all

Table 1. Pb-, Cd-, Zn-, Mn-, Cr- and Se-concentrations (µg/kg dried sample) in cellular fractions of bladder tissue ($n = 13$)

	Element					
	Pb	Cd	Zn	Mn	Cr	Se
Mitochondrial fraction						
Tumor	2 –340	0.3–2.5	26– 660	3 –102	0.4– 9.5	0.01–0.6
Normal	0.5– 35	0.4–1.4	30– 740	5 – 36	0.5–17	0.2 –1.0
Nuclear fraction						
Tumor	0.4–196	0.1–1.3	40–2560	14 –350	0.1–58	0.01–0.9
Normal	1.2– 15	0.4–6.6	25– 450	2.5– 49	0.5–17	0.2 –1.2
Cytosol						
Tumor	0.1– 0.6	–0.09	2– 120	5 – 17	n.d.	–0.03
Normal	0.1– 0.4	–0.08	3– 70	3 – 14	n.d.	–0.03

cellular fractions. It does not seem sensible to give mean values and RSD values for each fraction and the elements tested. But it is possible to monitor the following tendency:

Concentr. in tumor tissue	Element	Concentr. in normal tissue
Nucl. fr. > Mitochondr. fr.	Mn	Mitochondr. fr. > Nucl. fr.
Nucl. fr. > Mitochondr. fr.	Se	Mitochondr. fr. > Nucl. fr.
Nucl. fr. > Mitochondr. fr.	Cr	Mitochondr. fr. > Nucl. fr.

We could not find significant differences for the concentration of Pb, Zn and Cd between the cellular fraction of the normal bladder and of the urinary bladder tumor.

The comparison of the concentration values in the nuclear and the mitochondrial fractions of normal and carcinogenic bladder tissues shows:

Nuclear fraction	Element	Mitochondrial fraction
Tumor > Normal	Cr	Not significant
Tumor > Normal	Mn	Normal > Tumor
Tumor < Normal	Zn	Normal > Tumor
Tumor < Normal	Pb	Not significant
Tumor < Normal	Cd	Normal > Tumor
Not significant	Se	Normal > Tumor

Table 2. Examples for the molar relationship of several elements inside the cellular fractions of normal and carcinogenic tissues

	µMol metal/g tissue (dried)		
	Se	Σ (Pb, Mn, Cr, Cd)	Σ (Pb, Mn, Cr, Cd, Zn)
Patient A			
Mitochondrial fraction			
Tumor	0.014	1.36	3.66
Normal	0.023	0.15	1.36
Nuclear fraction			
Tumor	0.0018	0.219	5.289
Normal	0.0022	0.160	0.540
Patient B			
Mitochondrial fraction			
Tumor	0.0025	1.77	4.067
Normal	0.0037	0.45	1.67

We obtained no distinct differences in the concentration values of all elements analyzed in the cytosol fractions of normal and tumor tissues.

Studied of several authors (Webber 1985; Dürre and Andreesen 1986; Vernie 1984) suggest that selenium may play a role in the inhibition of both the initation and promotion stages of carcinogenesis. Therefore, we compiled the molar relationship of the elements tested in the mitochondrial and nuclear fraction of normal and cancerogenic tissues. Because of the small number of probands tested ($n = 13$) it is not reasonable to give mean values and RSD-values. It also seems possible that several other trace elements could influence the etiology of urinary bladder cancer. Therefore, we only give two typical examples for probands with bladder cancer (see Table 2).

Discussion

Attempts to elucidate the role of several trace elements in the carcinogenicity of certain human organs have been the subject of intense investigations in the past few years, but so far little information is available on their exact function in the cell metabolism. The etiology of the urinary bladder tumor which seems to be a multistage carcinogenesis, is likely to connect with a change of the concentration of several elements inside the tumor cells compared with normal ones. Our preliminary results monitor differences in the concentration of Cd, Cr, Pb, Mn, Se and Zn in both nuclear and the mitochondrial fractions of carcinogenic tissue compared with the normal one of the same proband. The concentration of these trace elements does not differ significantly in the cytosol between tumor and normal tissues.

In normal bladder tissue we could find higher Mn, Cr and Se levels in the mitochondrial fraction compared with the nuclear one. We observed a reverse relation in the carcinogenic tissue. We measured higher Mn, Cr and Se concentrations in the nuclear fraction. This should likely be of importance in the malignant transformation of the cells.

The mitochondrial fraction of tumor tissue is also characterized by a distinct lower concentration of manganese, zinc, selenium and cadmium as compared with that of normal tissue. This diminuition of Zn, Se and Mn is held responsible for mental cell oxidation inside the tumor tissue.

We found a distinct unpropitiousness diminuition of selenium in the mitochondrial fraction of carcinogenic tissue, if the molar concentration of selenium is compared with the sum of the molar concentration of the other elements tested. This fact could be caused by the protective effect of selenium discussed in view of carcinogenesis. In connection with the etiology of bladder cancer this observation is an aspect for further investigations.

References

Dürre P, Andreesen JR (1986) Die biologische Bedeutung von Selen. Biologie in unserer Zeit 16: 12–23

Feustel A, Wennrich R (1984) Zinc and Cadmium in cell fractions of prostatic cancer tissues of different histological grading in comparison to BPH and normal prostate. Urol Res 12: 147–150

Feustel A, Wennrich R (1986) Zinc and Cadmium plasma and erythrocytes levels in prostatic carcinoma, BPH, urological malignancies, and inflammations. The Prostate 8:75–79

Feustel A, Wennrich R, Steiniger D, Klauß P (1982) Zinc and cadmium concentration in prostatic carcinoma of different histological grading in comparison to normal pristate tissue and adenofibromyomatosis (BPH). Urol Res 10:301–303

Feustel A, Wennrich R, Dittrich H (1985) Verteilungsmessungen von Zn and Cd im Hodengewebe bei Patienten mit Prostatakarzinomen im Vergleich zu normalen Hoden. In: Harzmann R, Jacobi GH, Weißbach L (eds) Springer Verlag, Berlin, pp 315–322

Feustel A, Wennrich R, Dittrich H (1986) Studies of Cd, Zn and Cu levels in human kidney tumours and normal kidney. Urol Res 14:105–108

Habib FK, Dembinski TC, Stitch SR (1980) The zinc and copper content of blood leukocytes and plasma from patients with benign and malignant prostates. Clin Chim Acta 104:329–335

Kunze E (1984) Die multifaktorielle Mehrstufenkarzinogenese am Harnblasenurothel. In: Das Harnblasenkarzinom. Springer, Berlin Heidelberg New York

Rehn L (1895) Blasengeschwülste bei Fuchsinarbeitern. Arch Klin Chr 50:588–600

Rice JM, Frith CH (1983) The nature of organ specificity in chemical carcinogenesis. In: Langenbach R, Nasow S, Rice JM (eds) Organ and species specificity in chemical carcinogenesis. Plenum, New York London, pp 1–22

Vernie LN (1984) Selenium in carcinogenesis. Biochim Biophys Acta 738:203–217

Versieck J, Cornelis R (1980) Normal levels of trace elements in human blood plasma or serum. Anal Chim Acta 116:217–254

Webber MM (1985) Selenium prevents the growth simulatory effects of cadmium on human prostatic epithelium. Biochem Biophys Res Comm 127:871–877

Long-Term Experimental Study of Intravesical Chemotherapy: Effect on the Normal Urothelium in Dogs

F.-J. Deutz[1], F. Moll[1], R. Friedrichs[1], H. Rübben[1], R. Knüchel[2], and W. Lutzeyer[1]

Introduction

In recent years intravesical chemotherapy has become accepted worldwide in the treatment of superficial bladder cancer. The main problem treating these patients is the high frequency of recurrences even after complete transurethral resection of all visible lesions (Barnes et al. 1977; Miller et al. 1969). Depending on the grade of the primary tumor recurrences are observed between 50 to 70% (Heney et al. 1982; Dalesio et al. 1983). Concerning the results of randomized studies a maximum of 10 to 20% of the patients will profit from an adjuvant intravesical chemotherapy. More than 70% of the patients are treated unnecessarily (Rübben and Giani 1986). Thus local and systemic side effects as well as late complications of topical chemotherapy have to be considered and weighed against the therapeutic benefit (Lutzeyer et al. 1982).

The potential carcinogenic activity of cytotoxic agents is well known. On normal female Wistar rats a low carcinogenicity of adriamycin (ADM) and mitomycin C (MMC) could be documented, which was dependent on concentration and frequency of intravesical application (Rübben 1983). To analyze the risk of tumor induction by intravesical instillation of cytotoxic agents in the daily clinical practice, the experimental study was repeated in dogs.

Material and Methods

20 female mongrel dogs weighing between 10 and 15 kg entered the study. All dogs received a standard diet (Altromin Nr. 4130). Water was offered ad libidum. Transurethral manipulations were performed under intravenous pentobarbital anesthesia (1.2 ml per kg body weight, pentobarbital natrium ad us. vet., Ceva Laboratories).

The dogs were randomly divided into 2 groups: Adriamycin (ADM, Farmitalia) or cisplatinum (DDP, Bristol) (10 ml, 2.5 mg/ml, 2 h) was instilled via a transurethral catheter into the bladder and removed at the end of instillation time. The instillations were repeated each fourth day up to a total of 36 instillations; after 6 instillations an interval of 2 weeks was inserted for recovery of the animals. Every 3 months all dogs underwent cystoscopy and biopsy. Antibacterial prophylaxis was performed by giving 0.5 ml per 5 kg body weight Tardiomyocel (Bayer, Leverkusen) i.m. before each manipulation. After a 3-year-observation period the animals were killed by intravenous pentobarbital and the bladders were removed for analysis by light microscopy, immunocytometry and scanning electron microscopy. Before the final

[1]Department of Urology, Medical Faculty, RWTH Aachen, Pauwelsstr., D-5100 Aachen
[2]Department of Pathology, Medical Faculty, RWTH Aachen, Pauwelsstr., D-5100 Aachen

Investigative Urology 2
Edited by G. H. Jacobi et al.

phase of anesthesia the bladders were fixed by transaortal perfusion of 2.5% glutaraldehyde, when 2.5 h before 0.05 g/kg BrdU (Sigma Chemical Co., St. Louis, USA) was injected intravenously for immunocytometric staining. All bladders were divided into 4 rings and 2 lateral cups separated for cell cycle analysis by monoclonal anti BrdU technique (Becton Dickinson immunocytometry, Division Europe, Mechelen, Belgium) and scanning electron microscopic investigation respectively. 3 rings were embedded in paraplast for hematoxilin and eosin staining. Each bladder ring was divided into 16 parts and the predominant lesion in each part documented on a data card.

The morphologic criteria of evaluation were:

- light microscopy (HE-staining):
  vacuolization of the cytoplasm, mucosal necrosis, cellular infiltration of the bladder wall, neovascularization, epithelial hyperplasia, pseudopolyps, epithelial proliferation, tumor and nuclear changes.
- immunocytometry with BrdU labelling technique:
  incorporation of Bromodeoxyuridine, a thymidine analog, into DNA.
- scanning electron microscopy (SEM):
  cellular form, microridges, uniform and pleomorphic microvilli.

Results

Eleven of the 20 dogs died during the instillation period (5 in DDP group, 6 in ADM group) due to severe urinary tract infection with bladder shrinking, ascending infection and pyonephrosis. The remaining 9 animals, which could be observed over the 3-year period, provided data for analysis.

Cystoscopy and Biopsy. There was no evidence for urothelial carcinoma seen by cystoscopy or biopsy. Polypous alterations were biopsied and histologically characterized (Figs. 1, 2).

When focussing the results of randomized biopsies obtained by light microscopy, cytoplasm showed a moderate vacuolization which was marked in the apical parts of superficial cells and coarse chromatin in the nuclei. These findings were pronounced in the beginning of instillations, but could be seen all over the observation period. Cellular infiltration of the bladder wall and focal mucosal necrosis could be observed during the total study, with a maximum at the end of the instillation period. Pseudopolyps and epithelial hyperplasia were found, but there was neither evidence for neovascularization nor epithelial proliferation or tumor. All changes persisted even after the end of the instillation period (Table 1).

Immunocytometry. By way of monoclonal anti-BrdU technique no increased proliferation of cells could be demonstrated. The proportion of labelled basal – to superficial cells was 3 to 1 in all areas (Fig. 3).

Scanning Electron Microscopy. The scanning electron microscopy visualized only unspecific reactions to the instillation of the cytotoxic agents. The urothelium showed normal appearance of superficial cells forming a flat pavement-like surface. The cells

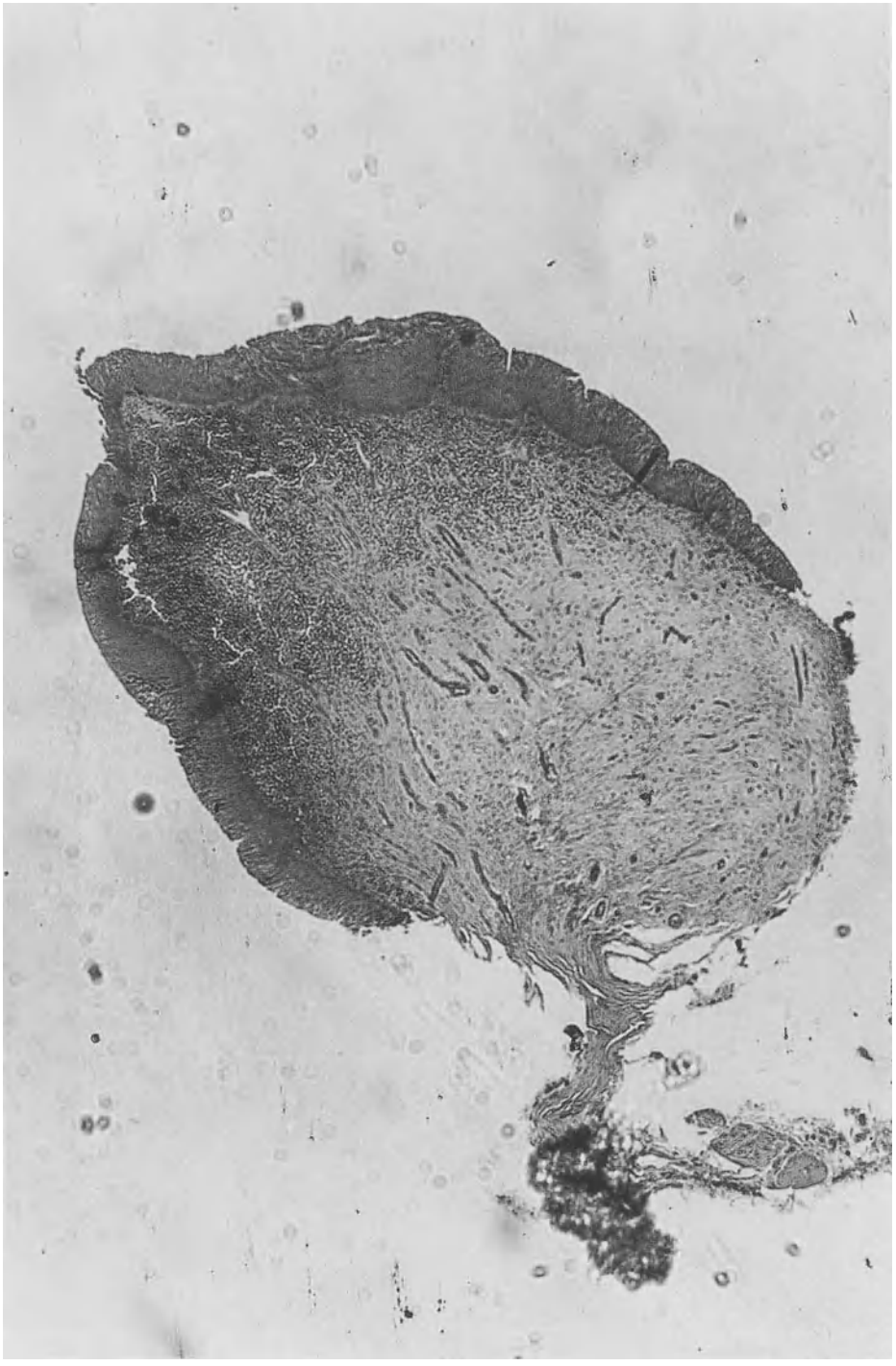

Fig. 1. Pseudopolyp with epithelial hyperplasia. HE, × 40

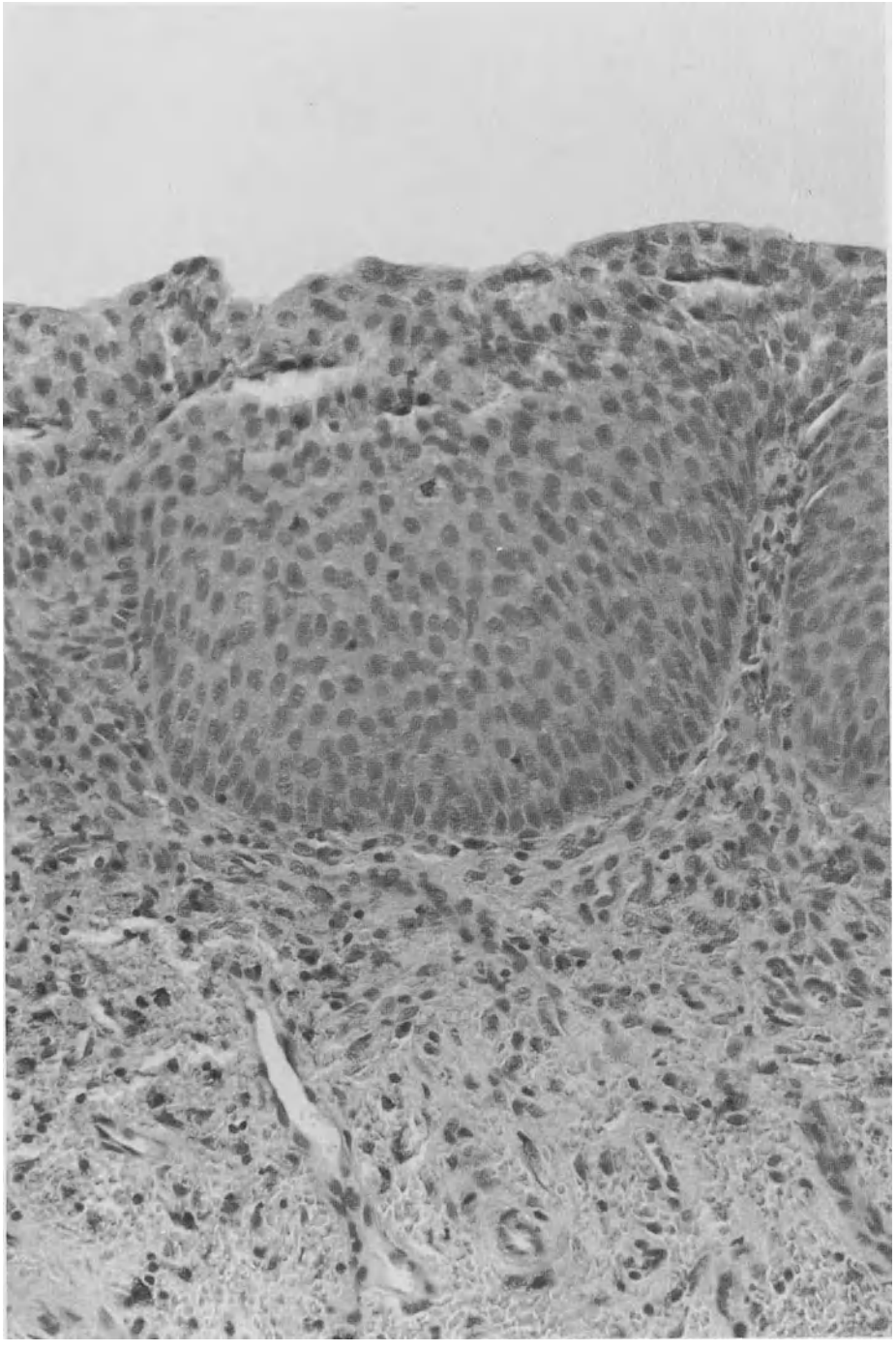

Fig. 2. Polypous hyperplasia without atypia. HE, $\times 100$

Table 1. Morphologic findings after instillation of 2.5 mg/ml ADM or DDP

	No. of instillations				Post instillation control	
	5	10	20	36	24 months	36 months
Vacuolization	++	+	+	+	+	+
Coarse chromatin	++	++	+	+	+	+
Mural infiltration	+	+	+	+	+	+
Mucosal necrosis	−	+	+	++	(+)	+
Hyperplasia	−	−	(+)	(+)	(+)	+
Pseudopolyps	−	−	+	+	(+)	+
Neovascularization	−	−	−	−	−	−
Proliferation	−	−	−	−	−	−
Tumor	−	−	−	−	−	−

− Normal; (+) focal, slight; + multifocal, moderate; ++ diffuse, severe

were polygonal in shape, the majority having 5 sides. In some areas the superficial cells were defoliated or necrotic and coated with mucus and leucocytes. The microridges were focally replaced by small uniform microvilli (Fig. 4). Pleomorphic microvilli as a sign of malignant transformation could not be observed.

Discussion

A precondition for the use of cytotoxic agents with a prophylactic aim is their activity against bladder tumor growth when given systemically in advanced disease or intravesically without resection of the tumor. The therapeutic effect of intravesical instillation of thiotepa, adriamycin, mitomycin C and epodyl has been well described in the literature. Severe systemic side effects are not to be expected after topical ADM and MMC treatment, because of the proven minimal transvesical absorption of these agents (Engelmann et al. 1982; Jacobi and Kurth 1980; Pavone-Macaluso et al. 1976). Local side effects were reported in 10 to 40% of the cases. The induced chemical cystitis with transient hematuria and reduction of the bladder capacity mainly depended on the concentration and frequency of instillation of the drugs. It responded to spasmoanalgetics and required cessation of the therapy in less than 5% of the cases (Rübben and Lutzeyer 1982).

Since the early observation of Pott in 1775, who reported a strong association between environmental exposure and human malignancy, many epidemiological and experimental studies have confirmed the excessive risk of cancer because of the influence of various carcinogens.

Tumor induction of the bladder has been proven by analytic epidemiologic studies for the following agents or factors: chronic urinary tract infection, bladder stones, bilharzia, balkan nephropathy, exposure to aromatic amines, excessive and chronic cigarette smoking, phenacetin abuse and irradiation of the small pelvis.

Since the use of cytotoxic agents in the therapy of malignant disease, secondary tumors have been observed with increased frequency. Bladder tumors are described

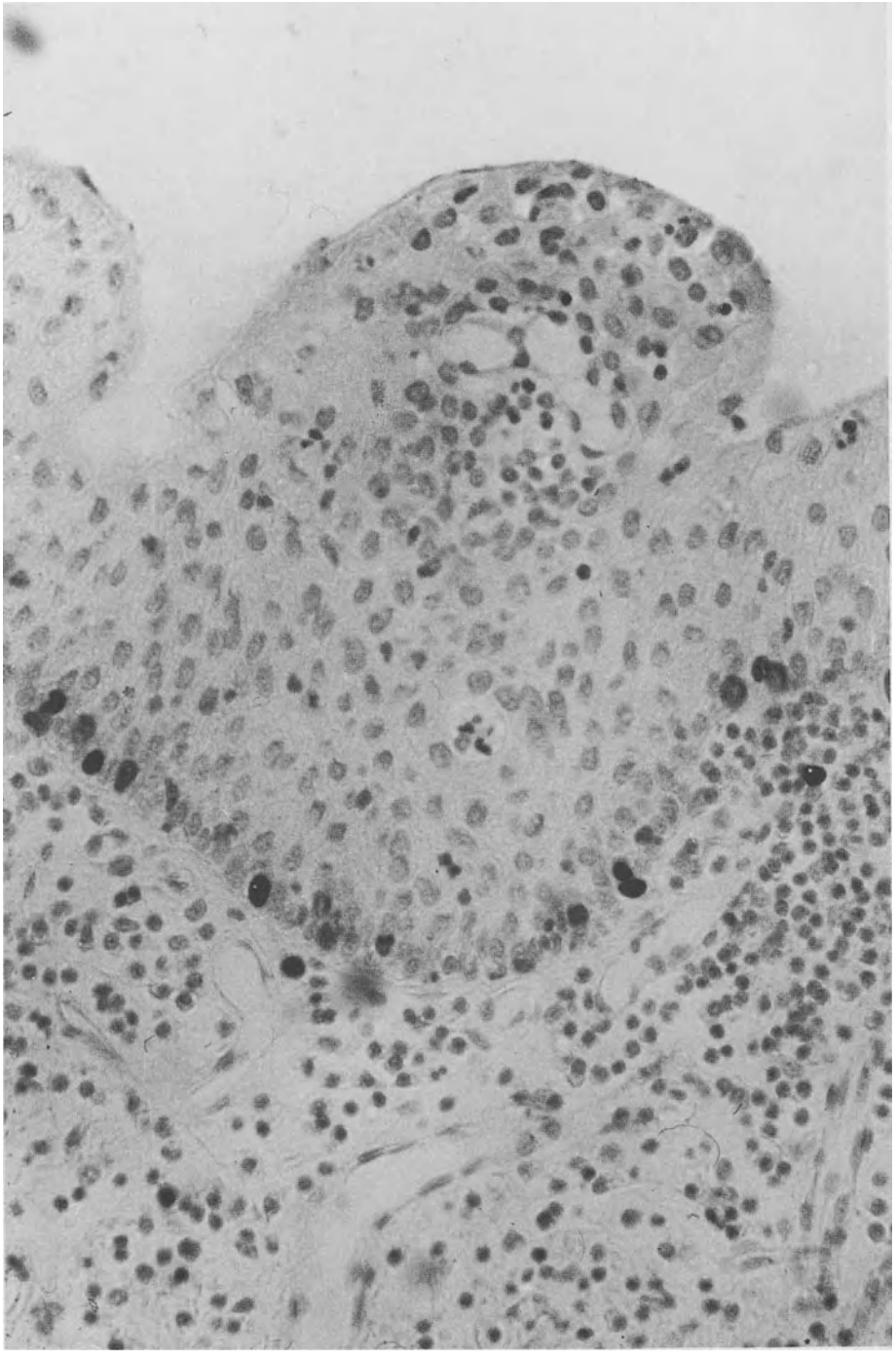

Fig. 3. Normal proliferation of urothelium. BrdU, × 40

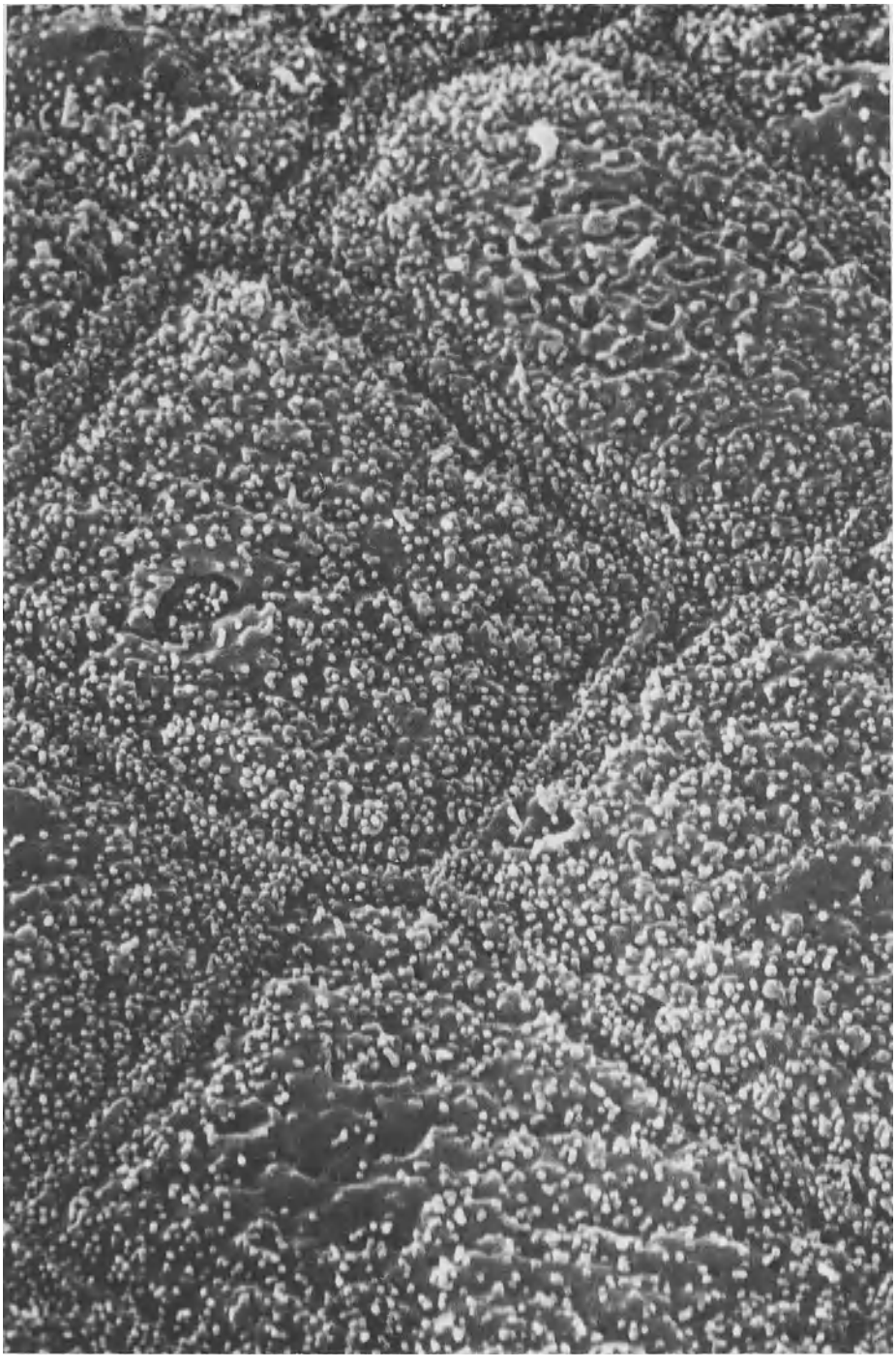

Fig. 4. Uniform microvilli as a sign of unspecific mucosal reaction. SEM, × 5,000

owing to aggressive systemic cyclophosphamide treatment after a latency period of 3–13 years (Dale and Smith 1974; Hoover and Fraumeni 1981; Plotz et al. 1979; Wall and Clausen 1975). Investigations about the effect of instillation of ADM, MMC, THI and DDP on the normal urothelium (Daskal et al. 1980; Murphy and Soloway 1980; Murphy et al. 1981a; 1981b; Rasmussen et al. 1980) showed only reversible lesions. The reason for these observations may be the short observation period with a maximum follow-up of 30 days and the low frequency of instillations. The findings after application of known carcinogenic agents given in very low dose and short time are also reversible when the administration is stopped at an early stage of the disease. Thus induction of malignant tumors depends on the dosage of the carcinogen, the frequency of application and the observation period.

The first evidence for induction of epithelial proliferations and tumors in the normal bladder mucosa of rats in long-term experimental studies after intravesical application of ADM was reported by Rübben 1983. The pathogenesis of the ADM-induced tumors is comperable to the carcinogenesis after administration of known carcinogens (Okajima et al. 1981; Frith et al. 1982). In the early postinstillation-phase induced epithelial proliferations and signs of repair could be observed. 3 to 6 months after repeated instillation severe dysplasia (carcinoma in situ) and invasive tumors could be observed. The scanning electron microscopy showed at this time pleomorphic microvilli as a sign of malignant transformation.

Contrary to these experiments on rats in this animal experiment 36 instillations of ADM and DDP into the bladder of 20 normal dogs induced neither infiltrative tumors nor carcinoma in situ during a total follow-up of 3 years. So the potential carcinogenicity of the investigated cytotoxic agents ADM and DDP in clinical dosages after intravesical administration seems to be low. But with regard to the high rate of ineffective intravesical chemoprophylaxis it is advisable to select those patients with a high risk of recurrency, who may profit from this form of adjuvant therapy and to avoid unnecessary treatment in patients with low risk superficial bladder cancer.

References

Barnes R, Hadley H, Dick A, Johnston O, Dexter J (1977) Changes in grade and stage of recurrent bladder tumors. J Urol 118:177–178

Dale GA, Smith RB (1974) Transitional cell carcinoma of the bladder associated with cyclophosphamide. J Urol 112:603–604

Dalesio O, Schulman CC, Silvester R, Depauw M, Robinson M, Denis L, Smith P, Viggiano G (1983) Prognostic factors in superficial bladder tumors. J Urol 129:730–733

Daskal Y, Soloway MS, De Furia MD, Crooke ST (1980) Normal mice and mice with N-(4-5-nitro-2-furyl)-2-thiazolyl formamide induced bladder neoplasms. Cancer Res 40:261

Engelmann U, Bürger R, Jacobi GH (1982) Experimental investigations on the absorption of intravesically instilled Mitomycin C in the urinary bladder of the rat. Eur Urol 8:176–181

Frith CH, Wiley LD, Shinohara Y (1982) Sequential morphogenesis of urinary bladder tumors in balb/c mice given 2-acetylaminofluorene. J Urol 128:1071–1076

Heney NM, Nocks BN, Daly JJ, Prout GR Jr, Newall JB, Griffin PP, Perrone TL, Szyfelbein WA (1982) Ta und Tl bladder cancer: Location, recurrence and progression. Br J Urol 54:152–157

Hoover R, Fraumeni JF Jr (1981) Drug-induced cancer. Cancer 47:1071–1080

Jacobi GH, Kurth KH (1980) Topical adriamycin for prophylaxis and treatment of superficial bladder cancer: studies on plasma and tumor uptake. J Urol 124:34–37

Lutzeyer W, Rübben H, Dahm HH (1982) Prognostic parameters in superficial bladder cancer: an analysis of 315 cases. J Urol 127:250–252

Miller A, Mitchel JP, Brown NJ (1969) The bristol bladder tumors registry. Br J Urol 41 (Suppl 1): 5–6

Murphy WM, Soloway MS (1980) The effect of thiotepa on developing and established mammalian bladder tumors. Am Can Soc 45:870

Murphy WM, Soloway MS, Crabtree WN (1981a) The morphologic effects of MMC in mammalian urinary bladder. Cancer 47:2567–2574

Murphy WM, Soloway MS, Finebaum PJ (1981b) Pathological changes associated with topical chemotherapy for superficial bladder cancer. J Urol 126:461–464

Okajima E, Hiramatsu T, Hirao K, Ijuin M, Hirao H, Babaya K (1981) Urinary bladder tumors induced by BBN in dogs. Cancer Res 41:1958

Pavone-Macaluso M, Gebbia N, Biondo S, Caramia G, Rizzo FP (1976) Permeability of the bladder mucosa to thiotepa, adriamycin and daunomycin in mice and rabbits. Urol Res 4:9–13

Plotz PH, Klippel JH, Decker JL, Grauman D, Wolf B, Brown BC, Rutt G (1979) Bladder complications in patients receiving cyclophosphamide for systemic lupus erythematosis or rheumatoid arthritis. Ann Intern Med 91:221

Pott P (1775) Cancer scroti. In: Hawes, Clark, Collins (eds) Chirurgical observations. London, p 63

Rasmussen K, Peterson BL, Jacobo E, Penick GD, Sal JS (1980) Cytologic effects of thiotepa and adriamycin on normal canine urothelium. Acta cytol 24:237

Rübben H (1983) Die intravesikale Chemotherapie des Blasenkarzinoms. Experiment und Klinik. Habilitationsschrift vor der Medizinischen Fakultät der RWTH Aachen

Rübben H, Giani G (1986) Experimentelle und klinische Grundlagen der topischen Chemotherapie des Blasenkarzinoms. Manz'scher Buchverlag, Wien

Rübben H, Lutzeyer W (1982) Klinische und experimentelle Gesichtspunkte der intravesikalen Behandlung superfizialer Blasenkarzinome mit Adriamycin. Urologe A 21:20–23

Wall RL, Clausen KP (1975) Carcinoma of the urinary bladder in patients receiving cyclophosphamide. N Engl J Med 293:271

Effects of Cisplatinum and Irradiation on the Proliferation of J-82 Transitional Cell Carcinoma*

G. Jakse[1], E. Rammal[2], F. Hofstädter[3], and H. Frommhold[2]

Introduction

Cis-diamminedichloroplatinum (CDDP) is currently the most active antineoplastic agent against transitional cell carcinoma. The response rate in metastatic disease is more than 30% (Soloway 1978; Yagoda et al. 1978). There is evidence from in vitro and in vivo experiments that CDDP might enhance the effects of irradiation (Douple et al. 1977; Wodinsky et al. 1974). Although the mechanisms of CDDP-radiation interactions are poorly understood, the combination of these modalities is an attractive therapeutic approach since there is a minimal overlap in toxic effects. Recent clinical studies did show that the simultaneous application of CDDP and irradiation resulted in a complete tumor remission of locally advanced bladder cancer in about 70% (Jakse et al. 1985; Shipley et al. 1984). The aim of this investigation was to find out the optimal sequence as well as dosage of CDDP in a combined chemotherapy and radiotherapy. Some preliminary results are presented here.

Material and Methods

Cell culture. The cell line J82 was maintained as a monolayer culture in 25 cm^2 flasks in Eagles' MEM supplemented with 10% heat-inactivated foetal calf serum at 37° in a humified atmosphere of 5% CO_2 in air. J82 cell line was derived from a poorly differentiated, invasive, transitional cell carcinoma, stage 3 (O'Toole et al. 1978).

Drugs. Stock solution of CDDP (Platinol, R) were made up just prior to use in PBSA and diluted in Eagles' MEM to following concentrations: 125 ng/ml, 150 ng/ml, 200 ng/ml, 250 ng/ml and 300 ng/ml.

Irradiation. We used a Gammatron 3 (R) with a Co-60 source of 3000 Ci activity. The irradiation field was 30 × 30 cm. The distance of the radiation source to the culture plates was 90 cm. 0.5 Gy were applied per min.

Experiments. Viable exponentially-growing cells were plated m microtest plate wells at a concentration at 40,000 cells per ml medium and incubated at 37.0°C in a humified atmosphere of 5% CO_2 in air for 24 h. The medium was then removed and

* This investigation was performed with the support of the "Fonds zur Förderung der wissenschaftlichen Forschung in Österreich" (P5727)

[1]Department of Urology, University of Innsbruck Medical School, Anichstr. 35, A-6020 Innsbruck
[2]Department of Radiotherapy, University of Innsbruck Medical School, A-6020 Innsbruck
[3]Department of Pathology, RWTH Aachen, Pauwelsstr., D-5100 Aachen

Investigative Urology 2
Edited by G. H. Jacobi et al.

1.0 ml aliquots of fresh medium containing the above mentioned doses of CDDP concentrations were added to the exponentially-growing cells. 6 h after starting the cisplatinum incubation the irradiation was performed with 2 Gy per fraction. After 24 h drug exposure the cells were washed 2 times with MEM and plated again in medium. The cells were detached using 0.5% trypsin on days 2, 5, 7 and 9. They were counted by means of a coulter counter. The viability was proven by dye-exclusion test. The experiments were done in triplicate.

Statistics. The results are expressed as percentage of surviving cells and were computed and analysed by multivariate analysis. The statistical significance was calculated by Dunnet-T-test.

Results

The surviving growth fraction was maximally reduced to 21% on day 7. This cell reduction was achieved by CDDP incubation for 24 h with 300 ng/ml (Fig. 1). A single dose of 2 Gy irradiation resulted in the reduction of the surviving cells to 69%. Combining both modalities a significant growth reduction could be achieved with dosages of 125 and 250 ng/ml compared to either modalities alone (Fig. 2). No enhancement could be demonstrated with the combination of 300 ng/ml CDDP and 2 Gy over 300 ng/ml CDDP alone.

Simulating the clinical situation of fractionated irradiation we applied 5 fractions of 2 Gy on 5 consecutive days. CDDP incubation with 125 and 200 ng/ml was performed either on days 0, 1, 2, 3 or 4. The greatest growth reduction could be achieved with CDDP incubation on day 1 or 2 (Table 1). This growth reduction was significantly ($P \leqq 0.005$) higher than those observed with radiation alone or CDDP incubation on day 0, 3 or 4.

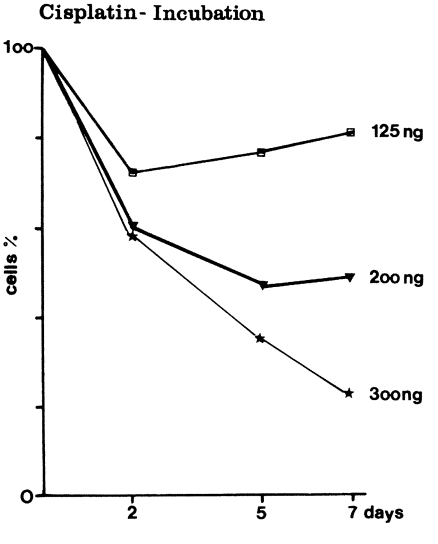

Fig. 1. Reduction of the surviving cells (%) by increasing doses of CDDP

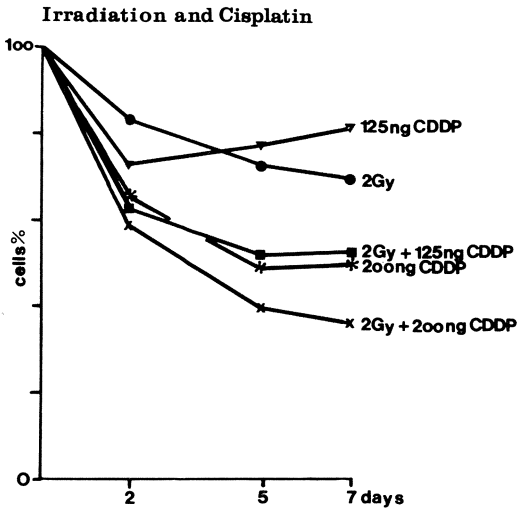

Fig. 2. Reduction of the surviving cells (%) by a single dose of irradiation (2 Gy) or a combined treatment with CDDP

Table 1. Consecutive irradiation (5 daily fractions of 2 Gy) and CDDP incubation on day 0, 1, 2, 3 or 4. Cell counts (%) on day 5 and 7

		D_0	D_1	D_2	D_3	D_4
Day 5	10 Gy			30%		
	CDDP (125 ng/ml)	14%	7%	14%	17%	20%
	CDDP (200 ng/ml)	12%	6%	9%	14%	18%
Day 7	10 Gy			13%		
	CDDP (125 ng/ml)	9%	3%	4%	11%	10%
	CDDP (200 ng/ml)	6%	2%	4%	9%	7%

D = day of CDDP incubation

Discussion

A synergistic or additive effect between CDDP and ionizing radiation has been observed by several researchers in vitro and in vivo (Douple et al. 1977; Kyriazis et al. 1983; Soloway et al. 1982; Weldon et al. 1979). Some possible mechanisms which may explain the enhancement of irradiation effects of CDDP are the following: 1) sensitization of hypoxic cells, 2) inhibition of sublethal and potentially lethal radiation damage repair, 3) cell cycle perturbation, 4) release of toxic ligands, 5) reaction with non-protein SH-groups (Douple et al. 1977).

Time sequence as well as the dose schedule of drug and irradiation administration are also important factors for the interaction between cystostatic drugs and irradiation.

Carde and Laval showed that CDDP had no radiosensitizing effect on exponential growing rat hepatoma cells (Carde and Laval 1981). However the repair of sublethal radiation damage was reduced by 50%. In plateau-phase cells a slight sensiti-

zation as well as a decreased repair of potential lethal radiation damage was noted. Dritschilo et al. demonstrated potent effects on repair of sublethal radiation damage with multifraction exposure of irradiation, whereas the effect of CDDP in single radiation dose experiments was minimal (Dritschilo et al. 1979). Twentyman et al. observed a variation of the extent of growth delay in 3 murine tumors by using different sequence of drug and radiation treatments (Twentyman et al. 1979). These investigators did not determine an interval which is the most effective. Bartelink and Kalman and Lilieveld et al. applied 5 daily doses of simultaneous or single higher dose of CDDP to the RIF-1 tumor (Bartelink and Kalman 1983; Lilieveld et al. 1985). Both schedules were more effective than several other schedules which were investigated. Ziegler and Trott showed that in B-14 Chinese hamster cells the modification of the dose response curve depends on the dose of CDDP as well as the interval between CDDP and irradiation (Ziegler and Trott 1985). The most effective interval was in this model up to 12 h. Overgaard and Khan used the mouse C3H-mammary carcinoma (Overgaard and Khan 1981). The interperitoneal application of CDDP 30 min before radiotherapy was superior to CDDP application 30 min or 4 h after radiotherapy.

Wodinsky and colleagues reported on an increased thrapeutic efficacy by combination of CDDP and radiation in P388 lymphocytic leukemia (Wodinsky et al. 1974). The same combination proved to the effective also in murine mammary adenocarcinoma and intracerebral rat brain tumor (Carde and Laval 1981). Implantation of MBT-2 transitional cell carcinoma in the hind limbs of mice and subsequent application of CDDP, 6 mg/kg on days 0, 7 and 14 combined with radiotherapy (36 Gy) resulted in tumor eradication in 7 of 9 mice. This result was significantly superior to radiation or chemotherapy alone (Soloway et al. 1978). The efficacy of CDDP and CDDP combined with radiotherapy could also be demonstrated on FANFT-induced tumors. However, there was no significant difference between CDDP alone and in combination with radiotherapy (Soloway et al. 1978).

Schuhmann and Göhde demonstrated on an Ehrlich ascites tumor cell model that an increase of G2 cells from 19% to 70% occurred 24–120 h after administration of CDDP (Kyriazis et al. 1983). These results would indicate that the optimal sequence of therapy is the administration of CDDP followed by irradiation several hours later.

However Kyriazis et al. demonstrated a potentiating effect of CDDP when it followed irradiation (Kyriazis et al. 1983). They used a transitional cell carcinoma cell line which was resistant to CDDP, thus enabling them to seperate the effect of CDDP from that of irradiation. Using this nude mouse model they also demonstrated that there was no difference between weekly or two weekly dose of CDDP.

Weldon and associates reported that animals receiving CDDP after termination of irradiation had the best survival compared to irradiation alone or CDDP before irradiation (Weldon et al. 1979).

Summarizing the reports mentioned above it becomes evident that there is no clear time sequence to achieve the maximal effect in terms of tumor response. Moreover the results indicate that the effects of the combined treatment will very much depend on the model which is used.

The dosage of CDDP in the above mentioned animal investigations varied from 1–6 mg/kg body weight (Carde and Laval 1981; Jacobs et al. 1978; O'Toole et al. 1978; Overgaard and Khan 1981; Schuhmann and Göhde 1979).

Although it can be suggested that with increasing doses of CDDP a logarithmic response of the tumor volume occurs, it is a also evident that increasing the dose beyond a certain point results in a smaller tumor volume reduction. This fact can be deduced from the results of Soloway and coworkers showing an increased death rate and a lower reduction in bladder weights in animals receiving CDDP and 48 Gy versus those being given 25 Gy. Furthermore, the toxicity of the different treatment schedules as well as the different irradiation dosage (single dose of 10 Gy) used in these animal experiments prevents the transfer of comparable doses to the human setting (Jacobs et al. 1978; Overgaard and Khan 1981).

At present time the results of our experiments would indicate that CDDP should be given on day 0 or 1. The interval between CDDP application and start of irradiation is mostly influenced in the clinical situation by the fact that the patients have to recover from their severe gastrointestinal symptomes. In our hands the interval of 8–10 h to the first irradiation is practicable. Shipley et al. used an interval of 24 h (Shipley et al. 1984).

It is also not quite clear whether CDDP continous infusion or bolus injection is the superior way of administration in terms of tumor regression (Bartelink and Kallman 1983). However, it was shown that bolus injection decreased significantly more the crypt cell survival than continous infusions (Luk et al. 1979). Moreover clinical studies in head and neck cancer indicate that toxicity is less frequent with continous infusion than bolus injection (Douple et al. 1977).

References

Bartelink H, Kallman RF (1983) The effects of cisplatin and irradiation on tumor, skin and gut in mice. In: Broerse JJ, Barendsen GW, Kal HB, van der Kogel AJ (eds) Proceedings of the Seventh Int Congr Rad Research. Nijhoff, The Hague Boston London, Abstract D 7–03

Carde P, Laval F (1981) Effects of cis-diamminedichloroplatinum (II) and X-rays on mammalian cell survival. Int J Radiat Oncol Biol Phys 7:929–933

Douple EB, Richmond EC, Logan ME (1977) Therapeutic potentiation in a mouse mammary tumor and an intracerebral rat brain tumor by combin treatment with cix-dichloradiammineplatinum (II) and radiation. J Clin Hematol Oncol 17:585–603

Dritschilo A, Piro AJ, Kelman AD (1979) The effect of cisplatinum on the repair of radiation damage in plateau phase Chinese hamster (V-79) cells. Int J Radiat Oncol Biol Phys 5:1345–1349

Jacobs C, Bortino JR, Goffinet DR, Fee WE, Goode RL (1978) Twenty four-hour infusion of cisplatinum in head and neck cancer. Cancer 42:2135–2140

Jakse G, Frommhold H, Zur Nedden D (1985) Combined radiation and chemotherapy for locally advanced transitional cell carinoma of the urinary bladder. Cancer 55:1659–1664

Kyriazis AP, Yagoda A, Kereiakes JP, Kyriazis AA, Whitmore WF (1983) Experimental studies on the radiation-modifying effect of cisplatinum in human bladder transitional cell carcinomas grown in nude mice. Cancer 52:452–457

Lilieveld P, Scoles MA, Brown JM, Kallman RF (1985) The effect of treatment in fractionated schedules with the combination of x-irradiation and six cytotoxic drugs on the RIF-1 tumor and normal mouse skin. Int J Radiat Oncol Biol Phys 11:111–121

Luk KH, Ross GY, Phillips TO, Goldstein LS (1979) The interaction of radiation and cis-diammino-chloroplatinum in intestinal crypt cells. Int J Radiat Oncol Biol Phys 5:1417–1420

O'Toole C, Price ZH, Ohnuki Y, Unsgaard B (1978) Ultrastructure, karyology and immunology of a cell line originated from a human transitional-cell carcinoma. Br J Cancer 38:64–76

Overgaard J, Khan AR (1981) Selective enhancement of radiation response in a C3H mammary carcinoma by cisplatin. Cancer Treatm Rep 65:501–507

Schuhmann J, Göhde W (1979) Experimentelle studien zur Inaktivierung von Tumorzellen durch Kombination von Chemo- und Strahlentherapie. In: Kombinierte Strahlen- und Chemotherapie. Urban und Schwarzenberg, München Wien Baltimore, pp 27–33

Shipley WU, Coombs LJ, Einstein AB, Soloway MS, Waisman Z, Prout GR (1984) Cisplatin and full dose irradiation for patients with invasive bladder carcinoma. J Urol 132:899–903

Soloway MS (1978) Cis-Diamminedichloroplatinum II in advanced urothelial cancer. J Urol 12:716–719

Soloway MS, Morris CR, Sudderth B (1982) Radiation therapy and cis-diamminedichloroplatinum (II) in transplantable and primary murinary tract: An Eastern Cooperative Oncology Group Study. Cancer Treatm Rep 66:405–409

Twentyman PR, Kallman RF, Brown JM (1979) The effect of time between x-irradiation and chemotherapy on the growth of three solid mouse tumours. III. Cis-diamminedichloroplatinum. Int J Radiat Oncol Biol Phys 5:1365–1367

Weldon TE, Kursh E, Novak LJ, Persky L (1979) Combination radiotherapy and chemotherapy in murine bladder cancer. Urology 14:47–52

Wodinsky I, Swiniarski J, Kensler CJ, Venditti JM (1974) Combination radiotherapy and chemotherapy for P388 lymphocytic leukemia in vivo. Cancer Chemother Rep 4:73–97

Yagoda A, Watson RC, Kemeny N, Barzell WE, Grabstald H, Whitmore WF (1978) Diammine-dichloride Platinum II and cyclophosphamide in the treatment of advanced urothelial cancer. Cancer 41:2121–2130

Ziegler W, Trott K-R (1985) Der Effekt einer kombinierten Behandlung mit Cisplatin und Bestrahlung auf das Überleben von chinesischen Hamsterzellen. Strahlentherapie 161:308–315

Tumor-Specific Antigen for Human Renal Cell Carcinoma: Ultrastructural Localization of the Antigen Using Immunoelectron Microscopy

T. Schärfe[1], St. Störkel[2], M. Yokoyama[1], R. Kaltwasser[1], G. H. Jacobi[1], and R. Hohenfellner[1]

Introduction

In clinical oncology, tumor markers are a valuable tool in therapy monitoring of tumor patients as well as for primary diagnosis. In renal cell carcinoma a number of tumor associated antigens were described which may also be expressed in normal kidney epithelium (Bander et al. 1983; Bander 1984; Moon et al. 1982; Oosterwijk et al. 1987a, b; Ueda 1981). Only occasionally are antigens described which do not react in normal kidney tissue. The here described antigen is restricted to well differentiated human renal cell carcinoma (RCC) and does not show any expression in the normal kidney or other human organs (Table 1). The antibodies produced by hybridoma-technology are highly specific for the antigen: they are IgG1 antibodies. The antibody-production was achieved according to the method of Köhler and Milstein (Köhler and Milstein 1975).

The recognized kidney tumor specific antigen is expressed by all well differentiated renal cell carcinoma including their metastases but can only be stained by using cryostat-sections as normal fixative procedures (formaline/glutaraldehyde) will destroy the binding epitope (Table 2).

The localization of the antigen within the cell and definition of ultrastructural recognition was undertaken in order to shed light into possible physiological functions of the antigen. Great effort was put into finding a fixation process which would allow antigen preservation together with acceptable conservation of intracellular structures. The special fixation method described by Nakane et al. (McLean and Nakane 1974; Rota et al. 1978) guaranteed good morphological integrity of the cells. The antibody binding epitope was preserved by prefixational coating with periodate.

Material and Methods

For fixation of the tissue used in electron-microscopy, tumor and macroscopically normal kidney tissue was removed immediately after nephrectomy and cut into cubes of 3 mm diameter. The fixative used was periodate-L-lysine-paraformaldehyde, incubating the tissue for 3 h and washing the tissue blocks thereafter with increasing concentrations of sucrose (7%, 15%, 25%). After embedding in Epon and preparing semithin sections the immune-peroxidase staining technique was employed to visualize monoclonal antibody binding. The slides were evaluated under the light-micro-

[1]Department of Urology, Medical School, Johannes Gutenberg University, Langenbeckstr. 1, D-6500 Mainz
[2]Institute of Pathology, Johannes Gutenberg University, D-6500 Mainz

Investigative Urology 2
Edited by G. H. Jacobi et al.

Table 1. Specifity pattern

Antibody:	E_8, C_8, E_6, B_7	
Class:	IgG_1	
Staining:	Cytoplasmic	
Positive binding:	Renal cell carcinoma G I–II ($n = 183$)	
	Bone metastases	(3)
	Lymph-node metastases	(2)
	Lung metastases	(1)
	Short-term tissue culture RCC	(3)
No staining:	Renal cell carcinoma G III ($n = 48$)	
	Sarcomatoide	
	Oncocytoma	(12)
	Microadenoma	(2)
	Leiomyoma	(2)
	Wilm's tumor	(3)
	Normal kidney	(231)
	Normal adult tissues	
	Fetal tissues (kidney and other)	
	Colon carcinoma primary	(2)
	Liver metastases	(2)
	Pancreatic carcinoma	(8)
	Mammary carcinoma	(2)
	Stomatic carcinoma	(2)
	Testicular carcinoma (MTU)	(1)
	Prostatic carcinoma	(1)
	Bladder carcinoma	(6)
	RCC cell-lines	(5)
	RCC transplanted tumors NMRI Na/Na	(25)

Table 2a. Antigen stability (crytostat sections)

Stable:	Acid = pH 2.0
	Temp. 100°C, 10 min
	Neuraminidase
	Detergents
	Organic solvents
	Prolonged washings 100 h
Sensitive:	Alkaline pH 9
	Fixatives (formaline/gluteraldehyde)
	Periodate
	Proteases (trypsine)

High MW-variant only stable at low temp. 4°C

Table 2b. Material and methods

1) Fresh tissue specimens were frozen immediately after nephrectomy
2) Intravital fixation for standard electronmicroscopy (Glutaraldehyde, Sorensen-buffer)
3) Fixation for Immune-EM
Incubation in 0.01 *M* Periodate, 0.075 *M* Lysine, 2% Paraformaldehyde
Incubation in 0.037 *M* Phosphate buffer (3 h, RT, pH 6.2)
Wash in 50 m*M* Phosphate buffer, 7% Sucrose (4 h, RT)
Wash in 50 m*M* Phosphate buffer, 15% Sucrose (4 h, RT)
Wash in 50 m*M* Phosphate buffer, 25% Sucrose, 10% Glycerine (2 h, RT)
Followed by embedding and sectioning for EM or light-microscopy

scope enhancing contrast by counter-staining with Meyer's Hemalaun (Fig. 1). For a second antibody a goat-anti-mouse immunoglobuline $(FAB)_2$ fragment was used conjugated to peroxidase (Jackson Labs/USA). For immuno-electron-microscopy the immuno-peroxidase technique did not render sufficiently clear localization of the antigen, so that an immuno-gold procedure using 5 nm gold-particles was preferred. Thus a precise correlation of antibody binding towards intracellular ultrastructures was possible. The incubation with the antibodies was performed at room temperature for 1 h in a water saturated atmosphere. For better contrast in electron-microscopy the tissue sections were counter stained with osmium-tetraoxide.

Results

For specificity testing of the monoclonal antibody 189 primary renal cell carcinoma were stained using the immuno-peroxidase technique. As controls the corresponding normal kidney tissue was included. Using cryostat sections the antibodies showed strong binding to well – and medium differentiated RCC whereas undifferentiated sarcomatoide renal cell tumors did not express the antigen. In Oncocytoma ($n = 12$) or Wilm's tumor ($n = 3$) or Angiomyolipoma of the kidney ($n = 2$) no staining was seen. The normal kidney tissue showed no antigen expression regardless whether peripheral or central portions were stained. In order to exclude cross reactivity of the antibodies towards normal adult or fetal human tissues a broad variety of different tissues were examined, only Panet's granular cells in the gastrointestinal tract showed non-specific binding of antibodies owing to the avidity of the mucoid substances. Other solid tumors investigated showed no antigen presence (Table 1). Studying antigen stability cryostat sections were exposed to various fixation processes in search for appropriate methodology. These experiments revealed that the antigen is extremely sensitive to the routinely used fixatives, it is sensitive to tryptic digestion and the inhibition of antibody binding after periodate incubation suggest glycoproteine nature of the antigen. The technique described by McLean and Nakane proved to be the method of choice. Using this fixative glycoproteines are stabilized in situ without loosing their immuno-reactivity. Ultrastructural preservation of the

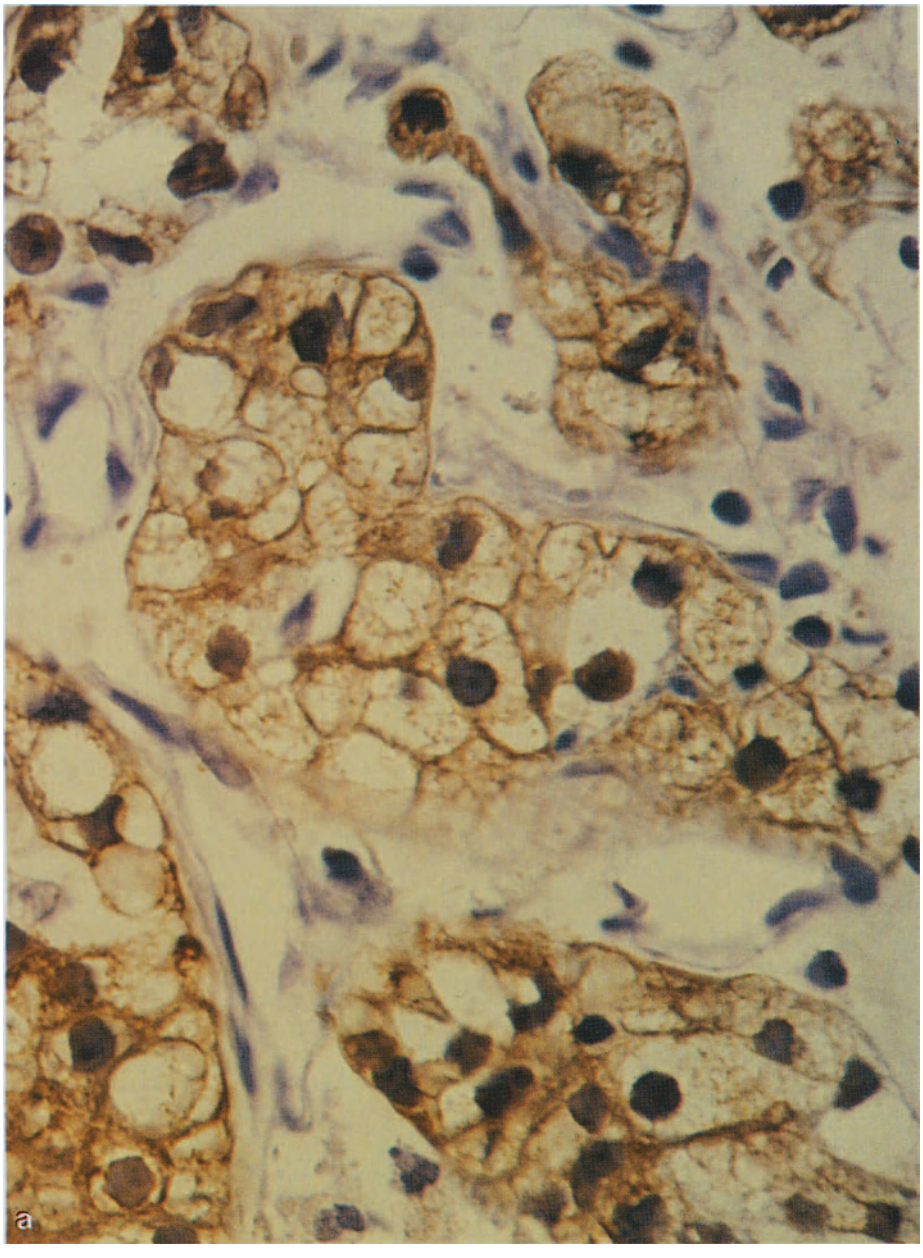

Fig. 1a, b. Renal cell carcinoma. **a** Immunoperoxidase stain. **b** TEM overview, × 6,336

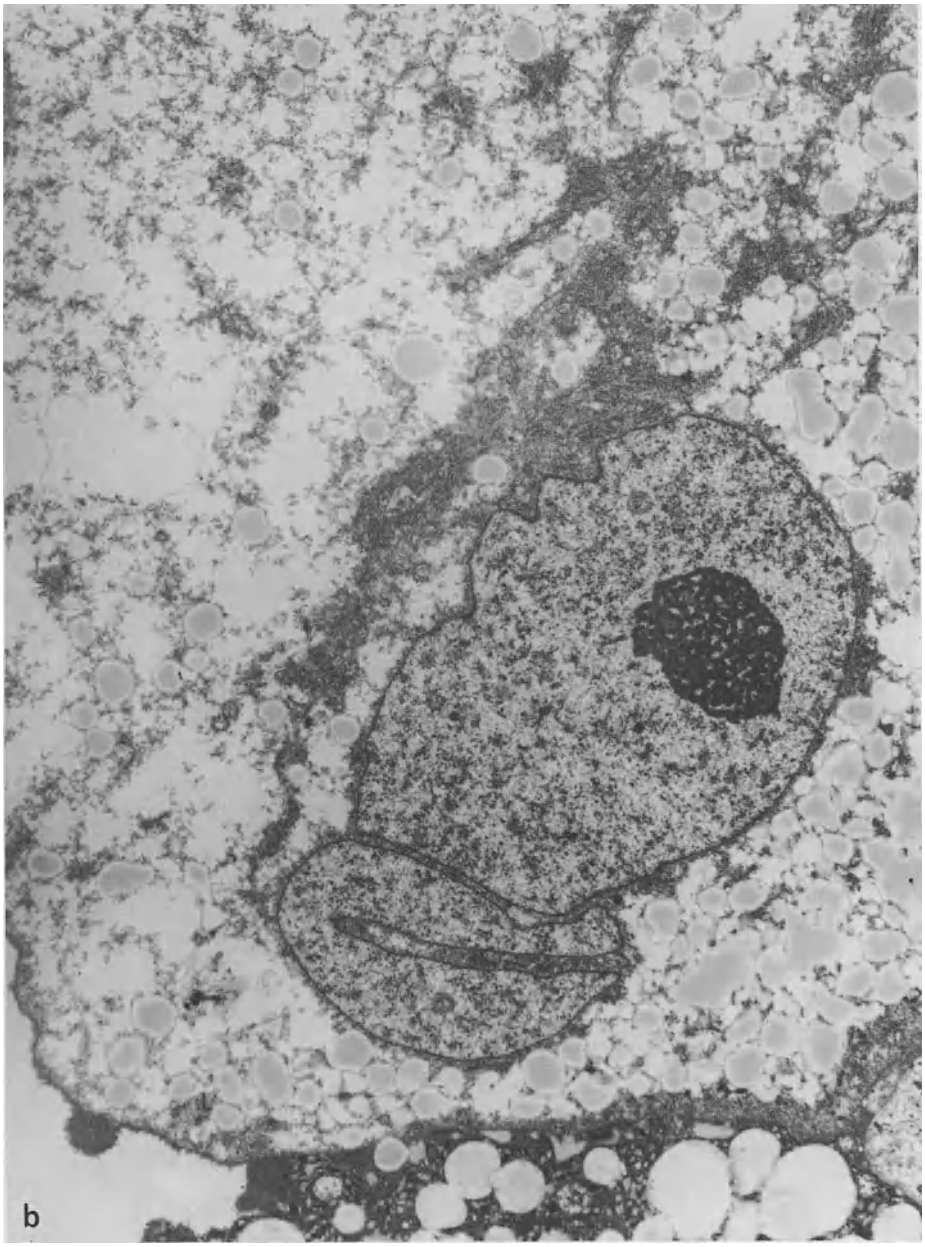

Fig. 1b

Fig. 2a–g. Renal cell carcinoma. **a** ×1,700; **b** ×8,200. **c, d** Immunoperoxidase stain, **c** ×6,500, **d** ×22,000. **e–g** Immunogold (5 nm), **e** ×26,000, **f** ×44,500, **g** ×90,000

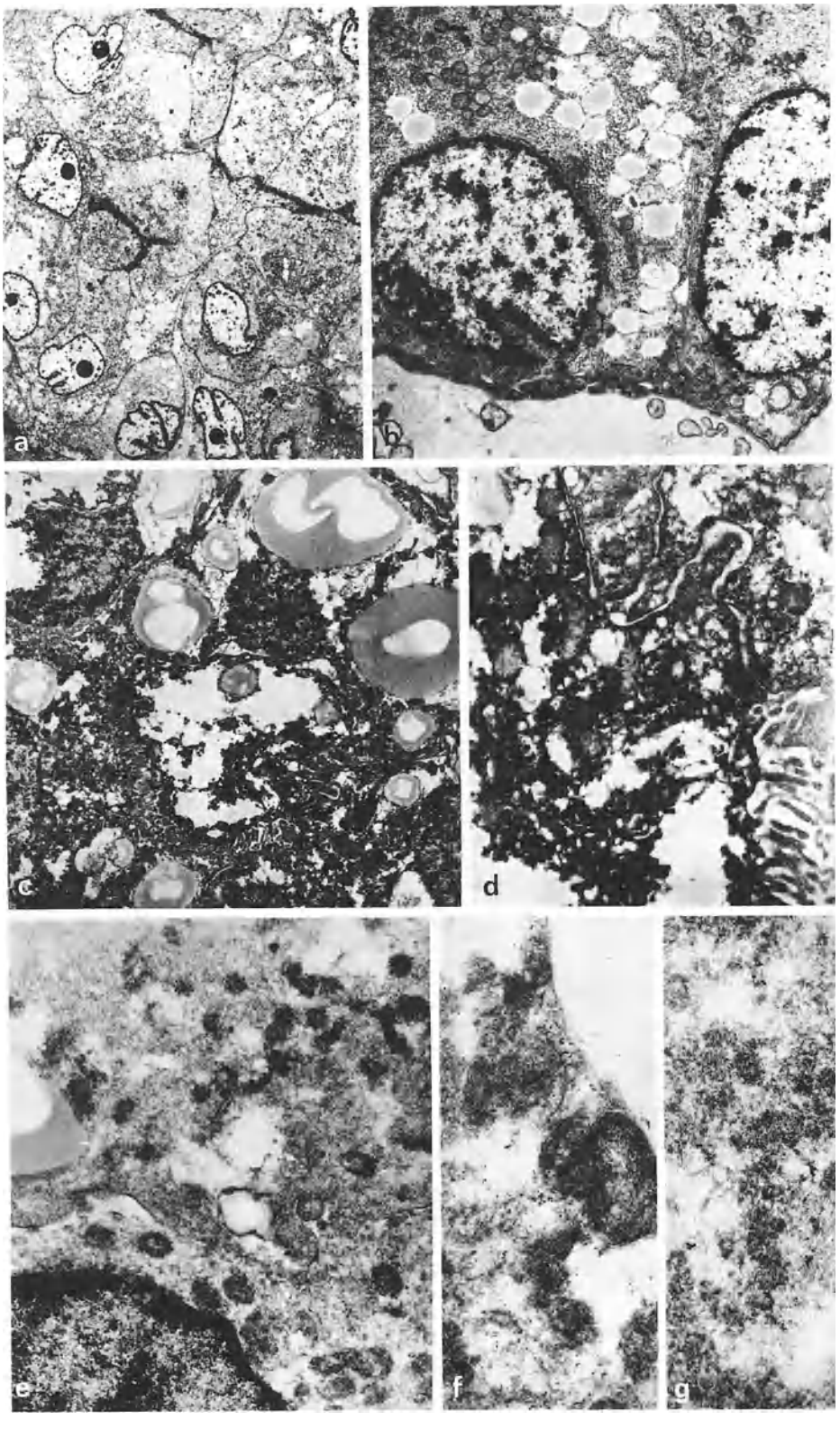
a
b
c
d
e
f
g

cells is adequate for electron-microscopical evaluation. The immuno-peroxidase reaction which produces electrondense precipitates around the antibody binding site does not render sufficiently precise localization of the antigen (Fig. 2). In order to pinpoint the antigen an immunogold staining was employed using a commercial Biotin-Avidin system with Colloidal-Avidin-Gold particles of 5 nm diameter. The very small particle size was chosen to facilitate diffusion into the tissue.

Using this technique the antigen was demonstrated to be intracytoplasmatic in close association to the typical glycogen particles. It did not stain the particles themselves nor fatty vacuoles, mitochondria, cell nuclei or cell membranes. From these findings we deduce that the antigen is expressed only in certain tumor cell types in which pathological glycogen synthesis is characteristic. This suggests that the antigen may be closely related to the pathological glycogen metabolism typical for these tumor cells.

Discussion

A number of tumor antigens were described defined by monoclonal antibodies. Some of these antigens are differentiation antigens which are also expressed in normal kidney tissues (Baldwin et al. 1985; Moon et al. 1983; Steplewski 1980; Ueda et al. 1981). To our knowledge, the here described antigen is only expressed by human renal cell carcinoma and exclusively by those cells which produce glycogen. The antibody is not only expressed in primary tumors but also in their metastases. Normal kidney tissue adult or fetal shows no antigen, other normal tissue are antigen negative. In contrast to other RCC specific antibodies (Moon et al. 1983; Oosterwijk et al. 1987a, b), our antigen shows no membrane-association, and it is intracytoplasmatically localized between the glycogen particles. This may suggest that the antigen plays a role in the pathological glycogen metabolism which is characteristic for these cells (Tannenbaum 1971). All well-to medium-differentiated human RCC showed positive antigen staining. Benign lesions of the kidney (oncocytoma, tubular microadenoma, angiomyolipoma) as well as undifferentiated RCC were antigen negative. Wilm's tumors showed no antigen expression. The frequently well differentiated clear cell type metastases of RCC showed strong antibody binding. Preliminary experiments have shown that this kidney tumor specific antigen may be used for immuno-szintigraphy with radiolabeled antibody.

The perfusion of tumor bearing kidneys shows strong specific binding of the monoclonal antibodies within the tumor but not in normal tissue. The specific expression of the antigen exclusively in human RCC with a high frequency rate (85%) of all operated RCC may suggest a close correlation to malignant transformation in tumorigenesis. Presently studies are under way to clone the tumor antigen encoding gene in order to lay hands upon a c-DNA-probe which will be used for localization of the gene within the cellular genome. The localization of this tumor activated gene by in situ hybridisation may shed light on the mechanisms responsible for the expression of tumor-markers in human cancer.

References

Baldwin RW, Embleton MJ, Pimm MV (1985) Monoklonale Antikörper zum Tumornachweis und -therapie. In: Die gelben Hefte, Immunbiologische Informationen 2/85:45–54

Bander NH, Whitmore W, Old L (1983) Monoclonal antibody defined cell surface antigens of human renal cancer. American Urologists Association Meeting, Las Vegas

Bander N (1984) Comparison of antigen expression of human renal cancers in vivo and in vitro. Cancer 53:1235–1239

Hellström KE, Hellström I, Brown JP (1982) Human tumor-associated antigens identified by monoclonal antigens. Springer Seminars in Immunopathology 5/2:127–146

Köhler G, Milstein C (1975) Continuous cultures of fused cells secreting antibody of predefined specificity. Nature 256:495

McLean IW, Nakane PK (1974) Periodate-Lysine-Paraformaldehyd fixative – a new fixative for immunoelectron microscopy. J Histochem Cytochem 22/12:1077–1083

Moon T, Vessella R, Lange P (1982) Hybridoma antibodies preferentially reactive with renal cell carcinoma. AUA Annual Meeting

Moon T, Seller R, Lange P (1983) Monoclonal antibodies in urology, a review. J Urol 130

Oosterwijk E et al (1987a) Monoclonal antibody G 250 recognizes a determinant present in renal cell carcinoma and absent in normal kidney. Int J Cancer (to be published)

Oosterwijk E, Ruiter DJ, Wakka JC, Huiskens JW, Meij VD, Jonas U, Fleuren G-J, Zwartendijk J, Hoedemaeker Ph, Warnaar SO (1987b) Immunohistochemical analysis of monoclonal antibodies to renal antigens: application in the diagnosis of renal cell carcinoma. Am J Pathol (to be published)

Roth J, Bendayan M, Orci L (1978) Ultrastructural localization of intracellular antigens – the use of protein A-gold complex. J Histochem Cytochem 26/12:1074–1081

Steplewski Z (1980) Monoclonal antibodies to human tumor antigens. Transpl Proc XII/3

Tannenbaum M (1971) Ultrastructural pathology of human renal cell tumors. Pathology Annual 6: 249–277

Ueda R, Ogata S, Morrissey D, Finstad C, Skudlarek J, Whitmore W, Oettgen H, Lloyd K, Old L (1981) Cell surface antigens of human renal cancer defined by mouse monoclonal antibodies: Identification of tissue specific kidney glycoproteins. PNAS 78/8:5122–5126

Extracorporeal Perfusion of the Tumor Bearing Human Kidney Using Tumor-Specific Monoclonal Antibodies: A Therapeutic Model

T. Schärfe[1], K. Bandhauer[2], E. Senn[2], P. Alken[1], G. H. Jacobi[1], and R. Hohenfellner[1]

Introduction

The use of monoclonal antibodies for tumor specific in vitro diagnosis is well established. With the possibility of producing tumor specific monoclonal antibodies, not only the in vitro application but also the in vivo use for tumor imaging is of great interest (Bander 1984; Mitchell and Oettgen 1982; Moon et al. 1983; Ritz et al. 1981). Methodology for radiolabelling of immunoglobulines is a well established and simple biochemical procedure thus making these antibodies ideal for immuno-szintigraphy (Greenwood et al. 1963; Hunter and Greenwood 1962; Mach et al. 1981; Scheinberg et al. 1982; Solter et al. 1982). Using alpha- or beta-emitting isotopes the therapeutic use of antibodies as tumor-targetted vehicles is feasible. With advances in biochemical conjugation procedures the coupling of cytotoxic drugs or cell toxines is now possible making the tumor specific antibody an ideal carrier for tumor specific application of drugs (Herlyn et al. 1980; Herlyn and Koprowski 1981; Houston and Nowinski 1981; Jansen et al. 1981; Krolik et al. 1983). Unfortunately presently only murine monoclonal antibodies are being produced which may cause problems in vivo being an alien proteine. A number of suggestions were made as how to circumvent the allergic complications possible after application of animal proteins (Baldwin et al. 1985; Craso and Griffin 1981; Gilliand et al. 1980). For the evaluation of our antibodies as possible carriers for radionuclides or cytotoxic drugs to the kidney tumor we developed an extracorporeal therapy model using the tumor bearing vital kidney.

Material and Methods

Tumor bearing human kidneys were perfused with cold Euro-Collins solution immediately after clamping the artery and vein. The procedure was performed in analogy to cold perfusion of cadaver-kidneys for transplantation purposes. Thus good organ vitality was guaranteed. 5 tumor bearing kidney were prepared in the described way and flushed with Euro-Collins solution intracorporeally immediately after ligation of the proximal artery and vein. After the organ had turned cold and blood-free the kidney was removed and taken to the laboratory. For antibody perfusion culture-supernatants from strongly antibody producing clones were used, mimicking a relatively low antibody concentration which has to be expected in vivo. The antibody perfusion was performed over 1 h at 4°C using a total of 50 ml of antibody super-

[1]Department of Urology, Medical School, Johannes Gutenberg University, Langenbeckstr. 1, D-6500 Mainz
[2]Department of Urology, Kantonsspital St. Gallen, CH-St. Gallen

Investigative Urology 2
Edited by G. H. Jacobi et al.

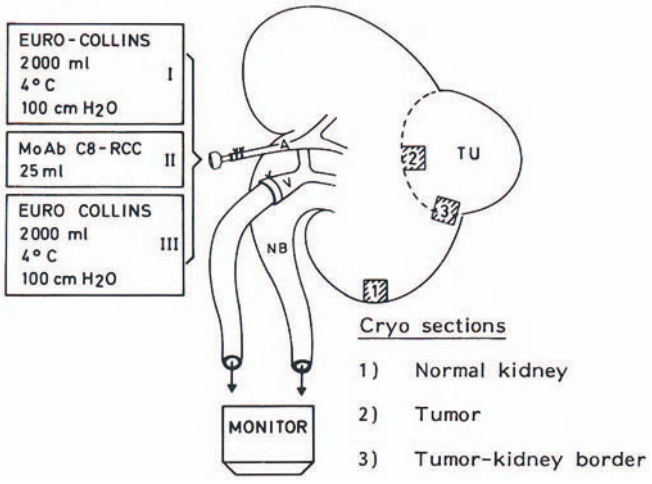

Fig. 1. Perfusion of the living organ with tumor specific monoclonal antibodies

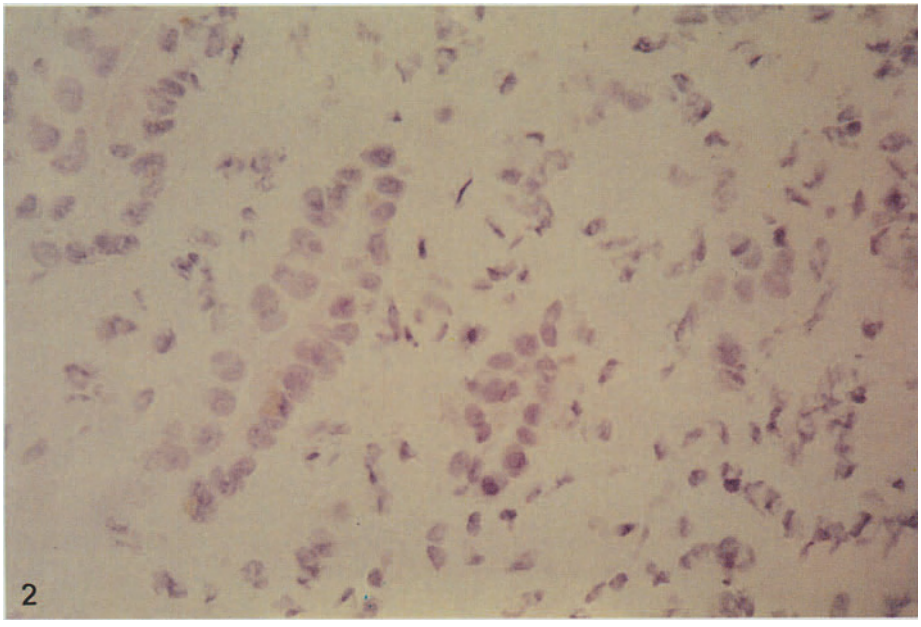

Fig. 2. Immunoperoxidase stain of the normal kidney section after perfusion

natants. Thereafter, the kidney was flushed with cold Euro-Collins again to remove unbound antibody. Then the kidney was dissected and tissue samples taken from mid-tumor, tumor-border and macroscopically normal kidney tissue. These were then stained using a goat-anti-mouse immunoglobuline antibody conjugated to peroxidase. A standard immunoperoxidase stain followed.

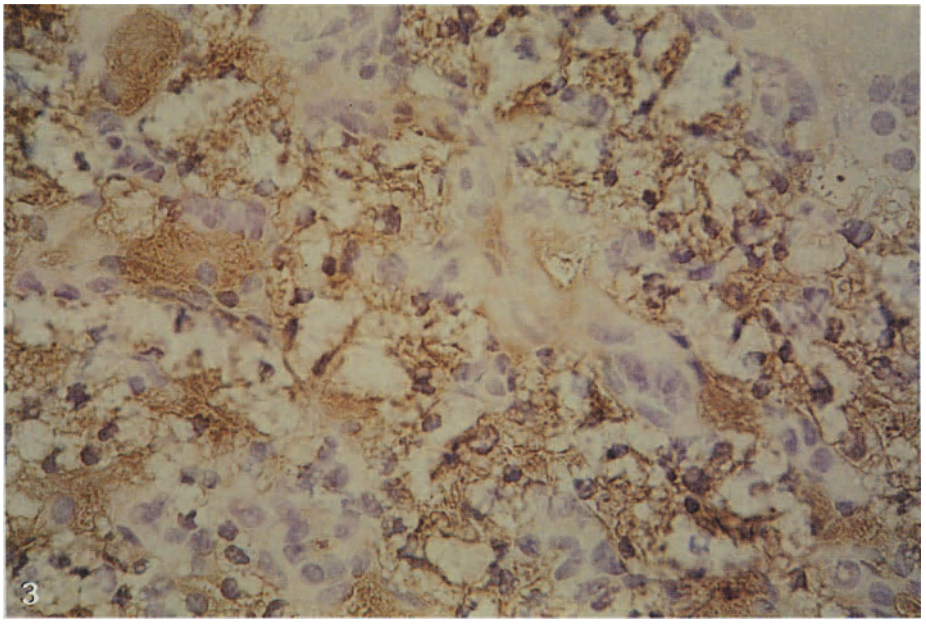

Fig. 3. Immunoperoxidase stain of the perfused tumor

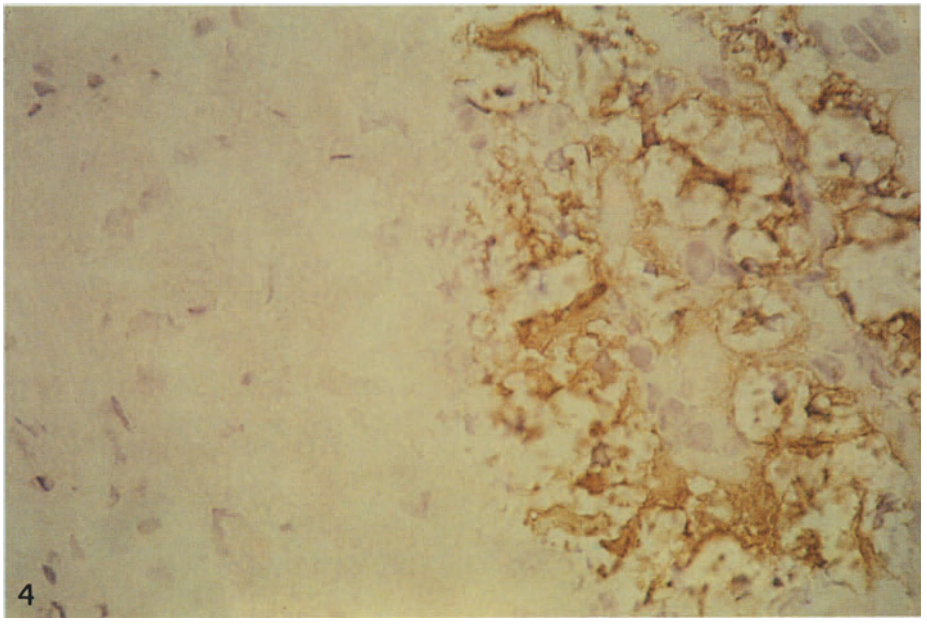

Fig. 4. Tumor-kidney border – immunoperoxidase after perfusion

Results

2 of the 5 kidneys showed no antibody binding within the tumor, routine immunoperoxidase stain revealed lack of antigen expression. In the other 3 tumors antibody binding was seen within the tumor mass, strongest around the vascular supply. Demarcation between tumor and normal kidney tissue was marked. The normal kidney epithelium showed no binding of antibodies. Intraluminal antibody was seen within the collecting system indicating antigen presence or filtration of the antibody to some extent.

Discussion

Tumor specific monoclonal antibodies have proven to be supreme tools not only in diagnostic but also for treatment of human neoplasia (Baldwin et al. 1985; Mitchell and Oettgen 1982). Using the antibody as a carrier molecule for various substances including radionuclides for imaging purposes or toxins for tumor cytotoxicity they could add a completely new dimension in the therapeutic concepts of tumor targetted chemotherapy (Moon et al. 1983; Solter et al. 1982). The specific binding of the cytotoxic drugs within the tumor promises high endotumoral concentrations at low systemic toxicity. For the evaluation of in vivo applicability of renal cell carcinoma specific antibodies, we think that the vital tumor bearing kidney perfused extracorporeally by Euro-Collins solution is a good therapy model for preclinical evaluation of antibodies. Using this model is safe for the patient and warrants good insight as to the clinical applicability of the antibody in question.

References

Baldwin RW, Embleton MJ, Pimm MV (1985) Monoklonale Antikörper zum Tumornachweis und -therapie. In: Die gelben Hefte, Immunbiologische Informationen 2/85:45–54

Bander N (1984) Comparison of antigen expression of human renal cancers in vivo and in vitro. Cancer 53:1235–1239

Bodmer WF, Epenetos, Mather, Granoska, Nimmon, Hawkins, Britton, Shepard, Taylor-Papadimitriou, Durbin, Malpas (1982) Targeting of iodine-123-labled tumor-associated monoclonal antibodies to ovarian, brest, and gastrointestinal tumors. Lancet 6th Nov:999–1005

Craso W, Griffin T (1981) Hybrid-Antibodies with dual specificity for the delivery of ricine to immunoglobuline bearings target cells. Cancer Res 41:2073–2078

Gilliand D, Steplewski Z, Collier R, Mitchel K, Chang T, Koprowski H (1980) Antibody-directed cytotoxic agents, use of monoclonal antibodies to direct the action of toxin-A chains to colorectal carcinoma cells. PNAS 77:4539

Greenwood FC, Hunter WM, Glover JS (1963) The preparation of ^{131}J-labelled growth hormone of high specific activity. Biochem J 89:114

Herlyn DM, Koprowski H (1981) Monoclonal anticolon carcinoma antibodies in complement dependent cytotoxicity. Int J Cancer 27:769–774

Herlyn DM, Steplewski Z, Herlyn A, Koprowski H (1980) Inhibition of growth of colorectal carcinoma in nude mice by monoclonal antibody. Cancer Res 40:717–721

Houston LL, Nowinski S (1981) Cell-specific cytotoxicity expressed by a conjugate of ricin and murine monoclonal antibody directed against Thy 1.1 antigen. Cancer Res 41:3913–3917

Hunter WM, Greenwood FC (1962) Preparation of iodine-131 labelled human growth hormone of high specific activity. Nature 194:495

Jansen, Blythman, Carrière, Casellas, Gros, Gros, Paolucci, Pau, Poulett, Richter, Vidal, Voisin (1981) Assembly and activity of conjugates between monoclonal antibodies and toxic subunits of ricin immunotoxins. In: Hämmerling, Hämmerlin, Kearny (eds) Monoclonal antibodies and T-cell hybridomas. Elsevier/North Holland Biomedical Press, Amsterdam New York Oxford

Krolik KA, Uhr WJ, Vitetta ES (1982) Selective killing of leukaemia cells by antibody-toxin conjugates: implications for autologous bone marrow transplantation. Nature 295:604f

Mach J, Buchegger F, Forni M, Ritschard J, Berche C, Lumbroso L, Schreyer M, Giardet C, Accolla R, Carrel S (1981) Use of radiolabelled anti-CEA antibodies for the detection of human carcinomas by external photoscanning and tomoscintigraphy. Immunol Today 2:239

Mitchell MS, Oettgen HF (eds) (1982) Hybridomas in cancer diagnosis and treatment. Prog Cancer Res Ther 21:1–26

Moon T, Seller R, Lange P (1983) Monoclonal antibodies in urology, a review. J Urol 130

Ritz J, Pesado JM, Notis-McConarty J, Clavell LA, Sallan E, Schlossmann SF (1981) Use of monoclonal antibodies as diagnostic and therapeutic reagents in acute lymphoblastic leukemia. Cancer Res 41:4771–4775

Scheinberg SA, Strand M, Gansow OA (1982) Tumor imaging with radioactive metal chelates conjugated to monoclonal antibodies. Science 215:1511–1513

Solter D, Ballou B, Reilan J, Levin G, Hakala RT, Knowles BB (1982) Radioimmunodetection of tumors using monoclonal antibodies. In: Mitchel, Oettgen (eds) Hybridomas in cancer diagnosis and use. Elsevier, Amsterdam, pp 241–244

Growth of Human Renal Cell Carcinoma in Nude Mice

V. Heller[1], I. D. Bassukas[2], J. W. Grups[1], and M. P. Wirth[1]

Introduction

In metastasized renal cell carcinoma successful treatment has not been established so far (McDonald 1982). Therefore, further experimental research is necessary to attack this problem. Such studies require reliable and well defined tumor models. Xenotransplantation of human renal cell carcinoma to thymusaplastic, congenital immune-deficient nude mice seems to be a useful model system provided that the human-specific characteristics are retained. Some human kidney tumors were successfully established in nude mice and accordingly characterized (Baisch et al. 1986; Clayman et al. 1985; Höhn and Schröder 1978; Otto et al. 1981; Otto et al. 1984).

Otto and coworkers (Baisch et al. 1986; Otto et al. 1984) revealed a wide conformity of the human renal cell carcinomas and the corresponding xenografts in nude mice. The statements concerning the growth kinetics, however, are contradictory since a distinct fraction of the carcinomas studied showed systematic alterations of the cell proliferation parameters as determined by flow cytometric (FCM) analysis of DNA histograms.

The purpose of the present study was to compare the proliferation parameters of both tumor parenchymal and endothelial cells as well as the histology of renal cell carcinomas with that of the corresponding xenotransplants growing on nude mice. This should reveal similarity or difference in cell proliferation and histology between the renal cell carcinoma growing in the patient and of tumors transplanted to nude mice. Such studies are necessary, if the results of testing cytostatic drugs on xenografts should be transfered to human tumor therapy, since the effectiveness of cytostatic treatment mainly depends on the growth kinetics of the tumors (Bhuyan 1977; Steel 1977).

Materials and Methods

Tissue specimens of 13 human renal cell carcinomas removed by radical nephrectomy and additionally of one lymph node metastasis were xenotransplanted into 4–6 male or female nude (nu/nu) mice with a BALB/c genetic background (own breeding colony). The nude mice were 6–8 weeks old. The animals received special food and were housed in temperature controlled laminar air flow facilities. For xenotransplantation small tissue specimens (about $1 \times 2 \times 2$ mm) of the periphery of the

[1] Urologische Klinik und Poliklinik der Universität Würzburg, Josef-Schneider-Str. 2, D-8700 Würzburg
[2] Institut für Medizinische Strahlenkunde der Universität Würzburg, Versbacher Str. 5, D-8700 Würzburg

Investigative Urology 2
Edited by G. H. Jacobi et al.

tumor were implanted subcutaneously bilaterally into the thoracic wall. Further passages from tumors growing on nude mice were transplanted in a corresponding manner.

For determining the "in vitro labelling index" (LI = % labelled cells) tumor tissue pieces (about 1 mm^3) of both the primary tumors and the metastasis as well as of their xenotransplants were incubated in 10 ml RPMI 1640 (+20% FCS) with tritiated thymidine (^{3}H-TdR; 5 µCi/ml; spec. act. 6.7 Ci/mMol) at 37°C and 2.25 bar carbogen (95% O_2 + 5% CO_2) for one hour (Helpap and Maurer 1969). Autoradiographs were prepared with the dipping method. The LI was determined simultaneously for the parenchymal and endothelial cells by counting a total of more than 5,000 cells. All cells with more than 4 grains per nucleus were counted as labelled.

Results

4 out of 13 renal cell carcinomas and one lymph node metastasis were successfully transplanted to nude mice and maintained by serial transplantation (take rate: 36%; see also Table 1). The cell kinetics of the tumors NT1, NT6, NT9, and the lymph node metastasis of NT9 as well as the 1. and 2. generation of NT1, of NT6 and of the metastasis were analyzed.

All tumors retained their cellular morphology throughout the passages. The LI of the *parenchymal tumor cells* from the excised primary renal cell carcinomas was lower than 1%, whereas that of the human lymph node metastasis was much higher (3.3%) especially when compared with its primary tumor NT9 (0.2%) (Figs. 1–3). The xenotransplants of the primary tumors and of the metastasis revealed a marked increase of the LI of parenchymal cells in the first passage (Figs. 1–3) and a further increase in the 2. generation of the tumors NT1 and NT6, whereas the LI slightly decreased in the 2. generation of the metastasis. However, large necrotic areas were observed in the latter tumor specimens.

Such marked differences were not found between the LI of *endothelial cells* of the primary tumors, of the lymph node metastasis and of their xenotransplants growing on nude mice (Table 2). Moreover the histological examination of the tumors revealed a progressive decrease of the relative number of endothelial cells during serial transplantations into nude mice.

Table 1. Staging and grading of the human renal cell carcinomas related to the established passages of their xenotransplants

Tumor	Staging and grading of the original human tumor	Established passages	Transplantation lines
NT1	$pT_2pN_0M_0$ GII	>5	Yes
NT6	$pT_4pN_0M_0pV_0$ GII	3	No
NT8	$pT_3pN_0M_0pV_1$ GII	1	No
Lymph node metastasis of NT9	$pT_4pN_3M_0pV_1$ GII	>5	Yes
NT12	$pT_3pN_0M_0pV_0$ GII	1	No

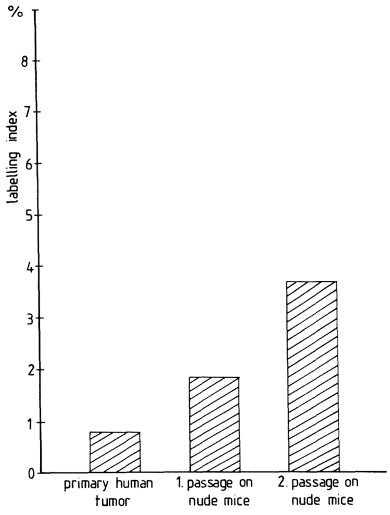

Fig. 1. After xenotransplantation of the renal cell carcinoma NT1 into nude mice the LI of parenchymal cells increased to double the value in the 1st and 2nd passage

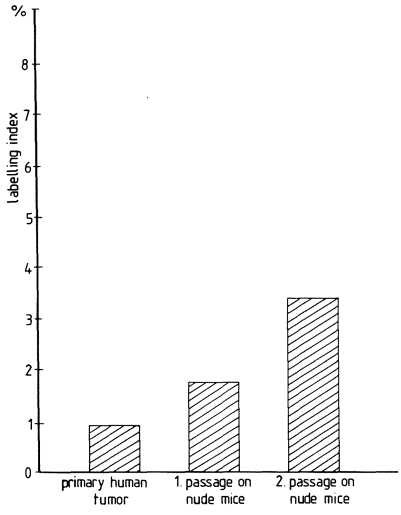

Fig. 2. Compared with the original tumor an increase of the LI of parenchymal cells was demonstrable in the xenographts of the renal cell carcinoma NT6

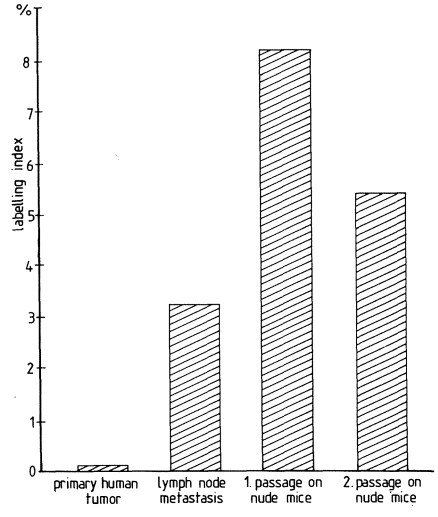

Fig. 3. The lymph node metastasis showed a higher LI of parenchymal tumor cells than the corresponding primary renal cell carcinoma NT9. Xenotransplantation of the metastasis led to an increase of the LI of parenchymal cells in the 1st passage, whereas in the 2nd passage the LI decreased

Discussion

The take rate of human renal cell carcinoma xenografts found in this study (36%) is comparable to that reported by other authors (Clayman et al. 1985; Giovanella and Fogh 1985) but contradicts the unusually high take rate (100%) reported by Baisch et al. (1986). It is noteworthy that the human tumor with the lowest LI (NT9, primary) failed to grow on nude mice.

Table 2. Fraction of endothelial cells related to parenchymal cells in renal cell carcinoma

Tumor	Original human tumor	1st passage on nude mice	2nd passage on nude mice
NT1	0.16	0.15	0.09
NT6	0.15	0.09	0.08
NT9	0.14	–	–
Lymph node metastasis of NT9	0.20	0.06	0.07

Table 3. Labelling index of the endothelial cells in renal cell carcinoma

Tumor	Original human tumor (%)	1st passage on nude mice (%)	2nd passage on nude mice (%)
NT1	0.39	2.00	1.87
NT6	3.34	2.83	3.54
NT9	0.03	–	–
Lymph node metastasis of NT9	5.38	6.43	8.62

The results further demonstrate that the fraction of parenchymal cells that actively incorporates ^{3}H-TdR, i.e., synthesizes DNA, apparently is higher in the xenotransplants than in the corresponding human tumors. Baisch et al. found an analogous increase of the % S-phase cells in a study of human renal cell carcinomas and their serial passages to nude mice applying the FCM method (Baisch et al. 1986). Other authors reported an increase of the mitotic index for a great series of different human tumors after xenotransplantation to nude mice (Otto et al. 1984; Sharkey and Fogh 1984).

Concerning the alteration of the LI after xenotransplanting the human tumor to nude mice it must be noted that generally the time interval between tissue removal and its incubation was longer (½–1 h) compared to that in the following passages (10–15 min). There are contradictory data in the literature how the prolongation of the time interval between tissue removal and beginning of the incubation influences the incorporation of ^{3}H-TdR (Hainau and Dombernowsky 1974; Helpap 1980; Meyer and Connor 1977). The fact that the LI progressively increases in the second passage of the primary human tumors (Fig. 1 and 2), suggests that the proliferation rate of the human renal cell carcinoma increases after xenotransplantation to nude mice.

The LI of the parenchymal tumor cells of the human metastasis was higher than that of the primary tumors, particularly the corresponding one, a difference which also persisted for the xenotransplants of these tumors (Fig. 1–3). This agrees with the

data on the % S-phase cells for a greater series of human renal cell carcinomas (Baisch et al. 1986).

In contrast to the progressive increase of the LI in the primary tumors studied (NT1 and NT6), the second passage of the metastasis showed a slightly lower LI than the first passage. This may be attributed to inappropriate tissue sampling for the incubation, because human tumors are quite heterogenous with respect to the proliferation parameters (Baisch et al. 1982; Frankfurt et al. 1984; Smallwood et al. 1983). This is further supported by the fact that only the specimens of the second passage of the metastasis showed a high fraction of necrotic material. It is known that the LI is minimal in the vicinity of necrotic areas due to a decrease of the growth fraction (Gabbert et al. 1982; Hirst and Denekamp 1979; Tannock 1968).

Although a similar increase of proliferation parameters as reported here was also observed by Baisch et al. (Baisch et al. 1986), these authors measured generally higher % S-phase cells compared to the in vitro LIs determined in the present study. This difference may be explained by the fact that many human renal cell carcinomas are composed of a hyperdiploid parenchymal cell population and a variable fraction of also proliferating euploid supporting cells (Baisch et al. 1986). Thus the values of % S-phase cells measured by the one-parameter FCM method may be biased by the presence of S- and G2 + M-phase euploid cells predominantly being registered together with the fraction of tumor parenchymal S-phase cells. This indicates that autoradiography is necessary to separately study the growth kinetics of different cell populations in tumor tissue.

Since both the induction (Folkman 1985) as well as the maintenance of endothelial cell proliferation (Denekamp and Hobson 1982) are obligatory prerequisites for tumor growth, the LI and the relative number of these cells were also measured in the present study. The LIs of endothelial cells of the xenotransplants tended to increase slightly during serial subtransplantation and were generally higher than those of the original human tumors. However, the relative number of the endothelial cells progressively decreased from the human tumors to the second passage on nude mice. Since no data are available on the absolute growth rate of the parenchymal cells, it is not possible to deduce, whether an excess of parenchymal cell proliferation or an increased endothelial cell loss or the combination of both led to the relative decrease of the number of the endothelial cells. In any case an increase of parenchymal cell proliferation seems to play a role, since the increase of the LI of the parenchymal cells exceeds that of the endothelial cells.

Another interesting fact is, that only from the tumor NT1 and the lymph node metastasis of NT9 permanent transplantation lines could be established in contrast to the tumor NT6, although this tumor showed the same alterations of growth kinetics and histology during the first 2 passages on nude mice.

In conclusion, the results indicate considerable differences between human renal cell carcinomas and the corresponding xenotransplants on nude mice, and between primary tumors and a lymph node metastasis respectively. Since the effectiveness of chemotherapy mainly depends on the growth kinetics of the malignant cells and on the blood supply of the tumor, the results of cytostatic treatment studies with xenotransplants are not simply transferable to the treatment of metastasized renal cell carcinoma in humans. Therefore, it is necessary to determine exactly all the differences between the xenotransplant and the human renal cell carcinoma. This present

lack of information may be one of the reasons, why chemotherapy which was successful in animal models, has led to disappointing results in the treatment of metastasized renal cell carcinoma in human.

Acknowledgements. The authors gratefully thank Prof. Dr. B. Maurer-Schultze for critical comments and helpful suggestions during the course of this research. They also thank Miss Th. Manger and Miss I. Weiglein for the skillful technical assistance. This work was supported in part by a grant (I.D.B.) from the Sander Stiftung, Neustadt/Donau, Germany.

References

Baisch H et al (1982) DNA content of human kidney carcinoma cells in relation to histological grading. Cancer 45:878–886

Baisch H et al (1986) Long-term transplantation of 30 different human renal cell carcinomas into NMRI (nu/nu) mice: Flow cytometric, histologic, and growth studies. J Natl Cancer Inst 76: 269–276

Bhuyan BK (1977) Cell cycle-related lethality. In: Drewinko B, Humphrey RM (eds) Growth kinetics and biochemical regulation of normal and malignant cells. Williams & Wilkins, Baltimore, pp 373–385

Clayman RV et al (1985) Transplantation of human renal carcinoma into athymic mice. Cancer Res 45:2650–2656

Denekamp J, Hobson B (1982) Endothelial-cell proliferation in experimental tumours. Br J Cancer 46:711–720

Folkman J (1985) Tumor angiogenesis. Adv Cancer Res 43:175–230

Frankfurt OS et al (1984) Flow cytometric analysis of DNA aneuploidy in primary and metastatic human solid tumors. Cytometry 5:71–80

Gabbert H et al (1982) The relation between tumor cell proliferation and vascularization in differentiated and undifferentiated colon carcinomas in the rat. Virchows Arch (Cell Pathol) 41:119–131

Giovanella BC, Fogh J (1985) The nude mouse in cancer research. Adv Cancer Res 44:69–120

Hainau B, Dombernowsky P (1974) Histology and cell proliferation in human bladder tumors. An autoradiographic study. Cancer 33:115–126

Helpap B (1980) Zellkinetische In Vivo und In Vitro Untersuchungen mit ^{3}H- und ^{14}C-Thymidin an Gewebsbiopsien von Experimental- und Human-Tumoren. Westdeutscher Verlag, Opladen

Helpap B, Maurer W (1969) Autoradiographische Untersuchungen zur Frage der Vergleichbarkeit des Einbaus von markiertem Thymidin unter in vivo-Bedingungen und bei Inkubation von Gewebsproben. Virchows Arch Abt B Zellpathol 4:102–118

Hirst DG, Denekamp J (1979) Tumour cell proliferation in relation to the vasculature. Cell Tissue Kinet 12:31–42

Höhn W, Schröder FH (1978) Renal cell carcinoma: Two new cell lines and a serially transplantable nude mouse tumour (NC-65). Invest Urol 16:106–112

McDonald MW (1982) Current therapy of renal cell carcinoma. J Urol 127:211–217

Meyer JS, Connor RE (1977) In vitro labelling of solid tissues with tritiated thymidine for autoradiographic detection of S-phase nuclei. Stain Technol 52:185–195

Otto U et al (1981) Transplantation von menschlichem Nierenadenokarzinomgewebe auf die nackte Maus. Urol Int 36:110–123

Otto U et al (1984) Transplantation of human renal cell carcinoma into NMRI nu/nu mice. I. Reliability of an experimental tumor model. J Urol 131:130–133

Sharkey FE, Fogh J (1984) Considerations in the use of nude mice for cancer research. Cancer Metast Rev 3:341–360

Smallwood JA et al (1983) The errors of thymidine labelling in breast cancer. Clin Oncol 9:331–335

Steel GG (1977) The growth kinetics of tumours. Oxford University Press, Oxford

Tannock IF (1968) The relation between cell proliferation and vascular system in a transplanted mouse mammary tumour. Br J Cancer 22:258–273

Short-Term In-Vitro Sensitivity Testing of Human Renal Cell Carcinoma

W. de Riese[1], S. Szücs[2], E. Hoene[1], G. Lenis[1], G. Kovacs[2], and E. Schindler[1]

Introduction

Renal cell carcinoma, particularly in advanced stages, responds only poorly to cytostatic therapy. Occasional partial remissions are described following chemotherapy. Although numerous agents have been known to achieve measurable response in individual cases of advanced renal cell carcinoma, the rate of therapy response documented for each agent is so inconstant that no single agent may be or has been recommended as a cytostatic of choice for this cancer (De Kernion 1986). This is the reason for present efforts to find means of determining the substance(s) best suited for renal cancer therapy in individual patients. Empirical-clinical measurement procedures are highly cost-intensive and require long and complicated instrumental means, besides placing an unnecessary burden on those patients showing no therapeutical response whatsoever to the agents tested.

The so-called "Soft-Agar-Clonogenic-Assay" (Lieber 1984; Salmon and Hamburg 1978) is widespread. This method is dependent on the rate of cell-division as a measure of the vitality and malignancy of the tissue cultured. In the cited procedure, the corresponding cytostatic agent is added to the culture medium. The single tumor cells grow within 2 or 3 weeks to form tumor-cell colonies. The number of cell colonies growing to a minimum size are counted. A comparison with the colonies growing from untreated cells permits a predictive statement with regard to possible therapeutic response in vivo. If, under the influence of a particular cytostatic agent, less than 30% of the colonies growing in control are counted, the tumor is regarded as sensitive to this substance (Lieber 1984; Mattern and Volm 1982; Mattern et al. 1986; Pavelic et al. 1986; von Hoff et al. 1983). Salmon et al. have, in this regard, documented numerous in-vitro investigations describing the effect of exposition to various chemotherapeutic agents in different concentrations within the culture medium. For clinical purposes, the plasma concentrations for in-vivo application was calculated individually on the basis of the concentrations within the culture medium (Albrecht et al. 1985; Lieber 1984).

Material and Methods

Figure 1 demonstrates schematically the preparation of the tumor cells. Following the customary transperitoneal tumor-nephrectomy, a sample is obtained under sterile conditions. The exact procedure of primary cell culture preparation is de-

[1]Department of Urology, Hannover Medical School, Konstanty-Gutschow-Str. 8, D-3000 Hannover 61
[2]Department of Cytogenetics, Hannover Medical School, Konstanty-Gutschow-Str. 8, D-3000 Hannover 61

Investigative Urology 2
Edited by G. H. Jacobi et al.

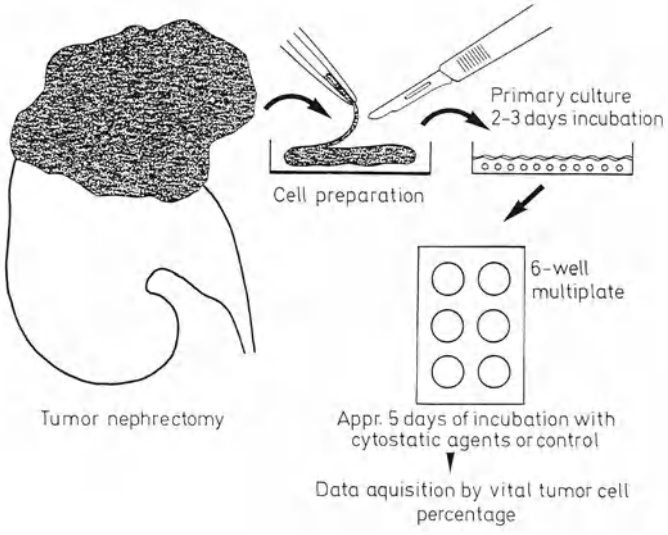

Fig. 1. Schematic representation of tumor cell preparation

scribed in a second report in this issue (Szücs et al. 1987). Proof that the tested cells were in reality tumor cells was obtained by karyotyping the primary culture cells. In all the primary cultures (i.e., those cultures used for cytostatic testing), clonal chromosome aberrations were demonstrated (Szücs et al., this volume).

The first cell passage then followed: after exposure to trypsin for 2–3 min at 37°C, the cells relinquish their attachment to the growth surface and go into suspension. The cell count was determined and the suspension was innoculated in 6-well culture plates, so as to attain an end-count of 10,000 to 50,000 per well. In preliminary testing, the well size of 3 cm diameter had proved optimal. Too large a well size proved impractical as the culture plates would have taken up inordinate space in the incubation cabinet. At smaller well sizes the quantity of culture medium applied would not have sufficed for consistent cultivation. The rate of successful cultivation was significantly reduced when the well size was below 3 cm diameter. We employed RPMI 1640 as a culture medium (Biochrome comp.), supplemented with 15% fetal calf serum. For each tumor, two control cultures and two culture wells per tested cytostatic concentration were innoculated. Five cytostatic agents were tested (see Table 2). The typical therapeutic concentration or simple multiples (X2, X5, X10) were employed.

The cells were cultivated in multi-well plates with canted covers under 5% CO_2-atmosphere at 37°C. On the average, the culture surfaces of the control groups were fully covered with tumor cells 2 days after innoculation. This was taken as the set time for evaluation of relative growth. After exposure to EDTA-trypsine for 2–3 min at 37°C, the cells were released from the culture surface to float freely in the medium where they were counted after transfer into counting chambers. Only vital cells were counted, the percentage of killed cells being determined by addition of a 1% solution of methylene blue.

Results

Table 1 delineates histological grade and TNM-stage for each of a total of 21 renal cell cancers tested. It is obvious that not only the undifferentiated tumors, but also highly differentiated tumors in an early stage were successfully cultivated in vitro. The success-rate for primary cultivation of renal cancer cells averaged 95%. For soft-agar-clonogenic-assay studies, the reported success-rate does not exceed 50% (Lieber 1984; Salmon and Hamburg 1978). This difference depends on the method of preparation: in the procedure outlined above (Szücs et al., this volume) the dis-aggregation of the tissue suspension is discontinued before reaching the single-cell suspension previously reported being arrested at a stage of 10–15-cell groups. For this reason, our method is based on the percentage of vital tumor cells in relation to the untreated control cultures rather than determination of established colony counts.

Figure 2 illustrates graphically the tumor-cell kill-rate under exposure to the agents mitomycin and epi-doxorubicin, in single, double, 5- and 10-fold concentra-

Table 1. Histological grading and staging for 21 renal cell tumors tested for cytostatic sensitivity in vitro

Histological grading and staging	Number of patients
G1, pT1	4
G1, pT2	2
G2, pT2	6
G2, pT3	4
G3, pT2	3
G3, pT3	2

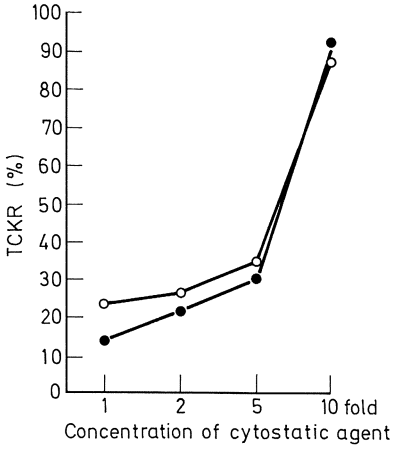

Fig. 2. Graphic representation of tumor-cell kill-rates (TCKR) for Mitomycin (○—○) and Epidoxorubicin (●—●) in single and 10-fold concentrations

Table 2. Tumor-cell kill-rates (TCKR) by cytotoxic drugs using single and 10-fold concentrations

Cytostatic agent	Concentration (ng/ml)	Tumor-cell kill-rates		
		Average	Minimum	Maximum
Mitomycin	0.5	9	2	16
Doxorubicin	1.9	9	4	17
Epi-Doxorubicin	1.9	10	3	22
Cis-Platin	3.0	7	0	23
Vincristin	0.04	8	5	21
Mitomycin + Doxorubicin	0.5 + 1.9	9	3	18
Mitomycin	5.0	94	82	99
Doxorubicin	19	95	78	98
Epi-Doxorubicin	19	93	84	97
Cis-Platin	30	86	49	93
Vincristin	0.4	72	44	86

tions based on the recommended therapeutic serum concentrations. The other agents tested generally showed the same dose-effect relationship as the 2 substances illustrated.

Table 2 outlines the chemotherapeutic sensitivity to all the cytostatic agents tested in this investigation. In conclusion, none of the agents examined showed a satisfactory kill-rate at the recommended concentration (variation between 2% and 23%). Improved kill-rates were not obtained, except at higher concentrations, i.e, doses that would be highly toxic in vivo. The cultures were carried out in a paired system with dual control of both cytostatic-exposed and untreated cells. The difference between the percentage counts of each pair *in no case* exceeded 5%. The kill-rates at higher concentrations varied from substance to substance and tumor to tumor (44%–99%).

Discussion

Investigations of chemotherapeutic sensitivity using soft-agar-clonogenic-assay and modifications of this method have been published, in which the predictive value for clinical applications was examined both retro- and prospectively (Albrecht et al. 1985; Kaufmann and Kubli 1983; Lieber 1984; Mattern et al. 1986). It could be documented that these procedures permitted correct prediction of the *resistance* of individual tumors towards particular agents in over 90%. In contrast, the prediction of *sensitivity* proved correct in only 50%–70% of the cases. Thus, in over a third of the cases, the tumor in vivo proved resistant to a cytostatic agent tested as sensitive

in vitro. At present, statistically sound data proving significant correlation between in-vitro results and extended survival time for correspondingly treated patients are rare. One investigation concerning lung-cancer patients, for instance, showed that, for all cases treated, those patients with tumors demonstrating in-vitro sensitivity towards doxorubicin evidenced a survival time extended by a factor of 2.5 in comparison with the patients whose cancer proved resistant in culture (von Hoff et al. 1983).

According to our results, cytostatic substances tested showed unsatisfactory kill-rates in vitro at recommended therapeutic concentrations. The kill-rates improved at higher doses, at which concentrations the agents would be highly toxic clinically. The kill-rates found, however, showed reproducible differences between individual tumors and different substances. This seems a promising starting point for further investigation.

Our study also corroborated the fact that renal cell cancer, irrespective of tumor stage or grade, generally shows poor sensitivity to all customary cytostatic agents (de Kernion 1986).

In comparison with the in-vitro cytostatic testing procedures previously described, our method presents a number of definite advantages. It is easier to implement and requires a good deal less sophisticated technical apparatus. The time required to obtain definite results with respect to chemotherapeutic resistance and possible sensitivity in each case averages 5 to 7 days. This interval correlates well with the post-operative recovery time, since adjuvant or palliative cytostatic therapy must, of necessity, be deferred this long to promote healing.

The known disadvantages of in-vivo testing procedures lie in the long duration of the experiments (taking months, for instance, in the nude-mouse model) and in the relatively high cost. The transplanted tumors are successfully established in the host at inconstant rates between 50% and 60%. Furthermore, the tumor grow under unphysiological conditions in the host organism exposed to immunological phenomena impossible to assess objectively (Arafah et al. 1986; Kurth et al. 1985; Mattern et al. 1986; Pavelic et al. 1986). The presently very critical public discussion concerning the moral justification for animal experimentation is a strong argument for intensifying the development of cell-culture models, especially in the light of the other advantages mentioned above.

The authors in the pertinent literature seem virtually unanimous in the opinion that in-vitro methods are capable of predicting the resistance of individual tumors to specific chemotherapies with a high degree of certainty. In contrast to empirical efforts, this presents a possibility of sparing each patient the additional burden of the side-effects of a chemotherapy that promises no benefit. That alone would be an important advancement in the development of individually tailored tumor therapy.

Methods of this kind may help in the development and trial of new cytostatic agents for incorporation in existing oncological therapy regimens, for they would permit objective comparison of such substances' effectivity with that of established drugs. If new agents were to show improved results under in-vitro conditions, that would present an important argument for the propagation of new regimens for widespread clinical use.

References

Albrecht M, Simon WE, Hölzel F (1985) Individual chemosensitivity of in vitro proliferating mammary and ovarian carcinoma cells in comparison to clinical results of chemotherapy. J Cancer Res Clin Oncol 109:210–216

Arafah BU, Griffin P, Gordon NH, Pearson OH (1986) Influence of Tamoxifen and Estradiol on the growth of human breast cancer in vitro. Cancer Res 46:3268–3272

de Kernion JB (1986) Renal tumors and renal cell carcinomas. In: Campbell's urology, 5th edn, vol 2. Saunders, Philadelphia, pp 1319–1323

Kaufmann M, Kubli F (1983) Gegenwärtiger Stand der Chemosensibilitätstestung von Tumoren. Dtsch Med Wochenschr 108:150–154

Kurth KH, Romijn JW, Schröder FH (1985) Assay-Verwertbarkeit humaner Nierentumorlinien. In: Harzmann R et al (eds) Experimentelle Urologie. Springer, Berlin Heidelberg New York, pp 475–482

Lieber MM (1984) Soft agar colony formation assay for in-vitro chemotherapy sensitivity testing of human renal cell carcinoma. J Urol 131:391–393

Mattern J, Volm M (1982) Clinical relevance of predictive tests for cancer chemotherapy. Cancer Treatm Rev 9:267–270

Mattern J, Wayss K, Volm M (1986) Stellenwert der Zytostatikatestung in der Therapie maligner Tumoren. Dtsch Med Wochenschr 111:676–678

Pavelic K, Bulbul MA, Slocum HK, Rustum YM, Bernacki RJ (1986) Growth of human urological tumors on extracellular matrix as a model for the in vitro cultivation of primary human tumor explants. Cancer Res 46:3653–3662

Salmon SE, Hamburg AW (1978) Quantitation of differential sensitivity of human tumor stem cells to anti-cancer agents. N Engl J Med 298:1321

Von Hoff DD, Clark GM, et al (1983) Prospective clinical trial of a human tumor cloning system. Cancer Res 43:1926–1931

In Vitro Colony Growth Dynamics of the MATLyLu Tumor and Six New Dunning Rat Prostatic Tumor Cell Lines

W. F. J. Feitz[1,3], A. J. M. C. Beniers[1], H. L. M. Beck[2], B. Th. Hendriks[1], W. P. Peelen[1], and F. M. J. Debruyne[1]

Introduction

Since the first description of the Dunning rat prostate tumor (Dunning 1963) several sublines of this tumor, originating from the dorsal lobe of rat prostatic tissue, have been described (Claflin and McKinney 1977; Isaacs et al. 1978; Isaacs et al. 1981; Smolev et al. 1977). One of these tumor lines, the MATLyLu tumor line which shows metastatic potential to lymph nodes and lung tissue (Isaacs et al. 1981), has been investigated over several years in our laboratory.

Recently 6 tumor cell lines have been developed from different sublines of solid rat prostatic tumor lines (Isaacs et al. 1986).

The development of the Human Tumor Cloning System (HTCS) led to extensive studies of this systems applicability for in vitro chemosensitivity tests (Hamburger and Salmon 1977; Salmon 1980). For studies of the dynamics of tumor cell colony development over time an automated colony counter can be used (Herman et al. 1983) and with this counting method the use of "temporal growth curves" was introduced for the evaluation of the HTCS cultures (Kirkels et al. 1983). This evaluation method can be used to study the growth potential of tumor cells and the effectivity of cytostatic agents in HTCS (Feitz et al. 1986; Verheyen et al. 1985). Recently, improvements of the HTCS have been described by using a cytotoxic control and a vital cell staining method (Alley and Lieber 1984; Lieber 1984; Shoemaker et al. 1985).

The purpose of the current study was to characterize the growth potential and growth pattern of the Dunning rat prostatic tumor MATLyLu as well as the six different Dunning rat prostatic cell lines in the HTCS. Also, the value of a cytotoxic control as well as a vital cell (colony) staining method in the temporal growth curve evaluation method of tumor colony development in HTCS was a subject of study.

Material and Methods

The MATLyLu tumor line as well as six different cell lines (AT-1, AT-2, AT-3, MATLu, MATLyLu and the G cell line) derived from solid tumors of the Dunning R 3327 rat prostatic tumor model system were used in this study. The MATLyLu tumor line was kept in serial passages in Fischer-Copenhagen (F336) rats. Each cell line was kept in a monolayer culture for maintenance and single cell suspensions

[1]Department of Urology, Radboud Hospital, Nijmegen University, P.O.Box 9101, NL-6500 HB Nijmegen
[2]Department of Pathologic Anatomy, Radboud Hospital, Nijmegen University, P.O. Box 9101, NL-6500 HB Nijmegen
[3]Department of General Surgery, SDZ, NL-Deventer

Investigative Urology 2
Edited by G. H. Jacobi et al.

were prepared from all cell lines by trypsinization of the cultures in a growing state. From a stock solution containing 3E6 cells/ml, eighteen 35 mm double layer soft agar culture plates at different concentrations of cells/dish were immediately plated without further processing as described before (Feitz et al. 1986; Herman et al. 1983; Kirkels et al. 1983; Verheyen et al. 1985; Salmon 1980).

The tumor cells from the MATLyLu tumor were plated in a cell concentration of 3, 5 and 10E3 cells/dish and an extra culture of 18 dishes with 5000 cells/dish was plated and treated with mercuric-chloride (HgCl2, 100 µg/ml, final culture concentration). From one of the growth cultures, part of the tumor cell suspension was fixed in 70% ethanol (−20°C) for flow cytometrical analysis. After colony formation in culture, they were washed out of the culture dishes and these cells were again fixed for flow cytometric analysis.

The cell lines AT-1, AT-2, AT-3 and MATLu were plated at 3, 5 and 10E3 cells/dish. The MATLyLu cell line was plated with 0.75, 1.5, 3 and 5E3 cells/dish and for the G cell line a concentration of 5, 10 and 15E3 was used. As a cytotoxic control 18 dishes of each cell line were plated for culture with 5000 cells/dish and treated with mercuric chloride as an overlayer of 200 µl/dish after plating of the cells (Alley and Lieber 1984; Shoemaker et al. 1985). The cultures were then incubated at 37°C at 6% CO_2 in a humidified atmosphere.

Assessment of in vitro colony formation was performed using the tetrazolium chloride (INT) (Aldrich Chemical Co., I-1040-6). Optimal colony staining was achieved by applying 200 µl of INT solution (1 mg/ml) to the surface of each culture followed by reincubation at 37°C, 6% CO_2, and 98% relative humidity for 20–24 h (Alley et al. 1982; Bol et al. 1977; Schaeffer and Friend 1976).

All colony counting was performed using the Omnicon Fas II automated colony counter (Milton Roy, Inc, Analytical Product Division, Rochester, NY) as previously described (Herman et al. 1983; Salmon et al. 1984; Feitz et al. 1986; Kirkels et al. 1983; Verheyen et al. 1985). 6 dishes were used as a control for counting procedures in which dots of indian ink (sized in the counting range) were dipped. These dishes were counted during all culture periods in which the variation in counted numbers was less then 5%. Colony formation was checked by optical control with a Leitz inverted microscope. Colonies were counted and characterized based on optical density, shape and diameter ranging between 60 and 400 µ in size by the Omnicon Fas II. 2 methods for the evaluation of colony growth with the Omnicon were used: 1) routine detection of colonies using a constant treshold for the discrimination of structures from the background and 2) a new method using INT stained colonies, detected by a constant treshold as described by Alley and Lieber (1984).

Flow cytometric analysis was performed using a Cytofluorograph 50 H (Ortho Instruments, Westwood, MA) as described before (Verheyen et al. 1985). All data was stored in correlated (list) mode on a PDP 11/34 computer (Digital, Malboro, MA) for subsequent data analysis.

Results

The MATLyLu tumor cells are preferentially growing in this Human Tumor Cloning System (HTCS). The cell suspension of the MATLyLu tumor contained a cell population with a normal as well as a cell population with an abnormal DNA stemline

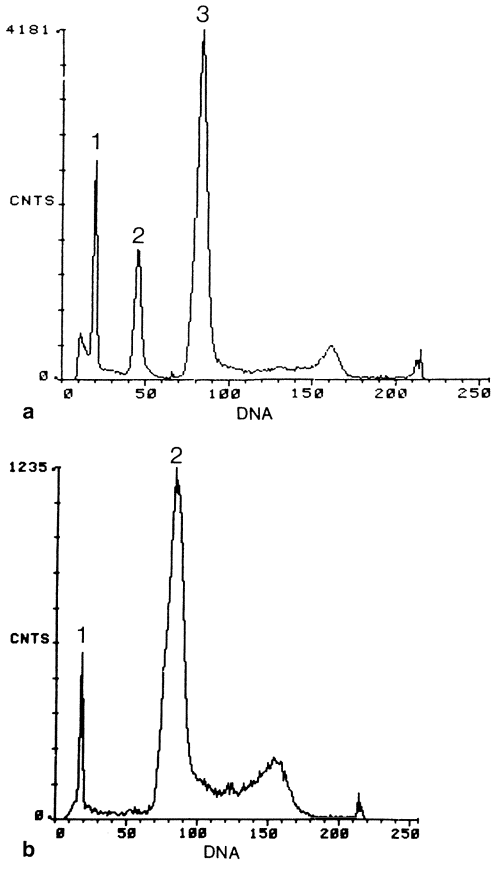

Fig. 1. a DNA histogram of the flow cytometric analysis of a cell suspension of the MATLyLu tumor line before culture showing an internal control of CRBC *(1)*, diploid cell population *(2)* and the aneuploid cell population *(3;* DNA-index = 1.8). **b** DNA histogram of cells from colonies harvested after culture in HTCS with CRBC as an internal standard *(1)* and the aneuploid cell population *(2;* DNA-index = 1.8). Notice the absence of the diploid cell population

(Fig. 1a). However, the FCM analysis of cells from colonies harvested after culture in the HTCS showed to contain only the cell population with an abnormal DNA content (Fig. 1b). When colony development in culture was evaluated with the temporal growth curve method, no major differences were seen between the normal counted dishes and the INT stained dishes 1 day later, in culture. Cultures of MATLyLu tumor cells were plated as normal but treated with mercuric chloride as described above on day 7 after cell plating when growth of colonies could be detected. The number of colonies counted thereafter, with or without INT staining, did not increase anymore, but viable structures were still present at day 14 of culture as could be detected by the omnicon counting and "viable" cells could be seen after the INT staining.

All Dunning rat prostatic cell lines used in this study showed the formation of tumor cell colonies in the HTCS. As these tumor cell colonies can be detected by the automated colony counter, a dynamic growth study was performed in which the growth patterns of the tumor lines of normal cultures and INT stained cultures were compared. An example of the growth patterns of a cell line culture in the HTCS is shown by the temporal growth curves of different cell concentrations plated of the MATLyLu cell line (Fig. 2a). This shows the colony development over time, evaluated

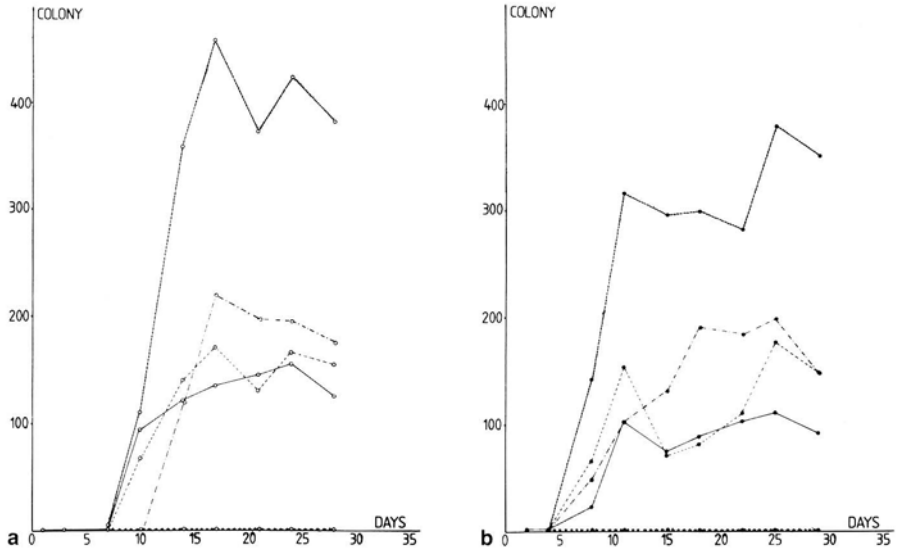

Fig. 2. a Growth curves of the MATLyLu tumor cell line in HTCS of colony formation with the routinely used automated colony counting method. Dishes were plated with 750 (○——●), 1,500 (○– – –●), 3,000 (○+++●) and 5,000 (○–·–●) cells/dish and as a cytotoxic control, a concentration of 5,000 cells/dish treated with mercuric-chloride, was used. **b** Growth curves of the MATLyLu tumor cells in HTCS of **a** after 24 h incubation with INT and evaluated with the automated colony counter. Note the decreased colony formation in the dishes plated with 5,000 cells/dish and the absence of colonies in the dishes treated on day 1 with mercuric-chloride

by the detection of objects larger than 60 μ in diameter. It also shows the presence of colonies of this size detected after 7 days in culture with the unstained routine counting procedure. A peak number of colonies arises around day 16 of culture for all cell concentrations plated but the highest number of colonies is seen in the culture plated with 3000 cells/dish with a plating efficiency of 13% (range: 4.4%–21.0% for the different cell concentrations plated). No colony growth was detected in the cultures treated with mercuric-chloride.

When these cultures are treated according to the INT staining method and counted for colony formation the next day, a resembling growth pattern is seen in comparison to the unstained cultures (Fig. 2b). The detection of colonies, as structures larger than 60 μ, starts after plating of the cell cultures on day 5 for all cell concentrations. A peak number of colonies is seen after 10–25 days in all concentrations of plated cells. The highest number of colonies is counted in the cultures with 3000 cells/dish with a comparable range of the plating efficiency (range: 4.0%–13.0%). Again, no growth of colonies was detected after the treatment of cultures with mercuric chloride on day 1.

The Temporal Growth Curves of the cell lines showed a time course of colony growth of all cell lines with a maximum colony number counted after 10–20 days in culture for the different lines.

For the AT-1 cell line colony formation was detected after 7–10 days in culture with a maximum colony number around day 20 of culturing in the dishes containing 10,000 cells/dish and a plating efficiency of 1.8% (range: 1.0%–1.8%).

AT-2 colony formation was detected after 3–7 days with a maximum colony number around day 20 of culture in the cultures with a concentration of 10,000 cells/dish with a plating efficienty of 2.5% (range: 2.5%–2.6%).

AT-3 colony formation was detected after 10 days and a maximum colony number was detected around day 22 in the cultures with a concentration of 10,000 cells/dish with a plating efficiency of 1.5% (range: 1.5%–2.6%).

For the MATLu cell line colony formation was detected after 4–7 days and a maximum colony number was seen around day 16 in the culture dishes with a concentration of 3,000 cells/dish which had a plating efficiency of 3.3% (range: 0.6%–3.3%).

In the G cell line colony formation was detected after 7 days in culture with a maximum colony number around day 30 of culture in the culture dishes with a concentration of 15,000 cells/dish with a plating efficiency of 2.2% (range: 1.6%–2.2%).

No growth of colonies was seen in any of the cytotoxic control cultures of the tumor cell lines.

Discussion

Since the introduction of the HTCS for chemosensitivity testing of human tumors, it has been propagated in the first years as an optimal system for individual patients tumor chemosensitivity testing (Salmon 1980; Sardosy et al. 1982). In recent years, critical remarks have been made about the system and its applicability in the clinical setting (Lieber 1984). Nowadays, it has been accepted as a research tool for the screening of the effectivity of new developed drugs and as a model system to study biological tumor cell potentials (Shoemaker et al. 1985; Verheyen et al. 1985).

The present study shows the growth capacity and growth patterns of tumor cells of the MATLyLu tumor in HTCS. It also shows that tumor cell growth in this system reflects a biological important potential related with the selection of tumor cell populations as tumor cells with an abnormal DNA content showed a preferential growth in our system (Verheyen et al. 1985).

In this study, also the growth potentials were compared of 6 recently developed different rat prostatic tumor cell lines and it could be shown that all cell lines contained colony forming cells. Also, the growth pattern over time was evaluated with the use of an automated colony counter and a temporal growth curve evaluation method (Herman et al. 1983; Kirkels et al. 1983). In this evaluation method, no major difference occurred between the growth patterns from unstained cultures in comparison to the INT stained colonies. The earlier detection of structures in the INT stained cultures might be explained by an increase of the density of cell clumps owing to the dark red color of the metabolized INT. Also, this increase in counted objects could be influenced by the diffusion of INT dye into the surrounding area of the cell clumps which gives an increase in the size of the counted structures. This shows, that there could be an advantage in the use of a vital cell staining method for the detection of early growth (Alley and Lieber 1984) but that this technique is not essential for colony growth detection of cell lines.

An essential contribution in the evaluation of the HTCS was given by the use of the application on day 1 of mercuric-chloride as a cytotoxic control which allows no colony growth at all. Interestingly we noticed that once there are cell clumbs or

colonies formed in culture, the application of a cytotoxic agent did not reduce the counted objects to zero, neither in the unstained or the INT stained cultures and that there are still viable cell clumbs left one week later in culture. The pattern of colony development over time in the growth control and the absence of colony formation in the cytotoxic control supplies the boundaries of possible tumor cell growth in this system.

References

Alley MC, Lieber MM (1984) Improved optical detection of colony enlargement and drug cytotoxicity in primary soft agar cultures of human solid tumour cells. Br J Cancer 49:225–233

Alley MC, Uhl CB, Lieber MM (1982) Improved detection of drug cytotoxicity in the soft agar colony formation assay through use of a metabolizable tetrazolium salt. Life Science 31:3071–3078

Bol S, Engh G, Visser J (1977) A technique for staining haematopoietic colonies in agar cultures. Exp Hematol 5:551–553

Claflin AJ, McKinney FMA (1977) The Dunning R3327 prostate adenocarcinoma in the Fischer-Copenhagen F1 rat: a useful model for immunological studies. Oncology 34:105–109

Dunning WF (1963) Prostate cancer in the rat. Natl Cancer Inst Monogr 12:351–369

Feitz WFJ, Verheyen RHM, Kirkels WJ, Vooijs GP, Debruyne FMJ, Herman CJ (1986) Dynamics of human renal tumor colony growth in vitro. Urol Res 14:109–112

Hamburger AW, Salmon SE (1977) Primary bioassay of human tumor stem cells. Science 197:461–463

Herman CJ, Pelgrim OE, Kirkels WJ (1983) In-use evaluation of the Omnicon automated tumor colony counter. Cytometry 3:439–442

Isaacs JT, Heston WDW, Weissman RM, Coffey DS (1978) Animal models of the hormone – sensitive and insensitive prostatic adenocarcinomas, Dunning R3327 H, R3327 HI and R3327 AT. Cancer Res 38:4353–4359

Isaacs JT, Yu GW, Coffey DS (1981) The characterization of a newly identified, highly metastatic variety of Dunning R3327 rat prostatic adenocarcinoma system: the MATLyLu tumor. Invest Urol 19:20–23

Isaacs JT, Isaacs WB, Feitz WFJ, Scheres J (1986) Establishment and characterisation of seven dunning rat prostatic cancer cell lines and their use in developing methods for predicting metastatic abilities of prostatic cancers. The Prostate 9:261–281

Kirkels WJ, Pelgrim OE, Hoogenboom AJ (1983) Patterns of tumor colony development over time in soft agar culture. Int J Cancer 32:399–406

Lieber MM (1984) Soft agar colony formation assay for in vitro chemotherapy sensitivity testing of human renal cell carcinoma: Mayo Clinic experience. J Urol 131:391–393

Salmon SE (ed) (1980) Cloning of human tumor stem cells. Alan R Liss, New York

Salmon SE, Young L, Leborowitz J (1984) Evaluation of an automated image analysis system for counting human tumor colonies. Int J Cell Cloning 2:142–160

Sardosdy M, Lamm DL, Radwin HM, Hoff DD (1982) Clonogenic assay and in vitro chemosensitivity testing of human urologic malignancies. Cancer 50:1332–1338

Schaeffer WL, Friend K (1976) Efficient detection of soft agar grown colonies using a tetrazolium salt. Cancer Letters 1:259–262

Shoemaker RH, Wolpert-DeFilippes MK, Kern DH (1985) Application of a human tumor colony-forming assay to new drug screening. Cancer Res 45:2145–2153

Smolev JK, Heston WDW, Scott WW, Coffey DS (1977) Characterization of the Dunning R3327 H prostatic adenocarcinoma. An appropriate animal model for prostatic cancer. Cancer Treatm Rep 61:273–287

Verheyen RHM, Feitz WFJ, Beck JLM (1985) Cellular DNA content – correlation with clonogenicity in the human tumour clonogenic cell culture (HTCS) system. Int J Cancer 35:653–657

Verheyen RHM, Feitz WFJ, Kenemans P, Vooys GP, Herman CJ (1985) Time course of ovarian tumour growth in soft agar culture. Br J Cancer 52:707–712

Monoclonal Antibodies Against Cell Surface Antigens of Human Prostate Carcinoma

M. P. Wirth[1], S. Bleistein[1], T. Papadopoulos[1], and J. W. Grups[1]

Introduction

In the past decade monoclonal antibody technique has been found to be a useful tool in the detection of new tumor-associated antigens on various tumor types. Monoclonal antibodies directed against such tumor-associated antigens have already been used to study their value in the immunodetection and immunotherapy of various tumors in animals and in man (Baldwin et al. 1982; Chatal et al. 1984; Mach et al. 1983; Moldofsky et al. 1983; Sears et al. 1984). In prostate cancer the monoclonal antibody technique has also been applied for the detection of new prostate-cancer associated antigens. Several new antigenic structures of prostate cancer could be demonstrated by monoclonal antibodies. The clinical importance of these antigens for immunotherapy or immunodetection depends on the restriction of these structures to only prostate cancer cells. A tissue specific prostate marker, however, could also be used in the immunodetection of metastases or immunotherapy. For immunotherapy and in vivo immunodetection only the detection of a tumor associated membrane antigen is necessary. The currently available tumor markers, the prostate specific acid phosphatase (PAP) and the prostate specific antigen (PSA), however, are intracellular structures. Therefore, the search for new prostate cancer or prostate tissue associated membrane antigens is necessary to achieve progress in immunodiagnosis and immunotherapy of prostate cancer by the use of monoclonal antibodies.

Material and Methods

Male BALB/c mice were immunized 4–8 times by intravenous and/or intraperitoneal injection of 5×10^6–10^7 viable tumor cells from prostatic cancer cell lines DU145, PC3, LNCAP, 1013L and PC93.

Spleen cells from immunized mice were fused with P3 × 63Ag8 and/or P3 × 63Ag8/653 myeloma cells using RPMI 1640 medium (Fa. Gibco, Karlsruhe) with 50% polyethylenglycol (Fa. Roth, Karlsruhe) with a molecular weight of 1,500. A ratio of 10 : 1 (spleen cells: myeloma-cells) was used. Following the cell fusion the cells were washed and resuspended in RPMI 1640 medium containing 10% fetal calf serum and $1 \times 10^{-4} M$ hypoxanthine, $4 \times 10^{-7} M$ aminopterin and $6.4 \times 10^{-5} M$ thymidine (Fa. Boehringer, Mannheim).

The cells were seeded in 96-well microtiter plates (Costar, Cambridge, MA) in 0.2 ml aliquots.

[1] Urologische Klinik und Poliklinik der Universität Würzburg, Josef-Schneider-Str. 2, D-8700 Würzburg

Investigative Urology 2
Edited by G. H. Jacobi et al.

Supernatants from growing hybridomas were screened for binding activity against various tumor-cells using the ABC immunoperoxidase staining technique (Fa. Vector, USA) as described by Hsu et al. (1981a). The cells used for specificity testing were attached to poly-L-lysin (50 µg/ml) pretreated microtiter-plates (Fa. Costar, USA) according to a technique described by Kennett (1980) and fixed with glutaraldehyde (0.5%). Hybridomas of interest were recloned for at least 2 times by the limiting dilution technique.

For further analysis of the binding activity of the monoclonal antibodies immunohistochemic analyses were performed applying the avidin-biotin-immunoperoxidase technique as described by Hsu et al. 1981b. Frozen sections and deparaffinized sections of 5 µm thickness were used for testing.

Antibody binding against prostatic acid phosphatase was measured by a modification of an enzyme immuno-assay (Fa. Behring Werke AG, Marburg).

Results

The development of 3 monoclonal antibodies directed against different membrane structures of human prostate cancer cells is reported. The hybridoma cells producing monoclonal antibodies H3, H5 and H7 have been doubly cloned by limiting dilution technique and expanded in cell culture. The binding specificity of these monoclonal antibodies was investigated on different cell lines and human tissues.

The enzyme immunological analysis of monoclonal antibodies on different human tumor cell lines is shown in Table 1. The monoclonal antibody H3 was directed only against 2 of the 3 tested prostatic carcinoma cell lines. The antibody H7 revealed a binding only on one of three prostatic carcinoma cell lines and not on other tumors tested. The antibody H5 showed a broader spectrum of binding specificity. Beside all 3 prostatic cancer cell lines, this monoclonal antibody reacted with a bladder tumor cell line, and leukemia cells also. None of these 3 monoclonal antibodies was directed against prostatic acid phosphatase.

The specificity of these monoclonal antibodies was further analyzed on a variety of human malignant and normal tissues (Table 2).

Table 1. Enzyme-immunological analysis of the specificity of monoclonal antibodies

Cell lines	Origin	Monoclonal antibody		
		H3	H5	H7
DU 145	Prostate cancer	+	+	−
PC 93	Prostate cancer	+	+	+
PC 3	Prostate cancer	−	+	−
T 24	Bladder cancer	−	+	−
Ca Ki 1	Renal cell carcinoma	−	−	−
Ca Ki 2	Renal cell carcinoma	−	−	−
K 562	Leukemia	−	−	−

Table 2. Immunohistochemical analysis of the specificity of monoclonal antibodies

Tissue	Monoclonal antibody		
	H3 n/+	H5 n/+	H7 n/+
Prostatic carcinoma	4/2	4/2	7/3
Benign prostatic hyperplasia	4/4	4/3	8/6
Bladder cancer	2/1	4/0	2/0
Renal cell carcinoma	1/1	1/1	1/1
Nephroblastoma	1/1	1/1	1/0
Ca of the stomach	1/1	–	1/0
Ca of the mamma	1/0	–	1/0
Cervix cancer	1/1	–	1/0
Ca of the pancreas	1/1	–	1/0
Normal colon	1/0	–	1/0
Normal skin	1/1	–	1/0

Fig. 1. Binding of monoclonal antibody H3 on benign prostatic hyperplasia. Visualized by immunohistochemical staining technique as dark parts

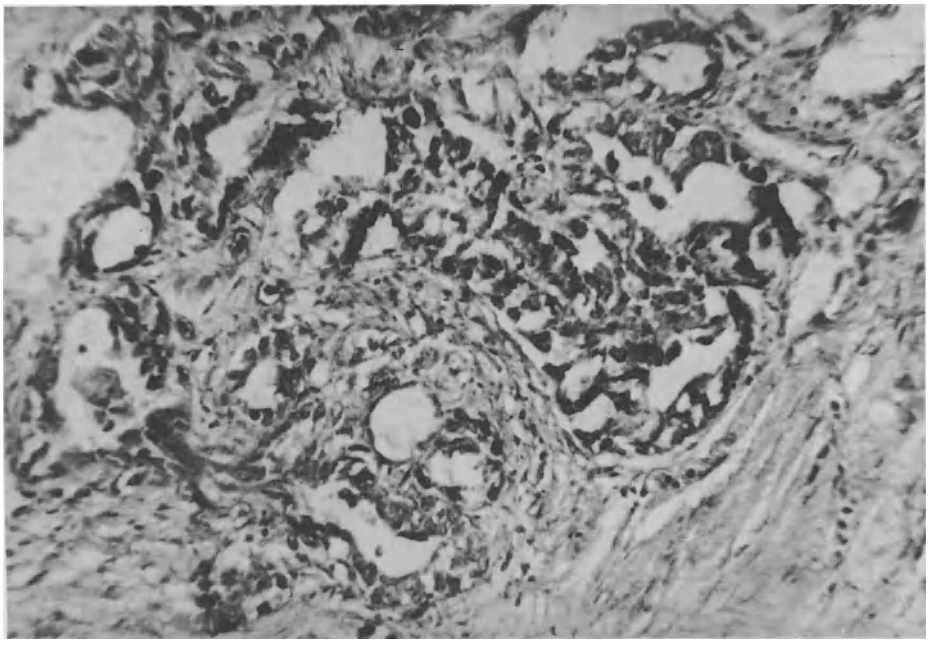

Fig. 2. Binding of monoclonal antibody H3 on prostatic carcinoma cells. Visualized by immunohistochemical staining technique as dark parts

The antibody H3 showed in this study a reaction with 2/4 prostatic carcinomas and with 4 of 4 cases of benign prostatic hyperplasia (Table 2; Figs. 1, 2). Binding of this monoclonal antibody was also observed on bladder cancer, renal cell carcinoma, nephroblastoma, cervix cancer, pancreatic cancer and normal skin.

Monoclonal antibody H5 did bind on a portion of the prostate cancer and benign prostatic hyperplasia tested (Table 2). No reaction was seen on bladder cancer. However, binding of this antibody occurred on renal cell cancer and nephroblastoma.

The monoclonal antibody H7 showed a binding on 3/7 prostatic cancer tissues and on 6/8 benign prostatic hyperplasia specimen from different patients. From 9 other tissues tested, a reactivity of this antibody was only present on renal cell cancer.

Discussion

Several monoclonal antibodies against prostatic cancer have been developed so far (Biermann et al. 1982; Carrol et al. 1984; Clarke et al. 1982; Frankel et al. 1982; Lowe et al. 1984; Raynor et al. 1984; Starling et al. 1982, 1986; Ware et al. 1982; Webb et al. 1983). However, until now, no monoclonal antibody directed against a membrane antigen only present on prostatic cancer cells has been reported.

The herein described monoclonal antibodies also bind on other tissues than prostate cancer. The specificity of these antibodies has been determined on different

human tumor cell lines and various malignant and normal human tissues. The results demonstrate that an analysis of the specificity of the monoclonal antibodies on cell lines is not sufficient. The testing on cell lines can only be used as a screening assay (Stuhlmiller et al. 1982).

The immunohistochemic studies on different tissues are a suitable method for further analysis of the specificity of such monoclonal antibodies. The monoclonal antibody H3 which originally showed promise for being specific for testing cell-lines showed a broad tissue binding activity.

The monoclonal antibody H7 which is directed against a part of prostate cancer tissue and benign prostatic hyperplasia, however, seems to be interesting. This antibody shwos in the specificity analysis an additional binding on only renal cell cancer out of 9 other normal and malignant tissues tested. This antibody possibly identifies a differentiation antigen of prostate cancer which is also present in benign prostatic hyperplasia and could be lost during malignant transformation.

Further analysis is required to investigate this problem. Whether this antibody is suitable for immunodiagnosis of a certain portion of prostate cancer is currently under investigation using xenotransplanted prostatic carcinoma in nude mice.

References

Baldwin RW, Embleton MJ, Pimm MV (1982) Monoclonal antibodies for radioimmunodetection of tumours and for targeting. Bull Cancer (Paris) 70:132–136

Biermann S, Goecke W, Cailloud R, Senge T, Falkenberg FW (1982) Monoclonal antibodies against antigens of human prostatic cancer. Immunbiol 162:328

Carrol AM, Zalutsky M, Schatten S, Bhan A, Perry LL, Sobotka C, Benaverraf B, Greene MI (1984) Monoclonal antibodies to tissue-specific cell surface antigens. I. Characterization of an antibody to a prostate tissue antigen. Clin Immunol Immunopathol 33:268–281

Chatal JF, Saccavini JC, Fumoleau P, Dozüllard JY, Curtet C, Kremer M, Mevel B, Koprowski H (1984) Immunoscintigraphy of colon carcinoma. J Nucl Med 25:307–314

Clarke SM, Merchant DJ, Starling JJ (1982) Monoclonal antibodies against a soluble cytoplasmic antigen in human prostatic epithelial cells. Prostate 3:203–214

Frankel AE, Rouse RV, Herzenberg LA (1982) Human prostate specific and shared differentiation antigens defined by monoclonal antibodies. Proc Natl Acad Sci 79:903–907

Hsu SM, Raine L, Fanger H (1981a) The use of avidin-biotin-peroxidase complex (ABC) in immunoperoxidase techniques. A comparison between ABC and unlabeled antibody (PAP) procedures. J Histochem Cytochem 29:577–580

Hsu SM, Raine L, Fanger H (1981b) A comparative study of the peroxidase-antiperoxidase method and an avidin-biotin complex method for studying polypeptide hormones with radioimmunoassay antibodies. Am J Clin Pathol 75:734–738

Kennett RH (1980) Enzyme-linked antibody assay with cells attached to polyvinyl chloride plates. In: Kennett RH, McKearn TJ (eds) Monoclonal antibodies. Hybridomas: a new dimension in biological analyses. Plenum Press, New York London, p 376

Lowe DH, Handley HH, Schmidt J, Royston I, Glassy MC (1984) A human monoclonal antibody reactive with human prostate. J Urol 132:780–785

Mach JP, Chatal JT, Lumbroso JD, Buchegger F, Forni M, Ritschard J, Berche C, Douillard JG, Carrel S, Herlyn M, Steplewski Z, Koprowski H (1983) Tumor localization in patients by radiolabeled monoclonal antibodies against colon carcinoma. Cancer Res 43:5593–5600

Moldofsky PJ, Powe J, Mulhern CB Jr, Hammond N, Sears HF, Gatenby RA, Steplewski Z, Koprowski H (1983) Metastatic colon carcinoma detected with radiolabeled F (ab') 2 monoclonal antibody fragments. Radiology 149:549–555

Raynor RH, Hazra TA, Moncure CW, Mohanakumar T (1984) Characterization of a monoclonal antibody, KR-p8, that detects a new prostate-specific marker. J Natl Cancer Inst USA 73:617–625

Sears HF, Herlyn D, Steplewski Z, Koprowski H (1984) Effects of monoclonal antibody immunotherapy on patients with gastrointestinal adenocarcinoma. J Biol Response Modifiers 3:138–150

Starling JL, Sieg SM, Beckett ML, Schellhammer PF, Ladaga LE, Wright GL Jr (1982) Monoclonal antibodies to human prostate and bladder tumor-associated antigens. Cancer Res 42:3084–3089

Starling JJ, Sieg SM, Beckett ML, Wirth PR, Wahab Z, Schellhammer PF, Ladaga LE, Poleskic S, Wright GL Jr (1986) Human prostate tissue antigens defined by murine monoclonal antibodies. Cancer Res 46:367–374

Stuhlmiller GM, Borowitz MJ, Croker BP, Seigler HF (1982) Multiple assay characterization of murine monoclonal anti-melanoma antibodies. Hybridoma 1:447–460

Ware JL, Paulson DF, Parks SF, Webb KS (1982) Production of monoclonal antibody α Pro 3 recognizing a human prostate carcinoma antigen. Cancer Res 42:1215–1222

Webb KS, Ware JL, Parks SF, Briner WH, Paulson DF (1983) Monoclonal antibodies to different epitopes on a prostate tumor-associated antigen. Implications for immunotherapy. Cancer Immunol Immunother 14:155–166

Determination of Nuclear Prostatic Androgen Receptors by FPLC (Fast Protein Liquid Chromatography)

D. M. Wilbert[1], M. Schauer[1], and G. H. Jacobi[1]

Introduction

The experimental detection of steroid receptors, quantitative as well as qualitative, has been received with wide-spread interest in the research of the various effects of steroid hormones during recent years. The quantitative measurement of cyto- and karyoplasmatic prostatic androgen receptors, carried out through such methods as the Dextran-Coated-Charcoal-Method (DCC) (Snochowsky et al. 1977), the gradient centrifugation method (Mainwaring and Milroy 1975; Menon et al. 1978) or the Hydroxyl-apatite process (Murthy et al. 1984; Pavlik and Coulson 1976), represent unprecise or complicated analytical processes, which are due to technical factors, such as proteolytical degradation, the time factor, temperature sensitivity, metabolic and biochemical reactions. Since the status of the estrogen receptors – especially regarding breast cancer – is currently a routine feature of therapeutic considerations, a practicable, valid check up process for hormonal therapeutic options as well as for the status of basic research relating to etiology and pathogenesis of benign and malignant prostatic changes appears to be a sensible project.

The goal of the method to be introduced is the qualitative and quantitative isolation of a specific nucleoplasmic androgen receptor via the process of Protein Liquid Chromatography (FPLC, Pharmacia, – Sweden) by selective column anion exchange resins and subsequent separation into protein fragments.

Material and Methods

Prostatic tissue samples (1–3 g) stored in liquid nitrogen were pulverized under refrigeration after the addition of TESM buffer (Tris HCl 0.01 *M*, EDTA 1 m*M*, Sodiummolybdate 10 m*M* and Monothioglycerol 12 m*M*, pH 7.4, T 4°C) by an "Ultra-Turrax-Homogenisator" (Firm Junke & Kunkel). 15 min later the cell organells were centrifuged in a minifuge (Heraeus-Christ) at a speed of 6,000 revolutions per min. After a renewed suspension of the sediment in solution and a 3-time washing with TESM buffer, the remaining sediment was flushed with TEDR buffer (Tris – HCl s.o., EDTA s.o., Dithiotreitol 1 m*M* and KCL 0.6 *M*) and was followed by a splitting of the nuclear membranes in an ultrasound machine (Braun, Melsungen, Braunsonic 300). The resulting extract was placed in an ultracentrifuge (Beckman Model 25–50, Rotor Ti 75, Acceleration 8.0) with 104,000 g at 2°C and was centrifuged for 1 h. The upper lipid layer was separated from the thus produced nucleoplasma. Sodiummolybdate as a phosphatase inhibitor and monothioglycerol influenced the pro-

[1] Klinikum der Johannes Gutenberg-Universität, Urologische Klinik und Poliklinik, Langenbeckstr. 1, D-6500 Mainz

Investigative Urology 2
Edited by G. H. Jacobi et al.

teinase suppression during the entire experiment as a receptor stabilizer (Gaubert et al. 1980; Hawkins et al. 1981; Noma et al. 1980), whereby the maintenance of a cooling chain of 4°C assisted the attempt to take care of the high temperature sensitivity of the receptor complex.

The incubation of the nuclear extract was performed in a 1 ml-volume with tritium-labelled dihydrotestosterone (^{3}H-DHT) (Firm NEN, specific activity 208 Ci/mmol) in gradually larger concentrations of 1 to 20 n*M* and a constant, 200 X excess of non-labelled DHT (Serva, Heidelberg) in a time-frame of 18 h.

Competition studies with constant concentrated radioactive nucleids (10 n*M* ^{3}H-DHT) and increasing excess of DHT (20 n*M*–5 µm), testosterone (100 n*M*–5 µm) and estradiol (100 n*M*–5 µm) (Sigma, Munich), were carried out just like in parallel experiments such as the above-mentioned DHT-incubation experiment, and with 20 n*M* ^{3}H-R1881 with and without 500 X excess in triamcinolonacetonide additive (progesterone receptor blockade) under otherwise identical conditions (buffer solutions, temperature, tissue samples).

In the DCC-Scatchard Plots, the incubation volume was 300 µl with a concentration of 1 to 20 n*M* ^{3}H-DHT and 200 X excess of cold DHT.

After equalizing the incubated nucleoplasmic extract (18 h) and separating the free steroid hormones with 330 µl (100 µl in case of the non-FPLC Scatchard Plot) of Dextran-Coated-Charcoal (1% activated charcoal, Sigma, Munich; Dextran T70, Pharmacia, Sweden; Tris-HCl 0.01 *M* and EDTA 1 m*M*, 4°C, pH = 7.4) as well as cleansing the sample with a Millex GS filter 0.22 µm (Millipore SA, France), the protein mixture can be separated out by the FPLC-system.

The principle of separating complex protein mixtures is carried out by column anion exchange resins "Mono Q" (Pharmacia, Sweden) via the employment of an individually programmable salt (NaCl)-gradient, which in turn reduces the proteins in form of anions which can be found in the buffer solution according to their specific parameters, i.e., nK-values, and through the increasingly concentrated salt solutions, out of whose electrostatic bonding a new carrier is selected.

A selected salt process is fed into the analytic programmer and control unit; the buffer solutions (Tris HCL, 0.01 *M*, EDTA 1 m*M*, Sodiummolybdate 10 m*M*, Monothioglycerol 12 m*M*) are mixed until they reach the identical NaCl level of 0.8 *M*/l in solution B).

500 µl of nuclear extract were fed into the system in a trial run of 1.5 ml/min, were divided into 36 groups of 0.63 ml per aliquot, and were measured by a tritium-β-Counter (Intertechnique, Type SL 30) with appropriate scintillation fluid (Unisolve I, Zimmer, France).

The resulting radioactivity, together with the protein concentration, achieved by absorption measurements within the system, is graphically reproduced.

The DNA-analysis for later quantitative receptor measurement was modified according to the diphenyl-reaction and was carried out photometrically according to Burton (Burton 1956; Leyva and Kelly 1974).

Results

The graphic illustration of the receptor contents according to the applied DCC method is shown in Fig. 1: Curve A shows the entire, curve B the nonspecific and curve C

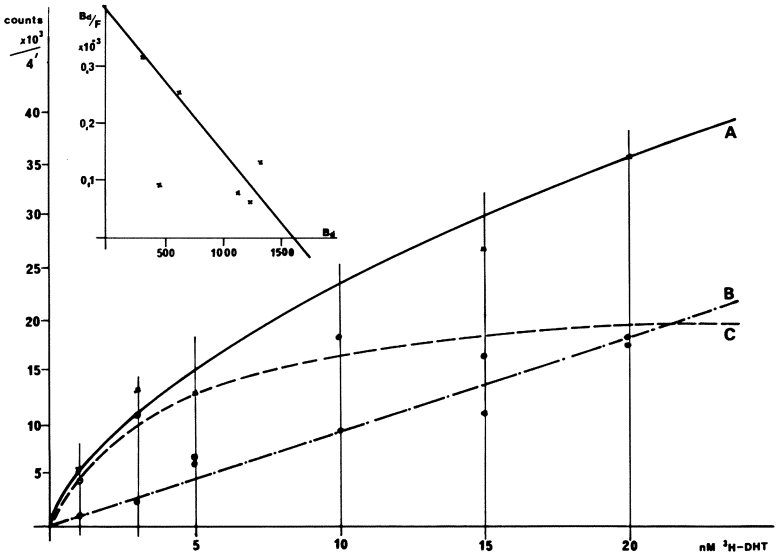

Fig. 1. DCC-Assay, DNA-concentration = 104 µg/ml. *A* 1, 3, 5, 10, 15, 20 n*M* ^{3}H-DHT; *B* 200 X excess of cold DHT; *C* specific androgen binding. *Insert:* Scatchard-Plot, regression rate (B/F). B_{max} = 1635 fmolg/mg DNA, K = $4.06 \times 10^{-9} M$

the specific binding of radioactive dihydrotestosterone in the concentrations of 1 to 20 n*M* ^{3}H-DHT. In the miniature "Scatchard Plot", the mathematical receptor result (B_{max}) of 1635 fmol/mg DNA is compared with a dissociation constant (K_D) of $4.06 \times 10^{-9} M$ (increase of regressions gradient). Comparable results have already been set up by authors like Lieskowsky (Lieskowsky and Bruchovsky 1979) or Sirett (Sirett and Grant 1978).

The relatively high values for the maximal bonding capacity appears to confirm the hypothesis of various authors, which state that the quantitatively largest percentage of the androgen-receptor-complexes are found in the nucleus and not in cytosol (Hicks and Walsh 1979; Menon et al. 1978).

Identical tissue samples, which were chromatographically divided in the above described system, lead to optimal results in the NaCl-gradient tests with medium increases and maximum salt concentrations of approximately 0.8 *M*/l in buffer solution 3. Exact adherence to the neutral pH values yielded high recovery rates of receptors.

The activity curve showing increasingly higher incubation concentrates of 2 to 20 n*M* ^{3}H-DHT ± 200X excess of cold DHT is labelled in Figs. 2–5 as "FPLC Assay".

A radioactive peak appears in both the 200 mmol/l and the 380 mmol/l-NaCl areas, whereby only the increase in the 200 mmol/l area shows a specific saturation. Protests that this could only be the transport protein SHBG and not a specific androgen-receptor can be refuted by several arguments: In controls with 20 n*M* ^{3}H-Methyltrienolone (R1881) incubated tests (results not shown), the specifically saturated peaks reappear; further use of dihydrotestosterone instead of R1881 was carried out because of the relatively small radioactivity of the R1881 (87.6 Ci/mmol) as compared with its natural analogue DHT (208 Ci/mmol) to achieve valid measurements in the liquid scintillation counter.

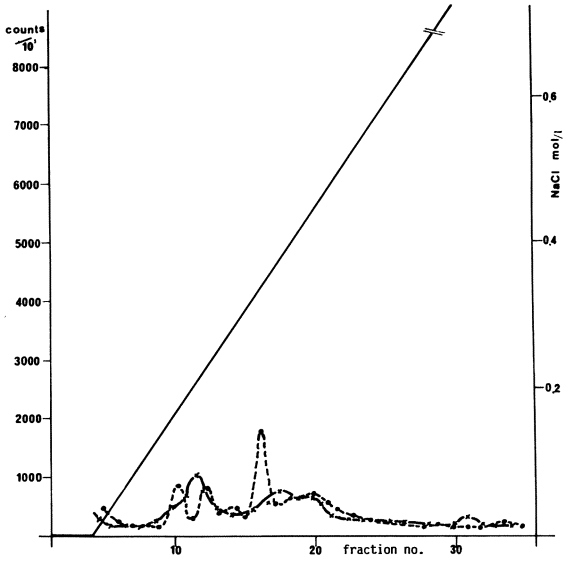

Figs. 2–5. FPLC Assay, DNA concentration = 166 µg/ml, NaCl-rate: 0–0, 8 *M*. 2, 5, 10, 20 n*M* ^{3}H-DHT. 2, 5, 10, 20 n*M* ^{3}H-DHT + 200 X excess of cold DHT

Fig. 2

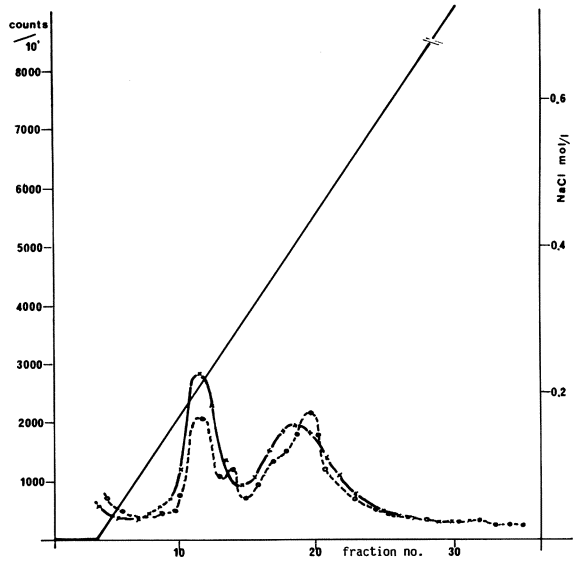

Fig. 3

Additionally, SHBG or albumin contaminations were avoided by intensive washings prior to the nuclear membrane sonication.

Experiments with cytosol and serum samples, which are not further described here, resulted in different peaks identified at concentrations of 165 mmol/l for SHBG and 220 mmol/l for albumin.

The depiction of the FPLC-trials as a Scatchard Plot (Fig. 6) shows a maximum bonding capacity of just 62.3 fmol/ng DNA and a dissociation constant of 9.2×10^{-9} *M* in corresponding tissue. Other tissue samples showed corresponding receptor

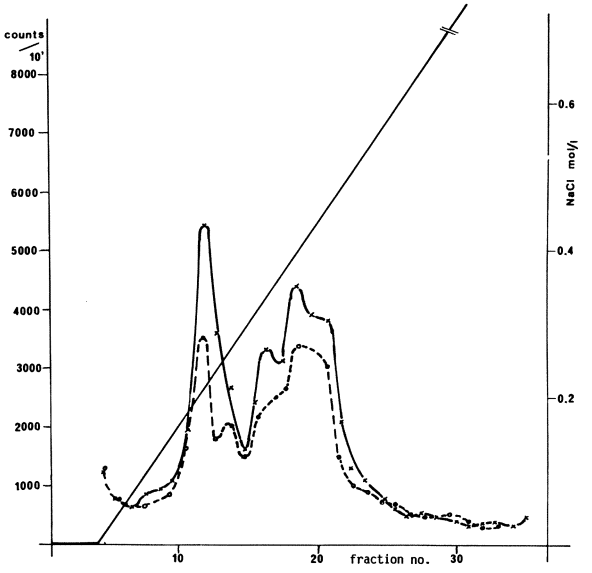

Fig. 4

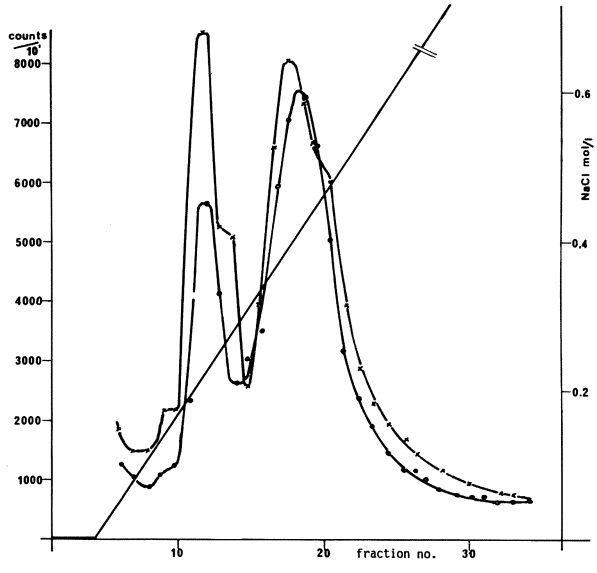

Fig. 5

contents of 202.2 fmol/ng DNA or 100.7 fmol/ng DNA respectively, thereby demonstrating the reproduceability of this method.

Accordingly, the applied chromatographic technique can also be used in competition studies.

The affinity of the androgen receptors to different steroids of increasing competitor hormone concentrations is pictured in Fig. 7 in a semi-logarithmic manner.

In accord with the above-mentioned nuclear-FPLC-tests, the 500 µl 10 n*M* ^{3}H-DHT incubated karyoplasmic samples were replaced step by step by higher concen-

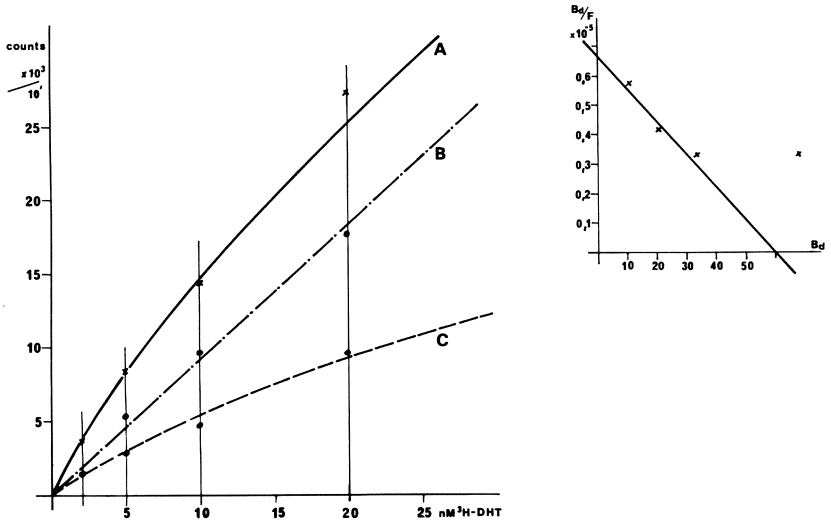

Fig. 6. FPLC-Scatchard-Plot illustration of Figs. 2–5. *A* 2, 5, 10, 20 n*M* ^{3}H-DHT; *B* 200 X excess of cold DHT; *C* specific androgen binding. *Insert:* Scatchard-Plot, regression rate (B/F). B_{max} = 62.3 fmol/mg DNA, K = $9.2 \times 10^{-9} M$

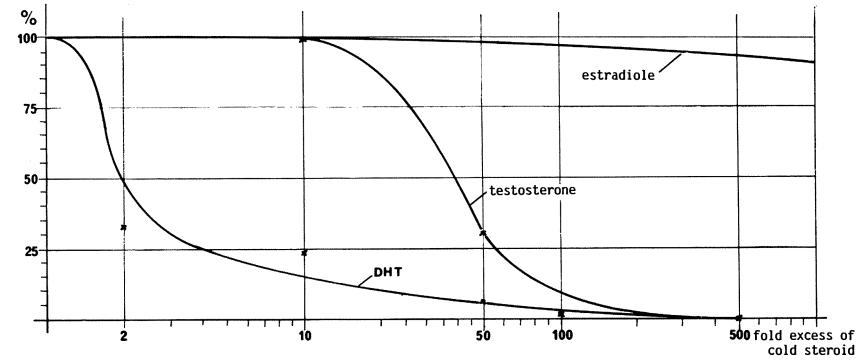

Fig. 7. Competitive binding (FPLC). *Ordinate:* percentage of the spec. given steroid; *abcissa:* logarhythm of the excess cold steroid

trations (20, 100, 500, 1000 and 5000 X excess) of cold DHT, testosterone (Serva, Heidelberg) and Estrodiol (Sigma, Munich).

Since the highly specific DHT-receptor complex is known for its reduced affinity to other steroid hormones (Hicks and Walsh 1979; Lieskovsky and Bruchowsky 1979; Menon et al. 1978), testosterone competed, as could be expected, in the higher than 200 X excess group. Estrodiol showed no competition up to the observed concentration level of 5 μ*M* (Fig. 7).

The results of the completed chromatographic extraction assays and competition tests proove the existance of the androgen-receptor and its required specifity (K_D) as well as low maximum binding capacity (B_{max}).

Discussion

With the application of the FPLC System, a new method for selected, qualitative and quantitative extraction of a specific nucleo-plasmic, androgen-receptor in human prostatic-adenomatous tissues has been found.

The discrepancy between the amount of receptor in the DCC and the FPLC confirms the problem of varying results also seen in density-gradient examinations. Therefore, the results of presently used quantitative receptor analysis methods have to be interpreted cautiously – at least in connection with androgens. It appears here that a variety of partially unspecific binding ligands have been included which do not belong to the androgen receptor complex (transport proteins, degraded receptors).

The measured receptors, as well as the calculated dissociation constant, lies within the region of the values published by other authors (Lieskowsky and Bruchovsky 1979; Sirett and Grant 1978; Trachtenberg and Walsh 1982) and confirms the required, high specificity at a low B_{max}, which in all tests is found in the "fmol-region". The tissue sampling through prostate biopsy is a prerequisite for the routine clinical receptor analysis.

Through application of the FPLC-system with approximately 500–700 mg – three biopsies respectively – appropriate microassays, as well as necessary histologies, may be performed as single point assays.

The advantage of the chromatographic method lies in the short separation time of approximately 15 min per run, which in turn greatly reduces the complex dissociation and metabolization; and, in the possibility of recovering a pure receptor protein.

Since publications by various authors like Trachtenberg and Walsh (1982), Wagner and Schulze (1978), or Walsh et al. (1979) indicate a correlation between the receptor status and hormonal therapy success rates, it can be said that a broad area of application for a viable nuclear receptor assay may exist.

References

Burton K (1956) A study of the conditions and mechanism of the diphenylamine reaction for the colorometric estimation of deoxyribonucleic acid. Biochem J 62:315

Gaubert CM, Tremblay RR, Dube JY (1980) Effect of sodium molybdate on cytosolic androgen receptors in rat prostate. J Steroid Biochem 13:931

Hawkins EF, Lieskowsky G, Markland FS (1981) Molybdate and the measurement of androgen receptors in prostate cancer. J Clin Endocrinol Metab 53:456

Hicks LL, Walsh PC (1979) A microassay for the measurement of androgen receptors in human prostatic tissue. Steroids 33:389

Leyva A, Kelly W (1974) Ann Biochem 62:173

Lieskowsky G, Bruchovsky N (1979) Assay of nuclear androgen receptor in human prostate. J Urol 121:54

Mainwaring WIP, Milroy EGP (1975) Metabolism and binding of androgens in the human prostate. In: Grayhack JT, Wilson JD, Scherbenski MJ (eds) Benign prostatic hyperplasia. CHEW Publication No (NIH) 76-1113:91–97

Menon M, Tananis CE, McLoughlin MG, Lippman ME, Walsh PC (1977) The measurement of androgen receptors in human prostatic tissue utilizing sucrose density centrifugation and a protamine precipitation assay. J Urol 117:309

Menon M, Tananis CE, Hicks LL, Hawkins EF, McLoughlin MG, Walsh PC (1978) Characterization of the binding of a potent synthetic androgen, methyltrienolone, to human tissues. J Clin Invest 61:150

Murthy BG, Chang CH, Rowley DR, Scardino PT, Tindall DJ (1984) Physiochemical characterization of the androgen receptor from the hyperplastic human prostate. Prostate 5:567

Noma K, Sato B, Nakao K, Nishizawa Y, et al (1980) Effect of molybdate on activation and stabilization of steroid receptors. Endocrinology 107:1205

Pavlik EJ, Coulson PB (1976) Hydroxylapatite "batch" assay for estrogen receptors: increased sensitivity over present receptor assays. J Steroid Biochem 7:357

Sirett DAN, Grant JK (1978) Androgen binding in cytosols and nuclei of human benign hyperplastic prostatic tissue. J Endocrinol 77:101

Snochowski M, Pousette A, Ekman P, Bression D, et al (1977) Characterization and measurement of the androgen receptor in human benign prostatic hyperplasia and prostatic carcinoma. J Clin Endocrinol Metab 45:920

Trachtenberg J, Walsh PC (1982) Correlation of prostatic nuclear androgen receptor content with duration of response and survival following hormonal therapy in advanced prostatic cancer. J Urology 127:466

Wagner RK, Schulze KH (1978) Clinical relevance of androgen receptor content in human prostate carcinoma. Acta Endocrinol (Suppl) 215:139

Walsh PC, Hicks LL, Reiner WG, Trachtenberg J (1979) The use of androgen receptors to predict the duration of hormonal response in prostatic cancer. In: Abstracts, Annual Meeting of the American Urological Association, New York

Receptor Analysis: Data Processing in the Presence of Nonspecific Binding Sites*

H. Moeller[1], Ch. Fusch[1], A. Kuch[1], N. Manolopoulos[1], and G. Oettling[2]

Introduction

In biochemical receptor analysis 2 parameters are of particular interest: the concentration of receptor binding sites and the dissociation constant of the receptor-ligand complex. For this purpose cell fractions or intact cells containing the receptor are incubated *in vitro* with radioactive ligand until equilibrium is achieved:

$$L + R + B \rightleftarrows RL + BL \quad (1)$$

L = free radioactive ligand, R = free receptor, B = free nonspecific binder, RL = radioactive receptor-ligand complex, BL = radioactive complex of ligand and nonspecific binder.

The concentrations in equilibrium depend on the dissociation constants of the complex of ligand and receptor (K_R) and ligand and nonspecific binder (K_B)

$$K_R = \frac{R \cdot L}{RL} \quad (2), \qquad K_B = \frac{B \cdot L}{BL} \quad (3)$$

as well as on the total concentrations of radioactive ligand (L_T), receptor (R_T) and nonspecific binding sites (B_T):

$$L_T = L + RL + BL \quad (4)$$
$$R_T = R + RL \quad (5)$$
$$B_T = B + BL \quad (6)$$

After incubation free and bound ligand are separated by physico-chemical methods which, however, generally fail to separate receptor-bound from non-specifically bound ligand. Therefore, separation yields the fractions L and b = RL + BL. RL must be known for further data processing to evaluate K_R and R_T. This may be performed by applying regression methods to the equation

$$RL = \frac{R_T \cdot L}{K_R + L} \quad (7)$$

Equation (7) follows from a combination of (2) and (5). Non-linear regression may be applied to equation (7). But usually methods of linearization are used (Scatchard 1949; Eisenthal and Cornish-Bowden 1974).

RL may be identified in the fraction b = RL + BL if the receptor binding sites are characterized by low capacity and high affinity and if the non-specific binding sites have a high capacity and low affinity for the ligand:

$$R_T \ll B_T \quad (8) \qquad \text{and } K_R \ll K_B \quad (9)$$

[1] Children's Hospital, University of Tübingen, D-7400 Tübingen
[2] Department of Anatomy, University of Tübingen, D-7400 Tübingen
* Supported by the Deutsche Forschungsgemeinschaft (Mo 315/3-2)

Investigative Urology 2
Edited by G. H. Jacobi et al.

Usually, for each concentration of radioactive ligand L_T a parallel assay (assay 2) is run containing unlabelled ligand $^\circ L_T$ in excess. Its concentration, however, must still be low compared to K_B:

$$L_T \ll {}^\circ L_T \ll K_B \tag{10}$$

Under these conditions (8, 9 and 10) binding of radioactive ligand to the receptor will be suppressed in assay 2 by the unlabelled ligand. Radioactive ligand will only be bound by the nonspecific binder.

In general, the concentration of the receptor-bound ligand in assay 1 $(RL)_1$ is calculated from the difference $\Delta = b_1 - b_2$ of radioactive ligand bound in assays 1 and 2 ("suppressible binding"):

assay 1 (only radioactive ligand L_T):	$b_1 = (RL)_1 + (BL)_1$	+
assay 2 (L_T + unlabelled $^\circ L_T$):	$b_2 = (RL)_2 + (BL)_2$	−

$$\Delta = b_1 - b_2 = (RL)_1. \tag{11}$$

$(RL)_2$ may be neglected when the conditions (8), (9) and (10) are fulfilled, and equation (11) may be used if $(BL)_1 = (BL)_2$ (12).

In the present work, however, we would like to show that in most cases condition (12) is not valid. The errors arising from equation (11) for the evaluation of receptor binding data will be discussed, and we shall prove that alternative methods of data processing as proposed by Rosenthal (1967) and Oettling (1987) yield correct results.

Methods

Calculation of Non-specifically Bound Ligand $(BL)_1$ in Assay 1

The concentration of the nonspecifically bound radioactive ligand is in both assays

$$BL = \frac{B_T \cdot L}{K_B + L} \tag{13}$$

Equation (13) follows from a combination of (3) and (6).

If the concentrations of radioactive (L_T) and unlabelled ($^\circ L_T$) ligand are negligible with respect to K_B (condition 10) equation (13) changes to

$$BL = \frac{B_T}{K_B} \cdot L \tag{14}$$

Thus the concentration of nonspecifically bound radioactive ligand BL is proportional to the concentration of free radioactive ligand L in both assays:

$$\frac{(BL)_1}{(BL)_2} = \frac{L_1}{L_2} \tag{15}$$

Using (15) the concentration of nonspecifically bound ligand in assay 1 $(BL)_1$ may be calculated from the measured concentrations of free ligand in both assays and from

the nonspecifically bound ligand in assay 2 where the concentration of receptor-bound radioactive ligand may be neglected (conditions 8, 9, and 10):

$$(BL)_1 = \frac{L_1}{L_2} \cdot (BL)_2 \tag{15a}$$

On the basis of equation (15a) the simplified equation (11) can be corrected as published by Oettling (1987):

$$\Delta corr = b_1 - b_2 \cdot \frac{L_1}{L_2} = (RL)_1 \tag{16}$$

Concentrations of Free and Bound Ligand when Two Binders Compete for the Ligand

In a system where a receptor and a nonspecific binder compete for the ligand the concentrations of free and bound ligand are described by equations (2), (3), (4), (5), and (6) which may be combined to

$$\begin{aligned} &L^3 + \\ &(R_T + K_R + B_T + K_B - L_T) \times L^2 + \\ &(K_R \times K_B + R_T \times K_B + B_T \times K_R - K_R \times L_T - K_B \times L_T) \times L - \\ &K_R \times K_B \times L_T = 0 \end{aligned} \tag{17}$$

The concentration of free and bound ligand may be calculated if K_R, K_B, R_T and B_T and the total concentration of the ligand L_T are known. We used this equation in order to test the validity of different methods of data processing for the evaluation of K_R and R_T.

For this purpose, we calculated the concentrations of free (L) and bound (b) ligands in a binding system comprising the receptor, a non-specific binder and the ligand. The constants chosen for the receptor were characteristic for high-affinity/low capacity binding:

$$K_R = 10^{-10} M; \quad R_T = 4 \cdot 10^{-10} M \tag{18}$$

while the K_B- and B_T-values of the nonspecific binder were varied within the range of low-affinity/high-capacity binders: $10^{-5} M$ to $10^{-3} M$. L and b were calculated for total concentrations of radioactive ligand L_T varying in the range $10^{-1} \times K_R < L_T < 10 \cdot K_B$. The concentrations of free and bound ligand were calculated for assays containing only radioactive ligand L_T (assay 1: L_1, b_1) and for assays containing the same concentrations of L_T and additional unlabelled $^{\circ}L_T$ in 100-fold excess (assay 2: L_2, b_2).

The concentrations of the free ligand L were calculated from (17) with the iteration method of Newton using the HP-1100-system (Hewlett Packard). The concentrations of the bound ligand b were calculated according to $b = L_T - L$.

Data Processing for Evaluation of K_R and R_T

The results for L_1, b_1, L_2 and b_2 were processed according to different methods for evaluation of K_R and R_T:

1. The concentration of receptor-bound ligand in assay 1 $(RL)_1$ was calculated with the generally used formula $\Delta = b_1 - b_2 = (RL)_1$ (11). Data of Δ and the concentrations of free ligand in assay 1 L_1 were processed according to Scatchard (1949).

2. $(RL)_1$ was calculated with the corrected formula given by Oettling (1987) $\Delta corr = b_1 - b_2 \cdot L_1/L_2$ (16). Data of $\Delta corr$ and the concentrations of L_1 were again processed according to Scatchard (1949).
3. Data of corresponding L_1 and b_1, L_2 and b_2 were processed according to Rosenthal (1967).

The calculated values of K_R and R_T were compared to the correct ones given in (18).

Results

The figures show plots of bound (b) and free (L) radioactive ligand in a system where the constants of the nonspecific binder are $K_B = 10^{-4} M$ and $B_T = 10^{-4} M$ and the true values of the receptor constants $K_R = 10^{-10} M$ and $R_T = 4 \times 10^{-10} M$ (18).

In Fig. 1 the values of b and L are separately plotted for the assays 1 and 2. The inset is the Scatchard plot of the same data. Considerable suppressible binding is seen in the range of $10^{-2} \cdot K_R < L < 10^2 \cdot K_R$ and again in the range $L > 10^{-2} \cdot K_B$. Only the former is due to saturation of receptor binding sites by unlabelled ligand °L while the latter indicates significant competition of labelled and unlabelled ligand for the non-specific binder.

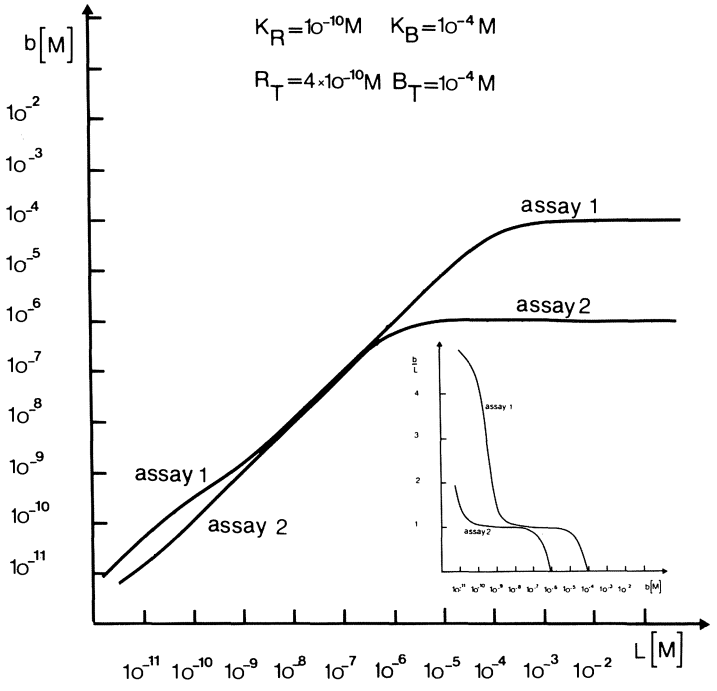

Fig. 1. Concentrations of free (L) and bound (b) radioactive ligand calculated from the simulated binding system. Assay 2 contains in addition a 100-fold excess of unlabelled ligand. The *insert* is the corresponding Scatchard plot

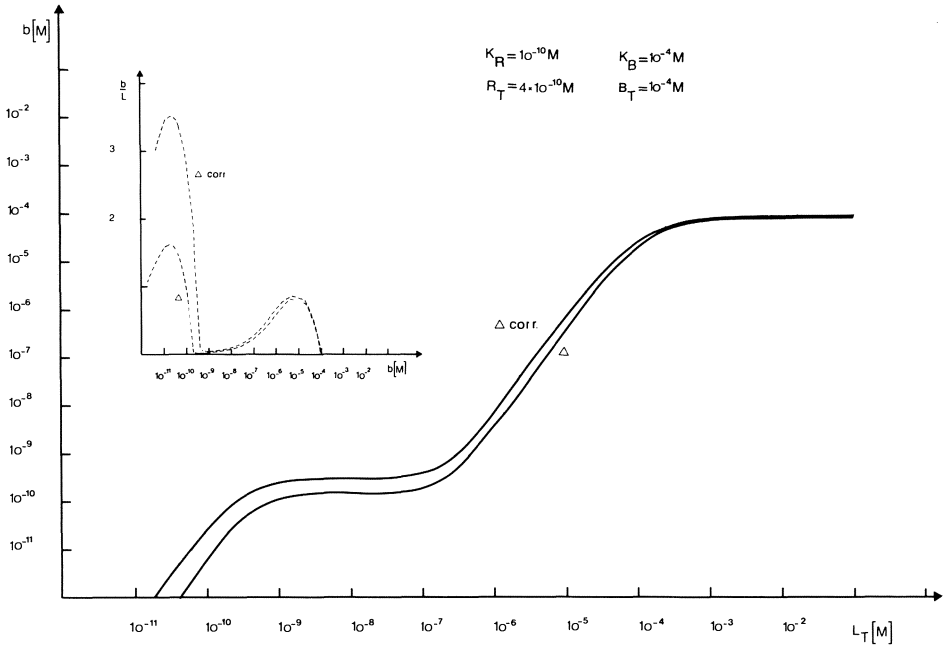

Fig. 2. "Suppressible binding" Δ (11) and corrected "suppressible binding" Δcorr (16) of radioactive ligand calculated from the simulated binding system. Assay 2 contains an additional 100-fold excess of unlabelled ligand. The *insert* is the corresponding Scatchard plot of the data

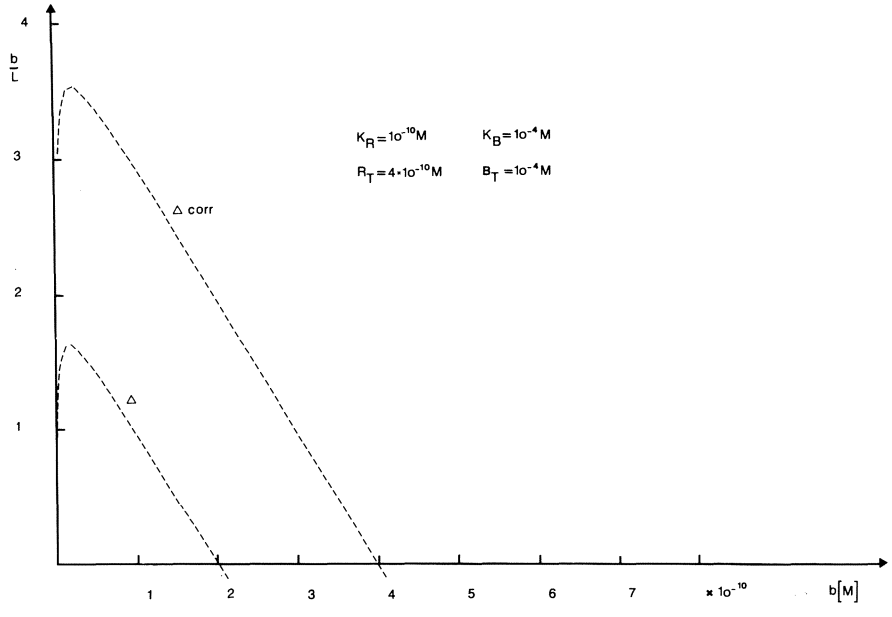

Fig. 3. Scatchard plot of the data given in Fig. 2 within the region of interest for evaluation of K_R and R_T. The correct values are $K_R = 10^{-10}M$ and $R_T = 4 \times 10^{-10}M$

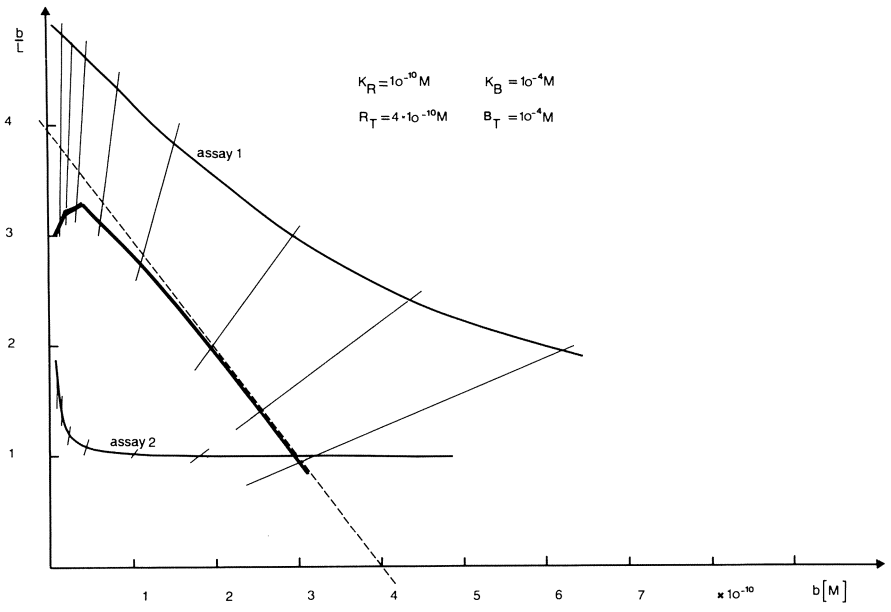

Fig. 4. Scatchard plot of the data given in Fig. 1 limited to the region of interest for the evaluation of K_R and $R_T \cdot K_R$ and R_T are estimated according to Rosenthal (1967)

Table 1. Evaluation of R_T in the simulated binding system by Scatchard plot using the concentration of "suppressible binding sites" Δ (11) as concentration of receptor-bound ligand. The correct value of R_T is 0.40 nM

B_T [nM]	0.01	0.10	1.00
K_B [nM]	R_T [nM]	R_T [nM]	R_T [nM]
0.01	0.20	0.04	0.005
0.10	0.36	0.20	0.040
1.00	0.39	0.36	0.200

Figure 2 shows apparent concentrations of receptor binding sites calculated from the dates given in Fig. 1 with formula (11) (suppressible binding Δ) and with the corrected formula (16) (corrected suppressible binding Δcorr). Both Δ and Δcorr indicate saturation of receptor binding sites in the range of $L_T = 50 \times K_R$ to $500 \times K_R$ [M]. In this range Δcorr yields the correct value of R_T, while Δ underestimates R_T. When L_T exceeds $100 \cdot K_R$ R_T will be overestimated by both formulas.

Figure 3 shows the Scatchard plot for Δ and Δcorr in the region of interest for evaluation of K_R and R_T. Both K_R and R_T are correctly estimated if Δcorr (16) is used while R_T is underestimated by 50% if Δ (11) is employed.

Figure 4 shows that estimation of K_R and R_T according to the graphic method of Rosenthal (1967) also yields the correct values for both constants.

The results shown in the figures may be generalized:

1. K_R is correctly evaluated by all 3 methods.
2. R_T is underestimated using formula (11). The magnitude of the error depends on both the capacity and the affinity of the nonspecific binding sites (Table 1).
3. R_T is correctly evaluated by both the arithmetic method of Oettling (1987), formula (16), and the graphic method of Rosenthal (1967) (Table 1) likewise.

Discussion

For the measurement of specific binding, 2 assays are usually run in parallel: assay 2 containing unlabelled ligand in excess to identify the concentration of specific binding sites. The difference of radioactive ligands bound in both assays $\Delta = b_1 - b_2$ (11) is considered to be identical with the concentration of receptor-bound ligand in assay 1 $(RL)_1$. This is correct if the concentrations of nonspecifically bound ligand in both assays are the same (12). In the present work we have demonstrated that condition (12) is never realized as $(BL)_2$ always exceeds $(BL)_1$. The correct relation of $(BL)_1$ to $(BL)_2$ is given by (15). Thus, $(RL)_1$ will be underestimated by the generally used method (11) of data processing.

We quantified the errors from the incorrect implication of condition (12) using a computer-simulated binding system. While correct values were obtained for the dissociation constant K_R of the receptor ligand complex, the binding capacity may be considerably underestimated. The magnitude of the error depends on the relation of B_T and R_T to B_R and K_R (Table 1).

Moreover, Scatchard plots of "suppressible binding sites" (11) may produce underestimation of R_T although the plots be linear and, therefore, no errors due to non-specific binding sites are suspected (Fig. 3).

The data shows that the evaluation of R_T according to (11) yields significant errors if considerable non-specific binding is encountered. Therefore, we compared 2 alternative methods of data processing: the arithmetic method of Oettling (1987) and the graphic method of Rosenthal (1967). Both give correct results for R_T and K_R (Table 1, Fig. 4).

We conclude that data of receptor analysis should be evaluated according to 1 of the 2 methods if non-specific binding sites are present in the system.

References

Eisenthal R, Cornish-Bowden A (1974) The direct linear plot. A new graphical procedure for estimating enzyme kinetic parameters. Biochem J 139:715–720

Oettling G (1987) Messung der freien und besetzten Androgenrezeptoren im Cytosol der ventralen Rattenprostata. Dissertation, Tübingen

Rosenthal HE (1967) A graphic method for the determination and presentation of binding parameters in a complex system. Anal Biochem 20:525–532

Scatchard G (1949) The attractions of proteins for small molecules and ions. Ann NY Acad Sci 51: 660–672

II. Neurophysiology

Evoked Responses for Differentiating Neurogenic Lesions in the Urogenital System in Patients with Diabetes Mellitus

H. W. M. Anten[1], E. S. C. van Waalwijk van Doorn[1], and F. M. J. Debruyne[1]

Introduction

Neuropathy is one of the most common complications in patients with diabetes mellitus. Normally, this neuropathy is classified as somatic or autonomic. Somatic neuropathy is seen very frequently and can affect every part of the peripheral nerve system (Ellenberg 1982) and autonomic neuropathy can cause functional disorders in almost any organ. In particular, the cardiovascular, gastro-intestinal, sudomotoric, vasomotoric, endocrine and urogenital systems are involved. In case of an autonomic neuropathy both afferent and efferent fibres of the sympathetic and/or parasympathetic nerve systems can be affected (Hosking et al. 1978).

Neurogenic disorders matching with a myelopathy are much less frequently seen. Dorsal column lesions (diagnosed by neuropathological methods) occur in 17%–44% of diabetics (Dolman 1963; Slager 1978).

The frequency of urogenital system dysfunctions is not known clearly. By means of urodynamic diagnostic methods such as flowmetry, cystometry, profilometry, pressure/flow studies and electromyography of the external anal and urethral sphincters, bladder neuropathy was diagnosed in 26% (Rundles 1945) and in 87% (Faerman et al. 1971) of insulin dependent diabetics. In studies on larger groups of unselected insulin dependent diabetics bladder neuropathy was found in approximately 44% (Frimodt-Møller, 1976). Potency disorders have been described in 15%–75% of male diabetics in different age ranges (Rundles 1945; Frimodt-Møller 1976; Fagerberg et al. 1967). Aagenaes (1963) and Faerman et al. (1971) diagnosed impotence as well as bladder neuropathy in 78%–83% of their diabetics. Data concerning sexual disorders in female diabetic patients are very scanty.

Normal micturition and sexual functions demand the integrity of the central and peripheral neural pathways involved (Bradley 1978). Part of these neural pathways can be tested by means of neurophysiological investigative methods. Bradley (1972) introduced a clinically applicable test. He stimulated the bladderneck electrically via 2 catheter-mounted surface ring electrodes. The latency time for the reflex response of the external anal sphincter was obtained by measuring the delay time at a surface electrode in an anal plug. Rushworth (1967), Haldeman et al. (1982a) and Vodusec et al. (1983) measured the latency time of the bulbocavernosus reflex after stimulation of the dorsal nerve of the penis and registration of the EMG activity of the external anal sphincter or bulbocavernosus muscles.

During this decade several authors (Kaplan 1981; Haldeman et al. 1982b; Badr et al. 1984) showed that after stimulation of the pudendal (dorsalis nerve of penis or clitoris) or pelvic nerves, cortical evoked responses could be obtained.

[1]Department of Neurology, "De Goddelijke Voorzienigheid" Hospital, Walramstraat 23, NL-6131 BK Sittard

Investigative Urology 2
Edited by G. H. Jacobi et al.

In the past few years these tests were standardized within our clinics. Electromyography of the external anal sphincter was added and, to increase the information, the tests were judged in combination. Nevertheless, not all the pathways involved are investigated in this study, so this combined method does not yet exclude all neurogenic causes for urogenital system dysfunctions. In the present study the frequency of occurrence of several neurogenic lesions in a group of diabetic patients, diagnosed by the combination of the tests mentioned above, will be described.

Materials and Methods

During electromyography, differences in electrical activity are measured in striated muscle fibres during straining and sometimes also at rest. A bipolar needle electrode is inserted into the external anal sphincter muscle. Commercially available EMG equipment is used to amplify and portray the electrical activity on a monitor. When motor axons are damaged, spontaneous activities such as fibrillations and positive sharp waves can be seen.

The bulbocavernosus reflex (BCR) is measured after supramaximal electrostimulation of the dorsal nerve of the penis or clitoris. The stimulus is given via an ordinary surface stimulator placed on the dorsal part of the organ. Eight stimuli are given at random time intervals with a duration of 0.1–0.2 ms (Fig. 1).

The vesico-anal reflex (VAR) is obtained after supramaximal stimulation of the bladderneck via 2 surface ring electrodes mounted on a silicone balloon catheter

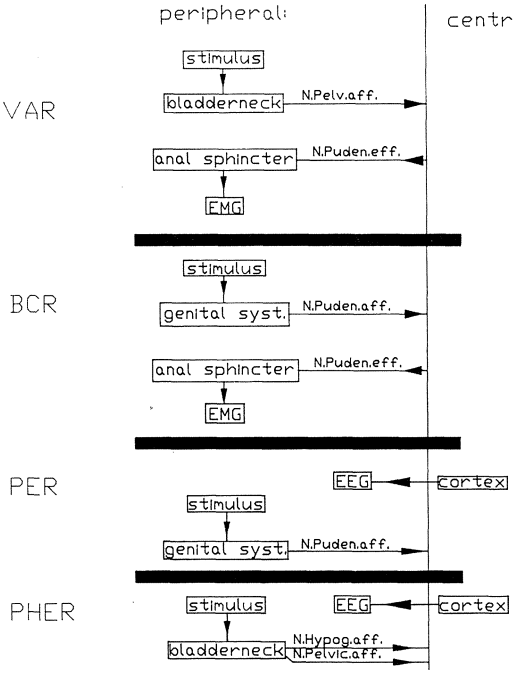

Fig. 1. Scheme of the various evoked responses: vesico-anal reflex *(VAR)*, bulbocavernosus reflex *(BCR)*, pudendus evoked response *(PER)* and pelvicus (hypogastricus) evoked response *(PHER)*

which is positioned transurethrally. Here also 8 stimuli are given, this time with a duration between 0.1–0.5 ms. The reflex responses of both the VAR and the BCR are derived from the external anal sphincter (Fig. 1).

The cortical evoked responses are the pudendus evoked response (PER) and the pelvicus (hypogastricus) evoked response (PHER). The PER is obtained after stimulation of the dorsal nerve of the penis or clitoris. The PHER can be measured after stimulating the bladderneck. Both cortical evoked responses are registered via EEG surface electrodes, positioned on the skin of the head according to the standard defined by Jasper: the active electrode is placed 2 cm behind Cz.

The current for the PER is increased to about 1.5 times the sensitivity threshold. For the PHER this is 2.5 times the sensitivity threshold. 100–300 stimuli are given (block pulse 0.2–0.5 ms) with a frequency of 1–2 Hz. The response signals are filtered out of the noise by a computerized averaging method which shows the result

Table 1. Differentiation between lesions in the neural pathways involved

	VAR	BCR	PER	PHER	Spontaneous activity	Interference pattern
Pelvic nerve (afferent)	−	+	+	+	+	+
Pudendal nerve (afferent)	+	−	−	+	+	+
Pudendal nerve (efferent)	−	−	+	+	+	−
Pudendal nerve (axon)	+	+	+	+	−	+
Central ascending (from pudendal nerve)	+	+	−	+	+	+
Pyramidal tract	+	+	+	+	+	−
Hypogastric nerve (peripheral or central)	−	+	+	−	+	+
Pelvic nerve (central) or hypogastric nerve (peripheral or central)	+	+	+	−	+	+

+ = normal; − = abnormal (delayed response)

Table 2. Normal values for the VAR, BCR, PER and PHER

Evoked response	Number of patients	Normal latency range
VAR	86	61 ± 14 ms
BCR	86	31 ± 9 ms
PER	86	(P1) 41 ± 6 ms
PHER	45	(P1) 66 ± 14 ms

for analysis on a monitor. Only averaged responses which are reproducible are accepted (Fig. 1).

By combining the results of the reflex latencies with the cortical evoked response latencies and the results of electromyography of the anal sphincter, it is possible to differentiate between peripheral and central lesions, between somatic and autonomic lesions, between afferent and efferent lesions, between ascending and descending central lesions and even between sympathetic and parasympathetic lesions (Table 1).

The VAR, BCR and PER have been investigated in 80 patients with diabetes mellitus. In the last 40 patients the PHER was also tested. There were 34 male and 46 female patients, with a mean age of 60.9 years. 38 patients were insulin dependent and 42 patients used oral antidiabetic agents or followed a diet. None of the patients drank excessive alcohol and 14 patients were receiving antihypertensive drugs.

In an earlier study normal values of each evoked response have been described (Anten et al. 1986) (Table 2) and found to be reproducible.

Results

The delay in latency time varied from 18% in the PER to 41% in the VAR (Table 3). The BCR was delayed in 29% of the diabetics and the PHER in 20%.

Table 3. Abnormal latency times in a group of 80 patients with diabetes mellitus. The PHER was only investigated in the last 40 patients

	VAR (*N:* 80)	BCR (*N:* 80)	PER (*N:* 80)	PHER (*N:* 80)
Delayed	37 (41%)	22 (29%)	14 (18%)	8 (20%)
Not evokable	3 (4%)	1 (1%)	1 (1%)	2 (5%)

Table 4. Occurrence and localization of partial lesions in 35 insulin dependent and 40 non-insulin dependent diabetics. The results do not include the PHER. Multiple lesions were found in some patients; no responses were generated in five

	Insulin dependent (35)	Non-insulin dependent (40)	Total (75)
Normal	9 (26%)	19 (48%)	28 (37%)
Pelvic nerve (afferent)	14 (40%)	9 (23%)	23 (30%)
Pudendal nerve (efferent)	11 (31%)	9 (23%)	20 (27%)
Pudendal nerve (afferent)	2 (6%)	3 (8%)	5 (7%)
Central ascending (from pudendal nerve)	3 (9%)	4 (10%)	7 (9%)

Table 5. Occurrence and localization of partial lesions in a group of 13 insulin dependent and 25 non-insulin dependent diabetics. These results do include the PHER. The sum of the percentages is not 100, because more than one lesion can occur in the same patient. No responses were generated in two patients

	Insulin dependent (13)	Non-insulin dependent (25)	Total (38)
Normal	3 (23%)	11 (28%)	14 (37%)
Pelvic nerve (afferent)	6 (46%)	7 (28%)	13 (34%)
Pudendal nerve (afferent)	1 (8%)	0	1 (3%)
Pudendal nerve (efferent)	2 (15%)	4 (16%)	6 (16%)
Central ascending (from pudendal nerve)	0	3 (12%)	3 (8%)
Central ascending (from pelvic nerve)	2 (15%)	2 (8%)	4 (11%)
Hypogastric nerve (peripheral or central)	3 (23%)	4 (16%)	7 (18%)

An attempt was made to localize the lesion in 75 diabetic patients with the combined use of the VAR and BCR together with the evoked responses (PER) and electromyographic study on the external anal sphincter (Table 4). No latency time could be generated in 5 patients.

Results showed 9 (26%) of the 35 patients in the insulin dependent group and 19 (48%) of the 40 in the non-insulin dependent group to have normal latency times. 14 patients in the first group (40%) and 9 (23%) in the second had partial lesions of the peripheral sensory pelvic nerve. Two insulin dependent patients (6%) and 3 (8%) non-insulin dependent ones showed partial lesions of the peripheral sensory pudendal nerve and 11 (31%) and 9 (23%) patients in the 2 groups had partial lesions of the peripheral motor pudendal nerve. Only 3 (9%) patients in the first group and 4 (10%) in the second had partial lesions of the central fibres of the pudendal nerve.

In addition to the VAR, BCR, PER and sphincter electromyography, the PHER was investigated in 40 diabetic patients (Table 5). No latency time was generated in 2 of them. In the 38 other patients we were able to show partial lesions of the central and/or peripheral sensory fibres from the hypogastric nerve in 3 insulin dependent patients (23%) and in 4 (16%) patients of the non-insulin dependent group. There were partial lesions in the central fibres of the pelvic nerve in 2 (15%) and 2 (8%) of the respective groups. Lesions of the central fibres of the pelvic nerve were always found in association with central or peripheral lesions of the hypogastric nerve (Table 5).

Discussion

Both motor and sensory components of the pudendal, pelvic and hypogastric nerves, as well as the spinal cord segments S2 to S4 have an important role in the peripheral nerve pathways. In the central nerve pathways, the long spinal tract, the reticular formation in the brainstem as well as cortical and subcortical structures all appear to be important (Bradley 1978).

By applying the reflexes described above, together with electromyography of the external anal sphincter, it is possible to distinguish between a lesion of the peripheral system or S2 to S4 cord segments from a lesion of the central nerve system in patients with urogenital dysfunction with a high degree of probability. In this way a disturbance in the innervation of the urogenital tract can be localized. Moreover, because the reflexes and evoked responses are reproducible, quantitative results may be obtained. This has been shown convincingly in transsection experiments (Barrington 1914) and after blockade of the sacral or lumbar nerve roots by local anaesthesia (Bradley et al. 1975; Rockswold et al. 1976).

The delays in latency times in the PER, VAR, as well as those in the BCR and PHER agree fairly well with those in the literature. For example, Andersen and Bradley (1976) found delayed VAR in 52% of diabetics but the reaction could not be generated in 30%. Ertekin et al. (1985) found a delayed BCR in 20% of the diabetics studied, but a delayed PER was only found in 10%. No comparable data has been found for the PHER in diabetics.

Clinical neurophysiological abnormalities were found in 47 (63%) of the 75 diabetics in whom the VAR, BCR and PER was carried out. Exactly the same percentage was found in the 38 patients who underwent the additional PHER procedure. However, application of the PHER led to an increase in the proportion of central lesions to 26%. In comparison, neuropathological studies have shown posterior tract lesions in 17%–44% of patients (Riedel 1965). By employing the PHER we were able to diagnose partial lesions of the sensory fibres of the hypogastric nerve (peripheral and/or central), and partial lesions of the central fibres of the pelvic nerve. We have not been able to find any comparable results with other such investigations in the published literature.

Not all components of the nerve system concerned in micturition and sexual function have been looked into in this investigation. In particular, the motor fibres of the pelvic nerves and the descending pathways (reticulo-spinal tract) have not yet been investigated. As a result, this study can not give absolute certainty about presence or absence of neurogenic lesions as cause of disturbances of urogenital function.

References

Aagenaes O (1963) Neurovascular examinations on the lower extremities in young diabetics with special reference to the autonomic neuropathy. Thesis. Reports of the Steno Mermorial Hospital, Copenhagen

Andersen JT, Bradley WE (1976) Abnormalities of bladder innervation in diabetes mellitus. Urology 7:442–448

Anten HWM, van Waalwijk van Doorn ESC, Debruyne FMJ (1986) Classification of neurogenic lesions in the urogenital system of EMG and evoked responses. In: Proceedings. ICS, Boston, pp 98–100

Badr GG, Fall M, Carlsson CA, Lindström L, Friberg S, Ohlsson B (1984) Cortical Evoked Potentials obtained after stimulation of the lower urinary tract. J Urol 131(2):306–309
Barrington FJF (1914) The nervous mechanism of micturition. Q J Exp Physiol 8:33
Bradley WE (1972) Urethral electromyelography. J Urol 108:563–564
Bradley WE (1978) Innervation of the male urinary bladder. Urol Clin North Am 5:279–293
Bradley WE, Timm GW, Rockswold GL, Scott FB (1975) Detrusor and urethral electromyelography. J Urol 114(6):891–894
Dolman CL (1963) The morbid anatomy of diabetic neuropathy. Neurology 13:135–142
Ellenberg M (1982) Diabetic neuropathy. Compr Ther 8(1):21–31
Ertekin C, Akyürekli O, Gürses AN, Turgut H (1985) The value of somatosensory-evoked potentials and bulbocavernosus reflex in patients with impotence. Acta Neurol Scand 71:48–53
Faerman I, Maler M, Jadzinsky M, Alvarez E, Fox D, Zilbervarg J, Cibeira JB, Colinas R (1971) Asymptomatic neurogenic bladder in juvenile diabetics. Diabetologia 7(3):168–172
Fagerberg SE, Kock NG, Petersen I, Stener I (1967) Urinary bladder disturbances in diabetics: A comparative study of male diabetics and controls aged between 20 and 50 years. Scand J Urol Nephrol 1:19–27
Frimodt-Møller C (1976) Diabetic cystopathy: Relationship to some late-diabetic manifestations. Dan Med Bull 23:279–287
Haldeman S, Bradley WE, Bhatia N (1982a) Evoked Responses from the pudendal nerve. J Urol 128(5):974–980
Haldeman S, Bradley WE, Bhatia NN, Johnson BK (1982b) Pudendal evoked responses. Arch Neurol 39:280–283
Hosking DJ, Bennett T, Hampton JR (1978) Diabetic autonomic neuropathy. Diabetes 27(10):1043–1055
Kaplan PE (1981) A somatosensory evoked response obtained after stimulation of the contralateral pudendal nerve: A preliminary report. Electromyogr Clin Neurophysiol 21:585–587
Riedel H (1965) Systematische morphologische Untersuchungen am Rückenmark von Diabetikern. Zentralbl Allg Pathol 107:506–513
Rockswold GL, Bradley WE, Timm GW, Chou SN (1976) Electrophysiological technique for evaluating lesions of the conus medullaris and cauda equina. J Neurosurg 45(3):321–326
Rundles RW (1945) Diabetic neuropathy: General review with report of 125 cases. Medicine 24: 111–160
Rushworth G (1967) Diagnostic value of the electromyographic study of reflex activity in man. In: Widen L (ed) Recent advances in clinical neurophysiology. Electroencephalogr Clin Neurophysiol [Suppl] 25:65–73
Slager U (1978) Diabetic myelopathy. Arch Pathol Lab Med 102(9):467–469
Vodusek DB, Janko M, Lokar J (1983) Direct and reflex responses in perineal muscles on electrical stimulation. J Neurol Neurosurg Psychiatry 46:67–71

Pelvic Floor Stress Response: Reflex Contraction with Pressure Transmission to the Urethra

J. W. Thüroff[1], F. Casper[2], and H. Heidler[2]

In 1961, Enhörning (1961) was the first to study the urethral closure mechanism by simultaneous recording of intravesical and intraurethral pressures. He found a substantial rise in intraurethral pressure during stress and concluded that this may derive from both, transmission of the intra-abdominal pressure to the urethra and contraction of the striated sphinteric muscles. These assumptions were substantiated with animal experiments by Thüroff et al. (1982a) and Heidler et al. (this volume). According to these experiments, the passive mechanism of transmission of the intra-abdominal pressure to the urethra, which is most effective at the level of the bladder neck and faints gradually distally, is complemented by an active stress mechanism at the level of the external urethral sphincter. This active mechanism plays an important role for urethral closure under stress conditions and derives from reflex contraction of the striated intramural and periurethral external sphincter muscles (Heidler 1986).

While the relative share of the stress response from intramural and periurethral striated muscles could not be determined by these experimental studies, there is some evidence from clinical data that the pelvic floor muscles play an important role in the mechanism of successful surgical repair of urinary incontinence: Some surgical techniques for treatment of male urinary incontinence use the intussusception of tissue into the membranous urethra [scrotal flap (Schmied and Wieland 1985), urethral diverticulum (Truss 1977), detrusor flap (Michalowski and Modelski 1972)]. The successful restoration of urinary continence under stress conditions by intussusception techniques suggests that the intussuscepted tissue provides a new substrate for the periurethral muscles to squeeze on, so that sealing of the urethral lumen improves.

To substantiate the assumption that the periurethral striated muscles play a major role for providing continence under stress conditions, we devised an animal experiment using a non-contractile substitute urethra to measure the contribution of the pelvic floor squeeze. For initiation and recording of urethral stress conditions, the animal model according to Thüroff et al. (1982a) was used. The experiments were devised to answer the following questions:

1. How much pelvic floor squeeze (active pressure transmission) is exerted on a non-contractile substitute urethra?
2. Can the pelvic floor squeeze on the substitute urethra be altered by suspension of the pelvic floor?

[1]UCSF Urinary Stone Center, University of California, San Francisco Medical School, 505 Parnassus Avenue, San Francisco, CA 94143, USA
[2]Department of Urology, Johannes Gutenberg University Medical School, Langenbeckstr. 1, D-6500 Mainz

Investigative Urology 2
Edited by G. H. Jacobi et al.

Material and Methods

6 adult male mongrel dogs (weight 18.5 kg–24 kg) were used for this study. Urodynamic recordings were obtained under neuroleptanalgesia with ketamine hydrochloride (20 mg/kg of body weight) without any further sedation. For simultaneous monitoring of intravesical and 3 urethral pressures, we used a custom designed 8F catheter with a central channel for bladder filling and 4 microtip transducers mounted at distances of 13 mm, 93 mm, 119 mm and 123 mm from the catheter tip (Gaeltec, Dunvegan, Scotland, model 16 CT/S 4/L). The pressure measurements were fed into a Siemens Sierecoust 404 and written on a Siemens Mingograph 62. The measurements were obtained at a bladder volume of 60 ml, the pressure readings were labeled as follows: B = Bladder, U_1 = proximal urethra, U_2 and U_3 = distal urethra (high pressure region of the external sphincter).

Experiment A: Intact Lower Urinary Tract

As controls, urodynamic measurements were obtained from the intact lower urinary tract. Urethral pressure profiles were recorded with mechanical continuous catheter withdrawal (3 mm/s). Functional urethral length and maximum urethral closure pressure were determined and the catheter was then placed with the most distal sensor (U_3) in the region of the highest urethral pressure and secured at the external meatus with a suture. To provoke a physiological stress condition with intrinsic rise of the intraabdominal pressure, sneezing was triggered in the dogs by stimulating the nose with irritating powder and compressed air. As a rule, several sneezes could be elicited and readings of intravesical and urethral pressures were recorded simultaneously.

Experiment B: Non-contractile Substitute Urethra

The abdomen was opened through a lower midline incision and the urethra was severed from the bladder neck. To eliminate any intrinsic urethral stress-reactions (e.g., by direct muscular extension from the bladder or by nerve mediated urethral contraction), non-contractile material was chosen for the substitute urethra. In 3 dogs, a Penrose-Drain was used as a substitute urethra, in the other 3 dogs a neourethra was created from a tubularized free skin flap. For this purpose, after thorough shaving, a free skin flap of 20 cm length and 2.5 cm width was obtained from the abdominal skin and tubularized over a 14F catheter by a running suture. In either case the substitute urethra was connected to the bladder neck by interrupted sutures. By blunt dissection a tunnel was created parallel to the original urethra through the pelvic floor, and after incision of the perineal skin, the substitute urethra was pulled through and a perineal stoma was formed. Before closing the abdominal incision, 2 strips of the external abdominal fascia of 15 cm length and 2.5 cm width with pedicles close to the symphysis were excised on either side in preparation for experiment C. These fascial strips were also pulled through the pelvic floor into the perineum, laterally on either side from the substitute urethra to avoid any direct compression. At this stage of the experiment, both fascial strips were not fixed in the perineum so that they were loose without tension. After closure of the abdominal wound, the microtip catheter was inserted in the substitute urethra and bladder and placed again with U_3 in the region of maximum urethral pressure. Repeat urodynamic

recordings were obtained during sneezing under otherwise identical conditions as in experiment A.

Experiment C: Substitute Urethra and Pelivc Floor Suspension

The previously fashioned fascial strips were now crossed over in the perineum and sutured to each other under tension, so that an elevation of the pelvic floor was the result. Under otherwise identical conditions as in experiment B, the urodynamic tests were repeated.

Results

Experiment A: Intact Lower Urinary Tract

The mean functional urethral length was 7.5 cm (range 6.5 cm–9.5 cm), the mean maximum urethral closure pressure in the dynamic measurements (pull-through of the catheter) 70.8 cm H_2O, in the static measurements 41 cm H_2O. During sneezing, the recorded pattern of intravesical and urethral pressure changes were very consistent intra-individually and inter-individually, but the absolute amount of pressure changes varied widely according to the intensity of the different sneezes. To allow comparison of the urethral responses from stress conditions of different intensities, the urethral pressure changes were expressed in percentage of the simultaneous intravesical pressure change (100%). This allows to evaluate the pattern of urethral responses rather than the absolute amounts.

With the lower urinary tract intact (experiment A), during sneezing a mean pressure rise of 101% of the intravesical pressure rise was recorded in the proximal urethra (U_1). In the distal urethra the stress response was 134% at U and 145% of the intravesical pressure rise at U_3 (Fig. 1).

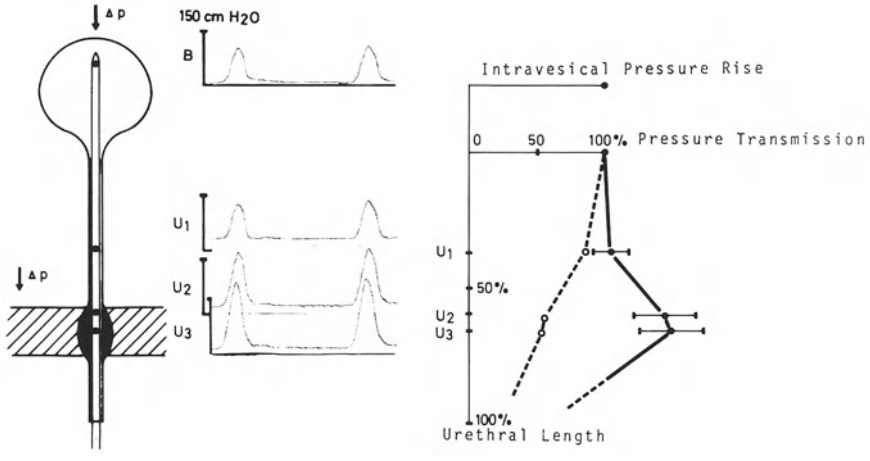

Fig. 1. Experiment A: Intact lower urinary tract, repeated sneezing. Simultaneous recording of intravesical and 3 urethral pressures (pelvic floor level: U_3). Urethral pressure response at the level of the external sphincter is 145% of the simultaneous pressure transmission to the bladder *(solid line)*. The *dotted line* illustrates the share of passive pressure transmission to the urethra as determined by Credé maneuver

Experiment B: Non-contractile Substitute Urethra

Measurements of urethral stress responses both with Penrose and skin flap substitute urethras revealed identical pressure patterns, thus the summarized data of both subgroups are presented: The pressure response dropped from the bladder to the proximal substitute urethra (U_1) to 69.3%. However, in the region of the pull-through of the substitute urethra through the pelvic floor (U_3) the stress response amounted to 135% of the intravesical pressure rise (Fig. 2).

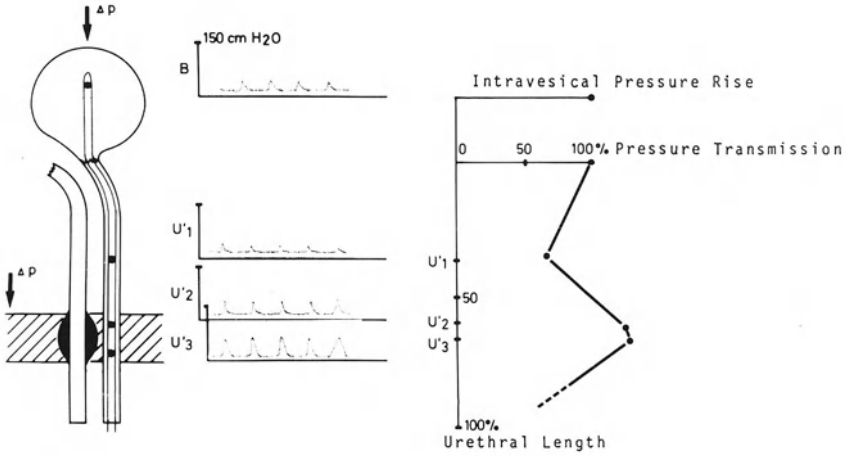

Fig. 2. Experiment B: Non-contractile substitute urethra and repeated sneezing: At the level of the pelvic floor muscles, intraluminal pressure response is 135% of the intravesical pressure rise

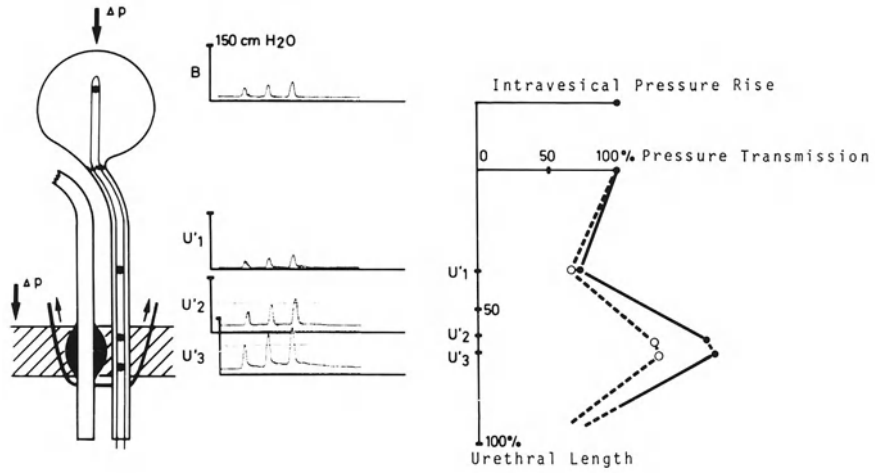

Fig. 3. Experiment C: Substitute urethra and pelvic floor suspension (fascial sling): Intraluminal pressure rise *(solid line)* at the level of the pelvic floor muscles is 174% of the simultaneous intravesical pressure rise during stress (*dotted line:* experiment B)

Experiment C: Substitute Urethra and Pelvic Floor Suspension

In the proximal substitute urethra (U_1) the pressure response amounted to 75% and at U_3 to 174% of the intravesical pressure rise during sneezing (Fig. 3).

Discussion

Under resting conditions, passive continence is related to the sealing effect of the muscosa under the resting tone of the urethra, which derives from the pressure in the submucous vessels, the tone of the smooth and striated urethral muscles and the tension of the elastic intramural and periurethral connective tissue (Awad and Downie 1976; Graber et al. 1974; Rud et al. 1980; Tanagho et al. 1969a, b). The tone of the striated intramural and periurethral muscles provides an about 50% share of the urethral resistance (Tanagho et al. 1969b). Under stress conditions, both an active and passive mechanism collaborates in securing continence while the intra-abdominal and intravesical pressure is increased (Enhörning 1961; Heidler et al., this volume; Thüroff et al. 1982). While there is only little debate on the mechanism of passive transmission of intra-abdominal pressure to the intrapelvic urethra during stress, the role of active pressure generation from contraction of the intramural and peri-urethral striated muscles during stress conditions and their relative share are still viewed controversially (Bunne and Öbrink 1978; Enhörning 1961; Heidler et al. 1979; Lapides et al. 1960; Öbrink et al. 1978; Rud 1981; Thüroff 1982a). However, both experimental (Thüroff 1982a) and clinical data (Constantinou and Govan 1981; Heidler et al. 1979) strongly suggest that the contraction of striated muscles plays an important role not only to maintain but augment urethral closure pressure during stress conditions. Nevertheless, the relative shares of both the intramural and periurethral striated muscles were still unknown.

In our experimental model, a non-contractile substitute urethra, connected to the bladder neck and pulled through the pelvic floor muscles, eliminated the possibility of any intrinsic urethral stress reactions and thus allowed assessment of the function of the periurethral striated muscle without the share of intramural sphincteric components. The lack of urethral tone of the non-contractile urethral substitute became evident from the reduction of resting closure pressure, which is not the case, if a neourethra is created from a bladder flap tube (Thüroff et al. 1982b, 1983; Tsuji et al. 1959; Zingg 1965). However, under the physiologic stress condition of sneezing, the intraluminal pressure rise in the region of the pelvic floor muscles was in the non-contractile substitue urethra only 10% lower as in the intact urethra and still 35% above the passive intravesical pressure rise. These results strongly support the concept of an active reflex contraction of striated muscles as being an important stress mechanism for urinary continence. This mechanism not only can balance a sudden intravesical pressure increase, but adds an edge of security to the urethral closure pressure under stress by boosting the urethral pressure way above the amount of the sudden intravesical pressure rise thus augmenting closure pressure in the moment of stress. This mechanism proved to be operational even in the presence of a non-contractile substitute urethra; however, under these conditions incontinence occurred due to the lack of a sealing mechanism of the substitute. Furthermore, these experiments demonstrate that the major share of this active continence mechanism

under stress derives from reflex contraction of the periurethral muscles of the pelvic floor, which remained functional without a contractile urethra. The intramural striated external sphincter muscle contributes less than 10% to the total striated sphincter response under stress conditions.
With suspension of the pelvic floor by a non-obstructing fascial sling, the pressure squeeze on the substitute urethra during stress could be enhanced 29% over the baseline recording to 174% of the bladder pressure rise. This underlines the importance of an anatomic and functional intact pelvic floor for urinary stress continence as well as the sound principle of those incontinence operations, which restore anatomy and function of the pelvic floor muscles by stretch and suspension.

Summary

There is still controversy regarding the active role of striated intramural and periurethral muscles and their relative share of function for urinary continence under stress conditions. To evaluate the function of the periurethral muscles, we subjected a dog model to the physiologic stress condition created by sneezing. Simultaneous measurements of intravesical and 3 urethral pressures were obtained in the intact urinary tract and in a non-contractile substitute urethra, which was pulled through the pelvic floor and studied with and without additional pelvic floor suspension.

The data clearly confirms the active role of striated sphincteric muscles for continence under stress conditions. The reflex contraction of the striated sphincteric muscles constitutes the majority of the distal urethral closure mechanism under stress conditions and generates intraurethral pressures which exceed those of passive transmission of intraabdominal pressure. The intramural striated sphincter contributes a share of less than 10% to this stress response, while the vast majority of the pressure rise is generated by the periurethral striated muscles. Surgical suspension of the pelvic floor can enhance effectivity of this stress mechanism and thus seems to be a sound physiological concept in surgical treatment of incontinence.

References

Awad SA, Downie JW (1976) Relative contributions of smooth and striated muscles to the canine urethral pressure profile. Br J Urol 48:347–354

Bunne G, Öbrink A (1978) Urethral closure pressure with stress – a comparison between stress-incontinent and continent women. Urol Res 6:127–134

Constantinou CE, Govan DE (1981) Contribution and timing of transmitted and generated pressure components in the female urethra. In: Zinner NR, Sterling A (eds) Female incontinence. Alan R Liss, New York, p 113

Enhörning G (1961) Simultaneous recording of intravesical and intraurethral pressure. Acta Chir Scand (Suppl) 276:1–68

Graber P, Laurent G, Tanagho EA (1974) Effect of abdominal pressure rise on the urethral profile. An experimental study on dogs. Invest Urol 12:57–64

Heidler H (1986) Die Rolle der quergestreiften Sphinktermuskulatur für die Speicherfunktion der Blase und ihre Beeinflussbarkeit durch Biofeed-back-Mechanismen. Veröffentlichung der Universität Innsbruck, Bd 157

Heidler H, Wölk H, Jonas U (1979) Urethral closure mechanism under stress conditions. Eur Urol 5:110–112

Kegel AH (1949) The physiologic treatment of poor tone and function of the genital muscles and of urinary stress incontinence. West J Surg Obstet Gynecol 57:527–535
Lapides J, Ajemian EP, Stewart BH, Breakey BA, Lichtwardt JR (1960) Further observations on the kinetics of the urethrovesical sphincter. J Urol 84:86–94
Michalowski E, Modelski W (1972) The replacement of the urethral musculature by detrusor flap: contribution of the operative treatment of incontinence. J Urol 107:791–794
Öbrink A, Bunne G, Ingelman-Sundberg A (1978) Pressure transmission to the pre-urethral space in stress incontinence. Urol Res 6:135–140
Rud T (1981) The striated pelvic floor muscles and their importance in maintaining urinary continence. In: Zinner NR, Sterling A (eds) Female incontinence. Alan R Liss, New York, p 79
Rud T, Andersson KE, Asmussen M, Hunting A, Ulmsten U (1980) Factors maintaining the intraurethral pressure in women. Invest Urol 17:343–347
Schmied E, Wieland W (1985) The scrotal flap technique as an operative method for the treatment of iatrogenic and posttraumatic male incontinence. In: Lutzeyer W, Hannappel J (eds) Urodynamics – Upper and lower urinary tract II. Springer, Berlin Heidelberg New York, p 203
Tanagho EA (1979) Urodynamics of female urinary incontinence with enphasis on stress incontinence. J Urol 122:200–204
Tanagho EA, Meyers FH, Smith DR (1969a) Urethral resistence: Its components and implications. I. Smooth muscle component. Invest Urol 7:136–149
Tanagho EA, Meyers FH, Smith DR (1969b) Urethral resistance: Its components and implications. II. Striated muscle component. Invest Urol 7:195–205
Thüroff JW, Bazeed MA, Schmidt RA, Tanagho EA (1982a) Mechanisms of urinary continence: an animal model to study urethral responses to stress conditions. J Urol 127:1202–1206
Thüroff JW, Bazeed MA, Schmidt RA, Tanagho EA (1982b) Urodynamic evaluation of a bladder flap tube as urinary sphincter. Neurourol Urodyn 1:113–122
Thüroff JW, Hutschenreiter G, Rumpelt HJ, Hohenfellner R (1983) Neourethra: A new two-stage procedure for reconstruction of the functional urethra. J Urol 130:1228–1233
Truss F (1977) Inkontinenzplastik nach TUR. Urologe A 16:334–335
Tsuji J, Kuroda K, Ishida H (1959) A new method for the reconstruction of the urinary tract: bladder flap tube. J Urol 81:282–286
Zingg FJ (1965) Tierexperimentelle Untersuchungen über den plastischen Ersatz der Harnröhre. In: Verhandlungsbericht der Deutschen Gesellschaft für Urologie. Springer, Berlin Heidelberg New York, S 286

Neuroanatomy and Neurophysiology of the External Urethral Sphincter

K.-P. Jünemann[1], R. A. Schmidt[2], H. Melchior[1], and E. A. Tanagho[2]

The muscular architecture of the external urethral sphincter is heterogenous and can be separated into an intrinsic and an extrinsic element (Gosling et al. 1981). The intrinsic part consists of a rhabdosphincter surrounding the membranous urethra; the extrinsic component is formed by the pelvic floor muscles and the levator ani muscle. The external urethral sphincter is one of the most important urinary continence and urethral stability providing structures, however, its neuroanatomy and neurophysiology is still under debate. Starting out from the idea that adequate urethral pressure is a passive effect of the elastic and vascular urethral tissue (Lapides 1958; Woodburne 1961; Ruch 1965) the discussion about the continence-providing mechanism passed several different scientific standpoints, such as an active muscular tone derived from the smooth and the striated muscle elements of the sphincter (Tanagho et al. 1969; Raz and Caine 1972; Donker et al. 1972).

The opinions regarding the neuronal control of the urethral sphincter offer a wide range from primary autonomic (Donker et al. 1976) to selective somatic innervation of the external urethral rhabdospincter (El Badawi and Schenck 1974; Gosling et al. 1982).

From previous experimental studies it became clear that neurostimulation of the S2 to S4 sacral roots does have a significant occlusive effect on the membranous urethra (Thüroff et al. 1982; Brindley et al. 1982; Schmidt 1983).

To establish the exact nerve supply of the external urethral sphincter we studied the neuroanatomy on male cadavers and performed a combined neurostimulation/urodynamic study on human patients to elucidate the neurophysiology of the external urethral closure mechanism.

Material and Methods

3 male human cadavers (aged 31 to 69 years) were dissected by tracing the entire sacral plexus. The sacral nerves were followed from the cauda equina throughout the sacral foramen to their final destination. Special attention was given to the branching of the pudendal nerve as the main nerve trunk regarding the nerve supply of the pelvic floor and the lower genitourinary tract.

In 5 patients who underwent a neurostimulation implant for treatment of stress incontinence and that due to detrusor-/sphincter hyperreflexia or for a bladder pacemaker implantation, intra-operative S2 and/or S3 sacral root stimulation combined with urodynamic studies was performed. Selective neurostimulation of sacral root or pudendal nerve before and after neurotomy or xylocaine blockade of specific

[1]Klinik für Urologie, Städtische Kliniken Kassel, Mönchebergstr. 41/43, D-3500 Kassel
[2]Department of Urology, University of California, San Francisco Medical School, San Francisco, CA 94143, USA

Investigative Urology 2
Edited by G. H. Jacobi et al.

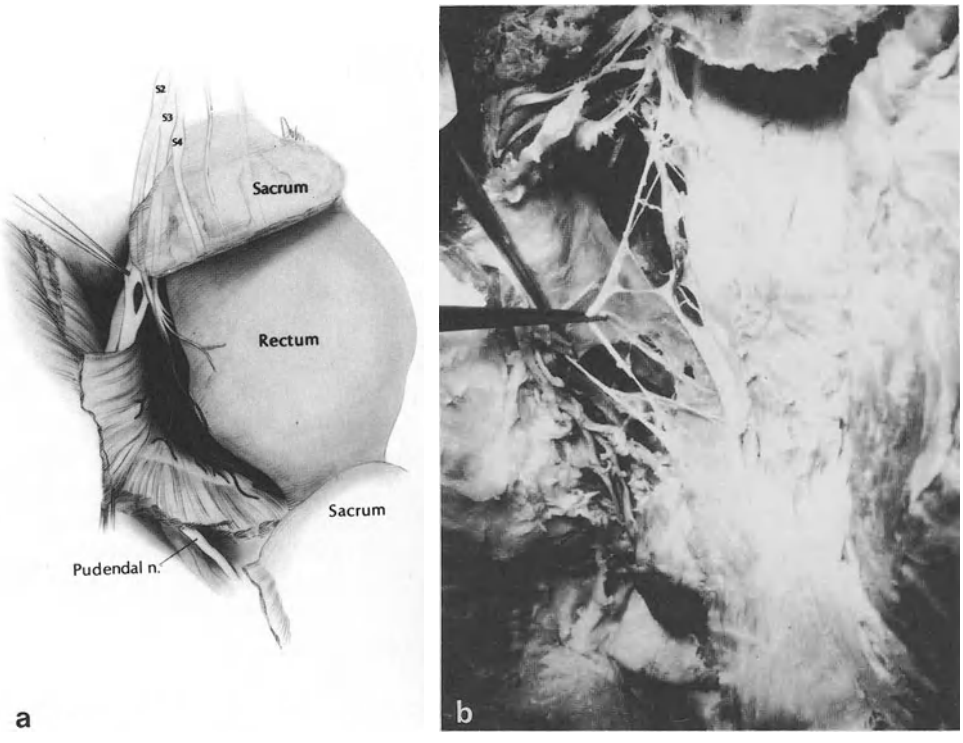

Fig. 1. a Nerve supply of the intrinsic rhabdosphincter of the membranous urethra and the levator ani muscle. **b** Dorsal view at levator ani innervation (pick-up); the coccygeus bone is partially removed

nerve branches should help to determine the contribution of each neuromuscular component to the external urethral closure pressure. Simultaneous pressure recordings of the bladder, bladder neck, urethral sphincter and rectum were performed with a three-balloon membrane catheter connected to a statham transducer.

Results

Neuroanatomy

Our dissections confirmed that the extrinsic urethral sphincter is formed by the rhabdosphincter around the membranous urethra and the levator ani and pelvic floor muscles. All three components are innervated by somatic nerve fibers that emanate from the sacral roots of S2 to S4.

After the S2–S4 nerves traverse the sacral foramen, they divide into autonomic and somatic fibers. The autonomic nerve branches which are primarily parasympathetic, form the pelvic plexus from which the nerve supply to the detrusor muscle and the smooth muscle of the urethra is derived. However, a few somatic nerve branches, emanating from S2 and S3 ventral roots, mainly S3, run in direct proximity to the autonomic nerve plexus to innervate the levator ani muscle and the external urethral rhabdospincter (Fig. 1). The levator ani, as one of the major muscular components

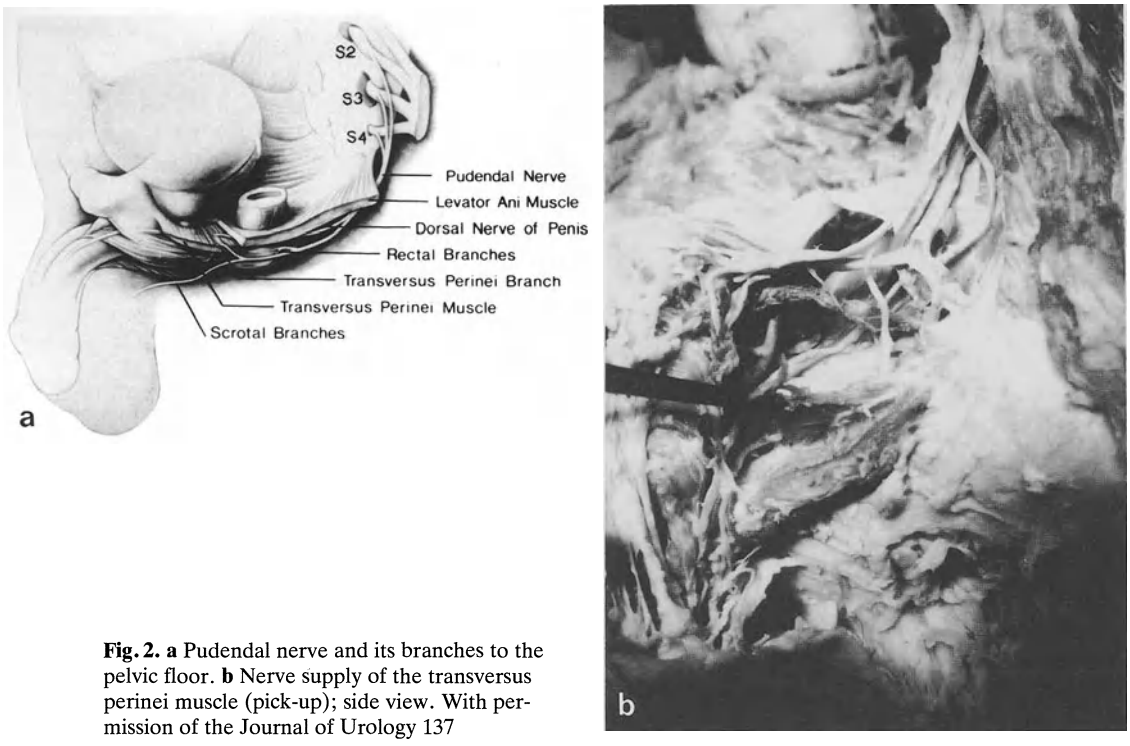

Fig. 2. a Pudendal nerve and its branches to the pelvic floor. **b** Nerve supply of the transversus perinei muscle (pick-up); side view. With permission of the Journal of Urology 137

of the pelvic floor, forms a muscular-fibrous peri-urethral sling around the urethral rhabdosphincter. Its nerve supply emanating from S2 and S3 somatic fibers runs on the inner side of the muscle.

The other contribution for the urinary continence mechanism derives from the pelvic floor muscles innervated by the pudendal nerve. Topographically, superior to the sacrospinous ligament the nerve branches from S2 to S4 ventral root form one major nerve trunk. At the caudal edge of the coccygeous muscle, right before the pudendal nerve enters the ischiorectal fossa, two nerve branches take off to target their final destination: the dorsal nerve of the penis and the perineal nerve fibers; both are carrying sensory fibers.

Further caudal, the remaining part of the pudendal nerve dives into the ischiorectal fossa. At the level of the anus the nerve splits into several branches: the anal branches that target the anal spincter muscle and the fibers to the bulbospongiosous muscle. At the level of the anal sphincteric nerve fibers, another single branch emerges from the mother trunk dorsolaterally to innervate the transversus perinei and the ischiocavernous muscles (Fig. 2).

This muscular complex consisting of the levator ani, external urethral rhabdosphincter and the pelvic floor muscles is essential for urinary continence.

Neurophysiology

The neuronal control of the lower urinary tract including the autonomic and the somatic components is located in the S2 to S4 sacral segments. With the newly acquired

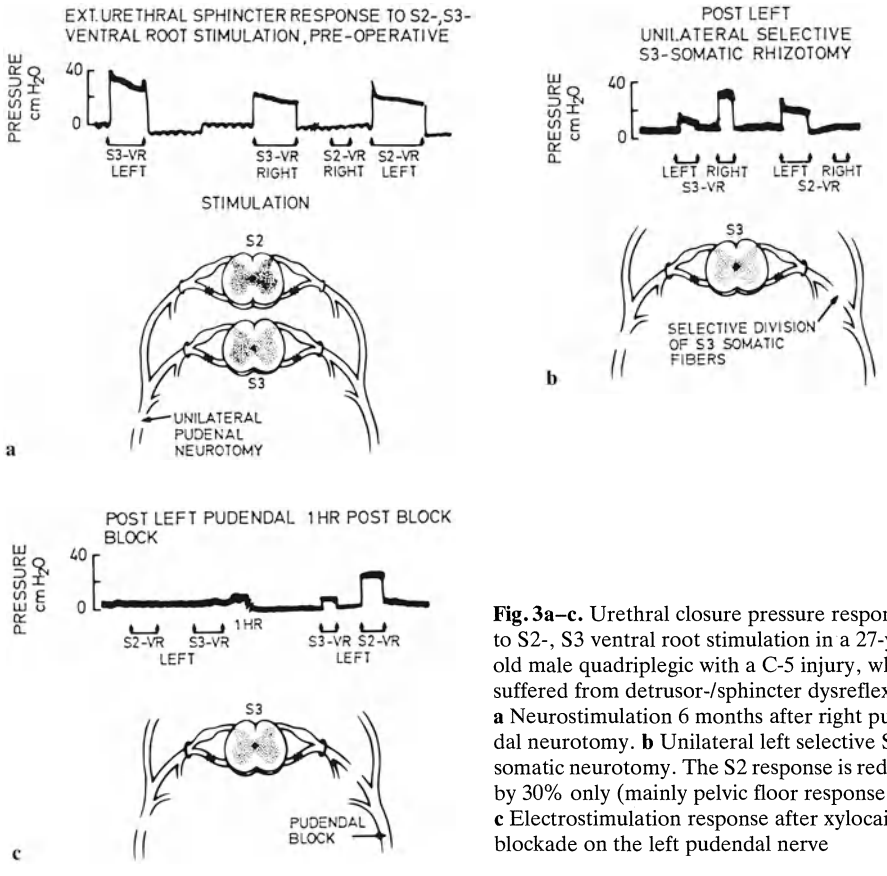

Fig. 3a–c. Urethral closure pressure responses to S2-, S3 ventral root stimulation in a 27-year-old male quadriplegic with a C-5 injury, who suffered from detrusor-/sphincter dysreflexia. **a** Neurostimulation 6 months after right pudendal neurotomy. **b** Unilateral left selective S3-somatic neurotomy. The S2 response is reduced by 30% only (mainly pelvic floor response!). **c** Electrostimulation response after xylocaine blockade on the left pudendal nerve

appreciation for the neuroanatomy of the external urethral sphincter we tried to elucidate the neurophysiologic and functional contribution of each sphincteric component to the external urethral closure mechanism with selective sacral stimulation and the pudendal nerve alone, before and after selective neurotomy or xylocaine blockade in 5 patients (vide supra).

The urethral closure pressure responses to sacral root stimulation as shown in Fig. 3 clearly show the different contributions of each neuromuscular unit to the intraurethral pressure. Right S2- and S3 ventral root stimulation showed a diminished or lost urethral closure pressure rise, 6 months after right pudendal neurotomy; the left side was intact and showed a strong urethral sphincter contraction (Fig. 3a). After unilateral selective S3-somatic neurotomy on the left side, the electrostimulation response of left S3 ventral root resulted in a 70% reduction in intraurethral pressure owing to the failure of the rhabdosphincter and levator ani muscle to contract (Fig. 3b). S2 sacral root stimulation alone showed a sphincteric pressure reduction of 30%; stimulation on the right remained unchanged. From this study, it became obvious that in this patient the major contribution to the pudendal nerve and its branches to the pelvic floor arise from S2, whereas the S3 somatic fibers mainly innervate the intrinsic urethral rhabdosphincter and the levator ani muscle.

To determine if the remaining sphincteric response to S3 stimulation is due to pelvic floor contraction, we blocked the left pudendal nerve with xylocaine. Repeated S2 and S3 ventral root stimulation on the left side showed a completely abolished external urethral sphincter activity; 1 hour later the intraurethral pressure response was restored (Fig. 3c).

Conclusion

From our neuroanatomical and neurophysiologic studies we conclude that the external urethral sphincter is innervated by somatic nerve fibers from S2 and S3. The nerve branches to the urethral rhabdosphincter (intrinsic component) and the levator ani muscle are mainly S3 fibers and emanate proximally to the sacrospinous ligament. The neural pathway to the pelvic floor (extrinsic component), in particular to the transversus perinei muscle, originates from S2 ventral root and runs via the pudendal nerve to its final destination.

Clinically, this neuroanatomic, neurophysiologic interrelationship of S2 and S3 somatic nerve fibers becomes significant for the treatment of incontinence (stress-, detrusor hyperreflexia, urethral syndrome) (Jünemann et al. 1986) and in the evaluation of bladder pacemaker candidates.

References

Brindley GS, Polkey CE, Rushton DN (1982) Sacral anterior root stimulators for bladder control in paraplegia. Paraplegia 20:365

Donker PJ, Ivanovici F, Noach EL (1972) Analysis of the urethral pressure profile by means of electromyography and the administration of drugs. Br J Urol 44:180

Donker PJ, Droes JThPM, Van Ulden BM (1976) Anatomy of the musculature and innervation of the bladder and urethra. In: Williams DI, Chrisholm GD (eds) Scientific foundations in urology, vol 2. Heinemann Medical Books, Chicago, p 32

El Badawi A, Schenck EA (1974) A new theory of the innervation of bladder musculature. III. Innervation of the vesico-urethral junction and external sphincter. J Urol III:613

Gosling JA, Dixon JS, Critchley HOD, Thompson S-A (1981) A comparative study of the human external sphincter and periurethral levator ani muscles. Br J Urol 53:35

Gosling JA, Dixon JS, Humpherson JR (1982) Functional anatomy of the urinary tract, chaps 4 and 5: Gross and microscopic anatomy of the urethra I and II. University Park Press, Baltimore; Gower Medical Publishing, London New York

Jünemann K-P, De Geeter P, Persson Ch, Melchior H (1986) Neuraltherapie der hyperaktiven Blase. Urologe A 25:288

Lapides J (1958) Structure and function of the internal vesical sphincter. J Urol 80:341

Raz S, Caine M (1972) Adrenergic receptors in the female canine urethra. Invest Urol 9:319

Ruch TG (1965) The urinary bladder. In: Physiology and biophysics. Saunders, Philadelphia, p 1010

Schmidt RA (1983) Neural prostheses and bladder control. Engineering in Medicine and Biology 2:31

Tanagho EA, Meyers FH, Smith DR (1969) Urethral resistance: its components and implications. II. Striated muscle component. Invest Urol 7:195

Thüroff JW, Bazeed MA, Schmidt RA, Lue DH, Tanagho EA (1982) Regional topography of spinal cord neurons innervating pelvic floor muscles and bladder neck in the dog: A study by combined horseradish peroxidase histochemistry and autoradiography. Urol Int 37:110

Woodburne RT (1961) The sphincter mechanism of the urinary bladder and urethra. Anat Rec 141:11

The Role of Striated Sphincter Muscle in Urethral Closure Under Stress Conditions: An Experimental Study

H. Heidler[1], F. Casper[1], and J. W. Thüroff[2]

Introduction

Decisive for urethral closure under stress is an increase in intraurethral pressure. This pressure increase is significantly affected by urethral tonus, passive pressure transmission and reflex pressure transmission. Approximately half of the urethral tonus is produced by the striated sphincter muscles (Rud et al. 1981; Tanagho 1979).

Passive pressure transmission is the transmittance of an intra-abdominal pressure increase to the urethral lumen. It decreases in intensity from the bladder neck to the external meatus.

Reflex pressure transmission is the total effect produced by the striated muscle of both the urethra and the pelvic floor. Under stress conditions it causes an additional increase in the intraurethral pressure in that segment of the urethra adjacent to the pelvic floor.

In this situation, a higher pressure transmission than expected is found in this region, which is furthermore initiated somewhat earlier than the simultaneous intravesical pressure rise. This observation led to the recognition of the role of the striated muscle in the production of the increased intraurethral pressure rise and was thus termed "reflex pressure transmission" (Constantinou and Govan 1981; Heidler et al. 1979; Tanagho et al. 1969).

Anatomically, the striated sphincter muscle is composed of 2 components: the intraurethral external sphincter muscle and the periurethral pubococcygeus muscle.

The aim of the experiment described herein was to determine to what extent reflex pressure transmission increases under stress conditions and which segment of the striated sphincter muscle is responsible for adequate reflex pressure transmission.

Methods

These functions can only be explored with an experimental animal model which offers anatomical conditions similar to those in the human, especially in regard to the pelvic floor and the urethra. Furthermore, several physiological conditions of the pelvic floor must be fulfilled:

1. In order to study passive pressure transmission, it must be possible to produce an extrinsic intra-abdominal pressure increase.

[1]Department of Urology, Johannes Gutenberg University, Medical School, Langenbeckstr. 1, D-6500 Mainz
[2]UCSF Urinary Stone Center, University of California, San Francisco Medical School, 505 Parnassus Avenue, San Francisco, CA 94143, USA

Investigative Urology 2
Edited by G. H. Jacobi et al.

2. In order to study reflex pressure transmission, a physiological stress situation must be created in which an intrinsic intra-abdominal pressure rise occurs.
3. It must be possible to surgically isolate the intramural striated sphincter in order to identify the output of the separate sphincter components.

The experiment was performed on 10 female German Shepherd dogs (weight 20–30 kg) under neuroleptanalgesia (Ketamine hydrochloride 20 mg/kg of body weight) without any further sedation so as to retain muscle reflexes.

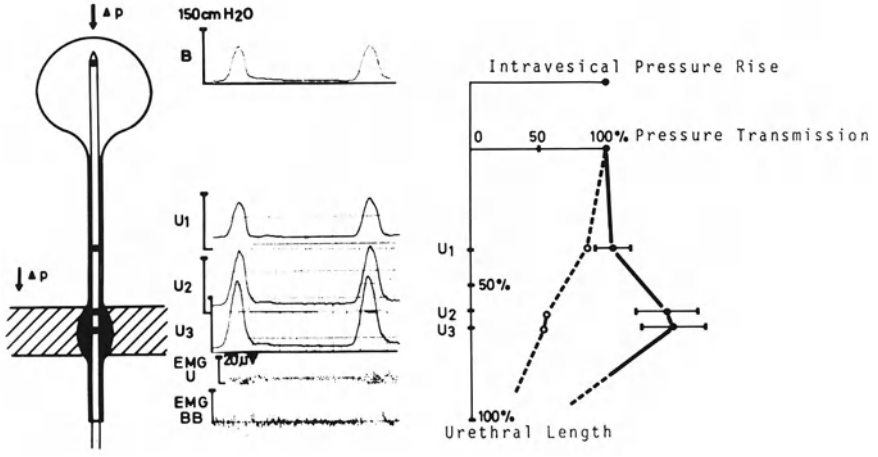

Fig. 1. Experiment Phase A: Urodynamic measurement with urethra in situ. *Left:* schematic drawing of the experimental set-up. *Right:* diagram of passive pressure transmission *(dotted line)* and reflex pressure transmission *(solid line)* from the bladder neck to the distal urethra

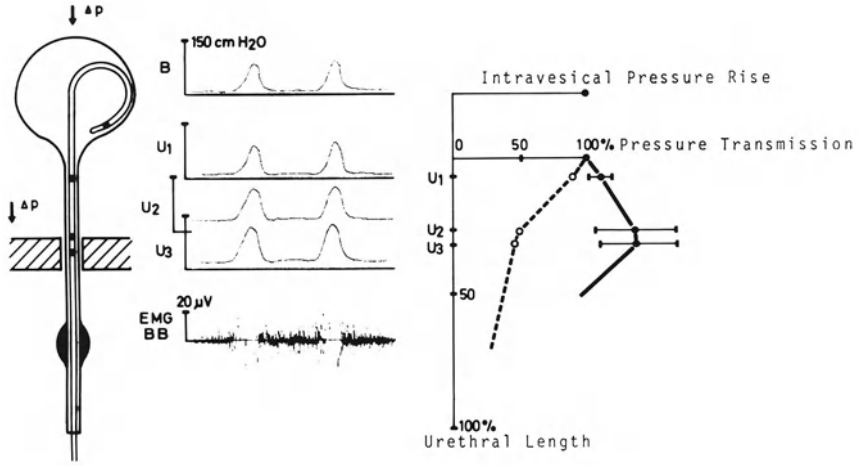

Fig. 2. Experiment Phase B: Urodynamic measurement after exposure of the urethra and isolation of the intramural striated sphincter. *Left:* schematic drawing of the operative site. *Right:* diagram of passive pressure transmission *(dotted line)* and reflex pressure transmission *(solid line)*

For simultaneous pressure monitoring (Fig. 1), we used an 8-French 4-membrane catheter with 1 measurement site in the bladder (B) and 3 along the urethra (U_1–U_3). Simultaneous measurements of the pelvic floor EMG were obtained with unipolar needle electrodes. To provoke a stress condition, sneezing was triggered by blowing compressed air and a mixture of sneezing powder and pepper in the dog's nose. In addition, the effect of passive abdominal compression (Credé maneuver) was examined.

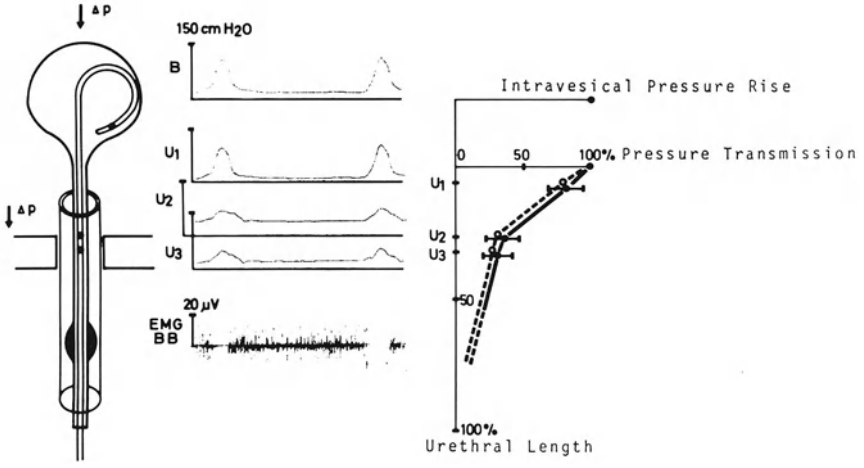

Fig. 3. Experiment Phase C: Urodynamic measurement of the shielded urethra. *Left:* schematic drawing of the operative site. *Right:* diagram of passive pressure transmission *(dotted line)* and reflex pressure transmission *(solid line)*

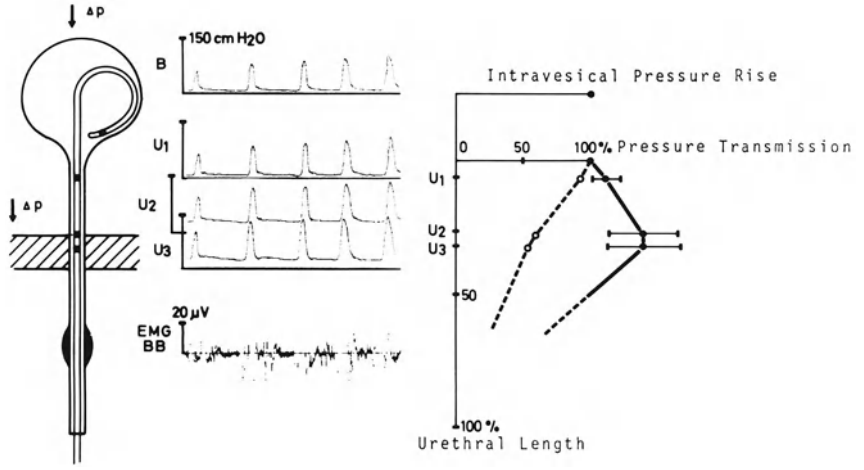

Fig. 4. Experiment Phase D: Urodynamic measurement after reconstruction of the pelvic floor: the intramural striated sphincter is still isolated. *Left:* schematic drawing of the operative site. *Right:* diagram of passive pressure transmission *(dotted line)* and reflex pressure transmission *(solid line)*

After recording the pressure transmission with the urethra in situ (Experiment Phase A), the urethra was dissected from the periurethral striated muscle of the pelvic floor (Experiment Phase B) thus interrupting muscular continuity of the urethra and the pelvic floor. The urethra was pulled down until only the smooth muscle of the proximal urethra was lying in the pelvic floor. For Experiment Phase C the urethra was shielded from the reflex contraction of the pelvic floor, and for Phase D the striated muscle of the pelvic floor was adapted to the smooth muscle of the proximal urethra (Figs. 1–4). Passive and reflex pressure transmission was recorded by urodynamic studies during each phase of the experiment.

Results

As the measurements obtained in this animal model showed variations of up to 160 cm H_2O in the passive and up to 320 cm H_2O in the active pressure transmissions, comparison of the absolute data for the individual animals was considered impossible. Therefore, the intravesical pressure rise was set at 100%, and the values for the intraurethral pressure changes were converted to percentage of 100% vesical pressure. The same anatomical length of the urethra was maintained during all urodynamic studies and experimental phases.

Experiment Phase A

The intraurethral pressure rise resulting from passive pressure transmission (Fig. 1, dotted line) was reduced at U_1 to 87% of the vesical pressure; at U_2 and U_3 it was reduced to 56%. We assumed that this nearly linear pressure decrease continued along the remaining length of the urethra. The intraurethral pressure rise resulting from reflex pressure transmission (Fig. 1, solid line) had risen at U_1 to 104%, and at U_2 and U_3 it had increased further to 145%. The external sphincter and pelvic floor EMG showed strong, synchronous activity which was interpreted as muscle contractions.

Experiment Phase B

After dissection of the urethra and isolation of the intramural striated muscle, a decrease of the intraurethral pressure rise resulting from passive pressure transmission (Fig. 2, dotted line) was also recorded. There was a continuous decrease to 90% at U_1, and a further reduction to 48% at U_2 and U_3. This is an 8% reduction of the passive intraurethral pressure rise as compared with Phase A.

Reflex pressure transmission (Fig. 2, solid line) surprisingly showed, in comparision with Phase A, a pressure increase to 109% at U_1 and 138% at U_2 and U_3. The EMG again registered sychronous pelvic floor reflexes. Despite isolation of the intramural striated sphincter, a nearly identical pressure rise was found which was apparently caused by contractions of the pelvic floor.

Experiment Phase C

With the urethra shielded, there was a continual decrease of passive pressure transmission (Fig. 3, dotted line) to 84% at U_1 and 36% at U_2 and U_3. As the urethral

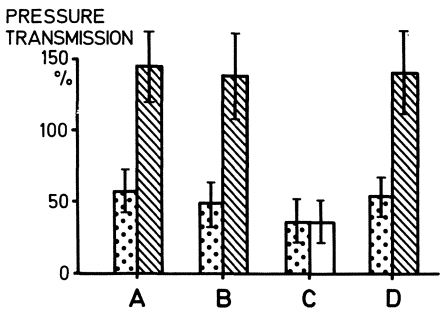

Fig. 5. Comparison of passive pressure transmissions *(dotted columns)* and reflex pressure transmission *(hatched columns)* obtained in Experimental Phases A–D

shield was located above the endopelvic fascia, this additionally reduced passive pressure transmission.

The intraurethral pressure use resulting from reflex pressure transmission (Fig. 3, solid line) was identical to the passive pressure transmission, thereby indicating that the urethra has no active contractile ability of its own. As the urethra was shielded, the pelvic floor contractions recorded on the EMG could not be transmitted to the urethra. It can therefore be deduced that the strong intraurethral pressure rise demonstrated in Phase B is a result of contractions of the pelvic floor.

Experiment Phase D

After reconstruction of the pelvic floor and further isolation of the intramural striated sphincter, there was a decrease in the intraurethral pressure rise resulting from passive pressure transmission (Fig. 4, dotted line) to 94% at U_1 and 54% at U_2 and U_3. This amounts to an only minimal difference of −2% after pelvic floor reconstructions, as compared with Phase A.

In the same manner, the intraurethral pressure rise resulting from reflex pressure transmission (Fig. 4, solid line) also showed a minimal increase to 109% at U_1 and a considerable increase to 141% at U_2 and U_3. This urethral pressure rise is nearly identical to the results obtained preoperatively (Phase A) with a minimal difference of −4%.

Summarizing the results of these animal experiments in an attempt to answer the questions posed at the start, it can be said that reflex pressure transmissions measured in the pelvic floor region reached an extent of 89%. This reflex pressure transmission compounds with a pre-existing passive pressure transmission of 56% to achieve the combined measured value of 145% (Fig. 5). Furthermore, the experiment showed that the reflex pressure transmission is almost exclusively a product of the periurethral striated sphincter with only 4% of the pressure transmission being produced by the intraurethral striated muscle.

Discussion

With this animal model it was possible to gain insight into the closure mechanism of the urethra, as it fulfilled the requirements of anatomical conditions and physiological stress reactions. The physiological stress reactions in the individual animals were

provoked by sneezing and were therefore converted into percentages as explained above. The data thus obtained showed an absolutely uniform trend in that strong sneezes led to higher intra-abdominal pressures and stronger pelvic floor contractions (Graber et al. 1974; Jonas 1975; Jonas and Tanagho 1976). This percental relationship confirms a reflex reaction of the pelvic floor rather than a transmitted intramural pressure increase. Similar results were also obtained by stimulation of the efferent nerve fibers (Nobuo Koinuma 1981) and in studies on the reflex arc performed by Jonas (Jonas and Tanagho 1975) and Thüroff (Thüroff et al. 1982). As Bruschini (Bruschini et al. 1977) found an increase in urethral closure pressure under tension, we were prompted to devise an experimental situation in which the urethra was not subjected to tension or elongation. Using external pressure application on the abdomen (Credé manouver), we were able to study pure passive pressure transmission, as EMG-activity was not measured. This corresponds to the findings in the literature (Öbrink et al. 1978). Passive pressure transmission of the intra-abdominal pressure rise therefore effects closure of the proximal urethra.

In the presence of a higher intra-abdominal pressure increase, such as in sneezing, a higher intraurethral pressure increase was observed – in contrast to Öbrink (Öbrink et al. 1978) – in the region where the smooth muscle of the urethra enters the pelvic floor than the principle of passive pressure transmission might suggest.

In the past, an active contraction of the striated sphincter muscle as a closure mechanism under stress was either denied (Gosling 1979; Rud 1981), disregarded (Bunne and Öbrink 1978; Drouin and McCurry 1970; Öbrink et al. 1978) or supported (Constantinou and Govan 1982; Enhörning 1961; Graber et al. 1974; Lapides et al. 1960; Tanagho 1979; Tanagho et al. 1969). Measurements of the intraurethral pressure increase in the midurethra, which partly exceeded the intravesical pressure (Constantinou and Govan 1982; Tanagho 1979; Tanagho et al. 1969) and preceded it (Constantinou and Govan 1981; Tanagho et al. 1969), have offered significant signs of external sphincter involvement. On the other hand, this pressure increase has been explained by passive pressure transmission caused by anatomical and mechanical factors (Asmussen and Ulmsten 1983; James 1976; Rud 1981). Our animal experiments, however, showed direct influence of the pelvic floor muscle on internal urethral pressure, and not via the bladder neck. In this experiment, the bladder neck was no longer in situ.

The anatomical description of the external sphincter by Miller (Miller 1964) as well as the surgical experience gained from Experiment Phase B show sufficient similarity to the human female urethra in order to be considered as fulfilling the requirements for an animal model. This agreement between the physiological reactions of the dog and human suggests the applicability of the results to the human situation.

References

Asmussen M, Ulmsten U (1983) On the physiology of continence and pathophysiology of stress incontinence in the female. Contrib Gynecol Obstet 10:32

Bruschini H, Schmidt RA, Tanagho EA (1977) Effect of urethral stretch on urethral pressure profile. Invest Urol 15:107

Bunne G, Öbrink A (1978) Urethral closure pressure with stress – A comparison between stress incontinent and continent women. Urol Res 6:127

Constantinou CE, Govan DE (1981) Contribution and timing of transmitted and generated pressure components in the female urethra. In: Zinner NR, Sterling A (eds) Female incontinence. Alan R Liss, New York, p 113

Constantinou CE, Govan DE (1982) Spatial distribution and timing of transmitted and reflexly generated urethral pressure in healthy women. J Urol 127:964

Drouin G, McCurry EM (1970) Catheters for studies of urinary tract pressure. Invest Urol 8:195

Enhörning G (1961) Simultaneous recording of the intravesical and intraurethral pressure. Acta Chir Scand Suppl 276

Gosling J (1979) The structure of the bladder and urethra in relation to function. Urol Clin North Am 6:31

Graber P, Laurent G, Tanagho EA (1974) Effect of abdominal pressure rise on the urethral profile. An experimental study on dogs. Invest Urol 12:57

Heidler H, Jonas U, Petri E (1979) Urethral closure mechanism under stress conditions. Eur Urol 5:110

James ED (1976) Transmission of abdominal pressure to bladder and urethra. Proc 6th Annual Meeting Int Continence Soc, Antwerpen

Jonas U, Tanagho EA (1975) Studies on vesicourethral reflexes. I. Urethral sphincteric responses to detrusor stretch. Invest Urol 12:357

Jonas U, Tanagho EA (1976) Studies on vesicourethral reflexes. II. Urethral sphincteric responses to spinal cord stimulation. Invest Urol 13:278

Lapides J, Ajemian EP, Stewart BH, Breakey BA, Lichtwardt JR (1960) Further observations on the kinetics of the urethrovesical sphincter. J Urol 84:86

Miller (1964) Anatomy of the dog. Saunders, Philadelphia

Nobuo Koinuma, Seigi Tsuchida, Osamu Nishizawa, Itaru Moriya, Ikuo Wada, Kenichi Ebina (1981) Urethral responses to nerve stimulation measured by strain-gauge force transducer. Proc 11th Annual Meeting Int Continence Soc, Lund

Öbrink A, Bunne G, Ingelman-Sundberg A (1978) Pressure transmission to the pre-urethral space in stress incontinence. Urol Res 6:135

Rud T (1981) The striated pelvic floor muscles and their importance in maintaining urinary continence. In: Zinner NR, Sterling A (eds) Female incontinence. Alan R Liss, New York, p 79

Rud T, Andersson KE, Asmussen M, Hunting A, Ulmsten U (1980) Factors maintaining the intraurethral pressure in women. Invest Urol 17:343

Tanagho EA (1979) Urodynamics of female urinary incontinence with emphasis on stress incontinence. J Urol 122:200

Tanagho EA, Meyers FH, Smith DR (1969) Urethral resistance: its components and implications. I. Smooth muscle component. Invest Urol 7:136

Thüroff JW, Bazeed MA, Schmidt RA, Tanagho EA (1982) Mechanisms of urinary continence: An animal model to study urethral responses to stress conditions. J Urol 127:1202

Myogenic Excitation Conduction After Microsurgical Anastomosis of the Ureter

D. Rohrmann[1], J. Hannappel[1], and W. Lutzeyer[1]

Introduction

Ureteral peristalsis originates in the proximal part of the urinary collecting system by way of spontaneous depolarization of smooth muscle cells (Bozler 1942; Golenhofen and Hannappel 1973).

In vitro studies on isolated smooth muscle strips of the pyeloureter reveal a frequency gradient of spontaneous activity. The average frequency of activity decreases markably the more distal the site of preparation (Fig. 1) (Hannappel et al. 1982).

In situ, the frequent but non-coordinated spontaneous depolarizations of proximal smooth muscle cells appear to produce a change of the resting membrane potential (RMP) in the region of the pyeloureteral junction resulting in an all-or-none reaction. This mechanism offers the possibility of modulation of ureteral activity: There seems to be some sort of blockade at the pyeloureteral junction (Morita et al. 1981). During diuresis, the peristaltic rate increases until ureteric contractions occur at the same peristalsis as that of the most proximal calyceal segments (Constantinou et al. 1976). Bozler (1938) described the ureter as a functional syncytium. Normally, electrical activity arises proximally – as shown above – and is conducted distally from one muscle cell to its adjacent cell across areas of close cellular contact (Notley 1970; Gosling and Dixon 1982). These socalled gap junctions function as electric synapses which conduct the electric excitation from one muscle cell to the other without any chemical substance as transmitter (myogenic excitation conduction).

In 1958, Murnaghan published his results of investigations on congenital hydronephrosis. He described a subtle change in the arrangement of the smooth muscle cells that could possibly be the histological correlate of disturbed contractility.

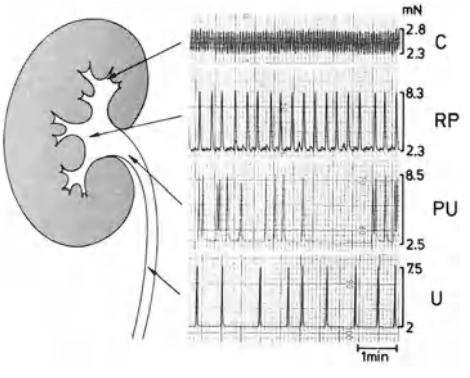

Fig. 1. In vitro study on isolated smooth muscle strips of the pyeloureter of the pig; spontaneous activity of strips originating from different parts of the pyeloureter. *C,* calyx; *RP,* renal pelvis; *PU,* pyeloureteral junction; *U,* ureter

[1] Abteilung Urologie der RWTH Aachen, Pauwelsstr., D-5100 Aachen

Investigative Urology 2
Edited by G. H. Jacobi et al.

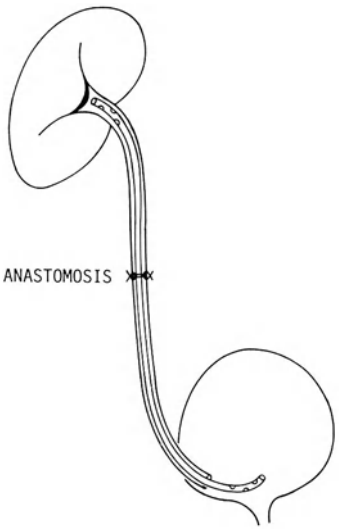

Fig. 2. Situation after complete transsection and anastomosis of the ureter. Indwelling ureteral stent

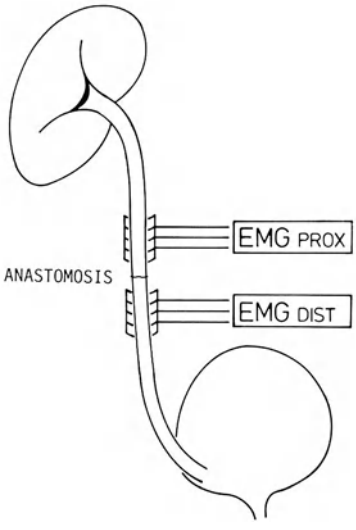

Fig. 3. Electromyography was done by installing 2 electrodes proximally and distally to the anastomosed area

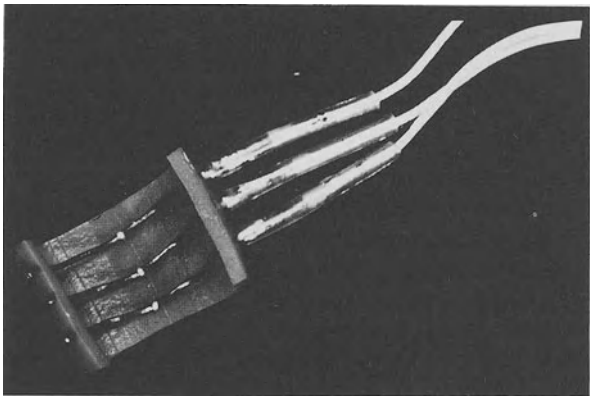

Fig. 4. One of the ring-shaped electrodes used for electromyographic recording

In order to get further information concerning this problem we started a series of experiments with special respect to ureteral activity after complete transsection and surgical anastomosis.

Material and Methods

In 15 rabbits, one ureter was exposed in its mid third by a median abdominal incision. It was carefully freed of its surrounding tissue and then transsected completely. A splint was inserted and advanced into the bladder. Then the 2 sides of the ureter were re-anastomosed by way of 4 end-to-end interrupted sutures (10–0 PDS). This

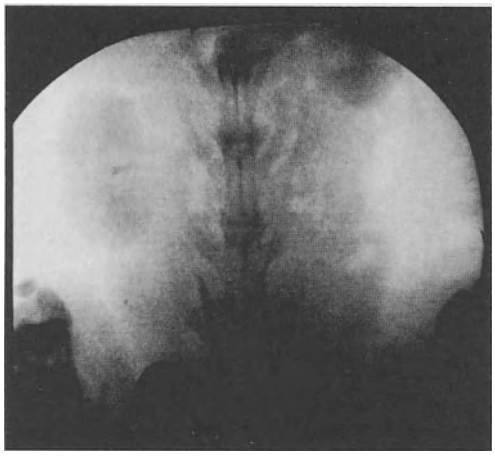

Fig. 5. X-ray of the urinary tract 5 min after the injection of contrast medium. The operation was done on the right ureter 3 months before

Fig. 6. Diagram showing several pictures taken from a permanent videotape recording after the injection of contrast medium. The operation was done on the right ureter 3 months before

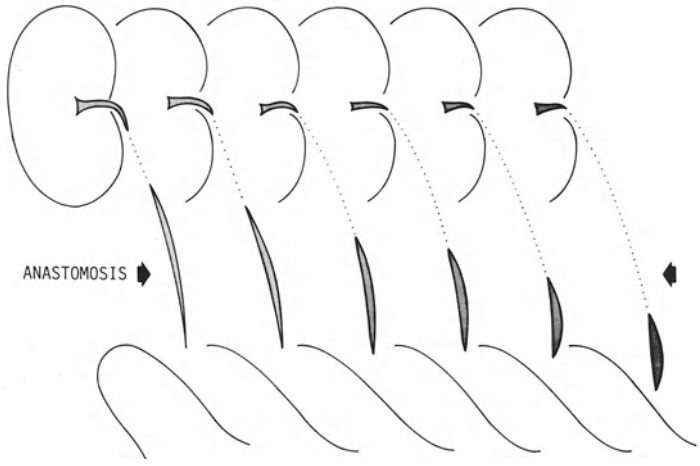

was performed by way of microsurgical techniques, using an operation microscope with a magnification of 25 (Fig. 2).

3 to 6 months after the operation ureteral activity was analyzed. Under anaesthesia, an X-ray of the urinary tract was done. We injected 6 to 8 milliliters of 70% contrast medium and did videotape recording. Then, the ureter was again exposed by a median laparotomy, and electromyography was done by installing 2 electrodes proximally and distally to the site of the anastomosis (Fig. 3). The contralateral ureter was investigated in the same way in order to compare both sides.

The ring-shaped electrodes consisted of 3 silvered copper wires fixed in some piece of plastic tube (Fig. 4). The inner diameter of the electrode was always more than the double ureteral diameter. As the electrode was only used for short-time measurements, the only disadvantage possible – permanent compression leading to a stenosis of the ureter – was without significance.

The animals were sacrificed 3 to 6 months after the operation and both ureters were investigated histologically. The site of the anastomosis was carefully examined for scar tissue and a special preparation was done to reveal tissue cholinesterase.

Results

After the injection of contrast medium, we observed the excretion by way of videotape recording. We found a normal and undisturbed excretion of contrast medium and an unobstructed ureteral peristalsis. Figure 5 shows the situation 5 minutes after the injection of contrast medium, the operation being done on the right ureter 3 months before. In order to make the peristalsis visible, we used a technique similar to that described by Durben et al. (1980). We took pictures from the videotape and combined them in one drawing, the frequency being 3 pictures per second (Fig. 6). The diagram clearly shows that the contraction ring at the proximal end of the urine bolus is propelled over the suture without any change in velocity.

Electromyography – done in the way described above – revealed spontaneous electrical activity proximally as well as distally to the anastomosis. Some instants after recording ureteral activity in the proximal part a similar activity is found distally to the anastomosis (Fig. 7). Compared to the contralateral side, no pathological time delay between the two electrodes occurred. Mechanic stimulation of the terminal ureter resulted in a phenomenon of retroperistalsis (Fig. 7).

Figure 8 shows the slow velocity record with multiple phases of activity, each of which reaches the distal electrode without any time delay.

The histological examinations have shown that groups of smooth muscle cells start growing into the site of the anastomosis. We are preparing to have a closer look

Fig. 7. On the left side you see normal ureteral activity as recorded proximally and distally to the anastomosis. On the right side a phenomenon of retroperistalsis. Rabbit ureter, 5 months after microsurgical anastomosis of the ureter

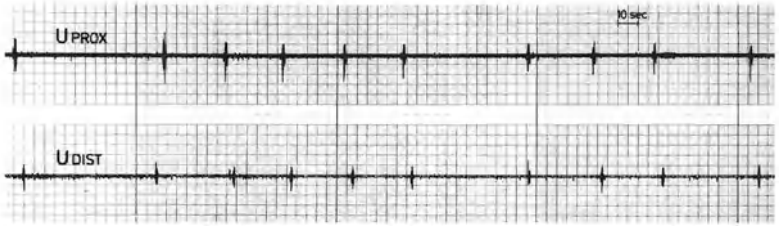

Fig. 8. Slow velocity record with multiple phases of activity. Rabbit ureter, 5 months after microsurgical anastomosis of the ureter

at the sutured area by way of electronmicroscopy in order to reveal whether newly formed areas of close cellular contact become evident after doing the anastomosis.

Discussion

The functional investigations after anastomosis of the ureter show an undisturbed excitation conduction. The histological investigations show the ingrowth of smooth muscle cells into the site of the anastomosis, but further investigations with special respect to electronmicroscopy are still necessary.

How to explain the undisturbed function after anastomosis of the ureter as measured by means of electromyography and radiology?

- As mentioned above, there is spontaneous activity all over the ureter. Thus, it is possible that the distal ureter develops its own new pacemaker after the cutting-off. This renders no explanation for the synchronization between proximal and distal ureter.
- The rise in pressure in the proximal ureter due to the peristalsis could induce the ureteral activity in the distal part by way of mechanical stimulation. This mechanism could achieve synchronization between proximal and distal ureter, but it would implicate a certain time delay between proximal and distal electrode.
- In our opinion, however, excitation conduction in the region of the anastomosis is created by new low resistance intercellular bridges that allow direct myogenic excitation conduction between neighboring cells. Long-term experiments to provide electronmicroscopic evidence of newly formed gap junctions are in preparation.

In cases of congenital hydronephrosis the open surgical approach (Pyeloplasty according to Anderson-Hynes) can provide an extensive contact area with an increased number of newly forming intercellular bridges. A simple dilatation or incision of the pyeloureteral region does surely not meet the requirements of an extensive contact area, but it only generates scar tissue.

References

Bozler E (1938) Electric stimulation and conduction of excitation. Am J Physiol 122:614
Bozler E (1942) The activity of the pacemaker previous to the discharge of a muscular impulse. Am J Physiol 136:543–552
Constantinou C, Hrynczuk J (1976) Urodynamics of the upper urinary tract. Invest Urol 14:233–240
Durben G et al (1980) The time-distance diagram. Invest Urol 18:207–208
Golenhofen K, Hannappel J (1973) Normal spontaneous activity of the pyeloureteral system in the guinea pig. Pflügers Arch 341:257–270
Gosling J, Dixon J (1982) Functional anatomy of the urinary tract. Gower Medical Publishing, London
Hannappel J et al (1982) Pacemaker process of ureteral peristalsis in multicalyceal kidneys. Urol Int 37:240–246
Morita et al (1981) Initiation and propagation of stimulus in the urinary tract. Invest Urol 19:157
Murnaghan GF et al (1958) The dynamics of the renal pelvis and ureter with reference to congenital hydronephrosis. Br J Urol 30:321–329
Notley RG (1970) The musculature of the human ureter. Br J Urol 42:724

Spongiosolysis for Erectile Dysfunction Due to Pathologic Cavernoso-glandular Shunts

C. G. Stief[1], P. Gilbert[1], W. F. Thon[1], and J. E. Altwein[2]

In about 20%–30% of impotent patients venous insufficiency is the only or a concomitant cause of erectile dysfunction. Until quite recently, ligation of the dorsal veins of the penis (Wespes and Schulman 1985) represented the only effective surgical procedure in the treatment of venous leakage. Already in 1902, Wooten suggested this operation for therapy of atonic impotence, as he called the pathological venous drainage of the cavernous bodies (Wooten 1902). The surgical technique is as follows: an infrapubic approach guarantees a good exposure of all dorsal veins of the penis. At first, the superficial dorsal veins are exposed, doubly ligated and cut through. The same procedure is performed on the deep dorsal vein, which must be isolated from both dorsal arteries beneath Buck's fascia. According to different authors, the operation is reported to be successful in 10%–85% (Wespes and Schulman 1985; Lewis and Puyau 1986). We in Ulm have operated on 32 patients. 14 of them are able to obtain spontaneous erections, considering a short-term follow-up of 6 months.

It is obvious that not all patients with venous insufficiency may benefit from ligation of the dorsal veins of the penis, since this operation does not solve the problem of distal venous leakage. The anatomical substrate of the latter consists of small venous

Fig. 1. Longitudinal section of the distal third of the penis

[1] Urologische Abteilung des Bundeswehrkrankenhauses Ulm, D-7900 Ulm
[2] Urologische Abteilung des Krankenhauses Barmherzige Brüder, Romanstr. 93, D-8000 München

Investigative Urology 2
Edited by G. H. Jacobi et al.

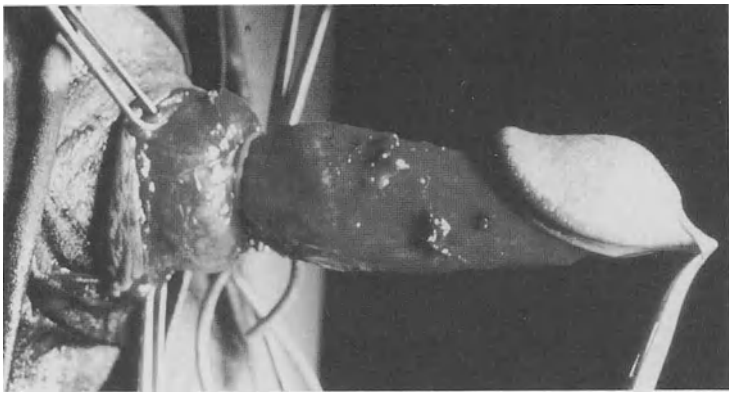

▲
Fig. 2. Sleeve technique

Fig. 3. Dissection of the C. spongiosum

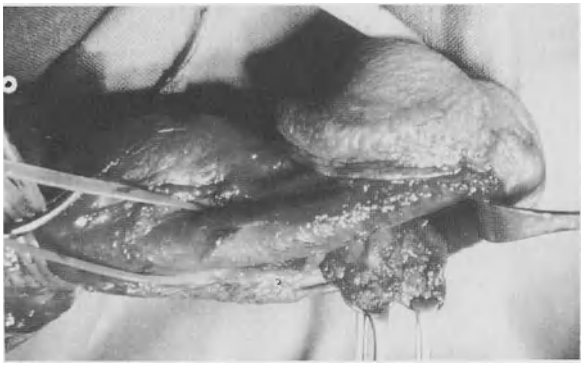

Fig. 4. Complete isolation of the tips of the C. cavernosa

shunts between the distal third of the corpora cavernosa and the corpus spongiosum, including the glans, as Tudoriu and coworkers have proved in their experimental studies (Ashdown and Gilanpour 1974; Tudoriu and Bourmer 1953). Figure 1 shows a longitudinal section of the distal third of the penis. In the histological section, venous vessels of various sizes were revealed between glans and cavernous body.

Basing on these morphological facts, we developed a new surgical procedure, called spongiosolysis, in order to close those distal venous shunts.

▲ **Fig. 5.** Pathological drainage via dorsum penis

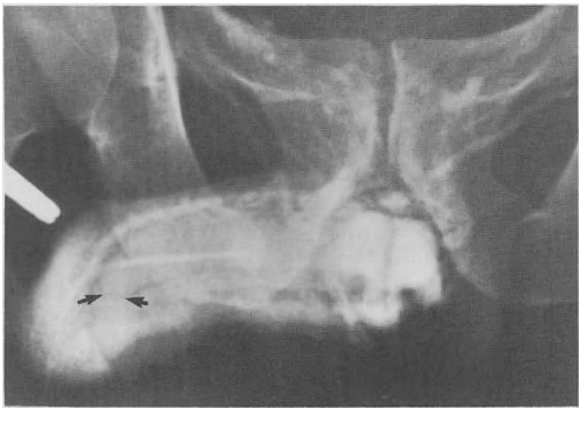

Fig. 6. Shunts between C. cavernosum and C. spongiosum/glans (→)

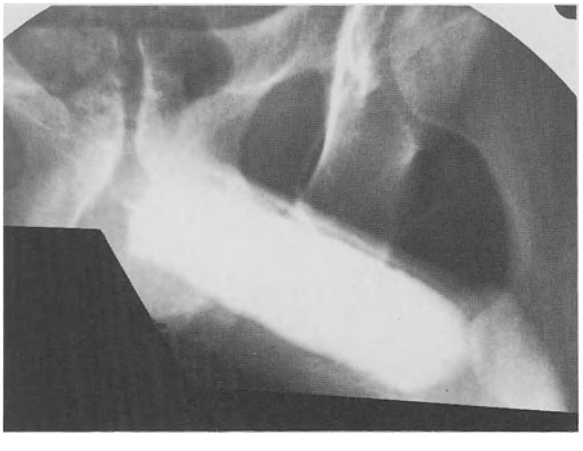

Fig. 7. Postoperative cavernosography

Surgical Method

The operation itself begins with circumcision and drawing back of the skin to the root of the penis (Fig. 2). A tourniquet proves useful. This step is followed by dissection of the corpus spongiosum (Fig. 3). An indewelling catheter facilitates the procedure. The tips of the cavernous bodies are cautiously dissected. Finally, the cavernous bodies are completely isolated in their distal third (Fig. 4, their tips are held by Allis-clamps). The operation is completed by hemostasis and skin sutures. A circular pressure bandage is kept for 3 days.

Results

Our short-term results (follow-up 6 months) in 5 patients are as follows: in every case but one, cavernosography showed no evidence of venous leakage; these patients regained the ability of erection with the help of cavernous autoinjectiontherapy, which became necessary because of concomitant arterial dysplasia in 3 cases and diabetic angiosclerosis in 1 case. One patient remained impotent. Cavernosography showed insufficiency of the deep dorsal vein to be the cause of continous erectile dysfunction. In this case ligation of the deep dorsal vein is stil necessary.

The importance of proper diagnosis and therapy shall be outlined by the example of combined venous insufficiency that is distal venous leakage and insufficiency of the deep dorsal vein, in a patient aged 35: preoperative cavernosography shows drainage of contrast medium via the dorsal veins and the glans (Fig. 5). After ligation of the dorsal veins, enhanced venous drainage via the glans and the corpus spongiosum is the consequence. The patient remained impotent (Fig. 6). Following spongiosolysis, no venous leakage is present (Fig. 7). Our patient regained the ability of erection by intracavernous injection of vasoactive drugs.

Discussion

In erectile dysfunction due to venous leakage, deep dorsal vein ligation (DDVL) is a systematic surgical approach to the pathologic cavernous drainage via the dorsum penis. After diagnosis of the venous leakage by dynamic cavernosography, the majority of the patients suffering from venous insufficiency will benefit from DDVL, at least in getting responders to the intracavernous injection of vasoactive drugs.

The successful closure of localized fistulas between glans and C. cavernosum, respectively as reason of impotence has been reported (Ebbehøj and Wagner 1979), but a systematic approach to distal venous leakage was lacking. The complete transsection of all venous shunts is guaranteed by careful dissection of the distal half of the C. spongiosum including the glans.

In combination with ligation of the dorsal veins of the penis it may solve the problem of venous insufficiency in erectile dysfunction. Nevertheless, a greater number of patients and long-term follow-up are required to confirm these preliminary results.

References

Ashdown RR, Gilanpour H (1974) Venous drainage of the corpus cavernosum penis in impotent and normal bulls. J Anat 117:159–170

Ebbehøj J, Wagner G (1979) Insufficient penile erection due to abnormal drainage of cavernous bodies. Urology 13:507–510

Lewis RW, Puyau FA (1986) Surgery for venous vasculogenic impotence. 5th Int Symposium of Operative Andrology, Berlin

Tudoriu T, Bourmer H (1953) The hemodynamics of erection at the level of the penis and its local detoriation. J Urol 129:741–745

Wespes E, Schulman CC (1985) Venous leakage: Surgical treatment of a curable cause of impotence. J Urol 133:796–798

Wooten JS (1902) Ligation of the dorsal vein of the penis as cure for atonic impotence. Texas MJ 18:325

RigiScan Penile Rigidity and Tumescence Monitoring in Impotent Patients as a Diagnostic Tool and as an Objective Assessment of the Effect of Intracorporeal Injection of Papaverine Hydrochloride

J. L. Bruins[1], A. E. J. L. Kramer[1], and U. Jonas[1]

Introduction

In order to obtain or sustain a penile erection with sufficient rigidity to allow intromission it is necessary that normal libido, good arterial supply to the cavernous bodies with normal decrease of venous outflow, normal functioning of the autonomic nervous system and good endocrine status coexist. In patients complaining of erectile impotence, each of these functions should be carefully evaluated before treatment is started. This includes detailed history and physical (including neurological) examination; determination of serum hormone levels; calculation of the penile brachial index; psychological screening and measurement of nocturnal penile tumescence and rigidity. If necessary, pelvic angiography and perfusion cavernosography are performed.

The primary goal of the evaluation of the impotence is to characterize patients into 2 therapeutic categories, one consisting of those patients for whom psychological counselling should be tried first and the second of patients without psychological abnormality in whom the sexual dysfunction is secondary to an organic disease process. Therapy in the second group will be the application of intracavernous vasoactive drugs or surgery.

The aim of this study is threefold:

- to test the value of continuous monitoring of tumescence and rigidity in the evaluation of patients with impotence,
- to settle the value of intracavernous injection of papaverine hydrochloride as a screening test for impotence,
- to test the possibility of replacing nocturnal RigiScan recording by real-time measurement after papaverine injection and during visual sexual stimulation.

Recording of Penile Tumescence and Rigidity

A normal pattern of nocturnal penile tumescence (Karacan et al. 1978; Bohlen 1981) indicates the integrity of neural supply, vascular supply and penile structures. If this pattern is found in a man with complaints of impotence this might be an indication of psychogenic impotence, while abnormal nocturnal penile tumescence is indicative of organic impotence. However, the common complaint is not lack of increasing volume during erection but lack of stiffness, so penile rigidity seems a more crucial variable than circumferential expansion (Marshall et al. 1981; Metz and Wagner

[1] Department of Urology, Leiden University Hospital, Rijnsburgerweg 10, NL-2333 AA Leiden

Investigative Urology 2
Edited by G. H. Jacobi et al.

1981; Wein et al. 1981; Wespes and Schulman 1984; Condra et al. 1986). Nocturnal penile tumescence monitoring alone is therefore of limited value in the diagnosis of impotence.

Penile rigidity measurements include recording of buckling force (Karacan et al. 1978); penile application of stamps (Barry et al. 1980), Erektiometer bands (Jonas 1982) or snap-gauge cuffs (Ek et al. 1983); or photography (Wein et al. 1983). These techniques, however, lack detailed documentation of frequency, quality or duration of penile rigidity and of possible difference in rigidity between penile base and shaft. A minimum duration of the rigid period appears to be of importance, too (Wein et al. 1983; Buvat et al. 1986; Sidi and Lange 1986).

Recently a new device (RigiScan) has been developed that measures more accurate tumescence and rigidity in patients with impotence (Bradley et al. 1985; Kaneko and Bradley 1986). The system features a self-contained micro-processor with clock, calender and data storage, and 2 loop strings connected to 2 D.C. motors. The system is battery-powered, with a separate long-life battery for the micro-processor and memory system. The weight is 2.3 kg. For a measurement the loop strings are placed near the base and near the tip of the penis respectively. During the measurement the loops are tautened every 15 s with a force of 1.7 N to measure penile circumference. The loop length is read from potentiometers. In between the loops are free and follow possible tumescence. When, after tautening, tumescence increase over 1 cm is noted, the loops are tautened with a somewhat higher force (2.8 N) and the resulting extra shortening of the loop is a measure for the penile rigidity. The rigidity measurement is taken once every 30 s during the erection phase and is stopped if the tumescence reading falls below the starting level of that phase again.

The penile circumference is measured with an accuracy of 0.05 cm in a range of 5–15 cm. If the circumference is outside this range, the data is lost during this period. The rigidity is given in a percentage, 100% rigidity meaning that no extra shortening is measured under the higher force. For each 0.05 cm extra shortening the rigidity figure is diminished by 2.3%. It must be appreciated that this rigidity measurement reads the circumferential rigidity of the penis and that in fact the axial rigidity, or buckling force, is the clinical important parameter. Bradley et al. (1985) showed that the circumferential rigidity is linearly related to the buckling force. The clinical impression is that rigidity or buckling force need to reach a fixed level.

After the recording the RigiScan's memory contains the record's identification data and 4 series of circumference measurement data: the base and tip circumferences, sampled every 15 s, respectively the base and tip circumferences at the higher force during rigidity testing, sampled every 30 s. If no rigidity has been tested the latter 2 data are coded as "no-test". The storage capacity of the instrument enables to hold the data of up to three 10-hour monitoring sessions. The instrument's memory contents can be dumped into a micro-computer memory and stored permanently on floppy disks. The RigiScan memory then can be erased and prepared for a new measurement.

Monitoring can be performed either with the stand-alone instrument or with the instrument connected to the microcomputer (real-time measurement). The first method is practised especially for nocturnal (sleep) monitoring in patients. Real-time studies are monitored directly on the graphic video terminal and both real-time and off-line studies can be displayed from the floppy disk storage on the terminal. The

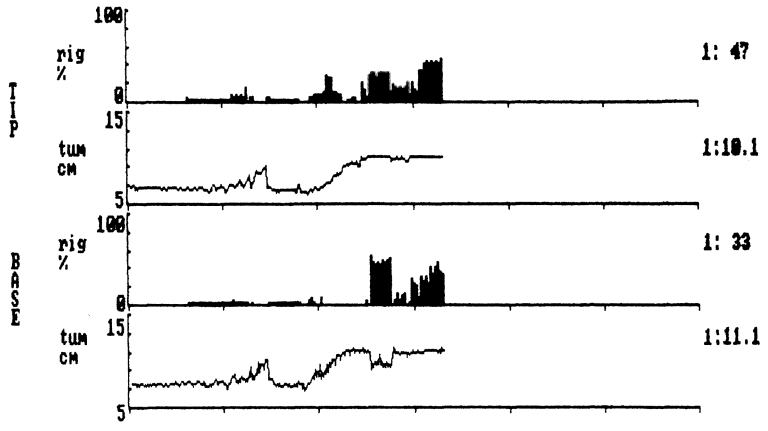

Fig. 1. Copy of real-time RigiScan session (2-hour screen)

Table 1. Normal findings with RigiScan monitor (Dacomed 1986)

Number of erections	3–6/8-h night
Duration of erections	10–15 min/event
Tumescence base	> +3 cm
Tumescence tip	> +2 cm
Rigidity insufficient	< 40%
Rigidity maybe sufficient	40%–70%
Rigidity sufficient	> 70%
Abnormalities	
Dissociation:	normal base readings with abnormal tip rigidity (with or without normal tip tumescence)
Uncoupling:	normal tumescence with abnormal rigidity (base and tip)

system software gives a representation of the data in 4 graphs: base and tip circumferences and rigidities, in cm and % respectively (Fig. 1). During the real-time study the most recent values of circumferences and rigidities are displayed also. All terminal screens can be hard-copied onto the computer printer.

Nocturnal sessions can be interrupted: the system will remain stand-by for 15 min after switch-off and the session will be continued if switched on again within this period. For nocturnal recordings to be reliable at least 2–3 night sessions are necessary. This corroborates findings of Bradley et al. (1985) and those in classical nocturnal penile tumescence recordings (cf. Buvat et al. 1986). Based on RigiScan data of over 500 patients in the Uro-Center of San Diego, Johnson summarized the guidelines of normal data as given in Table 1 (Dacomed 1986).

Intracavernous Injection of Vasoactive Drugs in Impotent Males

Intracorporeal injection of papaverine hydrochloride can produce drug-induced erection (Virag 1982). In normal men the smooth muscle around the sinusoidal channels in the corpora cavernosa relaxes, the arterial inflow increases and the venous outflow decreases (Abber et al. 1986). The method is used in management of neurogenic and vascular impotence (Sidi et al. 1986; Zorgniotti and Lefleur 1985).

Virag et al. (1984a, b) found after injection statistically different responses between non-organic impotence and impotence due to neurovascular lesions. This might qualify intracavernous papaverine injection as a screening test in differential diagnosis of erectile dysfunction.

Patients and Methods

8 healthy volunteers were monitored during a sexual stimulation video show. Their recording were performed on the off-line system. Afterwards they gave a subjective grading of the erection performance.

22 impotent males were studied. All patients underwent routine screening tests. 17 patients performed measurements with the RigiScan during 2 or 3 consecutive nights, mostly at home. The results were judged according to Johnson's guidelines (Table 1) with the exception of the number of erections: the occurrence of a single event was judged as positive.

Tumescence and rigidity were recorded in all patients during direct visual stimulation at the outclinic department. The procedure was as follows: after a habituation period of 5 min, a sexual stimulation video tape was run for a period of 25 min. After a resting period of 5 min, 80 mg papaverine hydrochloride were injected intracorporeal and the effect was recorded during 35 min. Between 15 and 20 min after injection compression of the penile base was performed by means of a rubber band. The session was ended with another 10 min of video stimulation (Fig. 2). The whole session was recorded with the RigiScan system in the real-time mode.

Results

All volunteers showed good tumescence increase (Fig. 3). Rigidity correlated well with their subjective interpretation. The results also corroborated Johnson's data in

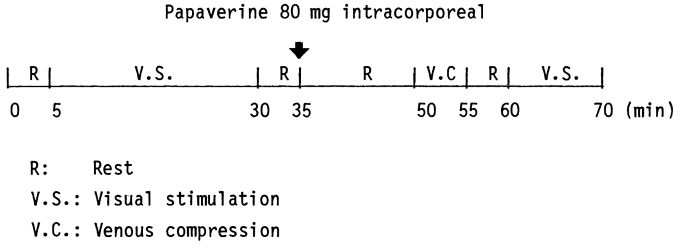

Fig. 2. Set-up of real-time session

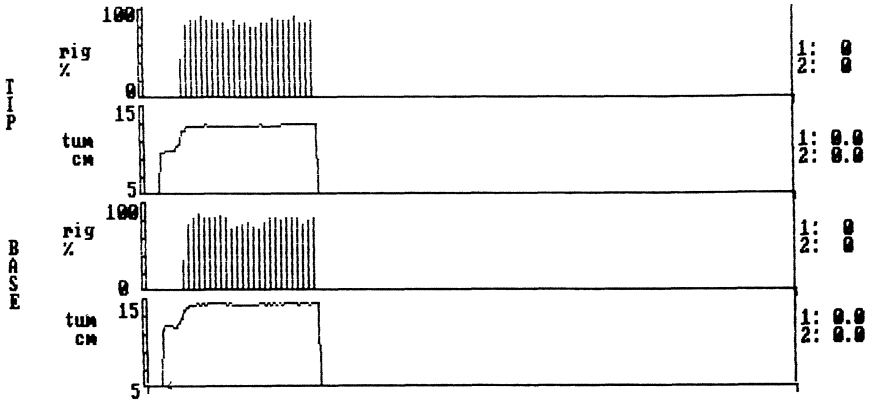

Fig. 3. RigiScan recording (volunteer; 1-h screen)

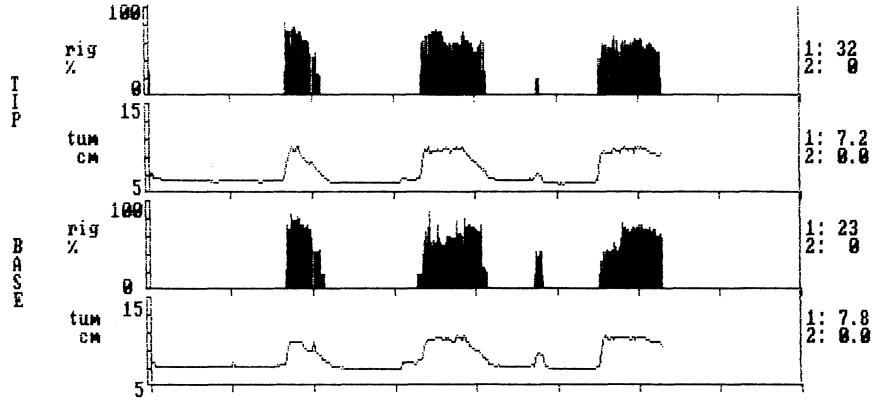

Fig. 4. Nocturnal RigiScan recording in psychogenic impotence (P5; 8-h screen)

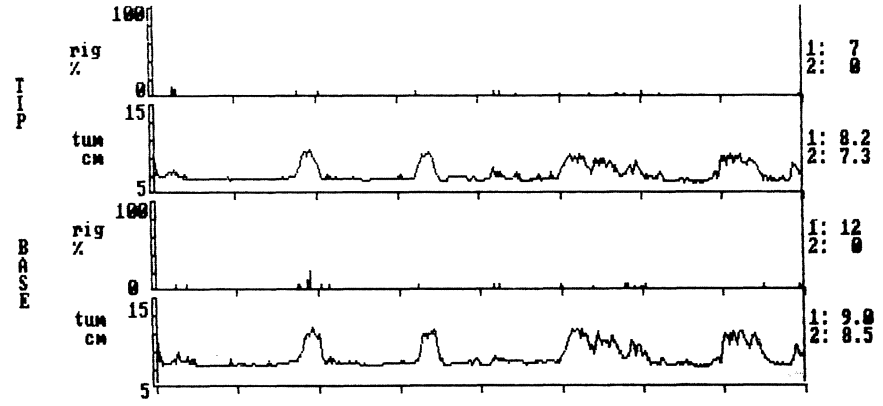

Fig. 5. Nocturnal RigiScan recording in organic impotence (O7; 8-h screen)

that rigidity of less than 40% was judged as insufficient, from 40%–70% as partly sufficient and over 70% as sufficient for coitus.

For the patient recordings therefore rigidity of at least 40% is regarded as adequate.

The patients were divided into 3 preliminary diagnosis groups, based on history and clinical investigation. Pure psychogenic impotence was diagnosed in 5 men (2 with ejaculatio praecox), pure organic impotence in 9, and mainly psychogenic with co-existence of an organic factor in the remaining 8.

Figure 4 shows the nocturnal recording from a psychogenic patient. 3 periods of good erection lasting 15 min–30 min and a short fourth one are found. In an organic patient (Fig. 5) good tumescence is found, but no rigidity. This patient was a young man with vascular impotence after pelvic fracture.

The real-time measurements in the same patients (Figs. 6, 7) show in the end comparable results (Table 2).

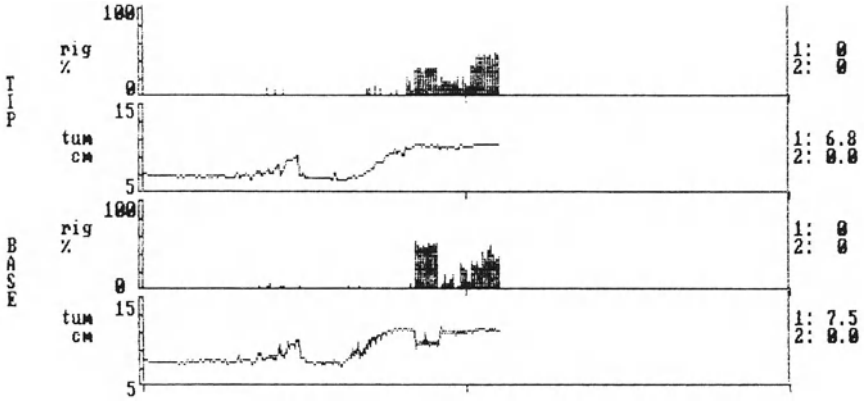

Fig. 6. Real-time RigiScan recording in psychogenic impotence (P5; 2-h screen)

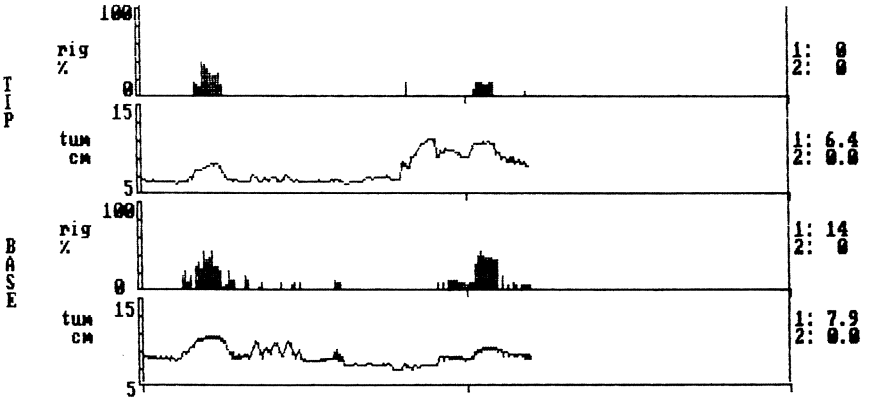

Fig. 7. Real-time RigiScan recording in organic impotence (O7; 2-h screen)

Visual stimulation alone elicited good tumescence increase in all 5 psychogenic patients, in 4 with adequate rigidity. 8 organic patients and 6 from the mixed group showed no reaction at all, the remaining one, respectively 2, only tumescence increase.

After injection of papaverine hydrochloride, tumescence increased with a 2 min–15 min delay in all but 5 organic and 1 mixed patient, however, in another mixed patient the result could not be checked because of a collapse. The same 4 psychogenic and 2 mixed patients now demonstrated adequate rigidity. Visual stimulation after injection elicited no tumescence increase in other patients, but the last psychogenic patient and another 3 from the mixed group now demonstrated adequate rigidity. Venous compression gave rise to tip tumescence increase and – of course – base tumescence decrease in all patients. Only in patients with rigidity before compres-

Table 2. Results of real-time and nocturnal RigiScan recordings in 22 impotent patients

Patients	Visual stimulation		Papaverine injection		+ Venous compression (Rig.)	+ Visual stimulation (Rig.)	Night recording	
	Tum.	Rig.	Tum.	Rig.			Tum.	Rig.
Psychogenic								
P1	+	+	+	+	+	+	+	+
P2	+	+	+	+	+	+	+	+
P3	+	+	+	+	+	+	+	+
P4	+	+	+	+	+	+	0	0
P5	+	–	+	–	+	+	+	+
Organic								
O1	–	–	–	–	–	–	0	0
O2	–	–	–	–	–	–	–	–
O3	–	–	+	–	–	–	0	0
O4	–	–	–	–	–	–	–	–
O5	–	–	–	–	–	–	–	–
O6	–	–	–	–	–	–	0	0
O7	+	–	+	–	–	–	+	–
O8	–	–	+	–	–	–	+	–
O9	–	–	+	–	–	–	0	0
Mixed								
M1	+	–	+	–	–	+	+	+
M2	+	–	+	–	–	–	+	–
M3	–	–	+	–	–	+	+	–
M4	–	–	+	–	–	+	+	+
M5	–	–	*	*	*	*	+	+
M6	–	–	+	+	+	+	+	+
M7	–	–	–	–	–	–	–	–
M8	–	–	+	+	+	+	+	+

0: No night recording performed
*: Patient collapsed after Papaverine injection

sion and in the fifth psychogenic patient an increase in rigidity was found, mainly at the base.

Nocturnal recordings were performed in 4 psychogenic, 5 organic and all 8 mixed patients. From the 17 sleep sessions (best of 2 or 3 in the same patient) no tumescence increase and rigidity was found in 4. 3 of these patients had a preliminary diagnosis of organic, 1 of mixed impotence. In 4 patients (2 organic, 2 mixed) nocturnal tumescence occurred, but without rigidity. The 4 psychogenic and 5 of the mixed patients showed good nocturnal erections.

From the 16 patients in whom both real-time and nocturnal studies have been completed, the tumescence and rigidity results are comparable in 15. One mixed patient (M3) showed tumescence during the night but rigidity lasted too short. Sufficient rigidity at the base was found during visual stimulation after papaverine injection.

Discussion

Reconsidering the real-time experiment it was decided that squeezing of the base of the penis by a rubber band was probably inadequate to reduce the venous outflow. It also might give artefactual recordings of rigidity at the base because of the constriction. Therefore, the results of this intervention are not evaluated.

The results on healthy volunteers indicate that the RigiScan monitor is a reliable and objective system to record and measure erection quality.

4 of the patients with a preliminary diagnosis of psychogenic impotence showed tumescence and rigidity already during the first visual stimulation, the fifth was only slightly tumescent. In this patient tumescence increased after Papaverine injection and rigidity was found at the later visual stimulation (Fig. 6). Nocturnal measurements in all 4 patients with sleep studies in this group show sufficient erections. Especially also the duration of these erections was within normal ranges. The conclusion is that this type of patients can be diagnosed by a positive response to sexual stimulation video tapes, when necessary combined with intracorporeal injection of papaverine hydrochloride.

None of the organic patients showed rigidity during the real-time session, neither during the night. These patients thus can be diagnosed by a negative result after intracorporeal injection of papaverine hydrochloride combined with visual stimulation. Tumescence increase only can occur, but their erection fails rigidity (Fig. 7).

In one mixed patient no results after injection could be evaluated because the patient collapsed after the injection. The night recordings of this patient show sufficient erections.

5 patients in this group demonstrated sufficient rigidity after injection or during the second visual stimulation. 4 of them had good nocturnal erections, too. It is therefore believed that their main problem is of psychological nature. The other patient (M3) is possibly mainly psychogenic, too, although this was not proven in the nocturnal recordings. However, sleeping disturbances were not ruled out because no simultaneous rapid eye movement recording was performed. If yet this patient's night registration is correct, then his impotence is caused mainly by an organic failure, that is sensitive to papaverine injection therapy. His impotence then might be neurogenic (Sidi et al. 1986; Sidi and Lange 1986). The remaining mixed patients had

no rigidity (M2) or not even tumescence (M7) during the real-time and the nocturnal recording and are supposed to be organic impotent.

Conclusions

The final conclusions of this study are:

- RigiScan monitoring of erections, by continuous recording of penile rigidity and tumescence, increases the quality of the diagnosis in impotent patients.
- Real-time monitoring with intracorporeal injection of papaverine hydrochloride and visual stimulation will separate out the major organic and papaverine-resistent types of impotence. These patients might show tumescence increase only without rigidity.
- Real-time monitoring with papaverine injection and visual stimulation obviates the necessity for nocturnal recordings in impotence.
- Real-time monitoring with papaverine injection and visual stimulation will give positive results for tumescence and rigidity in patients with psychogenic impotence.

References

Abber JC, Lue TF, Orvis BR, McClure RD, Williams RD (1986) Diagnostic tests for impotence: a comparison of papaverine injection with the penile-brachial index and nocturnal tumescence monitoring. J Urol 135:923–925

Barry JM, Blank B, Boileau M (1980) Nocturnal penile tumescence monitoring with stamps. Urology 15:171–172

Bohlen JG (1981) Sleep erection monitoring in the evaluation of male erectile failure. Urol Clin North Am 8:119–134

Bradley WE, Timm GW, Gallagher JM, Johnson BK (1985) New method for continuous measurement of nocturnal penile tumescence and rigidity. Urology 26:4–9

Buvat J, Buvat-Herbaut M, Dehaene JL, Lemaire A (1986) Is intracavernous injection of Papaverine a reliable screening test for vascular impotence? J Urol 135:476–478

Condra M, Morales A, Surridge DH, Owen JA, Marshall P, Fenemore J (1986) The unreliability of nocturnal penile tumescence recording as an outcome measurement in the treatment of organic impotence. J Urol 135:280–282

Dacomed Corporation, Minneapolis, Minnesota, USA (1986) RigiScan ambulatory rigidity and tumescence system. Selected case studies. Form number 750-156-0486

Ek A, Bradley WE, Krane RJ (1983) Nocturnal penile rigidity measured by the snap-gauge band. J Urol 129:964–966

Jonas U (1982) Erektiometer: Ein einfacher und sicherer Test in der Diagnostik der erektilen Impotenz. Akt Urol 13:324–327

Kaneko S, Bradley WE (1986) Evaluation of erectile dysfunction with continuous monitoring of penile rigidity. J Urol 136:1026–1029

Karacan I, Salis PJ, Williams RL (1978) The role of the sleep laboratory in the diagnosis and treatment of impotence. In: Williams RL, Karacan I, Frazier SH (eds) Sleep disorders: diagnosis and treatment. Wiley, New York

Marshall P, Morales A, Surridge D (1981) Unreliability of nocturnal penile tumescence recording and MMPI profiles in assessment of impotence. Urology 17:136–139

Metz P, Wagner G (1981) Penile circumference and erection. Urology 18:268–270

Sidi AA, Lange PH (1986) Recent advances in the diagnosis and management of impotence. Urol Clin North Am 13:489–500

Sidi AA, Cameron JS, Duffy LM, Lange PH (1986) Intracavernous drug-induced erections in the management of male erectile dysfunction: experience with 100 patients. J Urol 135:704–706

Virag R (1982) Intracavernous injection of Papaverine for erectile failure. Lancet 938
Virag R, Frydman D, Legman M, Virag H (1984a) Intracavernous injection of Papaverine as a diagnostic and therapeutic method in erectile failure. Angiology 79–87
Virag R, Spencer PP, Frydman D (1984b) Artificial erection in diagnosis and treatment of impotence. Urology 24:157–161
Wein AJ, Fishkin R, Carpiniello VL, Malloy TR (1981) Expansion without significant rigidity during nocturnal penile tumescence testing: a potential source of misinterpretation. J Urol 126: 343–344
Wein AJ, Arsdalen KV, Malloy TR (1983) Nocturnal penile tumescence. In: Krane RJ, Siroky MB, Goldstein I (eds) Male sexual dysfunction. Little/Brown, Boston
Wespes E, Schulman CC (1984) Parameters of erection. Brit J Urol 56:416–417
Zorgniotti AW, Lefleur RS (1985) Auto-injection of the corpus cavernosum with a vasoactive drug combination for vasculogenic impotence. J Urol 133:39–41

VIP – A Peripheral Neurotransmitter in Penile Erection

K.-P. Jünemann[1], T. F. Lue[2], H. Melchior[1], and E. A. Tanagho[2]

Vasoactive intestinal polypeptide (VIP), a 28-amino acid polypeptide, was first isolated from the human gut by Said and Mutt (1970) and is believed to possess all characteristics of a neurotransmitter. Recent studies have shown that the distribution of this neuropeptide is ubiquitous, mainly in the genitourinary tract (Larsson et al. 1977; Fahrenkrug and Schaffalitzky de Muckadell 1978; Fahrenkrug 1979; Ottesen et al. 1981; Steers et al. 1984). Its major effects are smooth muscle relaxation and vasodilation. These functional tissue reactions have led to speculation that VIP may be a neurotransmitter in penile erection (Rattan et al. 1977; Ottesen et al. 1984; Goldstein et al. 1985). Therefore, we designed an in vivo animal model to study the effects of VIP and VIP-antibody (VIP-AB) on penile erection, as well as its distribution in the erectile tissue by immunohistochemistry.

Material and Methods

In 7 adult, healthy, anesthetized, mongrel dogs (20.5–27 kg) the influences of VIP and VIP-antibody on the different stages of neurostimulation induced penile erection was studied. For this purpose, all dogs underwent cuff-electrode implantation around the cavernous nerve enabling us to induce a full erection by electrostimulation of the nervus cavernosus. After threshold parameters for neurostimulation – induced erection were determined and arterial inflow and venous outflow studies were performed, as described elsewhere (Jünemann et al. 1986a, b), VIP-antibody (1:10) was injected intracorporeally before the electrostimulation study was repeated. After the effect of VIP-antibody had worn off, the effect of VIP on penile erection was tested. Arterial inflow, corporeal pressure and systemic blood pressure were recorded simultaneously.

In a second immunohistochemical study, 4 dogs underwent in vivo fixation of the penis with 0.4% para-benzaquinone. Immunohistochemical staining was performed and the distribution of VIP in the erectile tissue was observed under an ultraviolet microscope.

Results

Intracorporal injection of 5–10 μg or 30–50 μg VIP caused a moderate-to-strong erection in all 6 dogs studied (Table 1). Interestingly, the arterial inflow increase was

[1] Klinik für Urologie, Städtische Kliniken Kassel, Mönchebergstr. 41/43, D-3500 Kassel
[2] Department of Urology, University of California, San Francisco Medical School, San Francisco, CA 94143, USA

Investigative Urology 2
Edited by G. H. Jacobi et al.

Table 1. Mean arterial inflow and corporeal pressure responses after VIP[a]

Dosage (μg)	Corporeal pressure (cm H_2O)			Arterial flow (ml/min)		
	Base-line	Peak	Rise	Base-line	Peak	% Rise
5–10	15.2	77.2	62	9.1	10.5	15.4
30–50	14.5	86.3	71.8	7.6	13.8	81.6

[a] 5 dogs were given the lower dosage range, 6 dogs the higher; the aorta was not clamped. All achieved erection

Table 2. Mean intracorporeal pressure responses to saline infusion before and after VIP in 3 dogs[a]

	Erection response	Corporeal pressure (cm H_2O)		
		Base-line	Peak	Rise
Before VIP	No	11.3	21	9.7
After VIP	Yes	9.3	187.3[b]	178

[a] Saline was infused at 1.9 ml/min (3.8 ml/min in 1 dog); VIP dosage was 5 μg. Each study was performed twice
[b] The recording ran off the scale

Table 3. Mean arterial inflow and corporeal responses to neurostimulation before and after VIP antibody in 5 dogs[a]

	Corporeal pressure (cm H_2O)			Arterial flow (ml/min)		
	Base-line	Peak	Rise	Base-line	Peak	% Rise
Before VIP-AB	21.6	145.2	123.6	7.9	55.2	599
After VIP-AB[b]	24.8	131.6	106.8	7	49.9	613

[a] VIP-AB was given as a 1:10 dilution with 0.9 ml normal saline solution; aorta open
[b] In 1 dog, VIP-AB did not block the venous outflow restriction (see Results) and 4 dogs were unable to maintain the erection

minor and was not significantly different from the baseline flow in a flaccid state. However, a venous outflow restriction after VIP injection was measured, due to corporeal smooth muscle relaxation (Table 2). By intracorporeal VIP-antibody application one should determine if the neurostimulation – induced erection response could be blocked. As Tables 3 and 4 clearly show, the VIP-antibody effect on the arterial inflow-rise, due to electrostimulation was minor; however, the venous outflow re-

Table 4. Mean intracorporeal pressure response to saline infusion without and with neurostimulation before and after VIP antibody in 5 dogs[a]

Stimulation	Erection response	Corporeal pressure (cm H_2O)		
		Base-line	Peak	Rise
Before VIP-AB				
Off	No	16	29.4	13.4
On	Yes	18.4	159.6[b]	141.2
After VIP-AB				
Off[c]	No	22	31	9
On	No	27.6	46.4	18.8[d]

[a] Saline was infused at 1.9 ml/min; VIP-AB was given as a 1:10 dilution with 0.9 ml normal saline solution; aorta occluded
[b] In 3 dogs, the recording ran off the scale
[c] 4 dogs only
[d] In 2 dogs, the pressure dropped 8 and 12 cm H_2O

striction during neurostimulation of the cavernous nervebundle was blocked completely after VIP-antibody injection (Table 4). 2–3 h after VIP-antibody application the blocking effect had worn off.

Theoretically, the observed influence of VIP-antibody on the erection response could have been due to another unknown inhibitor. We therefore examined the neurostimulation – induced erection response after VIP-antibody (1:10) had been preincubated with 50 µg of VIP. The preabsorbed VIP-AB/VIP-combination did not modify the erection response, indicating that the VIP-antibody inhibiting effect was specific.

By means of immunohistochemical evaluation of the penile tissue, the VIP distribution in the corpus cavernosum should be determined. Our microscopic observations showed VIP-immunopositive areas in the entire penis, in particular around blood vessels and close to the endothelium of the corporeal smooth muscle.

Conclusion

From our in vivo animal studies we conclude that VIP is one of the neurotransmitters in the penile erectile tissue that has been shown in the smooth muscle cells of the corpora cavernosa and in close proximity to penile vascular structures. Its effect on the penis is similar to that with neurostimulation – induced erection: increase of the arterial inflow and decreased venous outflow, due to sinusoidal relaxation.

References

Fahrenkrug J (1979) Vasoactive intestinal polypeptide: Measurement, distribution and putative neurotransmitter function. Digestion 19:149

Fahrenkrug J, Schaffalitzky de Muckadell OB (1978) Distribution of vasoactive intestinal polypeptide (VIP) in the porcine central nervous system. J Neurochem 31:1445

Goldstein I, Saenz de Tejada I, Krane RJ, Ottesen B, Fahrenkrug J, Wagner G (1985) Changes in corporeal vasoactive intestinal polypeptide (VIP) concentration following pelvic nerve stimulation. J Urol 133:218A

Jünemann K-P, Lue TF, Fournier GR Jr, Tanagho EA (1986a) Hemodynamics of papaverine- and phentolamine-induced penile erection. J Urol 136:158

Jünemann K-P, Luo J-A, Lue TF, Tanagho EA (1986b) Further evidence of venous outflow restriction during erection. Br J Urol 58:320

Larsson L-I, Fahrenkrug J, Schaffalitzky de Muckadell OB (1977) Occurrence of nerves containing vasoactive intestinal polypeptide immunoreactivity in the male genital tract. Life Science 21:503

Ottesen B, Staun-Olsen P, Gammeltoft S, Fahrenkrug J (1981) Vasoactive intestinal polypeptide (VIP): Specific receptors on smooth muscle membranes from porcine uterus. Protides of the Biological Fluids 29:527

Ottesen B, Wagner G, Virag R, Fahrenkrug J (1984) Penile erection: Possible role for vasoactive intestinal polypeptide as a neurotransmitter. Br Med J 288:9

Rattan S, Said SI, Goyal RK (1977) Effect of vasoactive intestinal polypeptide (VIP) on the lower esophageal sphincter pressure (LESP). Proc Soc Exp Biol Med 155:40

Said SI, Mutt V (1970) Polypeptide with broad biological activity: Isolation from small intestine. Science 169:1217

Steers WD, McConnell J, Benson GS (1984) Anatomical localization and some pharmacological effects of vasoactive intestinal polypeptide in human and monkey corpus cavernosum. J Urol 132:1048

III. Urolithiasis

Investigation of the Structure of Canine Urinary Stones Using Scanning Electron Microscopy

A. Hesse[1], G. Sanders[1], and D. B. Leusmann[2]

Introduction

According to the available literature, the incidence of canine urolithiasis lies between 0.4% and 3.3% (Brown et al. 1977; Pobisch 1969; Weaver 1970). Analysis of canine urinary calculi can provide important pointers for therapeutic concepts designed to prevent recurrence. In addition to this, structural examination provides information on the genesis of the stones and to analogies to urinary stone diseases in human beings.

Materials and Methods

741 canine concrements were examined using infrared spectroscopy and KBr press technique. A Type 598 Perkin-Elmer spectrometer with a wave number range from 4,000 to 200 cm^{-1} was employed (Hesse and Bach 1982; Hesse and Molt 1982). The scanning electron microscopical examinations were carried out on typical examples of canine urinary calculi. In addition to this, the fracture surfaces of certain concrements were sprayed with silver and examined under a Cambridge Stereoscan 180 SEM using an EPS 1000 PGT X-ray microprobe analysor.

Table 1. Composition of the canine uroliths, main constituents ($n = 741$)

Type of stone	%
Struvite	58.3
Cystine	21.4
Ammonium acid urate	6.4
Weddellite	4.5
Whewellite	3.5
Brushite	2.6
Carbonate apatite	0.4
Xanthine	0.4
Protein	0.5
For the time being not identified	2.0

[1]Experimentelle Urologie, Urologische Universitätsklinik Bonn, Sigmund-Freud-Str. 25, D-5300 Bonn 1
[2]Urologische Universitätsklinik Münster, Jungeblodtplatz 1, D-4400 Münster

Investigative Urology 2
Edited by G. H. Jacobi et al.

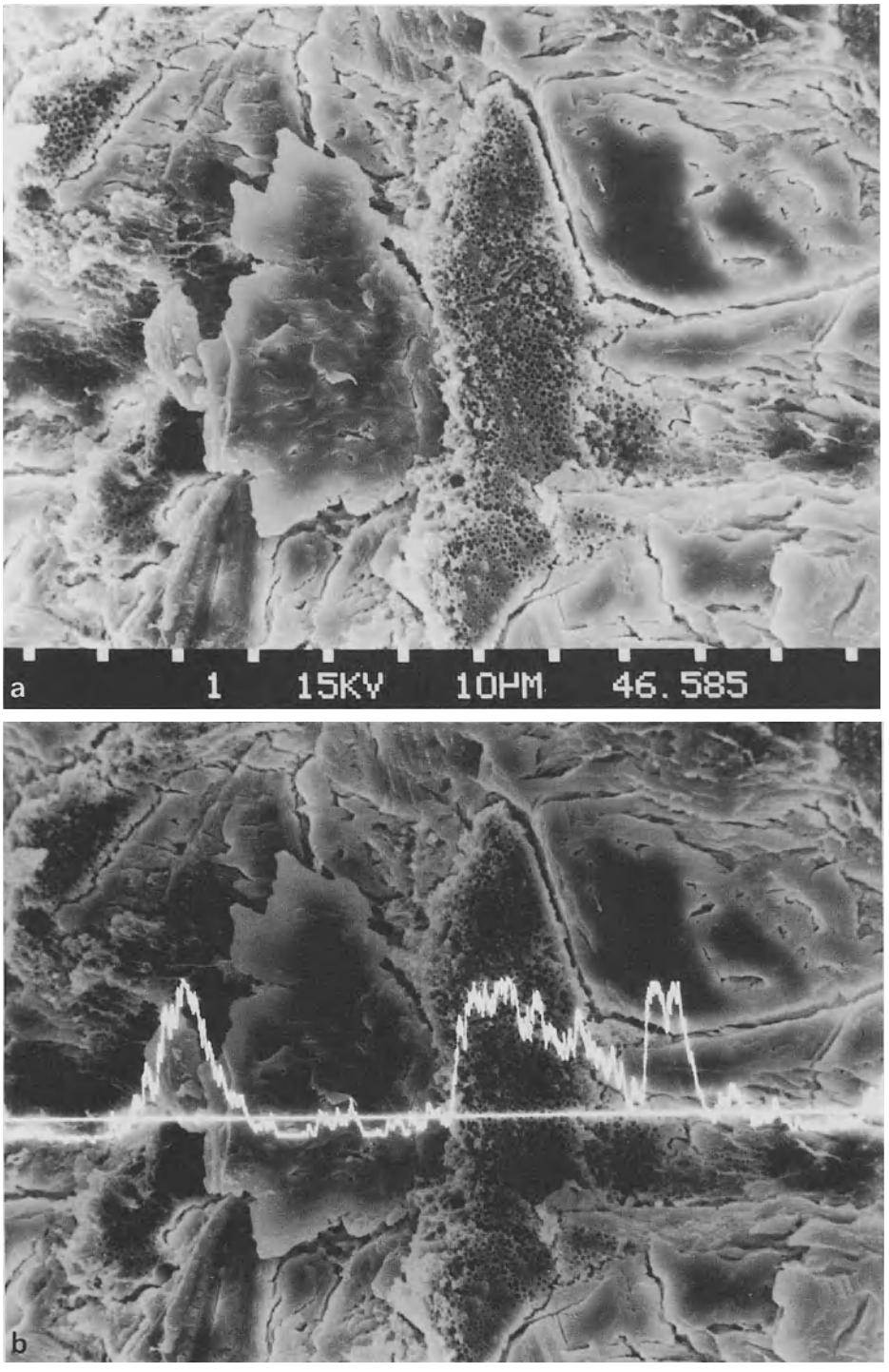

Fig. 1. **a** Struvite stone. Large, compact struvite crystals with pseudoamorphous apatite showing clear bacterial imprints. **b** As **a** with superimposed y-modulated EDXA signal of Ca; apatite detection. **c** Section of **a**. Bacterial imprints in the apatite zones

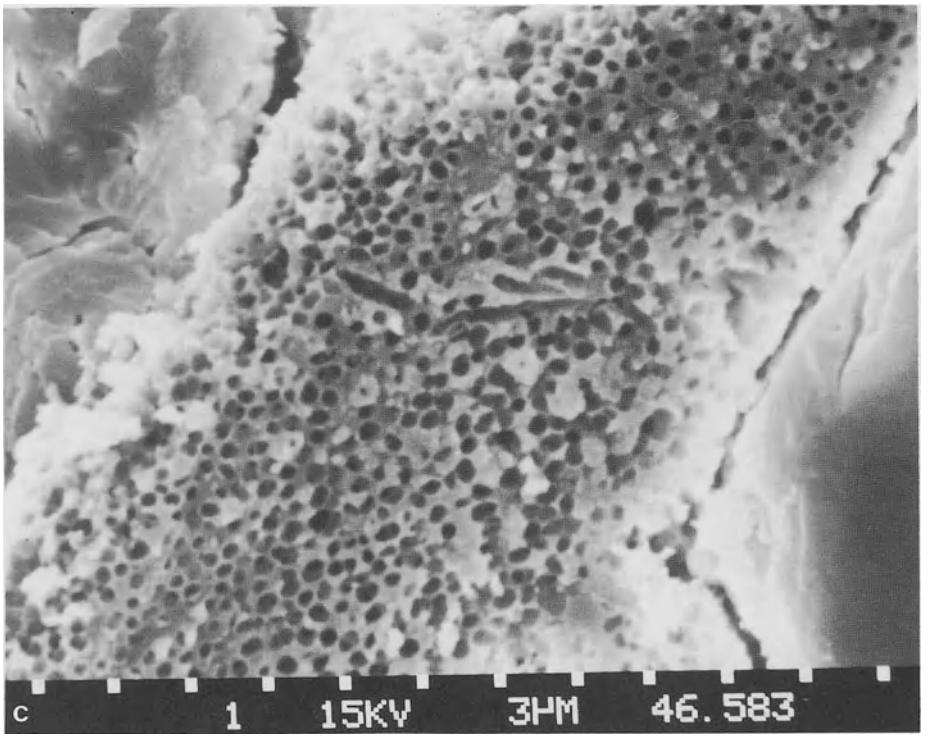

Fig.1c

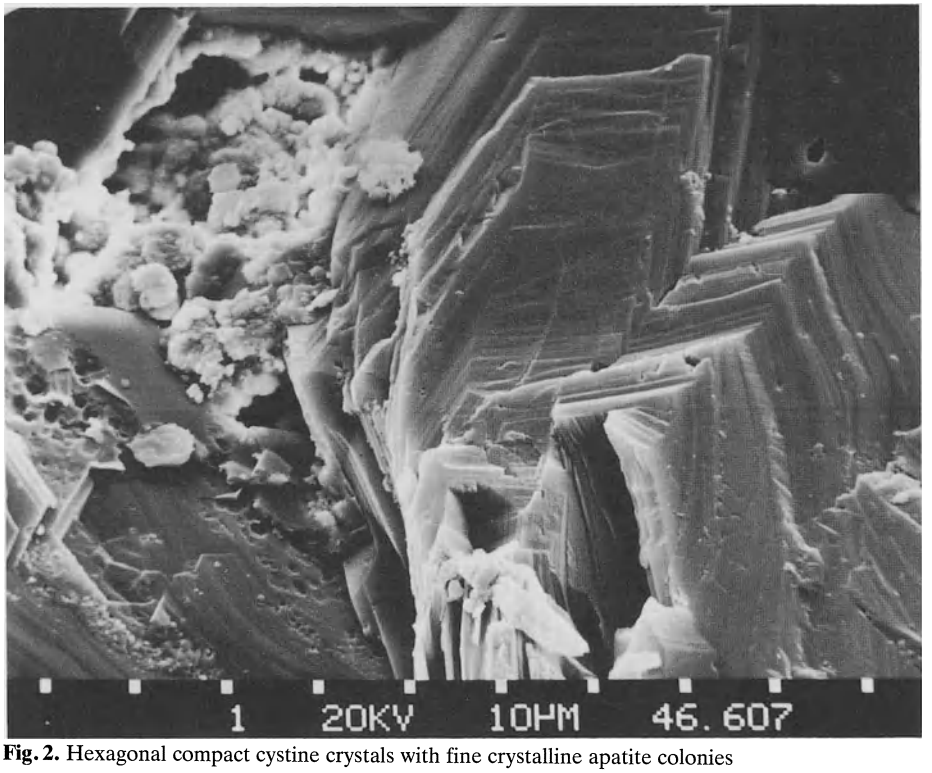

Fig. 2. Hexagonal compact cystine crystals with fine crystalline apatite colonies

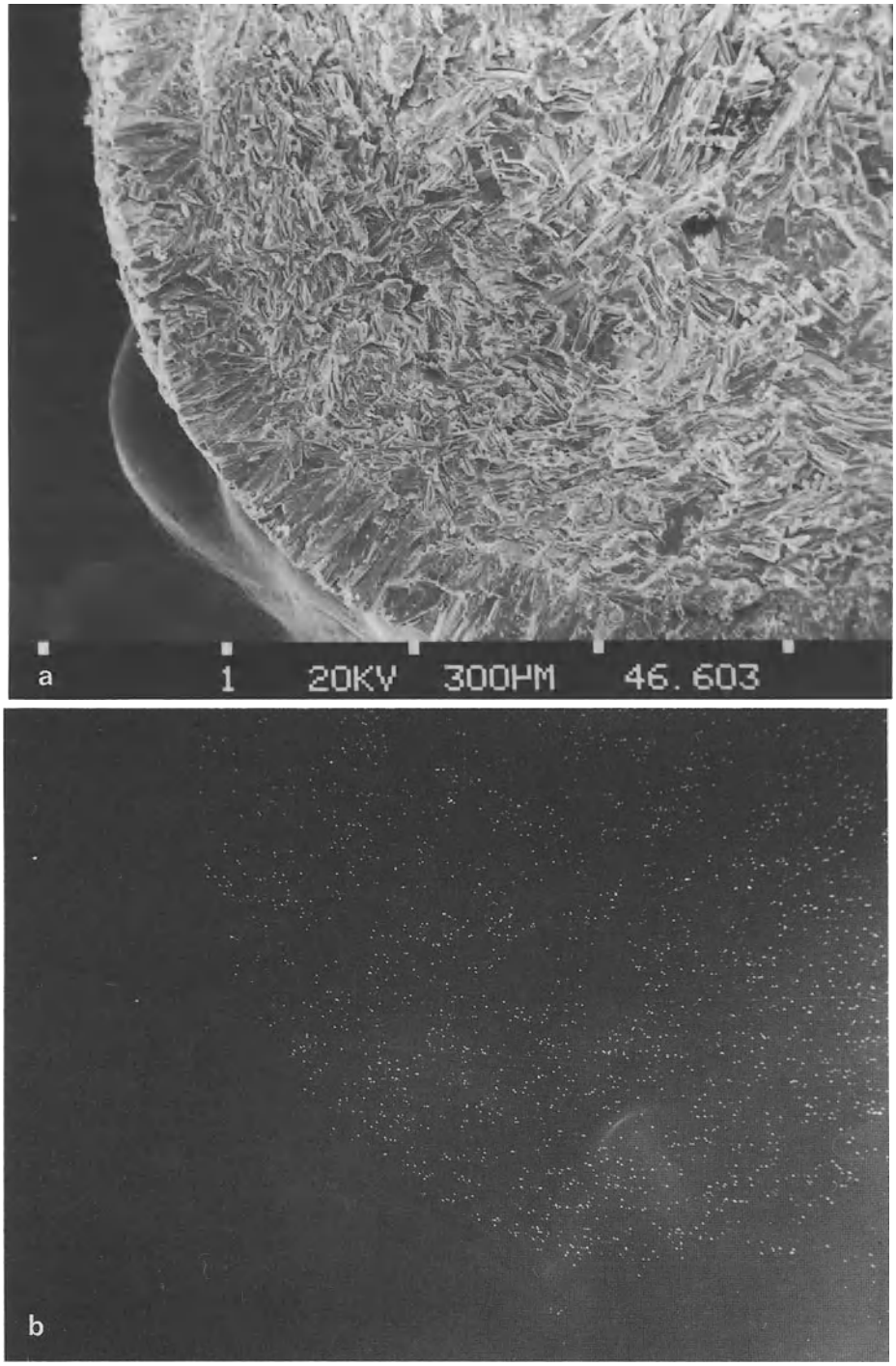

Fig. 3a, b

Fig. 3. a Cystine stone with firmly superimposed, evenly grown brushite envelope. **b** S distribution. Detection of cystine. **c** Ca distribution

Results

Infrared Spectroscopic Analysis

The IR spectroscopic quantitative analysis of the 741 concrements revealed great diversity of composition (Table 1).

Scanning Electron Microscopical Examination

SEM micrographs and element-distribution pictures were taken of characteristic fracture surfaces on the stones in order to describe the structure of these canine urinary calculi. In this way a stone containing a high proportion of struvite with large struvite crystals was also found to contain clear areas of pseudoamorphous Ca-phosphate (Fig. 1a, b).

The Ca-phosphate phase displayed a clearly perforated structure, probably attributable to the imprint of bacteria (Fig. 1c). Regular small nests of finely crystalline apatite were discovered in the majority of the cystine stones identified by IR analysis as monomineral (Fig. 2). This apatite structure was confirmed by element analysis (EDXA).

A rare phase combination was discovered in one cystine stone with a dense brushite envelope (Fig. 3a). The brushite crystals in the boundary layer were intermeshed with cystine crystals, although no mixed phases of the other component appeared in

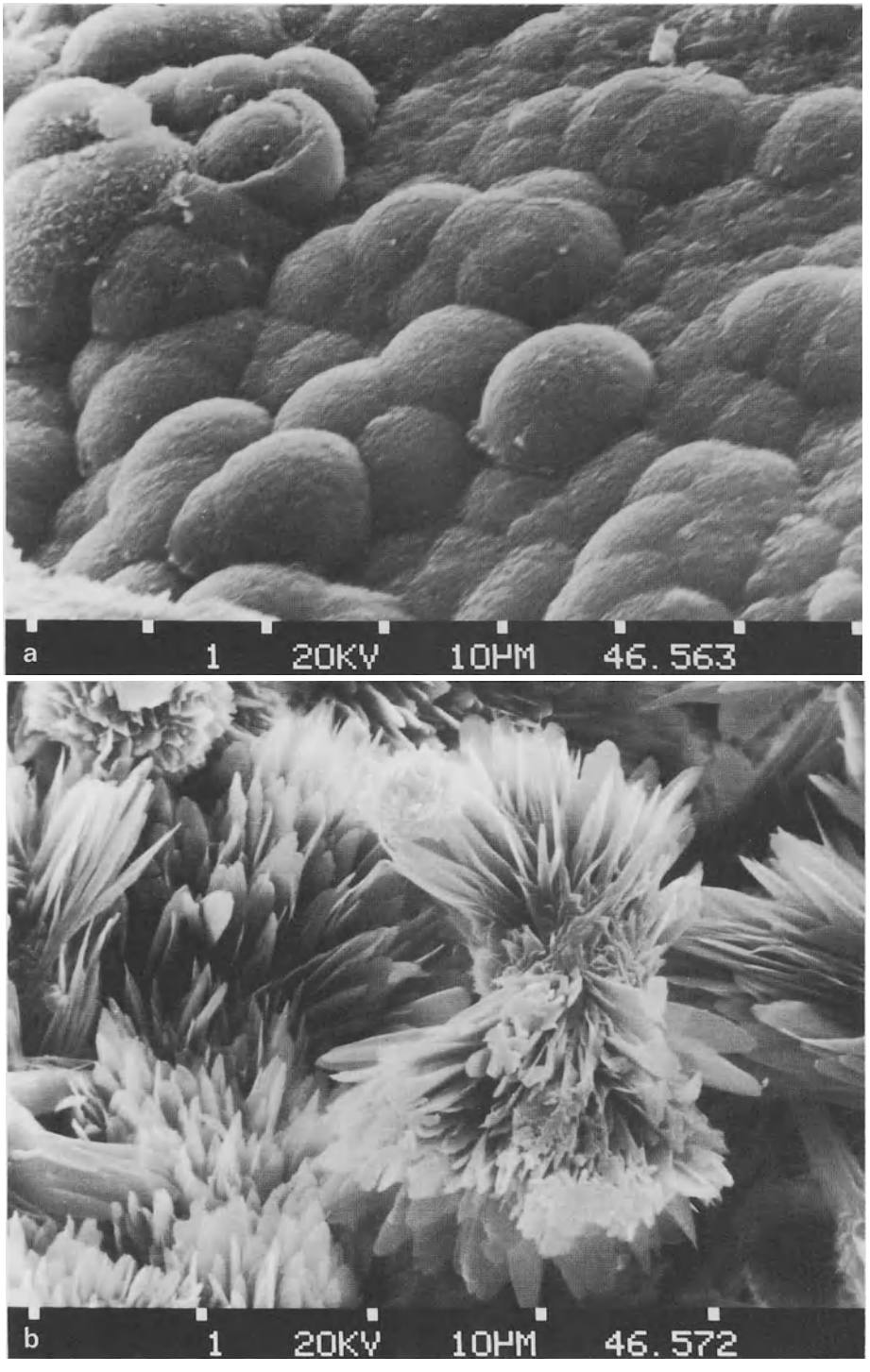
a
1 20KV 10PM 46.563
b
1 20KV 10PM 46.572

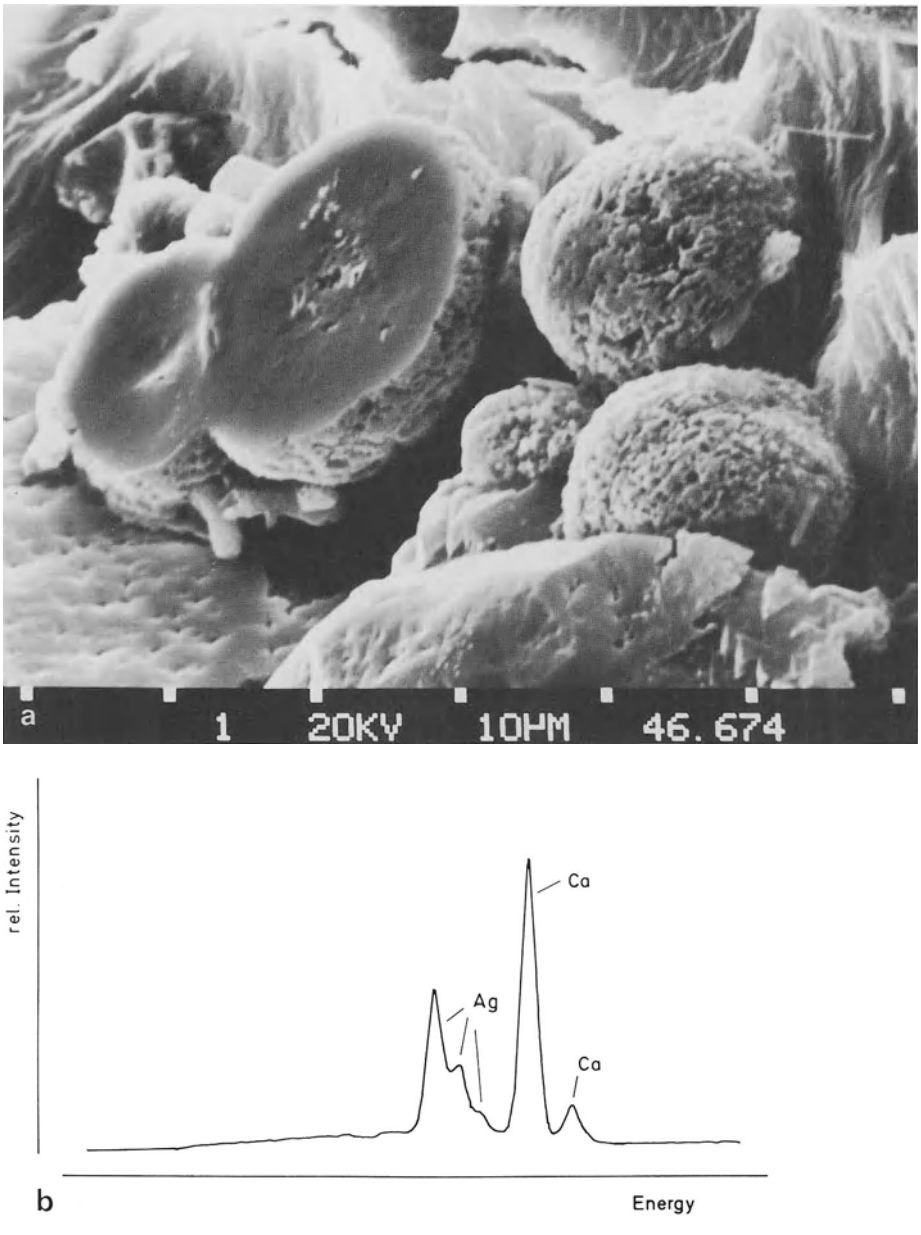

Fig. 5a, b. Mixed acid urate stone. **a** Compact, spherical form of Ca-urate. **b** EDXA, apart from Ca no other elements have been identified in the stone material (Ag due to sputter layer)

◂ **Fig. 4a, b.** Xanthine stone. **a** Spherical, compact structures. **b** Sheath-like crystalline arrangement

either the cystine or the brushite phases. This was confirmed by element analysis (Fig. 3b, c).

Xanthine calculi are also very rare in human beings. The SEM examination revealed two very different structures in the same stone. One was a compact sphere whose individual elements had grown in series of shells (Fig. 4a) and the other displayed lance-shaped crystals of sheath-like arrangement (Fig. 4b).

Ammonium acid urate appeared in the same fascicular form as it does in human stones, although the monomineral form is commoner in dogs than in human beings.

One group of urate stones proved impossible to classify precisely using IR spectroscopy and X-ray diffraction. During the SEM examination EDXA analysis revealed mixtures of urates in these concrements. Thus, one and the same stone was found to have a mono-Na-acid-urate core, adhesions between mono-Na-acid-urate and mono-K-urate and Ca-urate (Fig. 5a, b). The cations were identifiable in each case using EDXA (Fig. 5b).

Discussion

Pure canine struvite stones, and those containing high proportions of struvite, mostly result from an infection of the urinary tract by urea splitting bacteria (Klausner et al. 1977). The circular structures with a diameter of ~1 μm (Fig. 1c) agree with the size of bacteria. Therefore, bacterial ammonia production and concomitant alkalinization of the urine resulting in calcium phosphate and struvite crystallization are very probable. Similar structures have also been described in human calculi (Cifuentes-Delatte et al. 1984; Leusmann et al. 1984). Although, in the literature, cystine stones are always described as being particularly pure in composition (Krizek et al. 1973), we were constantly finding colonies of Ca-phosphate (Hesse and Bach 1982). Of special interest in canine urinary stones is the combination of cystine and brushite. This occurred in one stone as firmly connected layers (Fig. 3a).

We have not yet succeeded in examining xanthine in a urinary stone using SEM. The change from compact spheres to lance-shaped crystals in sheath-like arrangements was typical of the stones investigated. Also of interest in these canine stones were the mixtures of various urates, in which sodium and potassium urates occurred in the familiar form of fine needles (Hesse and Bach 1982; Leusmann 1983), in contrast to Ca-urate, which occurred in compact spherical structures. The reasons underlying the formation of these various urates in dogs have not yet been elucidated. SEM examination of canine urinary stones revealed a whole series of structures familiar in human stones. This enabled us to identify certain structures which had not previously been observed.

References

Brown NO, Parks JL, Greene RW (1977) Canine urolithiasis: retrospective analysis of 438 cases. J Am Vet Med Assoc 170:414–418

Cifuentes-Delatte L, Medina JA, Minon, Cifuentes JLR (1984) Cálculos papilares con placas atipicas. Arch Esp Urol (Ext 1) 37:569–576

Hesse A, Bach D (1982) Harnsteine. Thieme, Stuttgart, pp 150–179

Hesse A, Molt K (1982) Technik der infrarotspektroskopischen Harnsteinanalyse. J Clin Chem Clin Biochem 20:861–873

Klausner JS, Osborne CA, O'Leary P, Griffith DP (1977) Phosphate urolithiasis in dogs: pathophysiology, diagnosis, treatment and prevention. Gaines Vet Symp 27:25–37

Krizek V, Schneider HJ, Hesse A, Tscharnke J, Heide K (1973) Analytische Untersuchungen zur chemischen Zusammensetzung und Struktur von Zystinsteinen. Urologe A 12:183–187

Leusmann DB (1983) Routine analysis of urinary calculi by scanning electron microscopy. Scanning Electron Microscopy 1983:387–396

Leusmann DB, Meyer-Jürgens UB, Kleinhans G (1984) Scanning electron microscopy of urinary calculi – some peculiarities. Scanning Electron Microscopy 1984/III:1427–1432

Pobisch R (1969) Urolithiasis bei Hund und Katze. Wien Tierärztl Mschr 56:93–104

Weaver AD (1970) Canine urolithiasis: incidence, chemical composition and outcome of 160 cases. J Small Anim Pract 11:93–107

Urinary Supersaturation or Risk Index Calculations in the Assessment of Stone Formers

M. Hegemann[1], R. Pfab[1], M. Weitbrecht[1], M. Fisser[1], M. Niggl[1], and S. Stöhr[1]

Introduction

While recent progress in stone disintegration may have made obsolete metabolic evaluations and pharmacological treatment in idiopathic calcium urolithiasis, a considerable effort in time and money is still devoted to 24 h-urine analysis in the individual stone former (Pak et al. 1980). Disagreement prevails on the scope and therapeutic implications of urine examinations (Peacock 1982). Sophisticated calculations are said to reflect important pathogenetic factors operative in calcium oxalate stone formation. Since the thermodynamic pressure for urinary stone salt crystallization can be estimated by computer calculations, we have compared 24 h-urine stone salt supersaturation values (Finlayson 1977; Werness et al. 1985) to risk index calculations (Tiselius 1982; 1984; Leskovar et al. 1979; Hering et al. 1981) and simple concentration and excretion measurements in recurrent calcium oxalate stone formers and healthy controls.

Material and Methods

We examined the 24 h-urine of 113 stone formers with recurrent idiopathic calcium urolithiasis and 32 healthy subjects. The urine was collected under a non-restricted diet without preservatives in 2 l polyethylene bottles at least 2 months after the last hospitalization or outpatient treatment. Female/male ratio, average age and weight of the stone formers and controls is listed in Table 1. Urine was analyzed for calcium, inorganic phosphate, urate, chloride by means of a Technicon SMA autoanalyzer, for sodium and potassium by flame photometry, for oxalate (Hatch et al. 1977) and citrate enzymatically, for magnesium by atomic absorbance spectrophotometry, for sulfate colorimetrically (Swaroop 1973). Since variations of the pyrophosphate, am-

Table 1. Demographic data

	Patients ($n = 113$)	Controls ($n = 32$)
Age	44 ± 14	28 ± 6
♂/♀	76/37	26/6
Weight (kg)	68 ± 20	70 ± 11

[1] Urological Clinic of the Technical University Munich, Ismaninger Str. 22, D-8000 München 80

Investigative Urology 2
Edited by G. H. Jacobi et al.

monium, CO_2 concentration in the physiologic range have only a negligible influence on the urinary stone salt saturation, standard values were used. As observed in prior studies (Robertson et al. 1978) an uniform urin pH of 6.3 was assumed the risk of urinary crystal formation being the lowest in this pH-range (Berg and Tiselius 1986). Relative supersaturation values (SS) for calcium oxalate, brushite, hydroxyapatite, uric acid and mononatriumurate were calculated by a BASIC version of the EQUIL program (EQ11 from June 17, 1983) as published by Finlayson and kindly provided by L. H. Smith and P. Werness of the Mayo Clinic Foundation, Rochester Mn., USA (Werness et al. 1985). Since hydroxyapatite supersaturation grows exponentially (Smith et al. 1984) with calcium concentration, hydroxyapatite supersaturation was expressed as the Gibb's free energy (ln SS). To check the precision of ionic concentration calculations, the values of calculated ionic calcium concentrations in 80 patients were compared with concentration values of ionic calcium measured directly with the Orion Research Calcium Ion Electrode 93-20. The EQUIL program was part of a program package which concomittantly calculated stone salt supersaturation values (SS), "calcium oxalate stone risk indices" and "calcium oxalate activity product indices" as proposed by Tiselius and others (Tiselius 1982; 1984; Leskovar et al. 1979; Hering 1981) as well as 24 h-urine total and ionic concentrations of the analyzed lithogeneous and lithoprotective urinary substances. Patients were grouped according to metabolic anomalities as hyper-, normocalciuric, hypomagnesiuric, hyperoxaluric, hyperuricosuric, "without metabolic anomality". Small patient groups were studied before and after pharmacological treatment with hydrochlorothiazide and/or allopurinol. The differences between controls, patients, metabolic and pharmacological subgroups were evaluated by non-parametric statistics (U-test, Wilcoxon test). Correlation and regression was calculated parametrically by the method of the least squares. For better visualization of the data material and calculation of medians, percentiles, specifity, sensitivity, negative and positive predictive values and receiver operator characteristics (Griner et al. 1981; O'Brien et al. 1983), inverse distribution functions (Schwemmer et al. 1985) of the individual data were used in intergroup comparisons.

Results

Precision and Correlation of Methods

If a calcium ion sensitive electrode was used to check the precision of the EQUIL program in calculating ionic calcium concentrations of calcium, a highly significant correlation ($r = 0.94$) between calculated and directly measured values was found. EQUIL program calculated CaOx supersaturation values correlated very well with ion activity products estimated by the Tiselius AP(CaOx) Index ($r = 0.92$) (Tiselius 1982) or by Herings formula ($r = 0.88$) (Hering 1981). A much lower but still significant ($P = 0.001$) correlation coefficient could be computed for brushite supersaturation values calculated by the EQUIL-program and the Tiselius AP(Brushit) Index ($r = 0.48$) (Tiselius 1984). No significant correlation ($r = 0.12$) was found between the Tiselius Risk Index (Tiselius 1982) or similar calculations as published by Leskovar (Leskovar et al. 1979) and the calculated CaOx supersaturation values (EQUIL).

Supersaturation Calculations

There was no significant difference (Table 2, Fig. 1) in urine supersaturation for calcium oxalate, brushit, hydroxyapatite between healthy controls and hypercalciuric patients or stoneformers in general. As compared to healthy controls brushite and hydroxyapatite supersaturation was slightly lower ($P = 0.01$) in normocalciuric subjects. Again SS-CaOx did not differ significantly from normals in normocalciuric patients. Except for a few patients at the pH of 6.3 used in our calculations, the 24 h-urine was always supersaturated with calcium oxalate, brushite and hydroxyapatite. For calciumoxalate numeric values in the metastable range slightly below the formation product (Ahlstrand et al. 1984) could be calculated by the Tiselius AP(CaOx) Index. The relative supersaturation for calcium oxalate corresponded roughly to values computable on the base of micropuncture studies published by Hautmann (Hautmann and Osswald 1983). While there was no significant difference between controls and hyper- and normocalciuric stoneformers, the supersaturation values for calcium stone salts differed significantly between normo- and hypercalciuric patients. Hypercalciuric stone formers differed from normocalciuric patients much more significantly in calciumphosphate and especially hydroxyapatite supersaturation than in calcium oxalate supersaturation. While correlation between total calcium, total oxalate,

Table 2. Results of 24 h-urine analysis

	Controls ($n = 32$)	Hypercalciuric stone formers ($n = 57$)	Normocalciuric stone formers ($n = 56$)	Sum of stone formers ($n = 113$)
Ca (Mol/l)	0.0037 ± 0.0018	0.0048 ± 0.0022	0.0028 ± 0.0015	0.0038 ± 0.0021
Ox (Mol/l)	0.00024 ± 0.00009	0.00019 ± 0.00009	0.00022 ± 0.00009	0.00020 ± 0.00009
PO_4 (Mol/l)	0.0075 ± 0.0033	0.0060 ± 0.0031	0.0060 ± 0.0028	0.0060 ± 0.0029
SS-CaOx	6.56 ± 3.48	7.17 ± 3.43	5.65 ± 2.49	6.41 ± 3.10
SS-Brushit	3.56 ± 2.32	4.74 ± 5.07	2.42 ± 1.87	3.59 ± 4.00
DG-HAP ln(SS-HAP)	4.96 ± 0.92	5.32 ± 1.33	4.48 ± 0.80	4.90 ± 1.18
SS-H_2U	1.13 ± 0.469	0.889 ± 0.457	0.951 ± 0.470	0.919 ± 0.462
Tiselius Risk Index	363 ± 180	691 ± 368	483 ± 250	587 ± 331
Tiselius AP(CaOx) Index	1.59 ± 0.83	1.74 ± 0.90	1.32 ± 0.62	1.53 ± 0.80
Leskovar Risk Index	1556 ± 1689	89503 ± 119922	4391 ± 10127	17058 ± 87178
Urine volume (ml/24 h)	1639 ± 815	2012 ± 1049	1888 ± 1004	1950 ± 1024

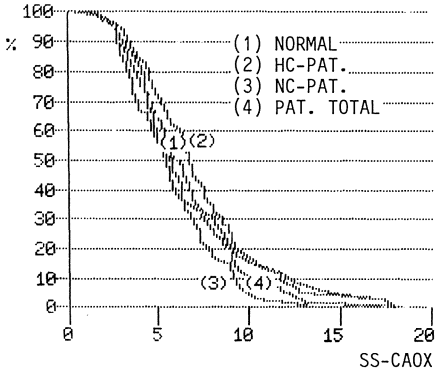

Fig. 1. Inverse cumulative distribution functions of calcium oxalate supersaturation values (SS-CaOx)

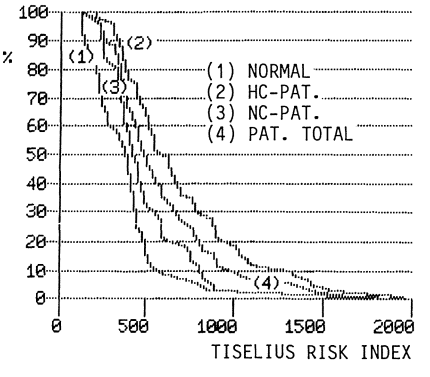

Fig. 2. Inverse cumulative distribution functions of Tiselius Risk Index values (Tiselius 1982)

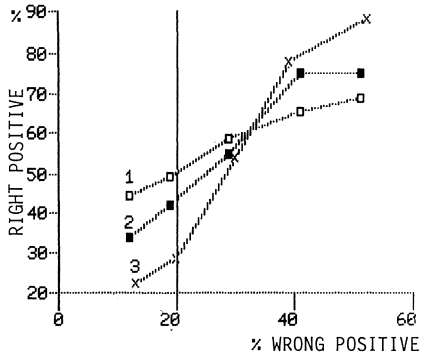

Fig. 3. Receiver operator characteristics comparing controls with all stone formers by *1* Tiselius Risk Index, *2* Leskovar Risk Index, *3* ionized magnesium concentration. *X-axis:* 1-Specifity, *Y-axis:* sensitivity

total phosphate concentration and calcium oxalate, brushite, hydroxyapatite supersaturation was similar ($r = 0.5$–0.7), not unexpectedly, differences in the molar oxalate concentration led to a relatively bigger change of SS-CaOx than a corresponding change in molar calcium concentration. Contrariwise, calcium rather than phosphate concentration had a predominant influence on hydroxyapatite supersaturation. Dependency of hydroxyapatite supersaturation on calcium concentration was much bigger than the dependency of calcium oxalate supersaturation on calcium concentration. Increased oxalate concentrations and reduced calcium concentrations or increased calcium concentrations and reduced oxalat concentrations in hyperoxaluric or hypercalciuric patients resulted in supersaturation values for calcium salts indistinguishable from controls. Patients with "no metabolic anomality" i.e., without hypercalciuria, hyperoxaluria, hyperuricosuria and hypomagnesiuria could not be discriminated from controls by calcium salt supersaturation calculations. The average urate excretion being the same in the control and stone forming group and the urine volume being slightly increased among stone formers, supersaturation for uric acid and mononatriumurate was slightly lower in the patient group (Table 2).

Risk Indices

Stoneformers as an entity, hyper- and normocalciuric and hyperoxaluric patients could be discriminated significantly (Table 2, Fig. 2) from controls by "risk indices", concentrations ratios of calcium, oxalate, citrate, magnesium, sodium as published by Tiselius or Leskovar. The usefulness of the ratio published by Leskovar was hampered by extreme values resulting in an excessive data variance. Patients with no metabolic anomality had risk index values almost identical to controls.

Concentration and Excretion Values

After metabolic grouping, subsets of patients could be identified which distinguished themselves significantly from controls by simple concentrations and excretion measurements: In hypercalciuric patients calculated calcium ion ($P = 0.001$) and citrate ion ($P = 0.001$) concentrations were a more significant parameter than total calcium ($P = 0.05$) or citrate ($P = 0.04$) when comparing controls and patients. Total ($P = 0.005$) and calculated ionic ($P = 0.0001$) magnesium concentrations were most significantly lowered in normocalciuric patients.

Hydrochlorothiazide and Allopurinol

Following hydrochlorothiazide and/or allopurinol administration 24 h-calcium ($P = 0.04$) and/or uric acid ($P = 0.005$) excretion decreased significantly. Similarily, a significant decrease of H_2U- or NaU-supersaturation ($P = 0.005$) could be found during allopurinol treatment. No significant decrease of CaOx supersaturation was noticed during hydrochlorothiazide administration, the decrease of calcium phosphate salt supersaturation being marginally significant in the group of patients treated with allopurinol and hydrochlorothiazides.

Diagnostic Value of 24 h-Urine Examinations

Statistically significant differences between stone formers and non-stone formers are a prerequisite for useful diagnostic urine examinations in stone disease. A comparison of all parameters mentioned (Table 2, Fig. 3) shows that only for the Tiselius Risk Index and similar indices significant differences are calculated between normals and normo- or hypercalciuric stone formers. If metabolically distinct subpopulations of patients were compared with normals, other parameters eventually had a bigger significance, but for no parameter other than the Tiselius Risk Index significant differences could be calculated while comparing the whole spectrum of stone formers with normals. Again patients with no metabolic anomality, i.e., without hypercalciuria, hyperuricosuria, hypomagnesiuria or hypocitraturia, were undistinguishable from normals by 24 h-urine analysis. If sensitivity, specifity, the positive and negative predictive value of the parameters were calculated and parameters with superior sensitivity and specifity identified be means of receiver operator characteristics (Fig. 3), the Tiselius Risk Index was the diagnostic parameter with the highest albeit quite low sensitivity of 50% at a specifity of 80% (Fig. 3). Generally this sensitivity of about 50% at a specifity of 80% could never be exceeded while comparing normals to patient groups or metabolic subpopulations. Only hypercalciuric patients could be distinguished from normals with a higher sensitivity by means of 24 h-

calcium excretion. Even at optimal cut-off points the sum of diagnostic misclassifications almost never fell below 30% and the positive or negative predictive value at a specifity of 80% and a prevalence of 50% almost never exceeded 70%. Normocalciuric patients fared even worse than the stone former population in general.

Discussion

Some conclusions can be drawn from our results which have some bearing on our current clinical practice of 24 h-urine analysis.

1) While the precision of supersaturation calculations is probably validated by direct control measurements of ionic calcium, the activity product of calcium oxalate can be calculated with similar precision by simple activity product indices (Tiselius 1982; Hering et al. 1981) necessitating only the analysis of 4 urinary constituents.
2) The individual or general pathogenesis of sterile calcium urolithiasis can probably not be attributed to differences in calcium oxalate supersaturation. Perhaps tides of hypercalciuria induce hydroxyapatite crystalluria and subsequent heterogeneous calcium oxalate nucleation, hydroxyapatite supersaturation being extremely sensitive to changes in calcium concentration.
3) Statistical distinction between normals and stone formers is feasible only with a very limited specifity and sensitivity the optimal parameter being the Tiselius Risk Index (Tiselius 1982). After metabolic grouping, simple concentration measurement have a diagnostic value similar to index calculations. From the clinical point of view, therefore the analysis of calcium, oxalate, citrate, magnesium in 24 h-urine seems to be all that is needed to assess – with a high margin of error – the risk of calcium stone formation.
4) The lack of diagnostic information obtained by comprehensive urine analysis for micromolecular substances indicates that other mechanisms like macromolecular inhibitors or particle retention in the kidney must play an important part in the pathogenesis of sterile calcium urolithiasis.

References

Ahlstrand CH, Tiselius HG, Larsson L (1984) Studies on crystalluria in calcium oxalate stone formers. Urol Res 12:125–130

Berg C, Tiselius HG (1986) The effect of pH on the risk of calcium oxalate crystallisation in urine. Eur Urol 12:59–61

Finlayson B (1977) Calcium stones: Some physical and clinical aspects. In: David SD (ed) Calcium metabolism in renal failure and nephrolithiasis. Wiley, New York, pp 337–382

Griner F, Mayewski J, Mushlin AJ, Greenland P (1981) Selection and interpretation of diagnostic tests and procedures. Ann Int Med 94:553–600

Hatch M, Bourke E, Costello J (1977) New enzymic method for serum oxalate determination. Clin Chem 23:76–79

Hautmann R, Osswald H (1983) Concentrations profiles of calcium and oxalate in urine, tubular fluid and renal tissue-some theoretical considerations. J Urol 129:433–436

Hering F, Burschardt WG, Pyhel N, Lutzeyer W (1981) The relation between relative supersaturation and crystal aggregation in urine. In: Smith LH, Robertson WG, Finlayson B (eds) Urolithiasis, clinical and basic research. Plenum Press, New York, pp 441–445

Leskovar P, Hartung R, Riedel J (1979) Kann allein aus der Harnanalyse auf ein erhöhtes Steinbildungsrisiko bei Steinpatienten geschlossen werden? Med Welt 30:937–941

O'Brien PC, Schampo MA, Robertson JS (1983) Statistics for nuclear medicine. J Nucl Med 24: 83–88, 165–171, 269–272, 535–541

Pak CYC, Britton F, Peterson R, Ward D, Northcutt C, Breslau NA, McGuire J, Sakhaee K, Busch S, Nicar M, Norman DA, Peters P (1980) Ambulatory evaluation of nephrolithiasis. Am J Med 69:19–30

Peacock M (1982) The mechanisms of hypercalciuria are unnecessary for treatment of recurrent renal calcium stone formers. Contr Nephrol 33:152–162

Robertson WG, Peacock M, Heyburn PJ, Marshall DH, Clark PB (1978) Risk factors in calcium stone disease of the urinary tract. Br J Urol 50:449–454

Schwemmer B, Schütz W, Kuntz RM, Lehmer A (1985) Simultaneous determination of six tumor markers in patients with prostatic carcinoma and bladder tumors. Urol Res 13:133–136

Smith LH, Jenkins AD, Wilson JWL, Werness PO (1984) Is hydroxyapatite important in calcium urolithiasis? Fortschr Urol Nephrol 22:193–197

Swaroop S (1973) A micromethod for the determination of urinary inorganic sulfats. Clin Chim Acta 46:333–336

Tiselius HG (1982) An improved method for the biochemical evaluation of patients with recurrent calcium oxalate stone disease. Clin Chim Acta 122:409–418

Tiselius HG (1984) A simplified estimate of the ion activity product of calcium phosphate in urine. Eur Urol 10:191–195

Werness PG, Brown CB, Smith LH, Finlayson B (1985) Equil 2. A basic computer programm for the calculation of urinary saturation. J Urol 134:1242–1244

Studies of Sulphate Excretion in the Urine of Healthy Individuals Compared to Recurrent Calcium Oxalate Stone Formers

R. M. Schaefer[1], A. Hesse[1], K. Klocke[1], H. v. Ahlen[1], and W. Vahlensieck[1]

Introduction

Sulphur is usually incorporated with the sulphur-containing amino acids cystine, cysteine and methionine, and only a small proportion is taken up as sulphate (Buddecke 1974). The oxidation into sulphate is taking place in the liver. It is either used for synthesis as "active sulphate" (sulphatide, chondroitin sulphate, keratin sulphate, heparin) or reaches the circulation as anorganic sulphate. It is then found as amino acid peptide sulphate, as ester sulphate or anorganic sulphate.

The renal excretion is simular to that of phosphate, the reabsorption takes place in the proximal tubule only (Deetjen et al. 1976). The threshold concentration is very low and the excretion which is proportional to the filtration rate only occurs with serum levels above 1.0 mmol/l (Dennis and Brazy 1982). There are hardly any investigations about the role of sulphate in stone disease (Hesse et al. 1985a; 1985b; Schwille et al. 1985).

The supersaturation of the urine is often an additional factor in calcium oxalate stone disease. Until now, the causes for this are unclear and it is unknown which role nutrition and changes in metabolism play (Hesse and Bach 1982).

Material and Methods

We have examined the sulphate excretion in 223 recurrent calcium oxalate stone formers, 152 males and 71 females. 24-h-urine was collected under individual and a standard diet. The control group consisted of 326 healthy individuals – 163 males and 163 females – under individual diet and 30 healthy subjects under individual and a standard diet, 17 males and 13 females. The sulphate excretion was measured nephelometricly.

Results

Under individual diet the average sulphate excretion in males was 21.6 mmol/d, in females 16.9 mmol/d; the difference was statistically significant. In the group of stone formers the average excretion in male individuals was 23.6 mmol/d, in females 18.0 mmol/d. The difference was statistically significant, too. Figure 1 shows the average sulphate excretion under individual diet. Under a standard diet (Fig. 2) the

[1] Urologische Universitätsklinik Bonn, Sigmund-Freud-Str. 25, D-5300 Bonn 1

Investigative Urology 2
Edited by G. H. Jacobi et al.

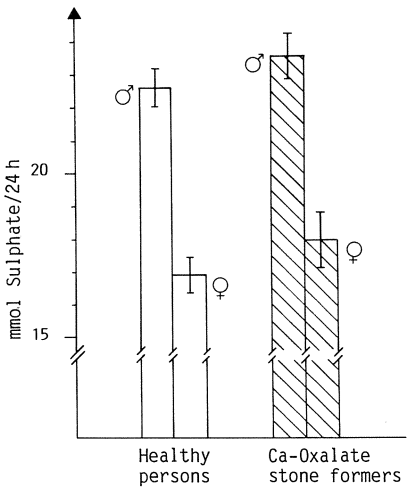

Fig. 1. Average sulphate excretion in 24-h-urine under individual diet

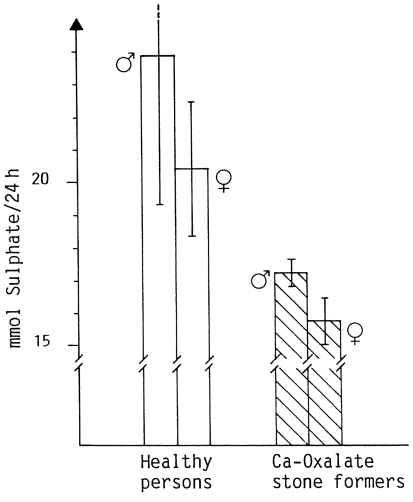

Fig. 2. Average sulphate excretion in 24-h-urine under a standard diet

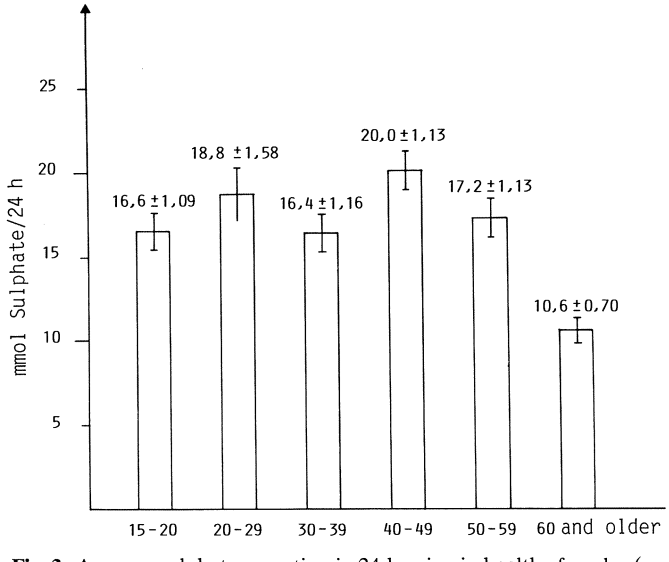

Fig. 3. Average sulphate excretion in 24-h-urine in healthy females ($n = 150$) according to age group

daily sulphate excretion was measured after a steady state had been reached after 7 days. In healthy male it was 23.9 mmol/d, in females 20.4 mmol/d; the difference was not statistically significant though. In male stone patients it was 17.2 mmol/d, in females 15.7 mmol/d (statistically significant difference).

Figures 3 and 4 show a clear change of the sulphate excretion in relation to the age of the patients. Males between 20 and 30 (Fig. 4) years of age show a maximum excretion while there is a marked decrease in patients over 60 years. Females show a

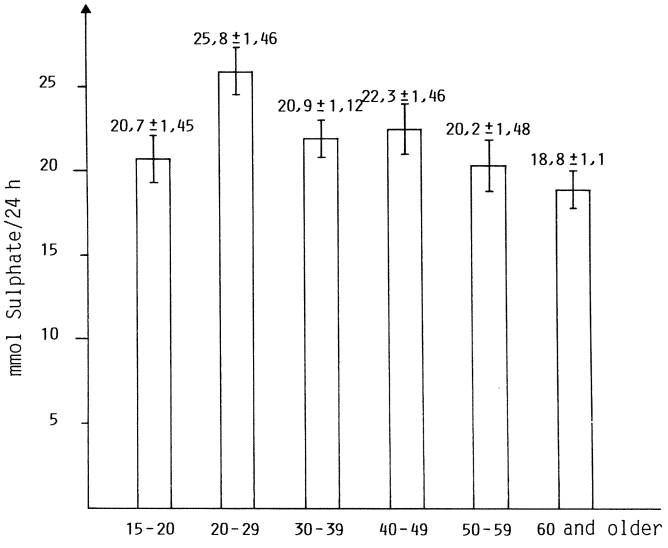

Fig. 4. Average sulphate excretion in 24-h-urine in healthy males ($n = 150$) according to age group

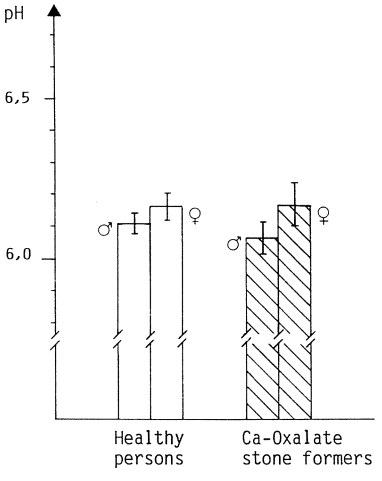

Fig. 5. Average pH in 24-h-urine under individual diet

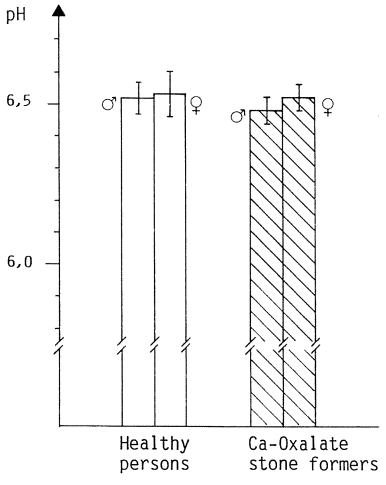

Fig. 6. Average pH in 24-h-urine under a standard diet

second peak between 40 and 50 years, and a marked decrease above 60 years, too (Fig. 3).

The urine pH under individual diet is shown in Fig. 5, it was almost identical in healthy males and females with 6.16 and 6.10, respectively. In male stone formers pH was slightly lower (6.05) than in females (6.15). Under the standard diet the pH increased, showing the same trend as above in healthy males and females with 6.53 and 6.52 (Fig. 6). In stone patients the same changes occurred, again with slightly lower values in males (6.48) than in females (6.51).

Discussion

Sulphate not only plays an important role in the acid base metabolism but has often been discussed as a complex former with calcium. Our investigations show that nutrition influences sulphate excretion. First of all, there is a clear sexual distinction, males always excret higher amounts of sulphate than females, which is probably because of the conjugation of sulphate with estrogens. While in healthy individuals sulphate excretion is slightly rising under a standard diet, it decreases significantly in stone formers. The age dependant changes in the first decades are certainly resulting from nutrition. The changes in the higher age groups are probably due to changes in metabolism, resulting in a reduced excretion. Different changes occur for the urine pH. In healthy individuals an increase in sulphate excretion also means a rise of pH, in stone formers urine pH increases considerably although the sulphate excretion diminishes. This is especially to be seen in the sexual distinction.

According to our investigations, a defect in the renal tubule must be considered in recurrent calcium oxalate stone formers, which preserves the function of sulphate excretion as a buffer on the one side and inhibits the complex forming capacity by a diminished excretion on the other side. Certainly further investigations will be necessary to evaluate this problem.

References

Buddecke E (1974) Mineralhaushalt. In: Grundriß der Biochemie. W de Gruyter, Berlin New York, p 280

Deetjen P, Boylan JW, Kramer K (1976) Niere und Wasserhaushalt. Urban & Schwarzenberg, München Berlin Wien

Dennis VW, Bracy PC (1982) Divalent anion transport in isolated renal tubules. Kidney International 22:498

Hesse A, Bach D (1982) In: Breuer H, Büttner H, Stamm D (eds) Harnsteine, Vol 5: Klinische Chemie in Einzeldarstellungen. Thieme, Stuttgart New York, p 80

Hesse A, Classen A, Klocke K, Vahlensieck W (1985a) The significance of the sexual dependency of lithogenic and inhibitory substances in urine. In: Schwille PO, Smith LH, Robertson WG, Vahlensieck W (eds) Urolithiasis. Plenum Press, New York, p 25

Hesse A, Classen A, Klocke K, Vahlensieck W (1985b) Untersuchungen zur Geschlechtsabhängigkeit der Ausscheidung von lithogenen und inhibitorischen Substanzen im 24-h-Harn von Gesunden und Kalziumoxalatsteinpatienten. In: Harzmann R et al (eds) Experimentelle Urologie. Springer, Berlin Heidelberg New York, p 129

Schwille PO, Hamper A, Sigel A (1985) Urinary and serum sulfate in idiopatic recurrent calcium urolithiasis. In: Schwille PO, Smith LH, Robertson WG, Vahlensieck W (eds) Urolithiasis. Plenum Press, New York, p 339

Scanning Electron Microscopic Microprobe Technique – Morphological and Chemical Analyses of Struvite Stones Exposed to Renacidin (Hemiacidrin)

TH. ZWERGEL[1], TH. GEBHARDT[1], U. ZWERGEL[1], and M. ZIEGLER[1]

Introduction

Magnesium ammonium phosphate (struvite) calculi may be dissolved by medical therapy, by chemolitholysis. Hereby renal stones are directly attacked through irrigation fluid in the pelvis and calices; struvite calculi respond to a solution of hemiacidrin (Renacidin) which consists of a puffered mixture of anhydrides, lactones of gluconic and lemon acid. In medical therapy a half-open circulation system is necessary, for instance, a combination of percutaneous nephrostomies and transureteral catheters. A controlled flowing in *and* out is indispensable and must be controlled by flow-meters.

Hemiacidrin (Renacidin) irrigations offer an auxiliary method in cases of special calculi therapy. Recurrent or retained stones after open surgical, percutaneous or shock wave therapy have to be mentioned, if in the analysis struvite could only and unequivocally be found.

Auxiliary investigations, for instance nephrostomies, are especially necessary in cases with great stones after extracorporeal shock-wave lithotripsy; they help to remove fractured calculi and to decompress temporarily hydronephrotic kidneys. With these nephrostomies open circulation system for Renacidin irrigation can easily be managed.

The in vitro influence of Renacidin on intact struvite stones, which had been removed by surgery, and also on those destructed by shock-wave lithotripsy, was analyzed.

Three points were of special interest:
- the time until the stones were completely dissolved
- the changes of the surfaces
- the chemical changes on the stone surface.

Material and Methods

The scanning electron microscopy (SEM) and the microprobe technique were used for simultaneous analyses of morphological and chemical changes on calculi surfaces.

The chemical composition (element analysis) of stone surfaces can be found with the distribution of energy, i.e., the distribution of wave length of emited X-rays after electron exposition. It is possible for elements up to an ordinal number of 5. The stone material for the analyses by SEM and by microprobe technique must be dried

[1]Urologische Universitäts- und Poliklinik der Universität des Saarlandes, D-6650 Homburg/Saar

Investigative Urology 2
Edited by G. H. Jacobi et al.

in an increasing alcohol sequence and then the pieces sputter-coated with graphite, silver or gold.

Intact and fractured struvite stones of defined largeness were exposed in vitro during different times to a perfusion of a 10% Renacidin solution, thereafter dried, sputter-coated and analyzed by SEM and microprobe technique.

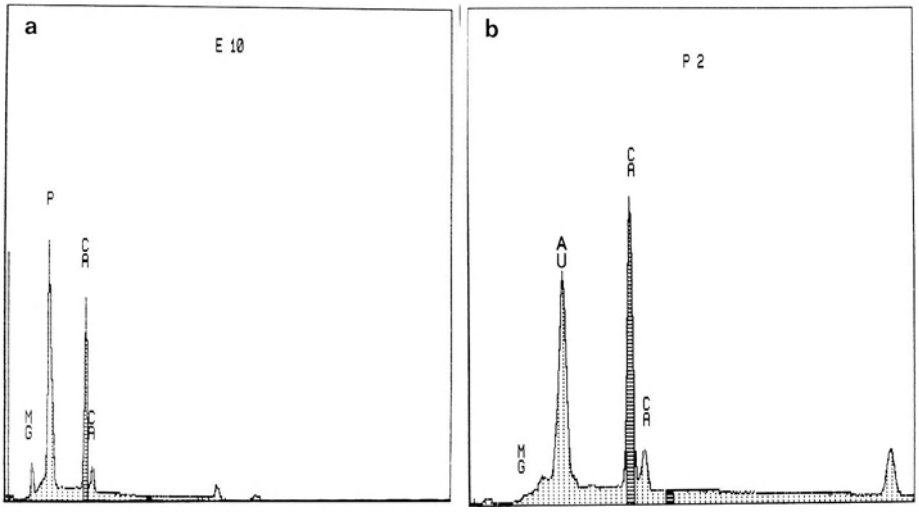

Fig. 1a, b. Example of the elementary analysis of a struvite-stone with an initial size of 1.1 cm; **a** before exposition to Renacidin, **b** after chemolitholysis with Renacidin (52.5 h). Magnesium *(Mg)* and phosphorus *(P)* cannot be found anymore. *Au,* sputter-coating with gold

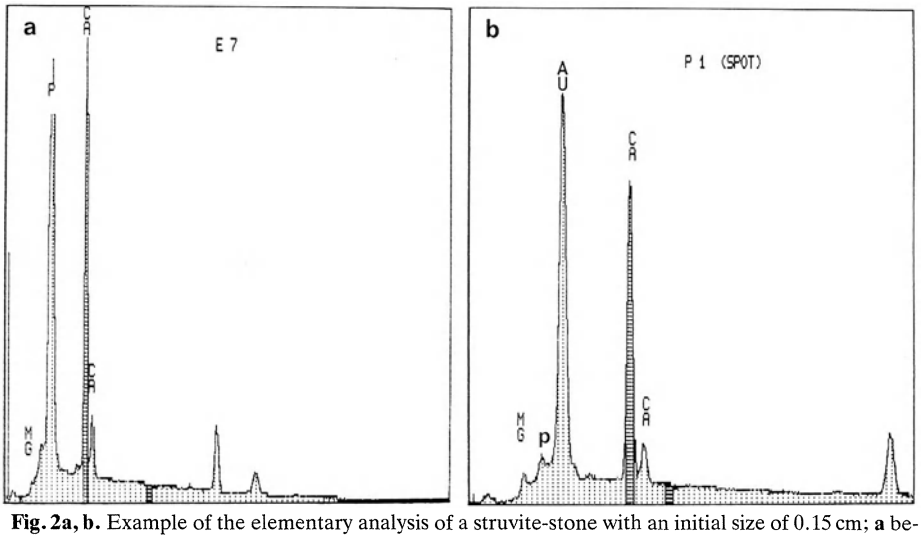

Fig. 2a, b. Example of the elementary analysis of a struvite-stone with an initial size of 0.15 cm; **a** before exposition to Renacidin, **b** after chemolitholysis with Renacidin (18.5 h). Magnesium *(Mg)* and phosphorus *(P)* are reduced. The semi-quantitative analysis of the elementary distribution on the surface also showed a relative reduction of calcium *(Ca)*

Results (Figs. 1–3)

Fractured struvite stones ($\varnothing > 1$ mm) after an exposition to Renacidin during an average time of 36.5 ± 11.9 h were significantly ($P \geq 0.5$) earlier dissolved than intact stones ($\varnothing \geq 1$ cm) with an averaging exposition time of 51.6 ± 14 h.

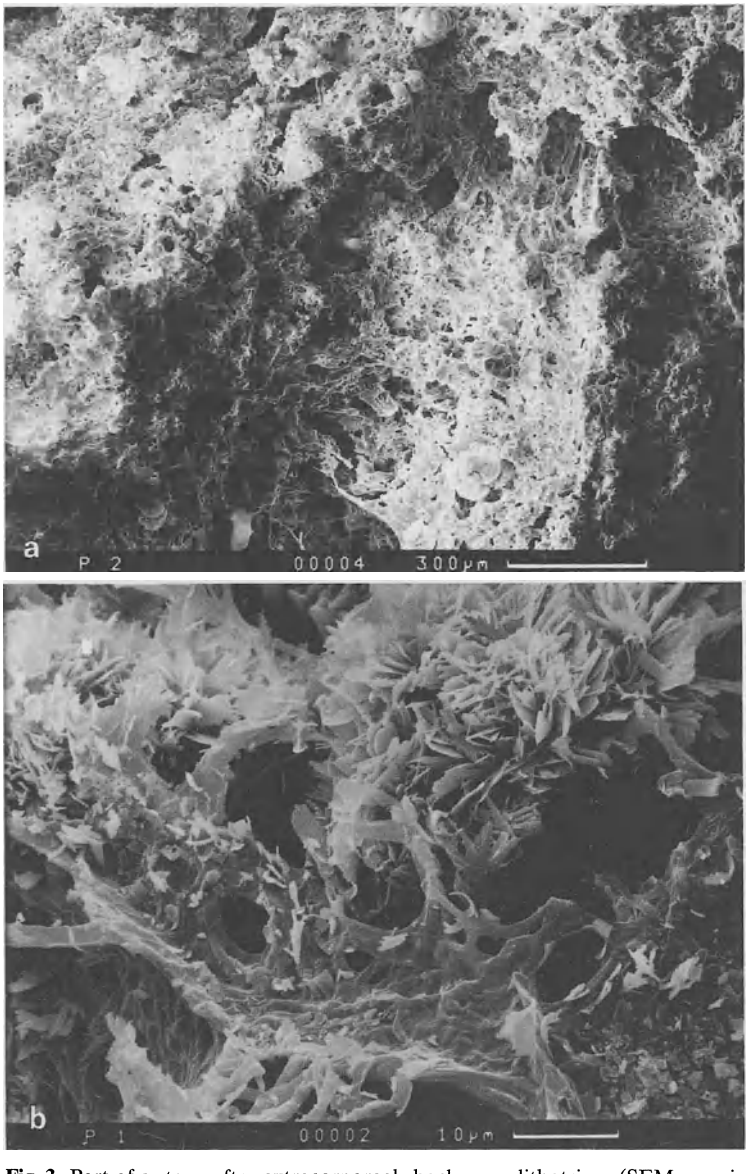

Fig. 3. Part of a stone after extracorporeal shock wave lithotripsy (SEM examination); **a** before exposition to Renacidin, **b** after chemolitholysis with Renacidin (18.5 h)

After Renacidin irrigation phosphorus is at first more reduced on the surface of all struvite calculi. This corresponds to a primary reduction of phosphate due to Renacidin, followed by diminutions of calcium and magnesium at the surface; this can be qualitatively analyzed by scanning electron microscopy.

The chemical elementary analysis of the surface could not determine qualitative differences in different stone sizes, independently whether fragmentory or intact calculi were analyzed.

With the micro-SEM-technique smallest stone particles can be analyzed morphologically together with the elementary analysis.

Renacidin-chemolitholysis is more effective in smaller calculi. This technique can be used as an auxiliary therapy after extracorporeal shock-wave lithotripsy of large struvite stones, at best done with half open systems for a good urinary flow and circulation.

Discussion

The indication for the application of hemiacidrin (Renacidin) is only given if there is a definite stone analysis of struvite.

Scanning electron microscopy is easy to apply requiring minimal sample preparation. The advantage of the described scanning electron microscopic technique consists in obtaining crystal habit and chemical composition both from the same sample using the same instrument. Analyses of composition range from the amorphous constituents to microcrystals and to macroscopic stones. As the method is non-destructive, the surface and the interior parts of the stone can be analyzed by first studying the stone surface and then the inside after fracture, before and after chemolitholysis.

Because very small particles are necessary, the method of urinary stone analysis with the energy dispersive X-ray microprobe technique is suitable for clinical routine in the urinary stone management in the above mentioned special cases, especially in combination with the extracorporeal shock wave lithotripsy and its auxiliary methods.

ESWL-Induced Renal Damage – An Experimental Study

R. Muschter[1], N. T. Schmeller[1], I. Reimers[1], K. R. Kutscher[1], A. Knipper[1], A. G. Hofstetter[1], and U. Löhrs[2]

Introduction

Since the clinical introduction of extracorporeal shock wave lithotripsy for the treatment of urolithiasis in 1980, approximately 200,000 treatments have been performed in the world (Eisenberger et al. 1977; Chaussy et al. 1978). The number of shock waves given in one single treatment varies in different urological departments and the relation of renal damage to treatment parameters is not known. Only a few authors published subcapsular hematomas in some cases and there are very few experimental studies in animals.

We examined the kind and size of ESWL-induced renal damage in dependance of the number and the pressure of given shock waves and tried to find clues to those damages in clinical examinations.

Materials and Methods

In 1985, we studied the effect of extracorporeally induced shock waves on the kidneys of healthy pigs using a Dornier kidney lithotriptor HM3.

Both kidneys of each individual animal were treated with an equal number of shock waves keeping the generator voltage constant. The groups were as follows: A – untreated control, B – 5,000 shock waves, 25 kV generator voltage, C – 2,500 shock waves, 25 kV generator voltage, D – 2,500 shock waves, 17 kV generator voltage, E – 1,400 shock waves, 17 kV generator voltage. 24 h after ESWL the left kidney was removed and histologically examined in order to judge the severity and localization of the renal damage. The animals living with the remaining shock wave treated right kidney were followed up for a period of 6 weeks, when the second kidney was removed and morphologically examined to show the healing and remaining defects.

We performed screening examinations of the electrolytes sodium and potassium, and of creatinine and urea before ESWL, 24 h after ESWL, before the first kidney was removed, 1 week, 3 weeks and 6 weeks after ESWL. In addition, we performed intravenous pyelograms and renovasograms 24 hours and 6 weeks after ESWL.

The control group was treated in the same way as all other groups including anesthesia but no shock waves were applied.

We used young healthy pigs of about 25 kg bodyweight. The animals were fixed in a special holding device of the lithotriptor. We performed intravenous anesthesia

[1] Department of Urology, Medical University of Lübeck, Ratzeburger Allee 160, D-2400 Lübeck
[2] Department of Pathology, Medical University of Lübeck, D-2400 Lübeck

Investigative Urology 2
Edited by G. H. Jacobi et al.

Fig. 1. Surface of an ESWL-treated pig kidney 24 h after treatment – 2,500 shock waves, 25 kV generator voltage

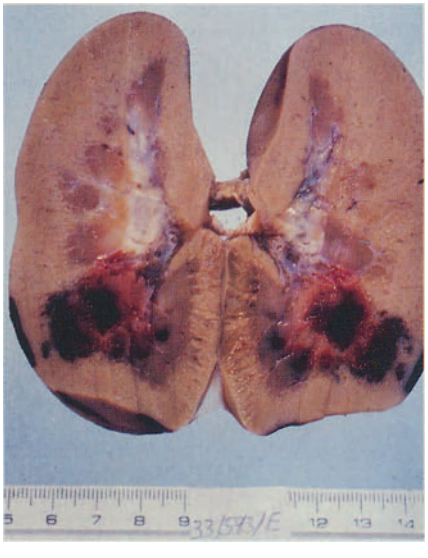

Fig. 2. Subcapsular and peripelvic hematoma in an ESWL-treated pig kidney 24 h after treatment – 1,400 shock waves, 17 kV generator voltage

with Pentobarbital. Shock wave localization and focusing was done via 2 X-ray devices. In order to picture the pelvi-calyceal system we infused contrast-medium, 4 ml of 30% Peritrast per kg bodyweight.

Results

All kidneys that were removed 24 h after ESWL revealed perirenal hematomas. There was no quantitative correlation with the number of shock waves or the generator voltage for perirenal hematoma.

The shock wave treatment resulted in significant morphological alterations. The most severe injuries were found in the center of the focus sharply demarcated towards intact kidney structures. All kidneys exhibited peripelvic and subcapsular hematomas, parenchymatous necrosis of the cortex and the medulla and fresh hemor-

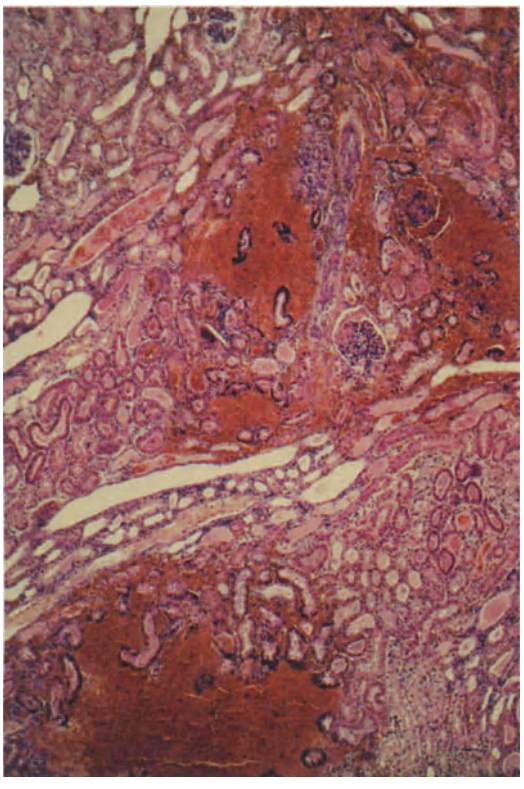

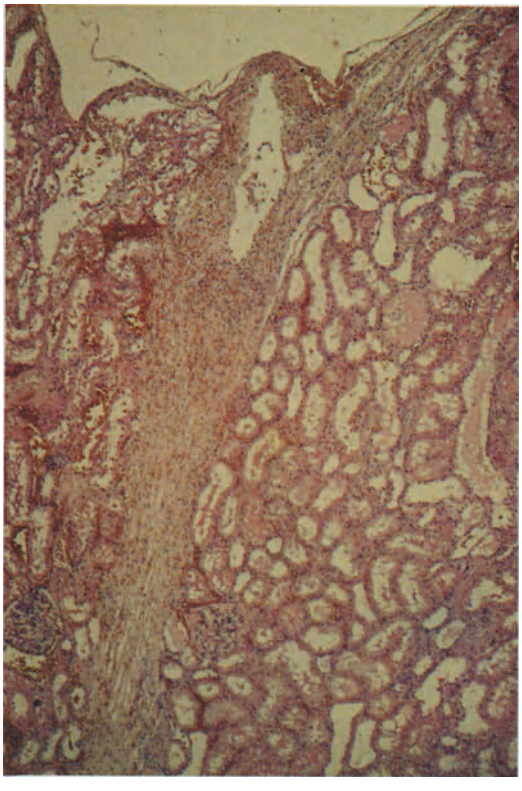

Fig. 3 **Fig. 4**

Fig. 3. Hematoma and parenchymatous necrosis in an ESWL-treated pig kidney 24 h after treatment – 2,500 shock waves, 17 kV generator voltage

Fig. 4. Fibrosis of the capsule and bandlike fibrosis of the parenchyma of an ESWL-treated pig kidney 6 weeks after treatment – 5,000 shock waves, 25 kV generator voltage

rhages of the pelvi-calyceal system. There were also initial inflammatory reactions with extravasal granulocytes.

The severity but not the size of renal damage directly correlates with the generator voltage. Surprisingly, no significant differences were noted in respect to the number of applied shock waves, provided the generator voltage was kept constant.

After 6 weeks, when the second kidney was removed, the morphological and histological examination showed healing with structural defects. In comparison to the primary renal damages, however, the extent of the residues was small.

There were adhesions between the kidney and the retroperitoneum. The structural defects were fibrosis of the capsule and bandlike fibrosis of the parenchyma, also lymphocytic infiltrates and siderophages. The Turnbulb blue staining was positive with no exception, indicating the residues of hematoma.

During the follow-up, sodium and potassium in serum did not change. Also there was no significant elevation of urea in all groups. Creatinin in serum rose in the term of 6 weeks from 110 µmol/l–150 µmol/l in average in all groups without difference between the ESWL treated and untreated solitary kidneys, regardless of the number of shock waves and generator voltage applied.

We were surprised that the severe morphologic damages could not be detected by intravenous pyelograms or renovasogram, even when performing the last method at the removed kidney.

Discussion

Our study shows that there is ESWL-induced renal damage. We think that the trauma would be reduced by decrease of the generator voltage. An increase of the number of shock waves from 1400 to 5000 seems to be not important. Our results were confirmed by Delius et al. (1986) who performed similiar experiments on dogs. Clinical determination of the renal damage is possible with modern imaging techniques (Kaude et al. 1985), but the real extent of tissue damage is still difficult to judge without histological examination.

References

Chaussy C, Eisenberger F, Wanner K, Forssmann B (1978) Extrakorporale Anwendung von hochenergetischen Stoßwellen – Ein neuer Aspekt in der Behandlung des Harnsteinleidens, Teil II. Akt Urol 9:95–101

Delius M, Enders G, Xuan Z, Rath M, Liebig G, Brendel W (1986) Effect of shock waves on the kidney. First Int Symp on Anesthesia and ESWL, München

Eisenberger F, Chaussy C, Wanner K (1977) Extrakorporale Anwendung von hochenergetischen Stoßwellen – Ein neuer Aspekt in der Behandlung des Harnsteinleidens. Akt Urol 8:3–15

Kaude JV, Williams CM, Millner MR, Scott KN, Finlayson B (1985) Renal morphology and function immediately after extracorporeal shock-wave lithotripsy. Am J Rad 145:305–313

Extracorporeal Piezoelectric Lithotripsy (EPL) – Generation and Application of Short High-Power Sound Pulses

R. Riedlinger[1], B. Kopper[2], and H. Wurster[3]

Introduction

The first attempts to disintegrate concretions extracorporeally using piezoelectric techniques date from the late fourties (Berlinicke and Schennetten 1951; Coats 1956; Lamport et al. 1950; Mulvaney 1953). These authors achieved a slight disruption of concretions by applying sound waves at intensities of about 5 W/cm^2 over a period of up to 30 min.

All such attempts were discontinued in the midfifties because of serious tissue lesions and insufficiently successful calculus disintegration. As we know today, these sound wave techniques were based on erroneous assumptions about the required time pressure profile.

Only the spark-gap shock wave procedures used since 1979 were successful in lithotripsy. However, the use of X-rays for calculus localization and the necessity of anesthesia because of the painful effects of the treatment appear disadvantageous.

Since 1980, a research group in Karlsruhe, Knittlingen and Homburg (W. Germany) has been investigating the possibility of developing an advanced technique of extracorporeal lithotripsy using piezoelectrically generated short sound pulses.

Important reasons for undertaking this project included:

- the possibility of varying the shape and amplitude of the sound pulse,
- the possibility of ultrasound localization of the calculus and its disintegration using one and the same transducer,
- the durability of the piezoelectric transmitter,
- the precise reproducibility of the high-energy sound pulse,
- the prospect of a painless treatment.

Material and Methods

Research and Development Aims

Since the beginning of our work various types of ultrashort (1–15 μs) high-energy sound pulses have been generated and tested. However, the amplitude, frequency spectrum, duration, profile and repetition rate of transient signals suitable for contact-free acoustic lithotripsy must be designed in such a manner that no lesions of the tissues in front of the concretions occur. In order to avoid detrimental tissue cavitation only highly transient signals could be considered.

[1] Fachgebiet Akustik IHE, Universität Karlsruhe, Kaiserstr. 12, D-7500 Karlsruhe 1
[2] Urologische Klinik, Universitätskliniken, D-6650 Homburg-Saar
[3] Wolf GmbH, Pforzheimer Str. 32, D-7134 Knittlingen

Investigative Urology 2
Edited by G. H. Jacobi et al.

On the surface of concretions, however, the cavitation can substantially contribute to disintegration. Only strongly focussing transducers of wide aperture protect anterior tissue sufficiently and provide a narrow cavitating focus.

Simultaneously, our aim was to work with low energy levels (< 0.1 mJ); this is possible if a directly focussing transducer is used.

Piezoelectric Sound Transmitter

Our Piezo-transmitters (Riedlinger 1986) are composed of a large number of small ceramic cylindrical elements mosaically covering the concave side of a spherical cap as illustrated in Fig. 1. The geometry of the components is determined by the desired periodicity of about 2 µs.

Diameter and focus length of the cap are adopted to the structure of the anatomy, on the one hand, and the energy requirements for calculus disintegration, on the other.

Pulse Generator, Signal Forms

The piezo-transmitter is stimulated by a high voltage electric signal and supplies a transient high-energy acoustic signal. By varying the input signal the force of the acoustic impulse can be continuously adapted to prevailing requirements within very wide range limits.

The pressure near the focal point can be increased up to about 60 MPa, thus being sufficient for calculus disruption. The pulse generator allows single pulse or continuous pulse operation with a repetition rate in the frequency range of 1–10 Hz.

In experiments conducted since 1980 we have generated the following signals depending on transmitter construction and input signal:

- High-energy-US-burst-signals with a carrier-frequency of 400 kHz and a decay rate of about 10 µs. Initial pressure: around 20 MPa.
- HE-bipolar-pulses (Profile approximates one-period sine wave) with pulse length of 2 µs and amplitudes of 30 MPa, approximately.
- HE-unipolar-pressure-pulses (Profile approximates positive half-wave sine curve) of 1 µs duration and pulse amplitude of appr. 40 MPa. The developed lithotriptor "Piezolith" generates such HE-unipolar-pressure-pulses.

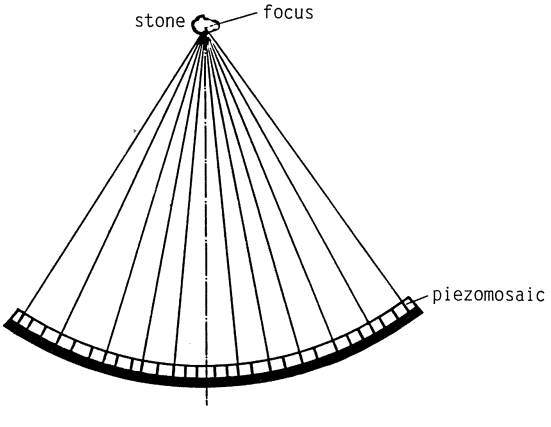

Fig. 1. Schematic drawing of the piezo-transmitter

Fig. 2. Piezoelectric lithotriptor with patient positioned for treatment

Technical Construction of the Lithotriptor, Installation

The piezoelectric lithotriptor has been constructed as a movable apparatus, the size of an operating table. The patient reclines in a supine-lateral position on the surface of the special table containing an opening into which the part of the body requiring treatment is immersed, without formation of air bubbles, and is thus coupled acoustically by means of water to the piezo-cap situated under the reclining surface (see Fig. 2).

The piezo-transducer can be positioned in all directions beneath the patient by observing the ultrasound signals until it is focussed within millimeters of the calculus (Fig. 4).

Each position of the focal point in the coordinate frame of the treatment table is displayed digitally on the operating console. Thus, interesting positionings can easily be retrieved. When requested by the operator, the original position is automatically aligned, the focus being centered on the coupled opening. Other positions can also be stored and automatically aligned.

The operating table concept also incorporates the entire water processing unit: The water is filtered, degassed and heated to body temperature in order to avoid even the smallest invisible bubbles which can dampen the generated sound pulses as well as irritate body tissue at the region of entry.

Installation of the mobile system merely requires an ordinary electrical outlet and a cold water supply. Since no building modifications are required and practically no depreciation costs occur, expenses are kept low.

The high-voltage equipment is contained in the operating table. The ultrasound positioning controls and displays are located in a movable console in the most convenient position for the physician. In order to determine the degree of calculus disintegration by the usual X-ray-C arm method, it is possible to elevate and translate the entire table surface without moving the patient until the table opening becomes accessible to the X-ray-C unit. After the X-ray procedure the table surface is automatically returned to the original position.

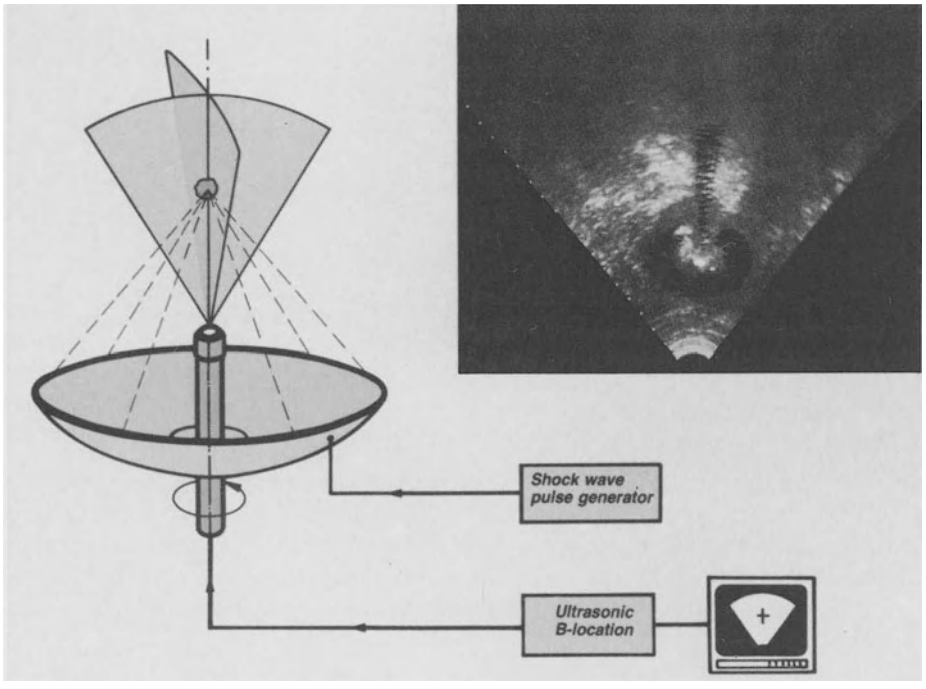

Fig. 3. Ultrasonic location system and display of B-scan image

Congruent Ultrasound Locating Device

Another important element of the apparatus is the locating device incorporating two different ultrasound locating systems. This is to the advantage of both doctor and patient. X-ray damage can be avoided to a large extent. X-rays are applied mainly for calculus diagnosis and confirmation of treatment success, as presently required. The treatment itself exclusively utilizes ultrasound methods for calculus localization and permanent observation. This is of particular advantage from a physical and acoustic point of view, since sound waves for calculus localization and disintegration use the same paths.

Sound wave refraction during tissue transition is accounted for.

Deviations of the focal point from the geometrical transmitter focus are thus taken into consideration during ultrasound positioning, which is not possible if X-rays are used. The similarity of the acoustic system for low-energy detection and high-energy sound transmission guarantees a precise positioning of the focal point on the calculus.

The locating system used consists of 2 components:

An imaging ultrasound device applying the B-scan method is useful for acoustic scanning. A special ultrasound scanner is located on the symmetry axis of the high-energy transmitter. It can be turned 90° automatically and thus provides image sections in 2 orthogonal planes (Fig. 3). By selecting different zoom adjustments, varying image sizes of body organs can be obtained. It displays the outer layer of the skin at the signal entry region as well as the kidney silhouette and the calculus.

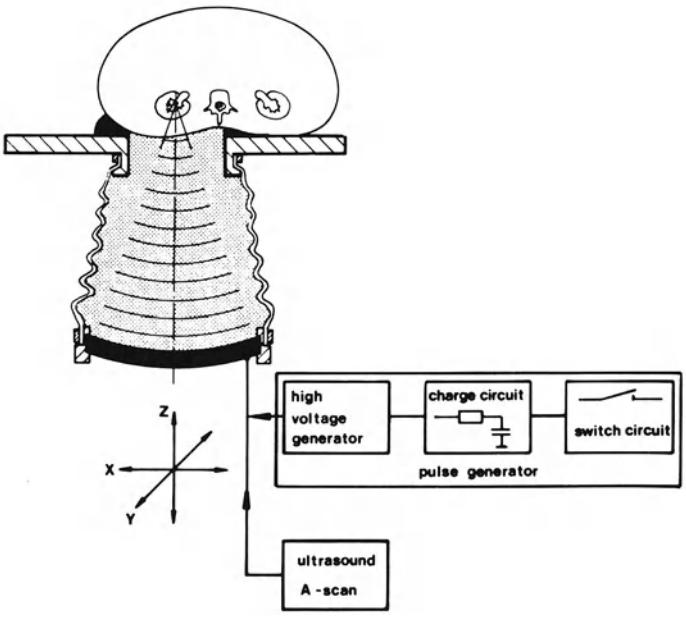

Fig. 4. Shock-wave application and congruent A-scan location system

Another ultrasound device applies the pulse-echo method (A-scan) and uses the Piezo-transducer for precise acoustic localization (Fig. 4). Here the high-energy sound transmitter simultaneously functions as an echo receiver. The echo signal produced at the calculus is analyzed on a monitor with respect to amplitude, polarity and time lag relative to the input signal. The positioning of this special A-scan method is accurate within millimeters. Reflections from bones or calculi can be distinguished by the echo pulse profile.

At the same time, this device can be used to supervise the quality of the acoustic coupling of the water-skin transition which seems imperative for avoiding skin irritation at the signal entry region as well as ensuring optimal energy transmission and focussing.

Results

Effects of Pulse Profile on Tissue and on Calculus Disruption

Under the effects of high-intensity CW-ultrasound the tissue is exposed to extremely heavy damage. Cell walls and vessels are disrupted by heat and cavitation originating in tissue fluids which are not free of blastulae. CW-US-methods are therefore totally inappropriate. Even if strongly focussed CW-US is applied only for seconds, the disruption of the tissue anterior to the calculus cannot be avoided if intensities required for calculus disintegration are used.

Through short-term bursts calculi can be disrupted very efficiently as long as the initial amplitude does exceed about 20 MPa. In this case, the cavitation effects on the

calculus surface intensify the disruption mechanism. Even if a sound intensity just enabling calculus disintegration is chosen, in-vivo experiments still show heavy tissue and vessel destruction. This occurs even if the sound pulse at 380 kHz and an initial amplitude of 20 MPa consists of only about five oscillations, and the focal diameter of the sound transmitter measured at half amplitude is only 5 mm.

Hence it can be inferred that the cavitation threshold in tissues is considerably lower than in tap water without special treatment, and thus tissue compatibility of sound pulses cannot be deduced from the lack of cavitation in in-vitro experiments.

If bipolar pulses of the same amplitude are applied, the efficiency of calculus disruption declines, but so does the degree of tissue damage. Significantly, better medical results are obtained using such bipolar pulses even at amplitudes of about 30 MPa and a pulse duration of 2 μs. However, even in this case, lesions have been observed with 1 μs-pulses of < 10 MPa.

The unipolar pulse appears particularly advantageous: extracorporeal disruption even at pulse amplitudes of 40 MPa and 2 μs duration is thereby possible without damaging the kidney or impairing its function.

The HE-unipolar-pulse presently appears as the most suitable signal profile for extracorporeal lithotripsy.

Animal Experiments

Sound therapy was used on 14 dogs after a partial ligature of the urethra and calculus implantation.

In all cases calculus disruption was achieved after the exact sonographic detection of the calculi.

The morphologic and functional kidney diagnosis after the piezoelectric treatment agree with the results known from animal experiments with shock wave therapy using the common ESWL-method.

Human Applications

Having shown by self-experimentation (1st co-author), that the piezoelectrically generated HE-pulses are painless for humans, all patients were treated without anesthesia. By June 1986, 108 treatments were applied to 89 patients including 2 children having calculi up to 2 cm in diameter in the kidney cavity system.

In 44 cases the stones were localized in the renal pelvis. 45 times calix stones were involved (5 upper, 11 middle and 29 lower calix concrements). 12 patients had undergone previous kidney stone surgery.

½ tablet of Flunitrazepam (Rohypnol) was administered to the patients as a sedative 30 min before the treatment began.

For all patients the concretions were easily localized using the 2 ultrasound systems. For 4 patients out of 93 intended for treatment the sonographic localization was used without result. 2 of these patients had left-side renal pelvic stones. The other two had upper kidney stones which were obscured by ribs when focussed.

The patients were placed in a semi-lateral position on the surface of the lithotriptor-table so as to facilitate a smooth coupling of the transducer. After sonographic calculus localization the treatment lasted 30 min on the average. On the average, 900–1200 sound pulses were applied to each calculus.

Patients perceived the sound pulses as a light painless pointed pressure in the kidney. Only in 2 cases did complaints of pain require the administration of an analgesic.

For 86 of 89 patients a complete disintegration into particles sufficiently small to leave the body was achieved. 19 patients were submitted to a subsequent treatment due to the large volume (diameter greater than 2 cm) or initially incomplete disintegration of the calculi. Auxiliary measures such as percutaneous nephrostomy and calculus dislodgement in the ureter using catheters were required in 13 cases.

At the time of their discharge from hospital after staying 4–6 days on the average, 33 of 89 patients (37%) were radiologically free of calculi. The other patients, having well disintegrated disposable calculus particles were submitted to outpatient urological supervision.

Serious complications, such as perirenal hematoma, have not been observed after Extracorporeal Piezoelectric Lithotripsy (EPL).

Discussion

Focal Dimensions

A significant difference between the new piezoelectric system and other lithotriptors is the small extent of the focal region within which disruptive sound pulses are generated. Its dimension is only about 3 mm radially and 5 mm along the axis. This means that the piezoelectric system exposes only a very small region to high-energy-impulses thus permitting, as has been demonstrated, the precise disintegration of calculi at chosen positions.

Disintegration and Disposal of Calculi

The piezoelectric system's pulse energy variability as well as the small dimensions of its focal region permit an extremely fine mode of calculus attack.

In general, stones are not split and reduced to initially large fragments, but small, fine, sandlike particles are crumbled off as long as the pulse energy is held sufficiently low. A high pulse energy, such as a spark-gap system generates, initially produces large fragments which are successively reduced to the size of sand grains during the course of further shock exposure. If the calculi masses are large, this may lead to problems in their disposal. Thus a high-focal energy density is not always desirable. By applying low-energy pulses, the surface of the calculus is eroded so that treatment interruption and disposal of pulverized material is possible, if existent stone masses are too large.

In vitro, renal calculi of about 1 cm in diameter can be disintegrated into particles the size of grains using approximately 1000 pulses. For human beings, 800–2000 pulses suffice, depending on anatomic conditions.

The onsetting stone disintegration can be detected sonographically by the increased diffusion and divergence of the originally intense stone-echo-image and the expansion of the US-shadow-region. Due to the permanent sonographic control during treatment, kidney movements caused by respiration, are of minor importance, since the sound pulses are manually triggered when the calculus is exactly in focus.

Mild Treatment and Painlessness

From a physical as well as medical point of view, EPL differs substantially from the ESWL-method used so far: The ESWL-method still applied uses a bubble-generating sound transmitter (underwater spark-gap). All these sound transmitters (including, e.g., wire explosion and transmitters with Laser-Induced-Breakdown) are based on the principle of exploding steam bubble whose expansion continues even after the desired shock wave has been generated. Thus low-frequency components of the sound spectrum result.

These components as well as the fact that the body surface itself is exposed to a shock wave, probably give rise to the painful effects of the other transmitter types. The ESWL-methods are tissue-preserving, in general, but disadvantageous tissue reactions cannot be excluded: for example, severe skin reddening may occur at the region where the sound waves enter the body.

Since the explosive-type transmitters are focussed by reflectors which cannot encompass the entire space angle of the generated sound wave, some unfocussed sound radiation will penetrate the body. In our opinion, cardiac arrhythmia occurring during treatment are sometimes caused by these basic properties of reflector-focussed ESWL-sound-transmitters.

The directly focussing EPL-system produces neither skin reddening nor pain sensations or extra systols.

We attribute this to the following special properties of the sound pulses we have applied:

The skin surface at the signal entry region is not exposed to a shock wave.

The EPL-sound signal does not contain the low frequency components which are produced by expanding and collapsing gas bubbles.

Since the EPL-sound signals are strongly focussed, the particle velocity in the focal region and elsewhere is considerably smaller than that of other more weakly focussing transmitters assuming identical pressure amplitudes are generated in the focal region.

Reproducibility, Depreciation

Dependable, permanent lithotriptor functioning requires that precisely reproducible sound pulses are transmitted through the body. The piezoelectric sound wave generating principle fulfils this requirement to a greater extent than a water spark-gap the separate impulses of which are subject to random deviations, the value of their time average depending on the degree of unavoidable electrode corrosion. Piezoelectrically induced impulses are reproducible with an average deviation of less than 2%.

As far as long term studies could determine, the piezo-system, despite high electromechanical strain is subject to no measurable wear. Material fatigue could not be determined, the transmitter system is practically without depreciation.

Compared to other systems, the piezoelectric lithotriptor being therapeutically highly efficient, offers various advantages:

- The calculus location causes no radiation damage because it only utilizes ultrasound techniques.

- There is no skin irritation at the sound entry region.
- Permanent sonographic control of the focussed calculus is possible.
- No extra systoles are induced.
- The Piezo-lithotriptor is a movable apparatus the size of a table with built-in water treating equipment and a small separate operating console. Power and water supplies suffice; no building modifications are required.
- Both purchase and treatment costs are comparetively low.
- Maintenance costs are low because the piezo-transmitter works without depreciation.
- No anesthesia is required, since the EPL-treatment is painless.

References

Berlinicke ML, Schennetten F (1951) Über Beeinflussung von Gallensteinen durch Ultraschall in vitro. Klin Wochenschr (Jg 29) 21/22:390

Coats CE (1956) The application of ultrasonic energy to urinary and biliary calculi. J Urol 75(5): 865–876

Lamport H et al (1950) Fragmentation of biliary calculi by ultrasound. Federation Proc (Mar) 9: 73–74

Mulvaney WP (1953) Attempted disintegration of calculi by ultrasonic vibrations. J Urol 70(5): 704–707

Riedlinger R (1986) Erzeugung transienter Hochenergie-Schallpulse. Proc DAGA '86, Oldenburg, pp 821–824

Experimental Evaluation of a New Electromagnetic Shock Wave Source

D. M. Wilbert[1], A. Jungbluth[2], T. Rosenkranz[1], H. Reichenberger[3], H. J. Rumpelt[2], H. Riedmiller[1], P. Alken[1], and R. Hohenfellner[1]

Introduction

Clinical application of new shock wave sources always warrants prior experimental evaluation of the stone disintegration capabilities and characterization of the shock wave impulses. The least possible tissue traumatization is necessary for successful clinical introduction. After the spark-gap generation of shock waves with semi-ellipsoid focussing had been introduced to the urological armamentarium for extracorporeal destruction of renal and ureteral stones in 1980 (Chaussy 1982), new modes of shock wave generation have been developed. In cooperation with the Siemens Company of Erlangen, Germany, a new electromagnetic shock wave source was evaluated by in vitro and in vivo animal experiments. The main question to be answered was: Does the shock wave retaining the capability of stone destruction harm viable structures such as connective tissue and parenchymal organs like the kidneys.

The shock wave device basically consists of an electromagnetic source and a local coupling unit to the experimental animal and later to the patient in order to avoid a surrounding water tank. A slap coil mounted on a hard carrier is separated by a thin insulating layer from a metal membrane. When a high-voltage pulse resulting from a capacitor discharge acts upon the slap coil, a current is induced in the membrane. The membrane is repelled rapidly from the coil which later results in a shock wave impulse. These waves are propagated through a small water-filled tube. Focussing is accomplished by a lense system with acoustic properties similar to water. Shock waves then are applied to the animal via a silicone coupling head which is held against the flank with constant pressure (Fig. 1). The focal zone is defined as an area of high pressure with a lateral extension of about 8–10 mm and a longitudinal exten-

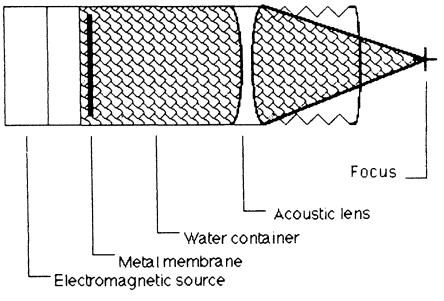

Fig. 1. Principle of electromagnetic shock wave generation and focussing by anacoustic lens

[1] Department of Urology, Johannes Gutenberg University, Langenbeckstr. 1, D-6500 Mainz
[2] Department of Pathology, Johannes Gutenberg University, D-6500 Mainz
[3] Siemens Company, D-8520 Erlangen

Investigative Urology 2
Edited by G. H. Jacobi et al.

sion of about 50 mm. Maximum pressure measured in this zone is as high as 550 bars (Reichenberger and Naser 1986).

Material and Methods

The device described above was initially coupled to a water container to perform in vitro experiments with human renal stones testing the desintegration capability and to perform shock wave exposure of human red blood cells in order to evaluate possible influence to erythrocyte membranes. Disintegration was performed on multiple small and large human renal stones. As an example a 10 mm calcium phosphate stone, a 13 mm uric acid stone, a 15 mm calcium phosphate and struvite stone were subjected to 200 shock wave impulses.

2 ml of human whole blood were subjected to shock wave exposure after 0.1 ml of potassium citrate had been added to prevent coagulation. The containers were placed in the focal zone and 10 impulses with increasing generator voltage from 17 to 20 kV were applied. In a second setting the generator voltage was kept constant at 17 kV and the number of shock wave impulses ranged from 10–40 impulses. Thereafter, the blood was centrifuged and the free serum hemoglobin was determined by a spectral photometric analysis at 450–400 nm wave length utilizing cyan-methemoglobin. The results expressed in mg % of free hemoglobin were plotted against the number of impulses or the number of the generator voltage.

As the next step, potential tissue traumatization was evaluated by exposing rats to serial shock waves. Knowing the extension of the focal zone of the EMS, (electromagnetic system) all organs were examined which are potentially localized in the focal area during disintegration of renal or ureteral stones. Essentially, all organs of the upper abdomen are at risk: particularly small and large bowels, liver, spleen, pancreas and the skin at the entrance and exit area of the shockwaves.

The difficulty of comparing directly the applied energy to a laboratory rat with 400 g in contrast to an adult human was circumvented by varying the applied energies. Thereby it was at least possible to evaluate the relative increase of potential tissue traumatization.

The rats were divided into three groups. In group 1 a laparotomy was performed and visceral organs such as the liver, small intestines and the kidney were exposed to shock waves after eventration. Half of these animals were sacrificed after the experiment, and gross and histological examinations were performed. 6 animals were retained in their cages for 14 days, then were sacrificed and also gross and microscopic examinations were performed.

The second group consisted of 30 rats which were exposed to shock waves as intact animals under ketamine anaesthesia. And finally, group 3 consisted of 3 rats in which the vertebral column and one of the legs were exposed to shock waves. In the intact animal group, 10 rats were sacrificed after the exposure and 20 animals were sacrificed after 14 days, and again gross and microscopic examinations carried out. For shock wave exposure of the eventrated organs the liver, kidney or small intestines were placed in front of the abdominal wall after laparotomy without compromising the anatomical blood supply. The organs were immersed into saline solution, which covered the coupling membrane. Consecutive exposure of segments of the small

bowels with increasing number of impulses from 1 up to 256 shock wave impulses was performed at 17 and 20 kV generator voltage. In 5 animals the lungs were exposed additionally. To evaluate the lesions of the small intestine a semiquantitative description was utilized. Small vascular erosions which were only visible under the microscope were judged as 1+. Gross visible hemorrhage was judged as 2+ and lacerations of the surface including hemorrhage were estimated as 3+.

For shock wave exposure the intact animals also were immersed in physiological saline solution and either 100 impulses with 17 kV or 20 impulses with 20 kV were applied.

The final experiments were performed with 15 male and female beagle dogs with a weight of 11–15 kg. In these dogs prior to shock wave application, human renal stones were implanted into the renal pelvis which were desintegrated after a healing period of approximately 8 days. In contrast to a previous protocol, – (Eisenberger et al. 1977) the stones were implanted into non-obstructed kidneys. This was facilitated by an intrasinusoidal pyelotomy and human renal stones of varying compositions of a size of 5–11 mm could be implanted utilizing this technique. The renal pelvis was closed with 6/0 chromic catgut. In some animals an additional human renal stone was implanted into a peritoneal pouch. Immediately after the operation a plain film was performed to control the correct positioning of the implanted stone. 8 to 10 days later, a plain film was repeated and sonography of the implanted kidney was performed. Only a few kidneys showed dilatation on sonography. Only one out of 15 implanted stones was dislodged in the upper ureter.

Then shock wave exposure was done with the animal under general intubated anaesthesia until the stone was desintegrated during radiological control. As the next step an IVP was performed in order to visualize not only the stone-bearing but also the opposite kidney which then was localized and subjected to high-dose shock wave exposure. In 9 animals selective shock wave exposure of the lungs was done with up to 200 impulses. 8 of these dogs were sacrificed after termination of the experiment and gross and microscopic examinations were performed. The stone fragments were removed from the kidneys, and their size was measured. 7 beagles were placed in cages for another 7 days and were then sacrificed. Gross and microscopic examinations were then performed and the hollow systems of the kidneys were examined for residual fragments.

Results

In Vitro Stone Desintegration. All stones were exposed to 100 impulses with 17 kV and 100 impulses with 18 kV generator voltage. In all instances, complete stone desintegration into particles smaller than 2 mm was achieved.

Shock Wave Exposure of Human Whole Blood. In both parts of the experiment, a pronounced increase of free hemoglobin was found with increasing shock wave exposure (Figs. 2, 3). It is conceivable that the cellular membrane of the erythrocyte is disrupted or at least the permeability of the cell membranes changed with shock wave exposure to set hemoglobin free.

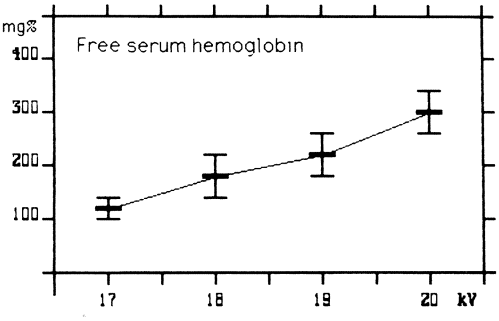

Fig. 2. Increase of free hemoglobin after shock wave exposure of 2 ml of human whole blood. 10 impulses with 17–20 kV, experiments performed with 5 samples each. (Normal range of free hemoglobin: 0–5 mg%)

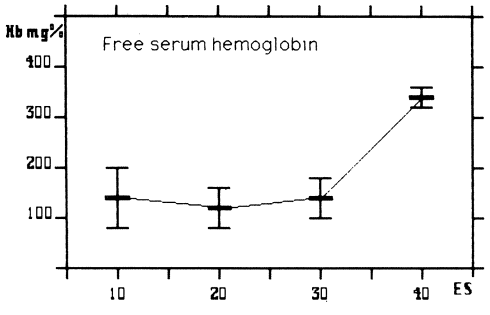

Fig. 3. Increase of free hemoglobin after shock wave exposure of 2 ml of human whole blood. 10, 20, 30 and 40 impulses at 17 kV, experiments performed with 5 samples each. (Normal range of free hemoglobin: 0–5 mg%)

Table 1. Serial exposure of small intestine in 7 rats. Shock wave impulses increase from 8–256 times. (For rating of trauma see description in Materials and Methods)

Nr./ES	1	2	4	8	16	32	64	128	256
5									2
6	1	1	1	2					
10				1	1	1	2	2,3	
7		1	2		2	2	3	3	
8				1	3,3,3	1			
9	1		1	2,3	2,2,2				
2	1	1	1	1	2				
Total	3/7	3/7	5/7	10/10	20/11	4/6	5/3	8/4	2/1
Index	0.43	0.43	0.71	1.0	1.82	0.66	1.66	2.0	2.0

Shock Wave Exposure of Eventrated Organs of WISTAR Rats. The kidneys and livers exposed to shock waves did not show any pathological changes on gross or microscopic examination, neither immediately after shockwave application nor 14 days later. The results of serial shock wave applications to the small intestines are summarized in Table 1 showing the evaluation of a total of 7 animals. In the lower row of the table an index was created presenting the quantitative tissue traumatization. If this is plotted against the number of shock waves, then a linear increase can be found as shown in Fig. 4.

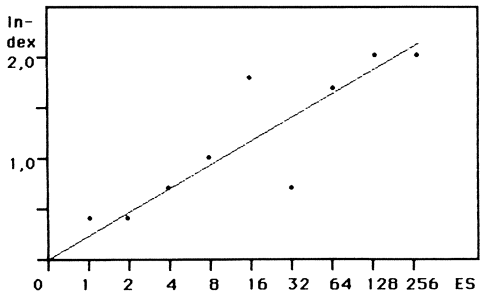

Fig. 4. Relation of "index of traumatization" with increased shock wave exposure

Table 2. Histological changes of abdominal organs and lungs immediately after shock wave application to Beagle dogs

Kidney (stone-bearing)	5/8
Kidney (opposite)	2/8
Heart, spleen	0/8
Pancreas	1/8
Intestines	1/8
Mesentery	1/8
Lungs (after select. exp.)	2/6

Table 3. Delayed histological changes of abdominal organs and lungs after shock wave application to Beagle dogs

Kidney (stone-bearing)	2/7
Kidney (opposite)	0/7
Heart, spleen	0/7
Pancreas	1/7
Intestines	0/7
Mesentery	0/7
Lungs (after select. exp.)	0/3

In those 3 rats where the vertebral column and the upper brim of one leg were exposed to shock waves, a local swelling of the extremities was found with slight petechial bleeding in 2 of the 3 animals at the site of the shock wave entrance. However, histological examination did not show any alterations of the vertebral bones, the medulla or the sciatic nerve.

Results of Shock Wave Treatment in Beagle Dogs. All 15 stones, which were composed of calcium oxcylate, struvite, uric acid or calcium phosphate were desintegrated with 150–1,000 single impulses and utilized generator voltages between 18 and 20 kV. The average fragment size was between 1 and 3 mm.

In general, only in those animals, in which autopsies were performed immediately after treatment, pathological changes were encountered. These include: Petechial bleeding, especially in the area of the mesentery, in the scarred area of the perirenal fat, and in the lungs, which were also exposed. Minor petechial bleeding was found in the pancreas and on the large bowels. Only 2 out of 8 acutely examined healthy kidneys showed minor punctual bleeding on the surface. Those alterations, which could be proven by histology, are summarized in Tables 2 and 3.

Selective exposure of the lungs did not show any changes when only 10–50 single impulses were applied with a generator voltage between 18 and 20 kV. Only after 100–200 single impulses subpleural hematomas were encountered. This also includes those animals which were subjected to delayed autopsy. None of the beagles had a hemoptisis or died from any changes related or unrelated to shock wave exposure or

Fig. 5. Stone-bearing canine kidney after shock wave application (500 S.E.) with small hemorrhage in an area of postoperative fibrosis. (HE, ×100)

anaesthesia. Figure 5 shows a localized hemorrhagical change on one of the stone-bearing kidneys after 500 shock wave exposures.

Discussion

Summarizing the results, the reproduceable stone desintegration was achieved with low number of shock wave impulses. The exposure of human erythrocytes revealed an alteration of the cellular membranes with increasing energy input. These findings compare well with previous results as published by Eisenberger et al. (1977) with one difference: the number of shock waves applied is 10 times higher in the experiments presented here. Shock wave exposure of anaesthesized animals, rats or dogs, only revealed minor pathological changes in terms of petechial bleeding or subserous hemorrhage in the area of the focal zone. In our canine experiments, complete stone desintegration could be achieved. Also, these findings are in keeping with previous reports (Eisenberger et al. 1977; Chaussy 1982). Even the non-stone-bearing kidneys which were exposed to 2,000 single impulses did not show any serious bleeding. Intrarenal alterations as described by Kopper et al. (1986) after application of shock waves from a piezoceramic source could not be reproduced with the electromagnetic shock wave source. Moreover, profound changes, as reported by Muschter et al. (1986) after high dose exposure with the Dornier System HM3 lithotripter also could not be found in the experimental setting described here. It is currently believed that the lower energy level at which stones are disintegrated with the electromagnetic system is responsible for the minimal changes found in the parenchymal organs.

References

Chaussy Ch (ed) (1982) Extracorporeal shock wave lithotripsy. Karger, Basel

Eisenberger F, Chaussy Ch, Wanner K (1977) Extracorporale Anwendung von hochenergetischen Stoßwellen – Ein neuer Aspekt in der Behandlung des Harnsteinleidens. Akt Urol 8:3–15

Kopper B, Ziegler M, Konrad G, Riedlinger R, Wurster H, Goebbels R, Stoll HP (1986) Extrakorporale piezoelektrische Stoßwellenlithotripsie – EpSWL. Abstract 78, Symposion für Experimentelle Urologie, Mainz

Muschter R, Schmeller NT, Hofstetter AG, Reimers I, Pensel J (1986) Art und Ausmaß von Nierenveränderungen nach extracorporaler Schockwellenlithotripsie in Abhängigkeit von der Anzahl der applizierten Schockwellen und der verwendeten Generatorspannung. Abstract 71, 8. Symposion für Experimentelle Urologie, Mainz

Reichenberger H, Naser G (1986) Electromagnetic acoustic source for the extracorporeal generation of shock waves in lithotripsy. Siemens Forsch Entwickl Ber 15:187–194

Action of the Ultrasound and Electrohydraulic Probe for Ureteral Stone Destruction on the Rabbit Ureter

N. T. SCHMELLER[1]

Introduction

Urinary stone destruction by the action of an energy transducer, that is activated next to or at the calculus, is possible by means of an ultrasound probe which is vibrating longitudinally, or by an electrohydraulic probe which generates a shock wave by an electric discharge. Most studies on the side effects of these devices on biological tissue are based on experiments with rabbit or canine bladder tissue.

As ureteroscopy is being more commonly introduced, the use of these energy transducers inside the ureter is increasing and an animal study on the side effects on ureteral tissue was desirable.

Material and Methods

Electrohydraulik Probe

2 different electrohydraulic generators available commercially in the F.R.G., were examined in vitro (Riwolith, made by Fa. Wolf GmbH, 7134 Knittlingen, probe diameter: 1.6 mm, and lithotron EL 21, made by Fa. Walz, 7271 Rohrdorf, probe diameter: 1.4 mm). With both generators the least possible energy level was used in all animal experiments. The spark area was determined by microphotography in a water chamber. By superposition of a chain of spark discharges under the microscope the maximum size of the spark area could be measured on the photography. By the same technique the spatial distribution of the pressure wave could be determined. Here the water chamber was filled with mineral water. The tension wave that is generated by the collaps of the cavitation bubble after each spark leads to small gas bubbles in the area of the pressure change (pseudo-cavitation). By photographic superposition a bubble cloud can be seen in the area of the pressure distribution.

Ultrasound Probe

The ultrasound probe catalogue no. 2167-30 made by Fa. Wolf, 7134 Knittlingen, was used for all experiments. The probe diameter is 1.5 mm and the vibration frequency 22 to 24 kHz.

The vibration amplitude was measured by microscopic photography. Microscopic photographs of the vibrating probe were first obtained in air, but thought not to be representative of the vibration of the ultrasound probe used under operating conditions. The microphotographs were therefore repeated with the sonotrode introduced

[1] Klinik für Urologie, Ratzeburger Allee 160, D-2400 Lübeck

Investigative Urology 2
Edited by G. H. Jacobi et al.

in an operating ureteroscope (Wolf, no. 8952.31) with irrigation running and the tip of ureteroscope and sonotrode in a water chamber. With magnification of 25- and 100-fold, the exact vibration amplitude was determined.

Temperature Measurements

The tip of the electrohydraulic or ultrasound probe was introduced into 1 cc of normal saline that was contained in a regular syringe. The tip of an electronic thermometer (Thermophil 444-1 B, Fa. Ultrakust, 8375 Ruhmannsfelden) was in this water chamber about 5 mm away from the tip of the stone destruction probe.

To simulate physiologic conditions in the ureter, this water filled 1 cc syringe was immersed in 10 liters of water at 30°C–35°C.

Pressure Recording

The pressure waves that are generated by the electrohydraulic probe were measured with a piezoelectric pressure transducer (PCB Piezotronics, model 109 A 02, Buffalo, New York, 14225) and recorded with a storage oscillograph (Fa. Hameg, model HM 208, 6000 Frankfurt 71).

Animal Experiments

18 rabbits of average weight of 3.5 kg were used. The abdomen was opened under sterile conditions and the kidney exposed. Ultrasound probe or electrohydraulic probe were introduced into the ureter in an antegrade fashion. During operation of the probes the ureter was perfused with normal saline to exclude thermal coagulation. The temperature was monitored immediately outside the ureter wall at the tip of the probe. The ultrasound probe was introduced into 30 ureters, 7 times without activation and in 23 ureters with activation (intensity 1) for 5 s ($n = 7$), for 10 s ($n = 8$) or for 60 s ($n = 8$). The electrohydraulic probe was introduced into the ureter in 5 cases and also 5 times into the bladder.

Results

Electrohydraulic Probe

The area of the spark discharge was as wide as the diameter of the electrohydraulic probe and at most 0.5 mm away from the tip of the probe in axial direction. Temper-

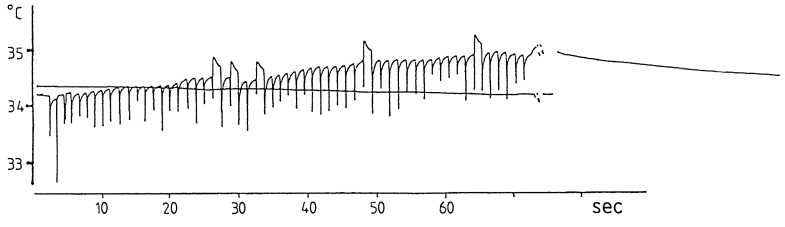

Fig. 1. Temperature of 1 cc of saline during electrohydraulic lithotripsy

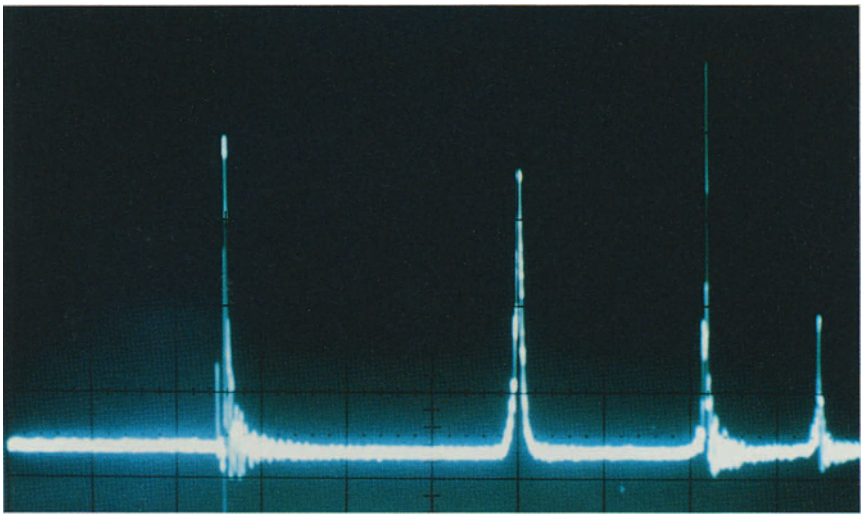

Fig. 2. Pressure reading after one spark discharge of electrohydraulic lithotripsy

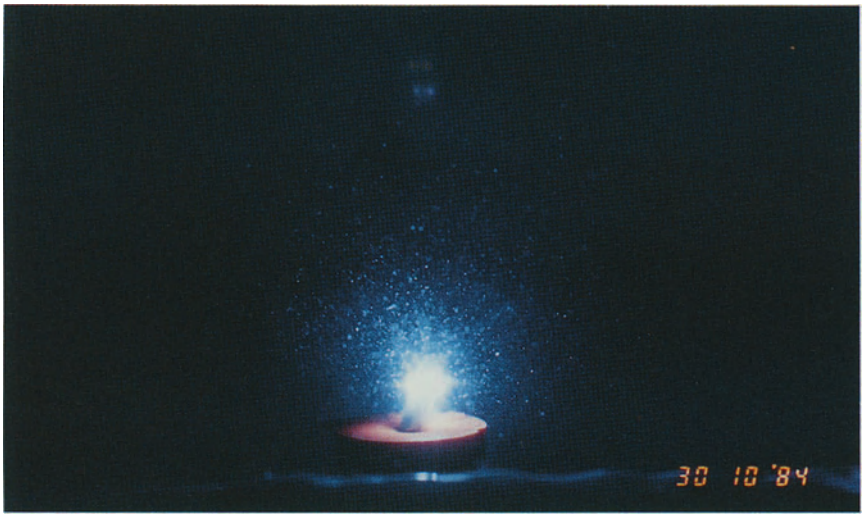

Fig. 3. Spatial pressure distribution of electrohydraulic lithotripsy shown by pseudocavitation

ature elevation in 1 cc of saline was minimal. During the period of 1 min the temperature rise was only 1°C (Fig. 1). Pressure measurements showed a peak pressure of the shock wave of 93 atmospheres at 3 mm distance. The duration of the shock wave was 2 μs at 50% of maximum pressure. 0.6 to 1.4 ms after the shock wave 3 to 4 pressure waves followed with a maximum pressure at or commonly above the shock wave for the first 2 following pressure waves. The third and forth pressure wave had a significantly smaller maximum pressure (Fig. 2). The pressure rise was slower than the shock wave and the duration longer with 5 to 6 μs at 50% maximum. These pressure

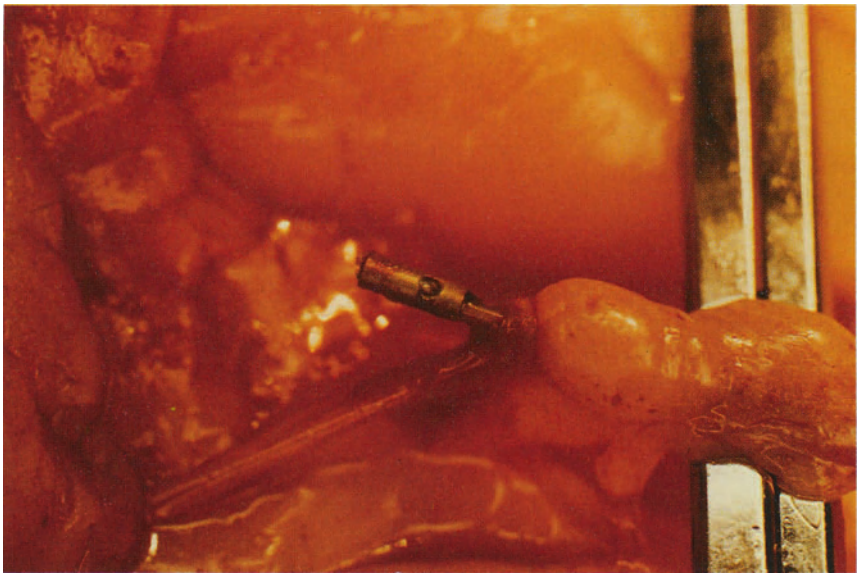

Fig. 4. Perforation of rabbit ureter by one spark discharge at lowest intensity

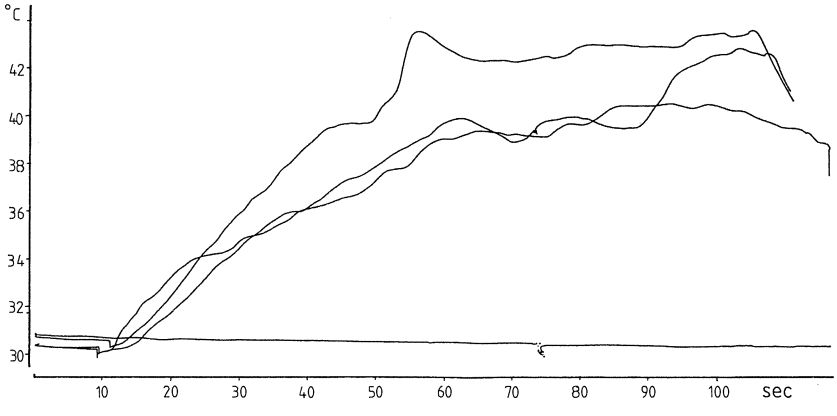

Fig. 5. Temperature of 1 cc of saline during activation of the sonotrode without irrigation running at 3 different intensities

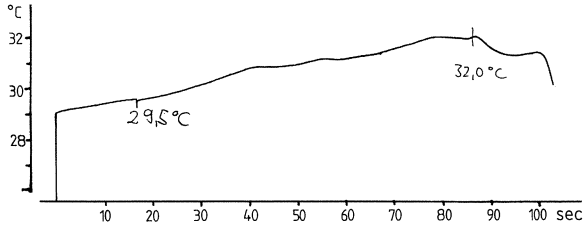

Fig. 6. Temperature of 1 cc of saline during activation of the sonotrode with irrigation running (height level of 1 m)

Fig. 7 **Fig. 8**

Fig. 7. Intravenous urogram of rabbit 6 weeks after activation of the sonotrode in the ureter

Fig. 8. Retrograde ureteropyelography of rabbit 6 weeks after activation of the sonotrode in the ureter

waves were produced by the oscillations of the plasma bubble generated by the spark discharge.

Pseudocavitation with mineral water demonstrated a spherical geometry of the pressure distribution (Fig. 3).

Activation of the electrohydraulic probe inside the ureter or in contact with the bladder wall led to immediate perforation of the wall at the first spark with lowest intensity (Fig. 4). When the probe was guarded by a silicone tubing protruding the tip for 3 mm, the tip of the probe could be kept at a defined distance of 3 mm from the wall of the bladder or renal pelvis. Activation of this probe with the protruding silicone tubing did not result in perforations, but defects in the urothelium and lamina propria as well as hematoma formation in the muscle wall and peripelvic/

perivesical tissue. Stone fragmentation is not possible when the tip of the probe is as far as 3 mm away from the stone. Perforations *are* observed when the silicone tubing is protuding for only 1 or 2 mm. Burn by the spark itself can therefore not be the mechanism of damage, as the spark area is only 0.5 mm long. The pure shock wave, like in ESWL, has a very similiar pressure curve and even much higher maximum, and does not lead to perforations of the renal pelvis or ureter. The reason for the tissue damage is found in the pressure waves of low frequency generated by the plasma bubble as others have shown also (Tidd et al. 1976).

Ultrasound

Vibration of the ultrasound probe in air can be observed under the microscope as mainly transversal with a small longitudinal component. With the probe fed through the ureteroscope and vibration observed in a water chamber there is a longitudinal amplitude of app. 60 micrometer and a transversal amplitude of 30 µm. The amplitude does not change whether the ultrasound generator is set to intensity 1, 2 or 3. Temperature elevation produced by the tip of the sonotrode in 1 cc of saline amounts to approx. 10°C in 60 s when there is no cooling by irrigation fluid (Fig. 5). With appropriate irrigation nevertheless there is only a temperature rise of 1° or 2° per min (Fig. 6).

In the animal experiments only in 2 cases a small hematoma developed at the tip of the vibrating sonotrode. In all other cases there was no macroscopic change. Histology demonstrated urothelial damage and small submucosal bleeding and edema, but these changes had reversed without scar formation by 2 weeks. Only in 1 ureter a stricture developed. The protocol in this animal experiment showed the suspicion of mechanical perforation when the ultrasound probe was introduced. A second ureter was obstructed by a ureteral calculus well above the point where the tip of the sonotrode had been. In all other ureters no stricture formation occurred and an IVP (Fig. 7) and retrograde filling (Fig. 8) showed a delicate upper tract.

Discussion

Stone fragmentation inside the ureter by electrohydraulic lithotripsy carries the risk of ureteral perforation if the spark discharge occurs within less than 3 mm away from the ureteral wall.

These results of our rabbit experiments were confirmed in similiar simultaneous experiments in dogs (Webb and Fitzpatrick 1985) and also observed when the electrohydraulic probe was used in patient treatment (Goodfriend 1984). This energy transducer for stone destruction can therefore only be used under good vision during ureteroscopy in a wide ureter where there is sufficient distance between the tip of probe and the ureteral wall. The sonotrode is less destructive for the ureter, but carries the risk of mechanical perforation by the rigid metallic rod and will lead to a significant temperature rise when it is not used correctly. With irrigation as used under clinical conditions nevertheless the temperature elevation is negligible. Similiar results were obtained when the sonotrode was applied to animal bladders (Howards et al. 1974; Bichler et al. 1984; Marberger et al. 1985) and also the use of the ultrasound

probe in the canine ureter produced no permanent damage (Webb and Fitzpatrick 1985). The ultrasound probe for stone destruction is therefore safe and atraumatic for use under ureteroscopic vision. Both methods, the electrohydraulic lithotripsy and the ultrasound lithotripsy, cannot be used under fluoroscopy as may become possible by the laser-induced techniques for stone destruction that are being developed.

References

Bichler KH, Erdmann D, Schmitz-Moormann P, Halim S (1984) Operatives Ureterorenoskop für Ultraschallanwendung und Steinextraktion. Urologe (Ausg A) 23:99–104

Goodfriend R (1984) Ultrasonic and electrohydraulic lithotripsy of ureteral calculi. Urology 23:5–8

Howards SS, Merill E, Harris S, Cohn J (1974) Ultrasonic lithotripsy: Laboratory evaluations. Invest Urol 11:273–277

Marberger M, Stackl W, Hruby W, Wurster H, Schnedl W (1985) Ultrasonic lithotripsy and soft tissue. World J Urol 3:27–32

Tidd MJ, Webster J, Cameron Wright H, Harrison JR (1976) Mode of action of a surgical electronic lithoclast – high speed pressure, cinematographic and Schlieren recordings following an ultrashort underwater electronic discharge. Biomedical Engineering 11:5–24

Webb DR, Fitzpatrick JM (1985) Experimental ureterolithotripsy. World J Urol 3:33–35

Urolithiasis Following Portacaval Shunt in Rats

P. SCHRAMEK[1], U. ENGELMANN[2], M. GRÜN[3], W. DOSCH[4], and P. GEMMER[2]

Introduction

A reliable technique for a portacaval anastomosis (PCA) in rats was first published by Lee and Fisher 1961. Since then the biological and biochemical consequences have been studied extensively in numerous investigations. The occurrence of a urolithiasis following PCA was first reported by Herz et al. 1972. Disturbances of uric acid metabolism that were caused by the shunt were thought to be responsible. They should lead to an increased production of endogenous uric acid and thus to hyperuricosuria. Investigations that were published since then mainly focused on chemical stone analysis (Bichler et al. 1974; Rasenack et al. 1977; Wallace et al. 1984).

The following study should investigate stone formation in male and female rats (so far mostly male rats had been studied), and for stone analysis scanning electron microscopy (SEM), X-ray diffractometry and X-ray dispersion microprobe analysis should be applied.

Material and Methods

In ketamine general anesthesia 115 Chbb Thom rats and 2 Sprague-Dawley-rats (63 males and 54 females weighing 250–350 g) were operated. Portocaval shunts were

Table 1. Distribution of operated and evaluable animals in treatment and control groups

	Male	Female	
PCA	36[a]/42	25[a]/41	
SOP	11[a]/11	3[a]/3	
St.I.	10[a]/10	10[a]/10	
Total	57[a]/63	38[a]/54	95[a]/117

[a] Available for evaluation
PCA, portacaval anastomosis; *SOP,* sham operated animals; *St.I.,* implantation of a bladder stone

[1]Department of Urology, Allgemeine Poliklinik, Mariannengasse 10, A-1090 Vienna
[2]Department of Urology, Medical School, University Hospital Mainz, D-6500 Mainz
[3]St. Vincenz und Elisabethen Hospital, D-6500 Mainz
[4]Institute of Mineralogy, Johannes Gutenberg University, D-6500 Mainz

Investigative Urology 2
Edited by G. H. Jacobi et al.

done following the technique of Lee and Fisher (1961) either under an operating microscope or with magnifying loups. The vessels were anastomosed end-to-side with interrupted sutures 10/0 or 8/0 Ethilon. Treatment and control groups are shown in Table 1. The pancreaticoduodenal vein was regularly included in the shunt. Control animals underwent a median laparotomy and clamping of the v. cava and portae for about 10′. Twenty rats received an implantation of a sterile stone (quarzit, 6 mm diameter) into the bladder; these animals were not shunted. The rats received a standard diet (Altromin) and tap water ad libitum. They were checked daily and weighed weekly; urine ph was measured repeatedly. The animals were sacrificed at intervals, mean follow up was 49.7 weeks (minimum 3 weeks, maximum 69 weeks).

95 animals (57 males and 38 females) were evaluable. Bladder stones were analyzed using X-ray diffractometry, scanning electronmicroscopy and energy dispersion spectrum (EDS).

Results

At the time of necropsy all animals had a wide open patent anastomosis (Fig. 1). The average weight loss in portacaval shunt groups was 25% at 4 weeks postop. 8–10 weeks postoperatively the rats had regained their preoperative weight, and when harvested they weighed 350 g (males) or 320 g (females) respectively.

29 out of 36 (80.5%) male PCA-rats had developed a urolithiasis (bladder stones: 21/29, kidney stones: 2/29, kidney and bladder stones: 5/25, ureter stones: 1/25) (Figs. 2, 3). The first stone was seen as early as 3 weeks postoperatively. Female shunt rats had a much lower incidence of urolithiasis, only 5/25 rats (20%) had

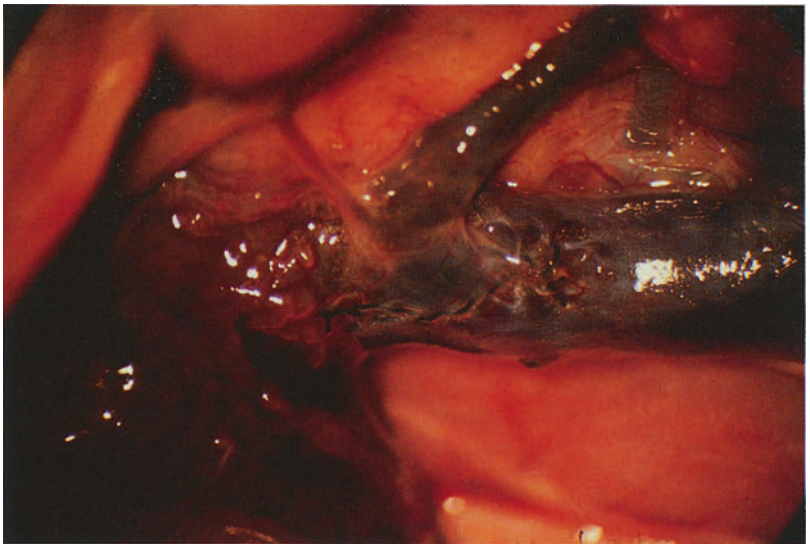

Fig. 1. Patent portacaval anastomosis, the pancreatoduodenal vein is included in the shunt

Figs. 2, 3. Extensive bladder stone formation following PCA 16 weeks postoperatively

Fig. 2a, b

stones when harvested. 3 rats had bladder stones only and 2 animals had kidney stones. Stone analysis was available in 24/29 male rats and classified 9 rats as having struvite stones (Fig. 4a, b), 13 stones were potassium-hydrogen-urate (KHU) stones (Fig. 5a, b), 2 stones were composite stones having about the same percentage of KHU and struvite or calcium phosphate, KHU and struvite respectively. 5 out of 24 stones contained up to 40% calcium phosphate. The stones of 2/5 female PCA rats could be analyzed, the remaining stones were two small for a complete analysis. One rat had a stone consisting of several components (struvite, calcium phosphate, KHU), the other had a struvite stone.

Fig. 3a, b

2 male rats out of 14 sham operated controls (11 males, 3 females) developed bladder stones spontaneously. In both cases these were struvite stones.

In group 3 (St.I.) with 2 exceptions all animals had formed bladder stones in addition to the implanted stones. 2 rats (1 male / 1 female) also had staghorn stones in both kidneys. 11 out of 20 analyses are evaluable: All additionally formed stones were struvite stones, 3 of these had 30% KHU, one had 20% KHU and another one consisted of 60% struvite, 20% KHU and 20% calcium phosphate. Only 2 implanted stones showed very little additionally formed stone material: in one animal the harvested stone showed a layer of KHU (3% of the total stone mass), in the other case it was struvite (10% of the total stone mass).

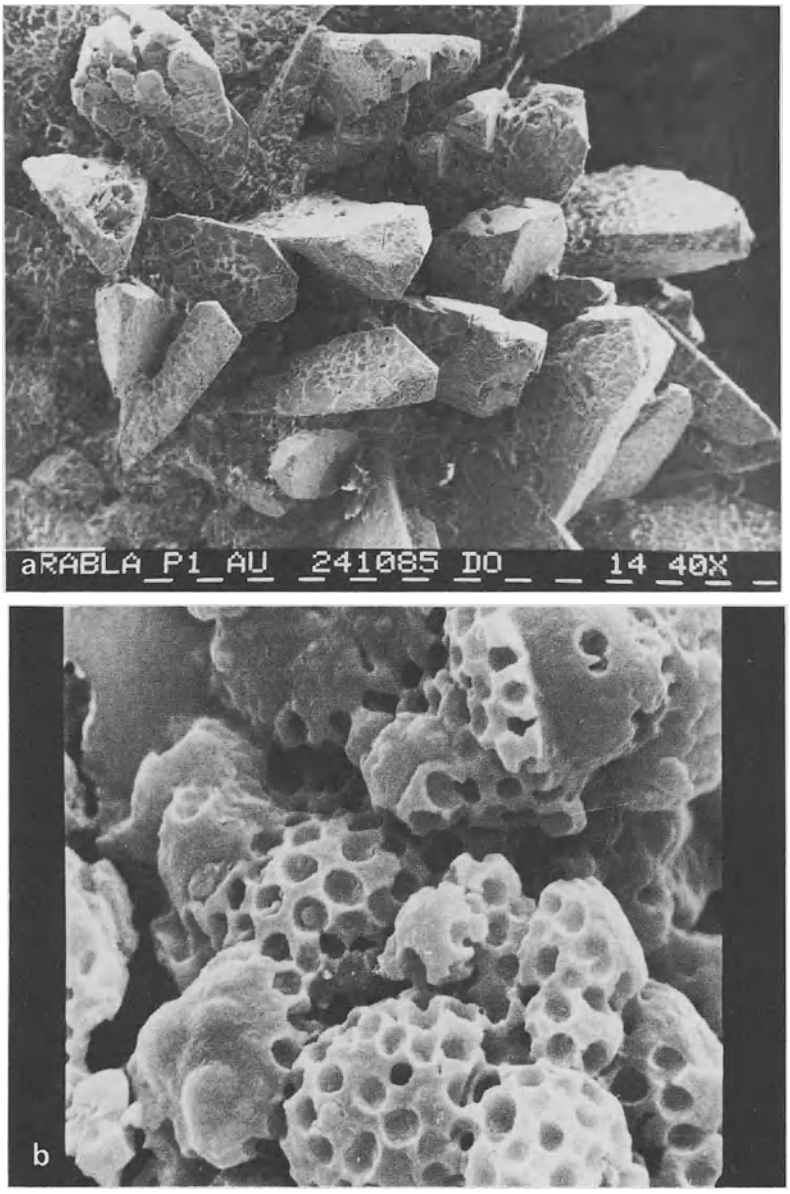

Fig. 4. **a** Slow struvite stone formation with idiomorphic crystals. **b** In comparison rapid struvite stone formation in presence of bacterial infection with bacteriae included in the stone

Discussion

Several investigators have described a urolithiasis following portacaval shunt in rats (Herz et al. 1972; Bichler et al. 1974; Wallace et al. 1984; Linnemann et al. 1986). In most cases stones were described as uric acid stones, one group (Linnemann et al.

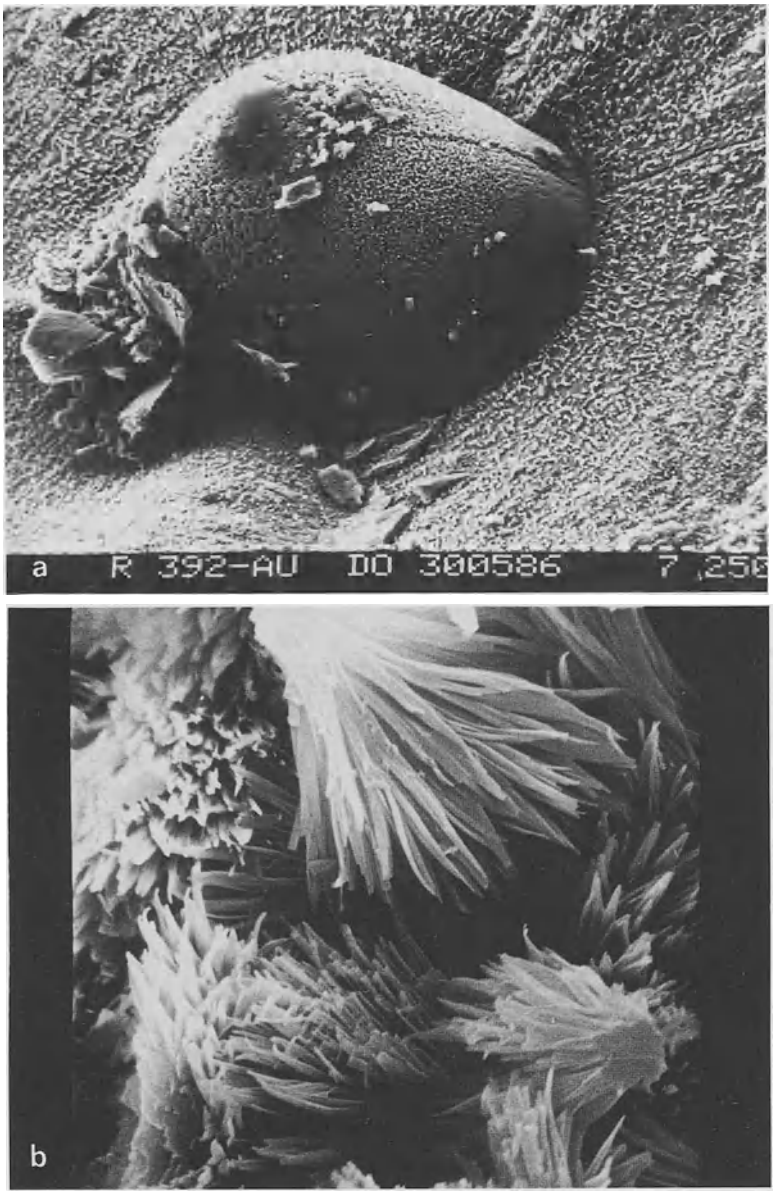

Fig. 5. a Scanning electron microscopy of a KHU bladder stone. **b** In comparison the characteristic appearance of NH_4HU stones

1986) described NH_4HU stones. We could confirm earlier findings (Wallace et al. 1984) that mostly male animals developed stones, however, the results of stone analyses differ considerably from those reported earlier: For the first time also struvite stones following PCA are described which were developed in the absence of bacterial infection (Fig. 4a, b). Slowly growing struvite stones, which are not caused by infec-

tion are for instance known in cats (Sanders and Hesse 1985). Secondly, stones which we initially regarded as NH_4HU-stones had to be reclassified later as KHU stones following the results of EDS. The striking sex difference in stone formation can not be explained sufficiently yet, changes in hormone levels (increase in estrogen and glucagon concentrations) could be responsible and these hypotheses are currently investigated.

References

Bichler KH, Kirchner Ch, Zelder O (1974) Erhöhung des Harnsäurespiegels im Serum und Urin der Ratte nach portokavalem Shunt. In: Vahlensieck W, Gasser G (eds) Harnsteinsymposium Bonn – Wien. Steinkopff, Darmstadt, pp 109–114

Herz R, Sautter V, Bircher J (1972) Fortuitous discovery of urate nephrolithiasis in rats subjected to portacaval anastomosis. Experientia 28:27–28

Lee SH, Fisher B (1961) Portacaval shunt in the rat. Surgery 50:668–672

Linnemann U, Kuch P, Schwille PO (1986) Ammonium-urat-urolithiasis in the rat with portacaval shunt – some aspects of mineral metabolism and urine composition. Urol Res 14:319–322

Rasenack U, Grün M, Liehr H (1977) Morphologische Untersuchungen der extrahepatischen Folgen einer portokavalen End-zu-Seit-Anastomose der Ratte. Z Gastroent 15:457–468

Sanders G, Hesse A (1985) Harnsteine bei Katzen Struvit – Steinbildung ohne Infektion. In: Gasser G, Vahlensieck W (eds) Pathogenese und Klinik der Harnsteine XI. Steinkopff, Darmstadt, pp 326–335

Wallace DMA, Ackermann D, Davis B, Hartmann WH (1984) Uric acid lithiasis and proliferative changes in the rat urinary bladder after portacaval anastomosis. In: Harzmann R, Jacobi GH, Weißbach L (eds) Experimentelle Urologie. Springer, Berlin Heidelberg New York, pp 430–433

IV. Various Innovations in Urological Research

Perfused Human Full-Term Placenta: A New Model for In Vivo Investigation of Aromatase Inhibitors

B. Wagner[1], A. Niemand[2], H. Klein[2], H.-P. Leichtweiss[3], and K.-D. Voigt[2]

Introduction

Interest in aromatase inhibitors is increasing since they are discussed as possible therapeutic agents in the treatment of mammary carcinoma and benign prostatic hyperplasia.

Experimental findings from recent years indicate a possible etiological role for estrogens in human benign prostatic hyperplasia, therefore introducing a new direction for therapy: Biochemical analysis of benign prostatic hyperplasia showed a preferential location of the estrogen receptor in the stromal fraction as well as a stromal nuclear location of estrogens (Krieg et al. 1981; Kozak et al. 1982). Administration of the estrogen precursor androstenedione to dogs led to an enlargement of the prostate histologically similar to benign prostatic hyperplasia and a simultaneous increase in circulating estradiol (Habenicht et al. 1985). Application of the aromatase inhibitor 4-hydroxy-androstenedione antagonized both the histological development of the prostate enlargement as well as the rise in serum estradiol.

However, despite the evidence for estrogen-dependence of development of benign prostatic hyperplasia and the possible therapeutic benefits of aromatase inhibitors, very careful analysis has failed to show aromatase activity in human prostatic tissue (Krieg et al. 1985; Bartsch et al. 1987). Therefore organ-specific prostatic steroid aromatization has so far been excluded as the underlying mechanism of these effects.

First clinical trials in men with the aromatase inhibitor testolactone indicate a therapeutic effect on the size of a preformed benign prostatic hyperplasia (Tunn et al. 1985). However, it has not been proven that these effects were a result of the inhibition of estrogen production. Vigersky postulated testolactone to be an antiandrogenic substance (Vigersky et al. 1983). In addition effects of the inhibitors on other metabolic pathways cannot be excluded in an intact organism.

In order to clarify the mechanism of action of aromatase inhibitors we initiated studies on their influence on in vitro steroid metabolism as well as in a new in vivo model. From our group in vitro investigations were performed to characterize 4 aromatase inhibitors: 19-acidoandrost-4-ene-3,17-dione, 1-methylandrost-1,4-diene-3,17-dione, 4-hydroxyandrost-4-ene-3,17-dione and 17-a-oxa-D-homo-androsta-1,4-diene-3,17-dione (testolactone) (Bartsch et al. 1987).

Obviously they cannot describe the action of the inhibitors under in vivo conditions in intact human tissue. On the other side the above mentioned animal model is neither useful to clarify the mechanism of action. Therefore, the extracorporally perfused placenta was chosen as a model to investigate the action of aromatase in-

[1]Department of Urology, University of Hamburg, Martinistr. 52, D-2000 Hamburg
[2]Department of Clinical Chemistry, University of Hamburg, Martinistr. 52, D-2000 Hamburg
[3]Department of Exp. Medicine, University of Hamburg, Martinistr. 52, D-2000 Hamburg

Investigative Urology 2
Edited by G. H. Jacobi et al.

hibitors under physiological conditions in intact functional human tissue without the complex pharmacodynamic problems encountered in the complete organism. Because of its easy accessibility and high aromatase activity the placenta readily lends itself to these studies. Excellent perfusion is possible for anatomical reasons.

In the present study the following questions have been investigated in our model:

1. Efficiency of the inhibitors in vivo?
2. Concentrations necessary for inhibitory effects?
3. Reversibility of the inhibition in vivo?
4. Interactions of the inhibitors with other pathways of steroid metabolism?

Material and Methods

Materials

The aromatase inhibitors 1-methylandrost-1,4-diene-3,17-dione, 4-hydroxyandrost-4-ene-3,17-dione and testolactone were gifts from Schering, Berlin. 19-acido-androst-4-ene-3,17-dione was donated by Organon, Os, Holland. Tritiated androstenedione was obtained from Amersham. Non-labeled steroids, solutions and Kieselgel were purchased by Merck, Darmstadt. Dextran T 40 and Sephadex LH 20 were obtained from Pharmacia, Uppsala, Sweden, bovine albumin from Behring, Marburg, and Medium 199 TC from Difco, Detroit, USA. The liquid scintillation fluid (Biofluor) was purchased from NEN, Boston, USA.

The 14 placentas were obtained following 6 cesarean sections and 8 normal deliveries in the clinic of gynecology and obstetrics, University of Hamburg. Only macroscopically intact placentas were used.

Perfusion-Technique

The extracorporal perfusion of the placenta was performed according to the technique described by Schneider et al. as modified by Carstensen et al. (Schneider et al. 1972; Carstensen et al. 1977). From many experimental systems described in the literature we chose for our perfusion the single cotyledo in an open system because of the easy access to end-arteries and optimal control of substrate and inhibitor concentrations without the complications introduced by recirculation. Similar to the physiological situation of separated fetal and maternal sides we have 2 independent perfusion systems.

One cotyledo from each placenta was connected to the perfusion system through canulation of fetal artery and vein using PVC-catheters within 10 to 15 min post partem. Following initiation of perfusion the placenta was placed in the perfusion chamber. The perfusion of the maternal side was then immediately established by insertion of 5 PVC-catheters into the intervillous space in the vicinity of the spiral arteries. The veinous drainage from the maternal side was through openings in the basal membrane. Immediately after canulation maternal perfusion was started. However, because exact canulation is possible only from the fetal side, the administration of substrate and inhibitors was solely from this side.

The medium consisted of TC medium 199, pH 7.4, 3 g/l bovine albumin and 20 g/l Dextran 40 and was equilibrated with 95% oxygen and 5% CO_2. The perfusion rates were 3.2 ml/min on the fetal side and 6.4 ml/min on the maternal side. Both the

perfusate and the perfusion chamber were maintained at 37°C. 15 minutes following the canulation of the fetal side 0.2 ng/ml ^{3}H-androstenedione and 1.2 ng/ml non-labeled androstenedione were added.

For the determination of the metabolites, veinous perfusion solution was collected at one minute intervals simultaneously on the fetal and maternal sides. In order to measure the steroids transferred to the maternal side, simultaneous collection of the perfusate is required. Incorrect conclusions resulting from different transitions on the maternal side are thereby excluded. Additionally the exclusive use of full-term placentas guaranteed maximal aromatase activity (Walsh et al. 1981; Gurpide et al. 1982; Tulchinsky 1973; Cedard 1971).

Steroid-Determination

Steroids were isolated from the perfusate aliquots by ethyl acetate extraction. Separation of estrogens and androgens was accomplished following evaporation of the ethyl acetate by addition of 2 ml NaOH, extraction of the androgens with iso-octane, addition 2 ml 1*N* HCl to the water-phase and extraction of the remaining estrogens with ethyl acetate. Further separation and quantification of estrone and estradiol were performed using Sephadex LH 20 column-chromatography. Androgens were quantified using thinlayer chromatography as described previously (Krieg et al. 1981).

Results

Viability of the Perfused Placenta

The percentage of estrogens (estrone and estradiol) from all labeled steroids recovered from the placenta reaches a plateau after 15 to 20 min (Fig. 1a) which persists at least 180 min during perfusion with a constant and approximately physiological androstenedione concentration of 1.2 ng/ml (Fig. 1b). After reaching this plateau possible influences of endogenous steroids from placental tissue on the aromatization rates and sequestration of the infused steroids obviously are constant. So viability of the placenta for at least 180 min is proven under conditions of our model. Therefore, the aromatase system could be investigated without artefacts within this time interval. In the plateau region between 80% and 90% of the radioactivity is recovered from the venous side. From this 60% to 70% are composed of estrone and estradiol and the remaining 30% to 40% consist of androstenedione and testosterone. Therefore, androstenedione in the isolated human placenta appears to be almost exclusively metabolized by aromatase and 17β-hydroxysteroiddehydrogenase (Fig. 2).

Aromatase Inhibition and Reversibility

In preliminary experiments the minimal concentration of inhibitors required to obtain a visible reduction of aromatization were determined by addition of increasing amounts of inhibitor to be perfusate. The lowest concentration that was effective in the perfused placenta was approximately 17–45 × higher than the K_i-value as determined in vitro (Table 1).

Additionally, the concentration of substrate (androstenedione, 1.2 ng/ml) used in all inhibition experiments was proven to be far below the saturation limit of the

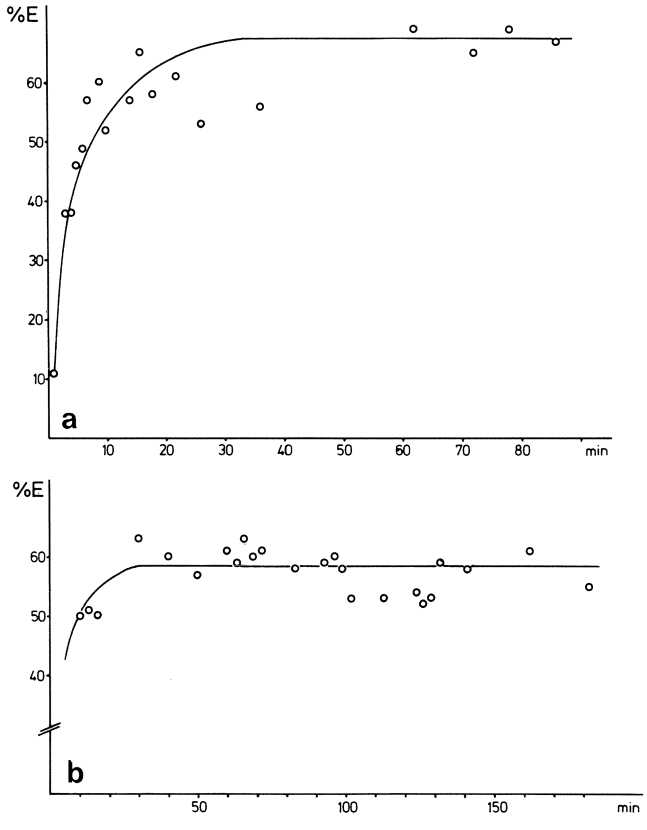

Fig. 1a, b. Aromatization of androstenedione in perfused human placenta. **a** Aromatization rate reaches a plateau 20 min after substrate was administered. **b** The plateau persists at least 180 min

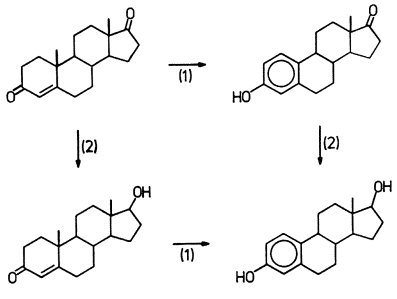

Fig. 2. Conversion of androstenedione to testosterone, estrone and estradiol by aromatase *(1)* and 17β-hydroxysteroiddehydrogenase *(2)*

Table 1. Aromatase inhibitors in perfused human placenta

Inhibitor	K_i	P_i	P_i/K_i
19-acidoandrost-4-ene-3,17-dione	7,5 nmol/l	410 nmol/l	55
1-methylandrost-1,4-diene-3,17-dione	15,0 nmol/l	1340 nmol/l	89
4-hydroxyandrost-4-ene-3,17-dione	37,0 nmol/l	3800 nmol/l	103
Testolactone	3700,0 nmol/l	680000 nmol/l	184

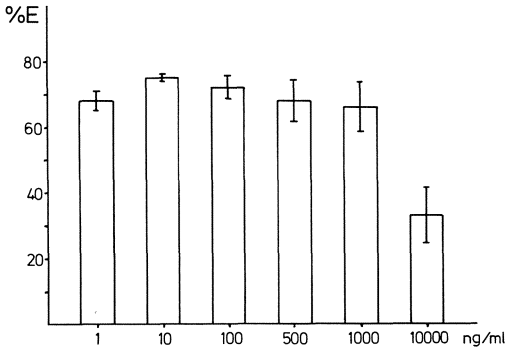

Fig. 3. Saturation of the aromatase system in vivo. Decrease of percentage of estrogens converted from androstenedione after addition of more than 1000 ng/ml androstenedione to the perfusate

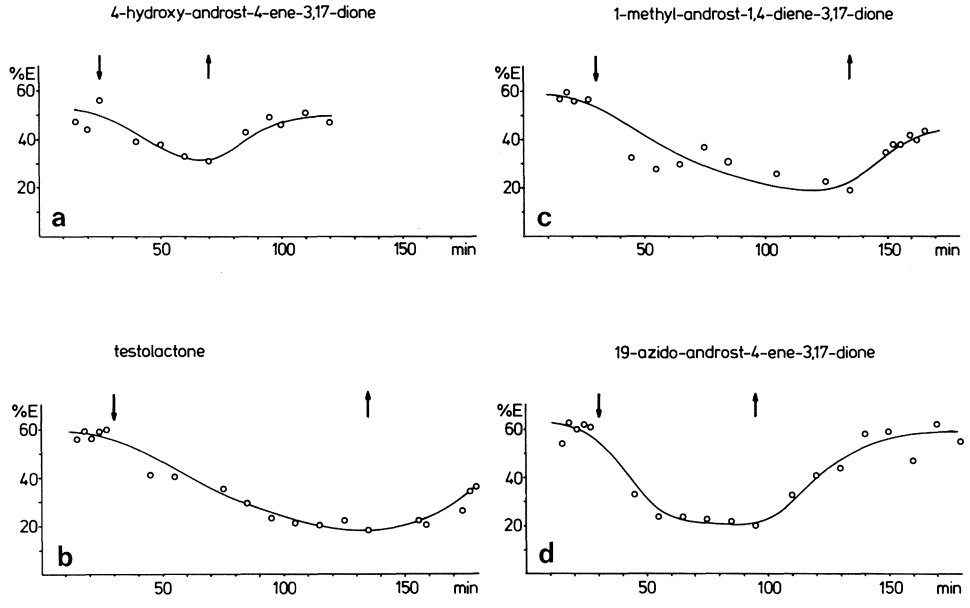

Fig. 4a–d. Inhibition and reversibility of the aromatase in perfused human placenta by the 4 inhibitors (**a–d**) investigated

aromatase system in our model. A decrease of the percentage of estrogens converted from the androstenedione administered was observed when more than 1000 ng/ml androstenedione were added to the perfusion medium (Fig. 3). In later experiments designed to establish the reversibility of the aromatase inhibition, the lowest effective concentration of inhibitor was used.

Following the first 25 min of perfusion the inhibitors were applied for a time period of 30 to 100 min during which there was a visible reduction in the aromatization rate followed by a recovery period after removal of the inhibitor. Under these conditions all 4 inhibitors investigated induced marked reduction of aromatization. After removal of the inhibitor from the perfusion system a return to baseline was seen in all cases (Figs. 4a–d).

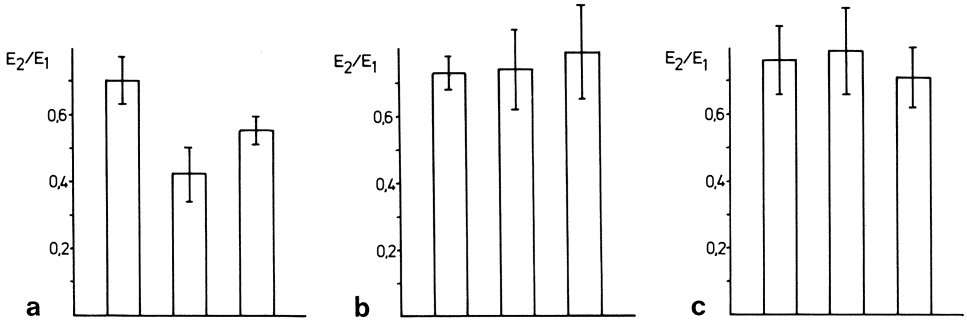

Fig. 5a–c. Estradiol/estrone ratio in the perfusate before, during and after administration of inhibitors. **a** 4-hydroxyandrostenedione, **b** testolactone, **c** without inhibitor

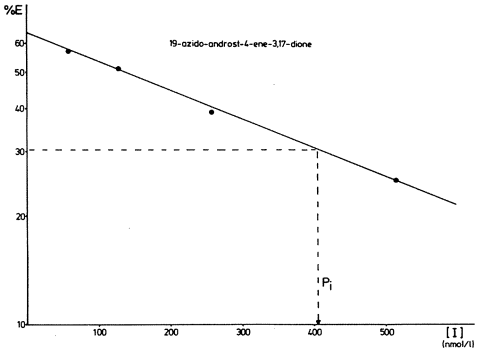

Fig. 6. Example for the evaluation of the inhibition potency P_i *(I)* = inhibitor concentration

Estradiol/Estrone Ratio

The distribution of estrogens in estrone and estradiol fractions is shown in Fig. 5. In the absence of inhibitors the percentage of estrone and estradiol in the placenta was constant over the entire perfusion time (Fig. 5c). Following addition of testolactone (Fig. 5b), 1-methyl-androstenedione and 19-acido-androstenedione, both estrogens were similarly reduced, the ratio of estradiol to estrone was not changed. Under the influence of 4-hydroxy-androstenedione the proportionality was lost since estradiol production was reduced to a greater extent than that of estrone (Fig. 5a).

In Vivo Inhibition Potency

Estimation of the reduction of aromatization with increasing inhibitor concentrations leads to the inhibition potency P_i: The concentration of inhibitor halving the inhibitor free aromatization rate in our model (Fig. 6). The P_i-values are listed in Table 1 together with in vitro K_i-values as determined from our group (Bartsch et al. 1987).

Discussion

All substances investigated were effective inhibitors of the human aromatase system in vivo as well as in vitro (Bartsch et al. 1987; Covey and Hood 1982a; Covey and Hood 1982b; Henderson et al. 1986). Effective intravasal concentrations differed widely between the four inhibitors as can be seen from the different P_i-values (Table 1). The relative inhibition potency P_i was defined in order to compare different inhibitors in vivo. In contrast to in vitro enzyme assays in the perfused placenta, aromatization is not measured under conditions of substrate saturation but instead using physiological androstenedione concentration. Therefore, all observed inhibitory effects allow conclusion to be drawn about local intravasal concentrations necessary for therapy.

The order of the P_i-values is the same as for K_i-values but with increasing K_i, P_i-values increase unproportionally; this means P_i/K_i ratio increases. Therefore, we may expect that low in vitro K_i gives us a hint for even better in vivo effectiveness of the aromatase inhibitor. It remains unclear if this unproportional effectiveness of the substance is a result of higher affinity to the intracellular mitochondrial aromatase system under physiological conditions or if it is resulting from different uptake into the cells.

Anyway, under in vivo conditions the effective intravasal concentration for the inhibitors was 17 to 45 × higher than under in vitro conditions. The range of inhibitors according to their effectiveness does not change in vivo compared to in vitro results. 19-acido-androstenedione is the strongest inhibitor, testolactone is the weakest one.

In our perfusion model all inhibitors showed biological reversibility. In all cases aromatase activity increased back to baseline within 30 minutes after removal of the inhibitor from the perfusate. This observation leads to the conclusion that continuous reduction of steroid aromatization can only be performed by repetitive administration of inhibitors.

In our model the estradiol/estrone ratio was significantly changed under the influence of 4-hydroxy-androstenedione only. Therefore, the production of estradiol, the most potent physiological estrogen, is reduced along 2 different pathways: inhibition of the aromatase and of the 17β-hydroxysteroiddehydrogenase. This enzyme converts androstenedione to testosterone and estrone to estradiol.

Our group proved the potency of 4-hydroxy-androstenedione and testolactone to inhibit both, aromatase and 17β-hydroxysteroiddehydrogenase in vitro. Testolactone is a weak aromatase inhibitor compared to 4-hydroxy-androstenedione. The inhibition of the 17β-hydroxysteroiddehydrogenase was tested in benign hyperplastic prostate tissue, where no aromatase activity was found. Possibly the aromatase inhibition by testolactone in our in vivo model was not strong enough to produce a visible changement of estradiol/estrone ratio owing to the extremely high aromatase activity in the placenta. This does not exclude, that the therapeutical benefit of this substance might be a result of local 17β-hydroxysteroiddehydrogenase inhibition in the prostate as well as of systemic aromatase inhibition and antiandrogenic effects of testolactone according to Vigersky (Vigersky et al. 1982).

Since 4-hydroxyandrostenedione is a very potent aromatase inhibitor which additionally inhibits the 17β-hydroxysteroiddehydrogenase it seems to be the most

promising substance to be used as a therapeutic agent for the treatment of benign prostatic hyperplasia in man.

References

Bartsch W, Klein H, Stürenburg HJ, Voigt KD (1987) Metabolism of androgens in human benign prostatic hyperplasia: Aromatase and its inhibition. J Steroid Biochem

Carstensen M, Leichtweiss HP, Molsen G, Schröder H (1977) Evidence for a specific transport of D-Hexoses across the human term placenta in vitro. Z Gynäkol 222:187–196

Cedard L (1971) Placental perfusion in vitro. 4th Karolinska Symposium on Research Methods in Reproductive Endocrinology, pp 331–340

Covey DF, Hood WF (1982a) Aromatase enzyme catalysis involved in potent inhibition of estrogen biosynthesis caused by 4-acetoxy- and 4-hydroxy-4-androstene-3,17-dione. Molecular Pharmacology 21:173–180

Covey DF, Hood WF (1982b) A new hypothesis based on suicide substrate inhibitor studies for the mechanism of action of aromatase. Cancer Res 42:3327–3333

Gurpide E, Marks C, de Ziegler D, Berk PD, Brandes JM (1982) Asymmetric release of estrone and estradiol derived from labeled precursors in perfused human placentas. Am J Obstet Gynecol 144:551–555

Habenicht UF, Schwarz K, Schweikert HU, El Etreby MF (1985) Development of a test model to investigate the influence of aromatase inhibitors on benign prostatic hyperplasia (abstr). Acta Endocrinol 108:152

Henderson D, Norbisrath G, Kerb U (1986) 1-methyl-1,4-androstadiene-3,17-dione (SW 489): Characterization of an irreversible inhibitor of estrogen biosynthesis. J Steroid Biochem 24: 303–306

Kozak I, Bartsch W, Krieg M, Voigt KD (1982) Nuclei of stroma: site of highest estrogen concentration in human benign prostatic hyperplasia. Prostate 3:433–438

Krieg M, Klötzl G, Kaufmann J, Voigt KD (1981) Stroma of human benign prostatic hyperplasia: preferential tissue for androgen metabolism and estrogen binding. Acta Endocrinol 96:422–432

Krieg M, Schlenker A, Voigt KD (1985) Inhibition of androgen metabolism, stroma and epithelium of the human benign prostatic hyperplasia by progesterone, estrone and estradiol. Prostate 6: 233–240

Schneider H, Panigel M, Dancis J (1972) Transfer across the perfused human placenta of antipyrine, sodium and leucine. Am J Obstet Gynecol 114:822–828

Tulchinsky D (1973) Placental secretion of unconjugated estrone, estradiol and estriol into the maternal and the fetal circulation. JCE & M 36:1079–1087

Tunn UW, Schweikert HU (1985) Conservative treatment of BPH-Clinical and experimental results. In: Matouschek E (ed) Endocrinology. Steinbrück, Baden-Baden

Vigersky RA, Mozingo D, Eil C, Purohit V, Briton J (1982) The antiandrogenic effects of testolactone (Teslac) in vivo in rats and rat prostate cytosol. Endocrinology 110:214–219

Walsh SW, McCarthy MS (1981) Selective placental secretion of estrogens into fetal and maternal circulations. Endocrinology 109:2152–2159

Comparison of MR-Sections and Anatomical Examinations of the Kidney

H. G. Zilch[1], T. Auberger[1], F. Köhler[2], P. Posel[3], and F. W. Baumgartl[1]

Introduction

Magnetic Resonance (MR) is a new method for diagnostic imaging of the kidney. Without any radiation-exposure multidimensional imaging with adequate resolution becomes possible. To evaluate the possibilities and the quality of renal MR-examinations comparison with anatomical sections have been performed.

Material and Methods

A total of 32 normal and pathological kidney-specimens has been examined by the use of a superconducting magnet (1.0 Tesla). The section thickness was 5 to 10 mm. All images were obtained with short T_1 and long T_2. Also special sequences have been adopted. The anatomical-macroscopic sections were performed in correspondence to the MR-slices.

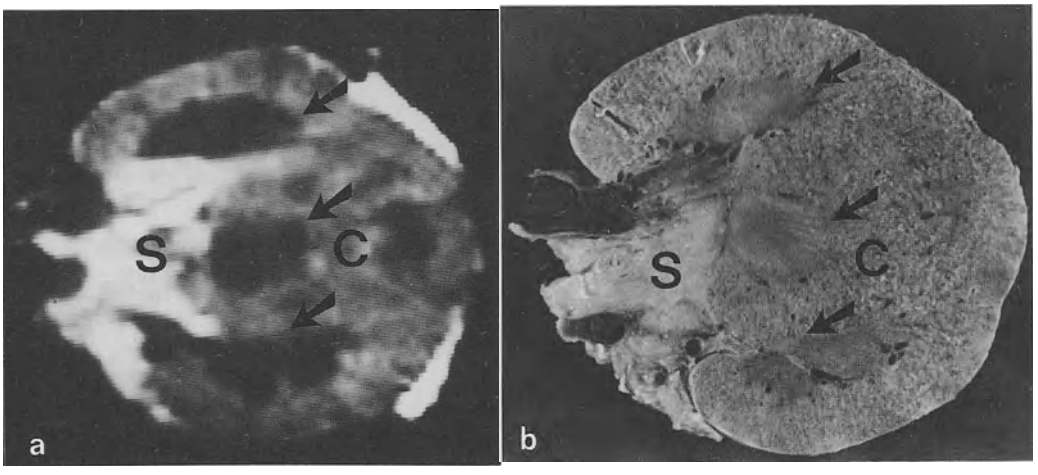

Fig. 1. a MR-section (axial plane, TR 0.5 s, TE 30 ms). **b** Corresponding anatomical section. Differentiation of the cortex *(c)* and medulla (➨); *s,* sinus

[1] Department of Radiology, Municipal Hospital Passau, Bischof-Piligrim-Str. 1, D-8390 Passau
[2] Department of Pathology, Municipal Hospital Passau, Bischof-Piligrim-Str. 1, D-8390 Passau
[3] Department of Anatomy, University of Munich, D-8000 München

Investigative Urology 2
Edited by G. H. Jacobi et al.

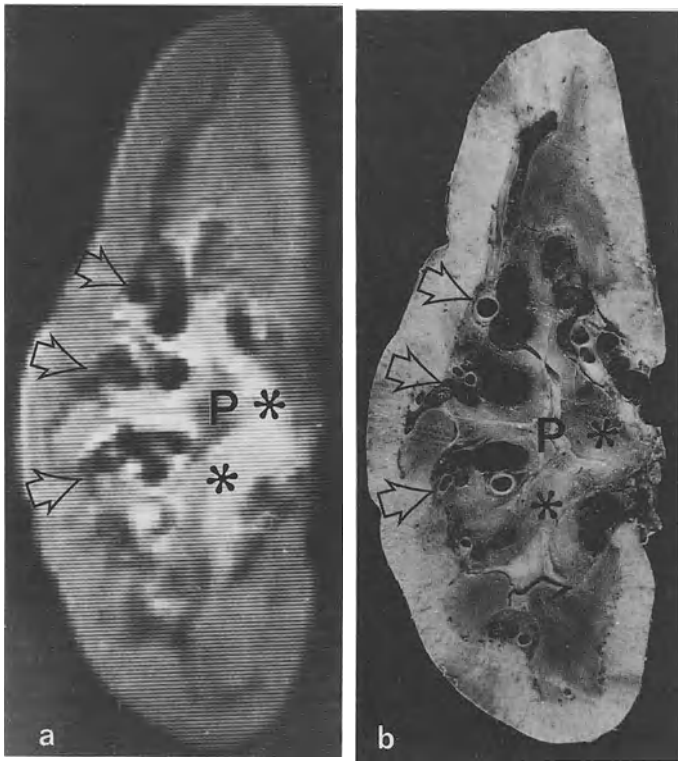

Fig. 2. a MR-section (coronal plane, TI 400 ms, TR 1.5 s, TE 30 ms). **b** Corresponding anatomical section. Differentiation of the sinus pelvocalyceal *(p)* system, adipose tissue (✻), vessels (⇨)

Results

In analogy of the macroscopical renal structure MR-images allow to distinguish the parenchyma and the sinus. Within the parenchyma one can separate the cortex and the medulla. The cortex extends toward the pelvis with the columnae renales ("columnae Bertini"). The medulla comprises 6–20 pyramids which show a signal pattern that in comparison to the columnae demonstrates lower intensity (Fig. 1).

In analogy of the anatomical sections the pyramids can present variable forms on the MR-images. The sinus of the kidneys can also be divided into different compartments (Fig. 2). The calices and vessels are structures with poor signals, whereas the fat on the sinus has a high signal intensity.

The examined hypernephromas ($n = 8$) could be precisely differentiated from the normal renal tissue. By selection of different acquisition-parameters one can also separate the vital tumor-tissue from necrotic or hemorrhagic areas (Fig. 3).

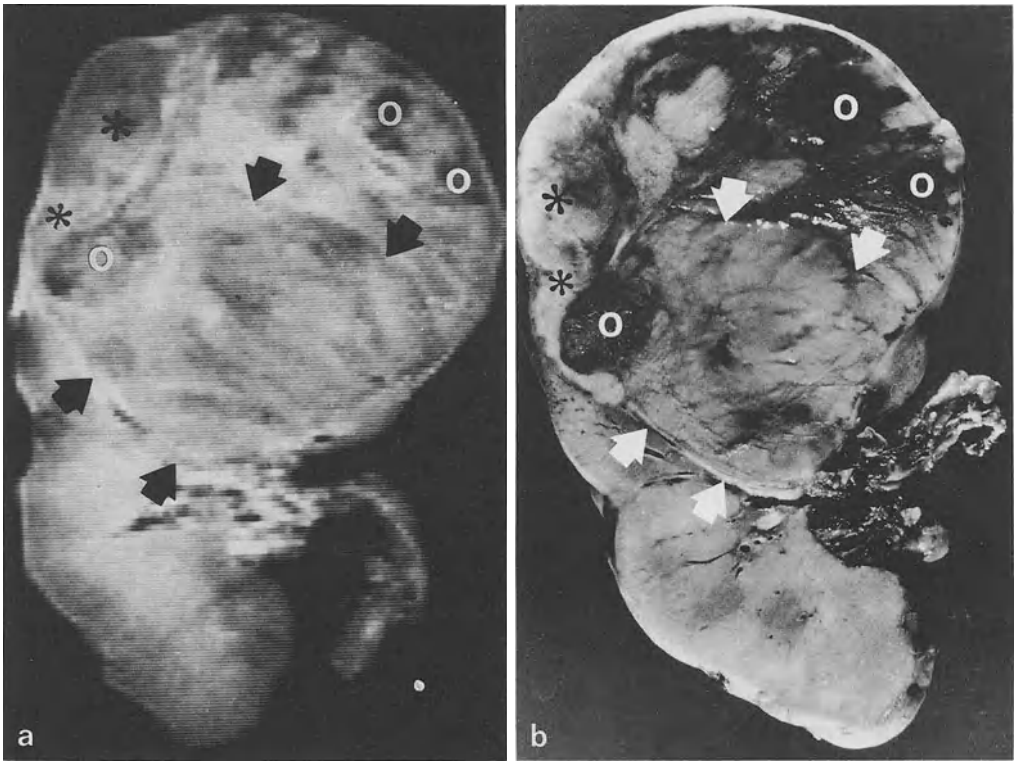

Fig. 3. a MR-section (coronal plane, TR 2.0 s, TE 100 ms). **b** Corresponding anatomical section. Hypernephroma with vital tumor-tissue (✻), necrotic (➨), and hemorrhagic areas (○)

Discussion

Comparisons of MR-sections of the kidneys with the corresponding anatomical sections have only been performed by a few groups (Zilch and Posel 1986). The great advantage of these studies is given by the possibility to precisely correlate the single structures seen on the images to the anatomical findings. The latter are only limited by vascular and physiochemical phenomenas which can occur on the specimen and have to be taken into consideration. Generally, the MR-images do not present fundamental differences in comparison to the MR-images in vivo. In accordance with Hricak and Moon (1983), Fiegler et al. (1984) and Ramm et al. (1986), the basic renal structural composition can be adequately demonstrated. By improved acquisition techniques one can even resolve details of the single structures (Zilch 1986; Zilch et al. 1986).

In fact, within the seen hypernephromas it was possible to separate necrotic and hemorrhagic areas from the still vital tumor-tissue. The future progress of MR-imaging will probably permit a detailed differentiation of renal tumors in patients.

References

Fiegler W, Felix R, Nagel R, Schörner W, Claussen C (1984) Die Kernspintomographie bei raumfordernden Nierenprozessen. Fortschr Röntgenstr 141:155–159

Hricak H, Moon KL (1983) Kidneys and adrenal glands. In: Margulis AR, Higgins CB, Crooks LE (eds) Clinical magnetic resonance imaging. Radiology Research and Education Foundation, San Francisco

Ramm B, Semmler W, Laniado M (1986) Einführung in die MR-Tomographie. Enke, Stuttgart

Zilch HG (1986) Renale Feinstrukturen im MR. Röntgenprax 39:378–380

Zilch HG, Posel P (1986) Magnetresonanztomographie von Nieren. Vergleich mit dem anatomischen Korrelat. Fortschr Röntgenstr 145/3:250–256

Zilch HG, Kett H, Baumgartl FW, Held P, Reisnecker E (1986) Renale Kernspintomographie – Fortschritte durch optimierte Untersuchungstechnik. Akt Urol 17:336–338

Analysis of T-Cell Subsets and DNA In-Situ-Hybridization – A New Diagnostic Tool for Virus Infections in Kidney Transplants

P. Hammerer[1], R. Arndt[1], K. Milde[2], Th. Loening[2], and H. Huland[1]

Introduction

The introduction of Cyclosporin A and successful anti-rejection-therapy with ATG or monoclonal antibodies has resulted in increasing organ transplantation rate (Ferguson et al. 1982; Land et al. 1985). The essential problem of transplantation immunology are virus infections under immunosuppression. Castro et al. (Castro 1985) recently described the influence of ATG/ALG-therapy on the CMV-infection which increased from 24% under immunosuppression without ATG to 49% under immunosuppression with ATG/ALG. ⅔ of the patients suffering from primary CMV-infections showed an impaired kidney function.

On the basis of morphological criteria it is not possible at the moment to differentiate between lymphocytic infiltration due to a reaction against the transplanted kidney versus virus infected cells. Frequently the origin of the biopsy causes the pathologist to interpret his findings as rejection. It is important whether these findings lead to a rejection therapy using high dose steroids and/or ATG or to a rescue therapy using specific hyperimmunsera.

The common diagnostic test for virus infections is based on the antibody-dependent immune response against the virus antigen. This seems to be paradox in immunosuppressed patients since primary and secondary immunresponses are depressed. Therefore, the results of serological tests are limited under immunosuppressive conditions. It is absolutely necessary for this reason to develop novel tests for the differentiation between virus infections and rejections.

Our aim was the direct identification of viral DNA in cells of transplanted organs, peripheral blood, and urine by in-situ-hybridization and visualization with indirect immunostaining.

In addition we examined the increase of the CD8 positive suppressor/cytotoxic cells in the peripheral blood caused by infections with lymphotropic viruses HSV, EBV, and CMV.

Material and Methods

Quantitative T-Cell Analysis

Peripheral blood mononuclear cells were separated from heparinized blood using Lymphoprep (Boyum 1968) (Nyegaard & Co, Oslo, Norway). The cells were washed with PBS, resuspended in RPMI-medium containing 10% fetal calf serum and incu-

[1]Universitätskrankenhaus Hamburg-Eppendorf, Urologische Klinik, Martinistr. 52, D-2000 Hamburg 20
[2]Pathologisches Institut, Universität Hamburg, Martinistr. 52, D-2000 Hamburg 20

Investigative Urology 2
Edited by G. H. Jacobi et al.

bated in a petri dish for 90 min at 37°C in order to adhere the macrophages and monocytes. The cell supernatant was washed again and incubated for 30 min at 4°C with antihuman Leu 1, antihuman Leu 2a, or antihuman Leu 3a (Becton Dickinson, Mountain View, USA) directed against the CD5 antigen found on pan T-cells, the CD8 antigen located on T-suppressor cells and the CD4 antigen found on T-helper cells, respectively. The cells were washed twice with cold RPMI-medium and incubated for 30 min at 4°C with a rhodamine conjugated goat-antimouse IgG. The cells were washed twice again and counted by a fluorescence microscope (Zeiss, Oberkochen, FRG).

In-Situ-Hybridization

The procedure was carried out on cytocentrifuged cell smears from peripheral blood, urine, and fine needle aspirations of kidney transplants.

The hybridization was slightly modified according to the procedure of Brigati et al. (1983). After fixation with methanol/acetic acid the cell smears were incubated with ribonnuclease B (Sigma, St. Louis, Mo, USA) for 1 h. The endogenous peroxidase activity was blocked with avidin (Sigma, St. Louis, Mo, USA).

For hybridization the cell smears were covered with 20 µl of the hybridization mixture containing the appropriate biotinylated DNA probe of 2 µg/ml (HSV-probe, CMV-probe, EBV-probe, Ortho, NY, USA), 2 × SSC (SSC = 0.15 *M* NaCl, 0.015 *M* Nacitrat, pH 7.0), 20% (v/v) formamide (Merck, Darmstadt, FRG), 10% (w/v) dextransulphat (Pharmacia, Uppsala, Sweden), 4% herring sperm DNA (Enzo Biochem, NY, USA).

DNA probes and cell smears were denatured by heating in a 90°C water bath and hybridized at 37°C for 1 h. After hybridization the cell smears were washed under nonstringent conditions at 37°C with SSC and 20% formamide, or under stringent conditions at 42°C with SSC and 45% formamide.

The specific DNA-bindings were visualized by sequential immunocytochemical reactions. The cell smears were incubated with a rabbit anti-biotin-antibody (Enzo Biochem, NY, USA). After washing with SSC the cell smears were treated with a second biotinylated anti-rabbit IgG (H + L)-antibody (Vector Burlingame, CA; USA) for 1 h at 37°C. After washing once again avidin-alkaline phosphatase (Jackson, Immunoresearch Lab, Avondale, PA, USA) was added.

The cell smears were washed again and the binding was detected by reaction with 0.3 ng/ml nitrobluetetrazolium (Sigma, St. Louis, Mo, USA) and 0.2 ng/ml 5-Brom-4-Chlor-3-Indolylphosphat (Sigma, St. Louis, Mo, USA).

The reaction was stopped with Tris-HCl and for documentation, the cell smears were then photographed.

Virus Serology

Serum antibodies directed against the herpes-simplex-virus-(HSV), cytomegalie-virus- (CMV), and Ebstein-Barr-virus- (EBV) antigens were estimated by the complement fixation test (CFT) and by IgG and IgM specific enzyme-immunoassay. To evaluate EBV-infections the Paul-Bunnell-test and the fluorescent antibody test against the virus capsid-antigen (VCA), the early antigen, and the EBV nuclear antigen were performed.

Primary infections were diagnosed when an initially seronegativ patient seroconverted and developed antibodies.

A reactivated infection required a 2-fold or greater increase in titer in a previously seropositive patient.

Table 1. Case 1, pat. Lew

	Relative %		Absolute c/nl	
	Pat.	Normal	Pat.	Normal
CD5 pos. T-cells	89	63–67	2.0	1.3–1.5
CD4 pos. T-cells	33	39–53	0.75	0.8–1.0
CD8 pos. T-suppressor cells	64	22–33	1.47	0.5–0.6

Ratio T-helper cells:	T-suppressor cells 0.51 (normal 1.1–3.1)
Immunosuppression:	CyA, Corticosteroide
Virus serology:	HSV-CFT I: 640 positive EIA IgM I: 40 positive
In situ hybridization:	HSV positive, CMV negative, EBV negative

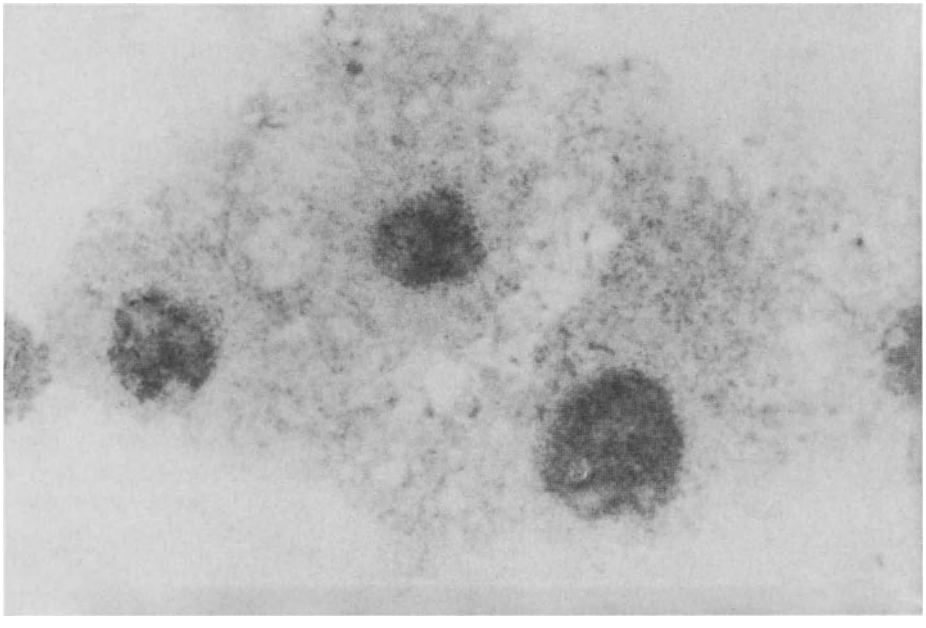

Fig. 1. In-situ-hybridization with HSV-probe. Fine needle aspirate of the transplant kidney, kidney cells, × 400. Staining of the HSV-positive cells

Table 2. Case 2, pat. Pog

	Relative %		Absolute c/nl	
	Pat.	Normal	Pat.	Normal
CD5 pos. T-cells	56	63–67	0.98	1.3–1.5
CD4 pos. T-cells	26	39–53	0.46	0.8–1.0
CD8 pos. T-suppressor cells	42	22–33	0.73	0.5–0.6
Ratio T-helper cells:	T-suppressor cells 0.62 (normal 1.1–3.1)			
Immunosuppression:	CyA, Azathioprine, Corticosteroide			
Virus serology:	CMV-CFT I: 20 positive			
	EIA IgG I: 5120			
	EIA IgM I: 40			
In situ hybridization:	HSV negative, CMV positive, EBV negative			

Table 3. Case 3, pat. En

	Relative %		Absolute c/nl	
	Pat.	Normal	Pat.	Normal
CD5 pos. T-cells	56	63–67	1.7	1.3–1.5
CD4 pos. T-cells	36	39–53	1.1	0.8–1.0
CD8 pos. T-suppressor cells	20	22–33	0.61	0.5–0.6
Ratio T-helper cells:	T-suppressor cells 1.81 (normal 1.1–3.1)			
Immunosuppression:	CyA, Azathioprine, Corticosteroide			
Virus serology:	HSV-CFT 1: 20 positive			
	EIA 0			
In situ hybridization:	HSV positive, CMV negative, EBV negative			

Results

By monitoring the T-lymphocyte subpopulations it is possible to recognize an early proliferation of CD 8 positive cells, which is due to a systemic infection with lymphotrop viruses. The proliferation of the CD 8 positive suppressor is demonstrated in Table 1. Because of this proliferation the amount of the peripheral T-cells was elevated.

By in-situ-hybridization with the corresponding virus-DNA, virus infections in transplanted organs can be visualized. Figure 1 shows the in-situ-hybridization with HSV-probe on kidney cells in the same patient. The virus positive cells are stained dark by the reaction of the substrate with the bound enzym-conjugated antibody. The serology gave a positive result in the HSV-CFT.

Patients immunosuppressed with CyA, azathioprine and steroids show a reduction of the peripheral T-cells and the T-subpopulations. In case of virus infections the proliferation of the CD 8 positive suppressor cells is not as high as compared to patients who are under immunosuppression only with CyA and steroids (Table 2, pa-

tient Pog.). The in-situ-hybridization gave a positive reaction with the CMV-probe on kidney cells. The virus serology showed elevated antibodies against CMV in IgG specific enzyme-immunoassay (same patient).

In patients without a positive virus serology and without a proliferation of T-suppressor cells, the direct identification of virus-infected cells in transplants is the only possibility to diagnose a virus infection (Table 3, pat. En.). This patient was immunosuppressed with CyA, azathioprine and steroids. 3 weeks after kidney transplantation and 1 week after a HSV-stomatitis the patient had a detoriation of the kidney function. The in-situ-hybridization of kidney cells from fine needle aspirates and from frozen sections of kidney biopsies showed HSV-positive kidney cells. At this point no antibody response against the virus nor a T-suppressor cell proliferation was seen.

Discussion

In contrast to the immunosuppression with steroids or azathioprine cyclosporin A acts selectivly on T helper cells by inhibition of T cell proliferation and T cell activation (Dos Reis and Shivach 1982; Meyawaki et al. 1983). The combination of cyclosporin A, steroids and azathioprine leads to a reduction of the CD4 positive T helper cells and normal CD8 positive T suppressor cells. The consecutive decrease of the ratio T helper cells/T suppressor cells can also be seen in patients with a proliferation of the T suppressor cells. For the differentiation of these 2 variables, a quantitative T cell-analysis is needed.

A quantitative rise of the T suppressor cells is seen in EBV, CMV, and HSV, as well as in other virus infections. Reinherz et al. (Reinherz and Schlossmann 1980) could show that this rise is related to the suppression of the lectin-induced immunglobulin synthesis. The CD8 positive cells might reduce the T cell response for delayed hypersensitivity and the T cell mediated cytolysis (Liew and Russel 1980).

By the immunological monitoring of organ-transplanted patients, the quantitative T cell analysis gives a new possibility for the early diagnosis of virus infections.

Under immunosuppression sometimes no development of virus-specific antibodies nor the proliferation of the T suppressor cells is seen. In such cases, the in situ hybridization is the only possibility to differentiate a virus infection from a rejection. This means that complications due to an intense anti-rejection therapy in case of a non-diagnosed virus infection will be avoided.

References

Boyum A (1968) Separation of leucocytes from blood and bone marrow. Scand J Clin Lab Invest 21:Suppl 97

Brigati DJ et al (1983) Detection of viral genomes in cultured cells and paraffin-embedded tissue sections using biotin-labeled hybridisation probes. Virology 126:32

Castro LA (1985) Zytomegalievirusinfektion nach Nierentransplantationen – die Bedeutung der primären Infektion. Immun Infekt 13:210

Dos Reis GA, Shivach EM (1982) Effect of cyclosporin A on T-cell function in vitro: The mechanisms of suppression of T-cell proliferation depends on the nature of the T-cell stimulus as well as the differentiation state of the responding T-cell. J Immunol 129:2360

Ferguson RM et al (1982) Cyclosporin A in renal transplantation, a prospective trial. Surgery 92:175
Land W et al (1985) Cyclosporin A bei Nierentransplantationen. Internist 26:549
Liew FY, Russel SM (1980) Delayed-type hypersensitivity to influenza virus: induction of antigen specific suppressor T-cells for delayed type hypersensitivity to haemagglutinin during influenza virus infection in mice. J Exp Med 151:799
Meyawaki T et al (1983) Cyclosporin A does not prevent expression of Tac antigen, a probable TCGF receptor molecule, on mitogen-stimulated human T-cells. J Immunol 130:2737
Reinherz EL, Schlossmann SF (1980) The differentiation and function of human T-lymphocytes. Cell 19:821

Partial Alloplastic Ureter Replacement with Polydioxanon and Vicryl Tube Implantations

H. Derouet[1], G. Seitz[3], B. Kopper[1], Th. Gebhardt[1], J. Günter[2], and U. Gonser[1]

Introduction

Since Boari's experiment in 1895 using a glass tube as a ureter replacement, different materials such as artificial prostheses (Ziegler et al. 1972; Dreikorn et al. 1978; Bergmann et al. 1978; Varandy et al. 1982; Homann et al. 1984) or umbilical cord veins (Klippel and Hohenfellner 1979) have been examined for their use as ureter replacements. Only a few good clinical long-term results were reported (Ziegler and Konrad 1981). Because of somewhat disappointing results with the materials used up to now, we first experimentally examined absorbable polydioxanon and polyglactin 910 (vicryl)-tube-implantation for their applicability as segmental ureter replacements.

Material and Methods

2 polydioxanon (PDS) and 3 vicryl tube implantations (kindly supplied by Ethicon GmbH) with a length of 4 cm and a diameter of 2 mm were implanted during nembutal anesthesia (30 mg/kg body weight) in the middle part of the ureter of 5 female beagles weighing between 12 and 15 kg. Additional treatment of the inside surface of the prothesis with an anti-incrustation lacquer was not done (Ziegler et al. 1972). The implantation of the ureter prosthesis was done transperitoneally by a midline laparotomy. After resecting 4 cm of the middle part of the ureter, the defect was covered by a correspondingly long prosthesis (Fig. 1). An end-to-end anastomosis between the end of the prosthesis and the ureter was made using an operating microscope (Zeiss OPMI 7D) and microsurgical instruments with X10 magnification. 8–10 interrupted suture stiches using 8–0 vicryl threads formed an exact adaption of both ends. The ureter was splinted with a self-supporting inner 5-charr ureter catheter which was cystoscopically removed after 8–12 weeks. In 4 cases the uretero-nephrectomy was done after 3 months and in 1 case after 7 months.

Results

I.V. urograms made 14 days postoperatively while the ureter was still splinted, showed in all animals no signs of contrast medium extravasation. Immediately after transurethral removal of the splint, only 2 animals, one with vicryl and one with PDS

[1]Department of Urology, University of Homburg/Saar, D-6650 Homburg/Saar
[2]Department of Urology, District Hospital of Idar-Oberstein, D-6580 Idar-Oberstein
[3]Department of Pathology, University of Homburg/Saar, D-6650 Homburg/Saar

Investigative Urology 2
Edited by G. H. Jacobi et al.

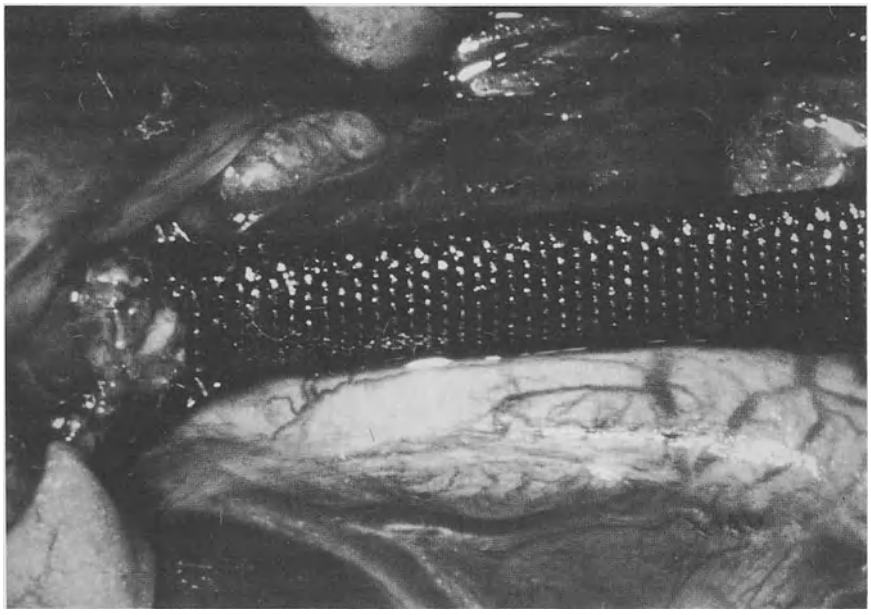

Fig. 1. Vicryl ureter tube prosthesis after implantation

Table 1. Results after implantation of 2 PDS and 3 vicryl tube prostheses with dog ureters

	Duration of ureter prosthesis implantation (months)	Morphology and function
PDS implants ($n = 2$):		
1.	7	Normal calibre ureter with normal urogram
2.	3	Moderate ureter stenosis with obstruction
Vicryl implants ($n = 3$):		
1.	3	Normal calibre ureter with normal urogram
2.	3	Filiform ureter stenosis, hydronephrosis
3.	3	Moderate ureter stenosis with obstruction

prosthesis, showed normal urograms (Fig. 2), while 3 animals showed more or less severe forms of obstruction (Table 1).

The ureter nephrectomic preparations in animals without obstruction showed a macroscopically almost normal ureter wall (Fig. 3) with the preparation of the replaced ureter part being difficult because of periureteral fibrosis. Macroscopic

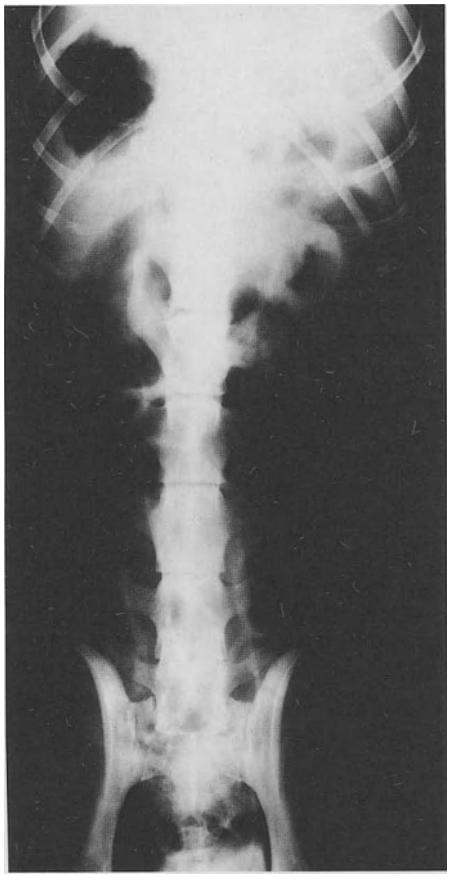

Fig. 2. Normal urogram 10 min after contrast medium was given 4 months after implantation of a PDS tube prosthesis on the right in the middle of the ureter

Fig. 3. Ureter 7 months after prosthesis implantation. The stenosis around the upper end of the prosthesis-ureter-anastomosis showed no impairment of the function (see corresponding urogram of Fig. 2)

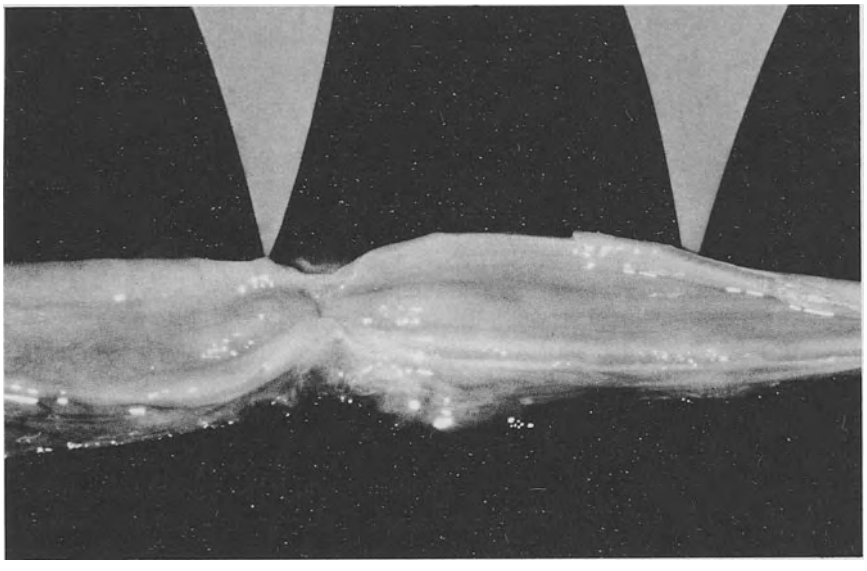

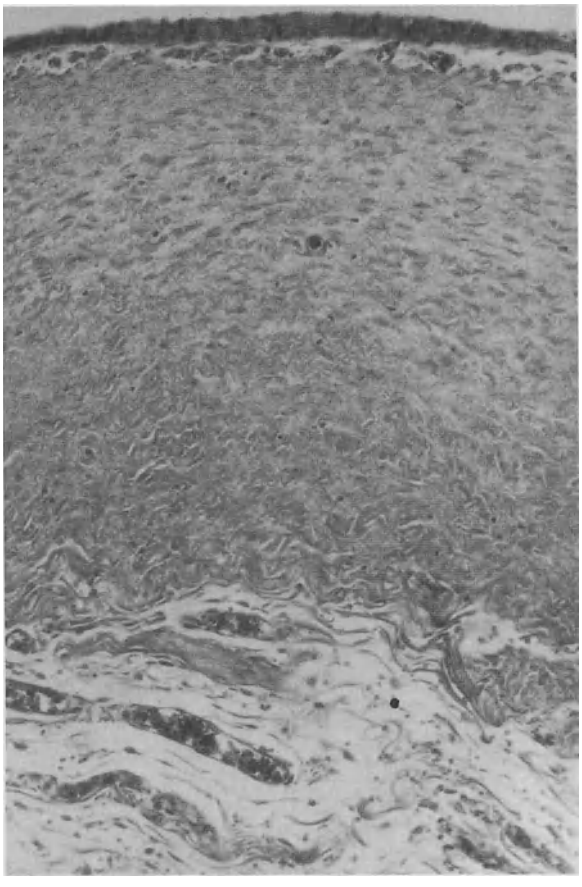

Fig. 4. Histological section through the ureter replacement 3 months after the implantation of vicryl prosthesis. *1,* Epithel; *2,* prosthesis transformed into connective tissue; *3,* bordering soft tissue

Fig. 5. Enlarged section of the newly formed regular urothel in the ureter replacement 3 months after implantation of a vicryl prosthesis. *1,* Urothel

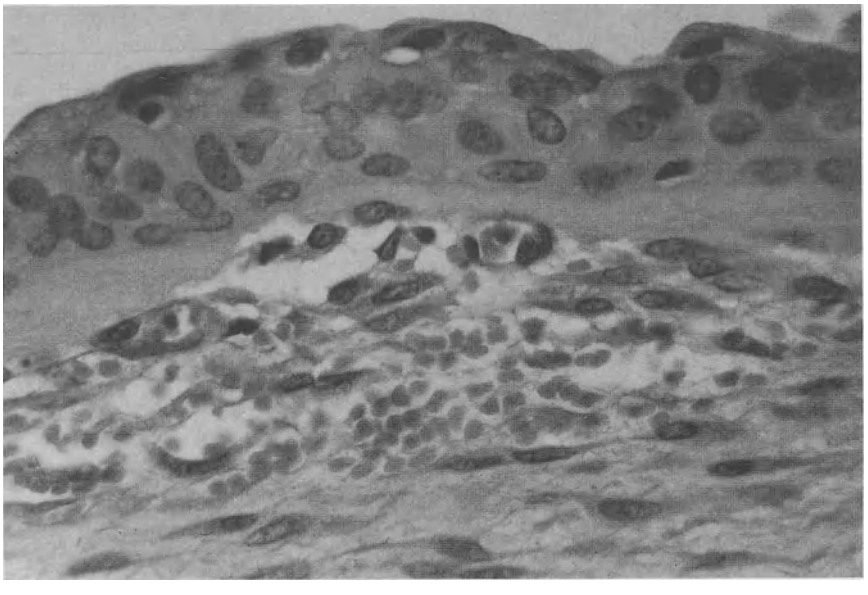

changes could be observed over a much shorter distance than the original length of the prosthesis. The ureter replacement in this area was completely epithelialized with regular statified urethel and imitated the normal histological structure. The layers corresponding to the muscularis propria and the lamina propria consisted only of cell-poor connective tissue (Figs. 4, 5). Smooth muscle cells could not be noted. No inflammatory infiltrates or foreign body reactions worth mentioning were found. Isolated subepithelial clasp-shaped calcifications were observed.

Discussion

Up to now the long-term results of segmental or total ureter replacements with alloplastic material have been to a great extent disappointing (Melchior et al. 1972; Grégoir 1984). Only a few good results with alloplastic replacements of the distal ureter were obtained with silicon ureter prostheses and by neo-implantation of the distal prosthesis end in the bladder (Ziegler, 1972 and 1981), while the segmental ureter replacement with ureter prosthesis ureter anastomosis led to a hydronephrosis of the kidney (Melchior et al. 1972).

The PDS and vicryl prostheses tested are both made of absorbable synthetic material. PDS is an aliphatic polyester which is made by polymerizing the monomer p-dioxanon. Vicryl or polyglactin 910, a copolymer of glycolide and lactide, is catabolized in the same way. Both substances cause extremely little tissue reaction during the absorption period. The duration of this reaction is longer with PDS which has an absorption time of up to 196 days as compared to vicryl with an absorption time of 80 days. Independent of the implantation material used, good results could be achieved in only 2 out of 5 cases with a PDS and a vicryl prosthesis.

By exact adaptation of the prosthesis with the ureter ends using a microsurgical operation technique and by application of a self-supporting inner ureter splint into the ureter lumen, no incidence of local fistulization in the area of the suture could be observed.

In 3 out of 5 cases different degrees of hydronephrosis were noted. This could be the result of stricture developing with stenosis of the ureter lumen, especially in the area of the anastomosis suture. The stasis determined by means of urography immediately after removal of the splint while the ureter lumen was still open, suggests a motility disturbance in the replaced segment (Melchior et al. 1972). This is supported by the fact that the ureter replacements lack the smooth muscularis propria muscles of a normal ureter as opposed to the case of implanted silicon tubes, where Ziegler et al. (1972) described a muscle development in the connective tissue canal around the prosthesis. The few cases of subepithelial calcification observed had no negative influence on the permeability of the ureter, because they did not obstruct the lumen. The inductive effect of the transitional epithelium forming calcification and bony tissue has already been known for some years (Huggins 1931; Friedenstein 1968). It is interesting that the inner prosthesis surface was completely coated with urothel.

In our opinion the PDS and the vicryl prosthesis used are suitable for ureter replacements with artificial material. Further experiments with neo-implantation of the distal prosthesis ends in the bladder are necessary because here the additional demand of a necessary secondary peristalsis in the distal ureter part, as in the seg-

mental ureter replacement, is absent. Furthermore, it seems conceivable that the prosthesis was still not fully absorbed when the splint was removed and that thus the ureter replacement was not yet completely formed when the prosthesis was removed. This is indicated by the fact that pathological anatomical changes were found over a much shorter distance than the length of the original implanted prostheses. Whether the operation results with the development of a complete neo-ureter can be improved by a longer splinting time, remains the subject of further investigation. Here the shorter absorption time speaks in favor of the use of vicryl prostheses.

References

Bartone Francis F et al (1977) Polyglactin 910 suture in urinary tract. Urology IX:5

Bergmann et al (1978) Biodegradable ureteral grafts in dogs. Invest Urol 16/1

Dreikorn K et al (1978) Alloplastic replacement of the canine ureter by expanded Polytetrafluorethylene (Gore-Tex) grafts. Eur Urol 4:379–381

Friedenstein AJ (1968) Induction of bone tissue by transitional epithelium. Clin Orth Rel Res 59: 121–135

Graw M (1985) Künstlicher Harnleiter mit körpereigenem Antrieb. In: Harzmann R et al (eds) Experimentelle Urologie. Springer, Berlin Heidelberg New York

Grégoir W (1984) Uretersubstitution heute. Therapiewoche 34:46

Homann W et al (1984) Long-term results of prothetic ureteral replacement in minipigs. Urol Int 39:95–99

Huggins CB (1931) The formation of bone under the influence of urinary tract. Arch Surg 22:377–408

Jonas D et al (1981) Splintless microsurgical anastomosis of the ureter in the dog. Urol Res 9:271–279

Klippel KF, Hohenfellner R (1979) Umbilical vein as ureteral replacement. Invest Urol 16/6:447–450

Melchior H et al (1972) Die Problematik des segmentalen Ureter-Ersatzes durch alloplastisches Material. Urologe A 11:41–45

Varandy S et al (1982) Ureteral replacement with a new synthetic material Gore-Tex. J Urol 128: 171–175

Ziegler M, Konrad G (1981) Long-term clinical follow-up after implantation of ureteral prosthesis. In: Wagenknecht L et al (eds) Genitourinary reconstruction with prosthesis. Thieme, Stuttgart

Ziegler M et al (1972) Harnleiterersatz durch Silikonschläuche: Experimentelle und erste klinische Erfahrungen. Verhandlungsber Dtsch Ges Urol, pp 204–209

Renal Vasodilatation After Inhibition of Renin or Converting Enzyme in the Marmoset

D. Neisius[1], J. M. Wood[2], K. G. Hofbauer[2], and M. Ziegler[1]

Introduction

In both experimental and clinical studies converting enzyme inhibitors have been reported to induce an increase in renal blood flow, which may be important for the chronic antihypertensive efficacy of these agents. A reduction in the renal vasoconstrictor action of angiotensin II (ANG II) may not be the sole mechanism for this increase in renal blood flow. In addition to blocking the conversion of ANG I to ANG II, converting enzyme (kinase II) inhibitors may block the degradation of bradykinin and other peptides (Johnston 1984; Sweet and Blaine 1984). Moreover, the increased concentrations of bradykinin may stimulate renal prostaglandin synthesis (McGiff et al. 1972). Both bradykinin and prostaglandins have been shown to increase renal blood flow after exogenous administration (Gerber et al. 1978; Lonigro et al. 1978). Thus, the renal haemodynamic effects of converting enzyme inhibitors may be mediated by several mechanisms (Clappison et al. 1981; Wong et al. 1981). It has not been possible to clearly elucidate the relative importance of the reduction of ANG II after converting-enzyme inhibition by the use of ANG II antagonists, since these antagonists also possess partial agonist activity (Arendhorst et al. 1977; Zimmerman 1979). The recently developed inhibitors of renin, which specifically block the formation of ANG I, are useful tools for this purpose (Hofbauer and Wood 1984; 1985).

In this study we compared the renal haemodynamic effects of the converting enzyme inhibitor enalaprilat and 2 different types of renin inhibitors. CGP 29 287 is a synthetic peptide (Wood et al. 1985) and R-3-36-16 is a purified monoclonal antibody (Wood et al. in press). Both compounds are potent and specific inhibitors of primate renin, but differ considerably in their molecular size, mechanism of inhibition, and pharmacokinetic properties. Their effects on blood pressure and plasma renin activity have been characterized in previous experiments in marmosets (Hofbauer et al. 1985; Wood et al. 1985). The renin inhibitors were shown to induce a hypotensive response comparable to the response to a converting enzyme inhibitor. In the present study, the effects of enalaprilat, CGP 29 287, and R-3-36-16 on regional blood flows were evaluated in conscious marmosets after acute treatment with a diuretic. Renal, mesenteric, and hindquarter blood flows were measured with chronically implanted ultrasonic-pulsed Doppler flow probes.

[1] Urologische Universitätsklinik, D-6650 Homburg/Saar
[2] Cardiovascular Research Department, Pharmaceuticals Division, Ciba-Geigy, CH-Basle

Investigative Urology 2
Edited by G. H. Jacobi et al.

Methods

Animals and Surgery

13 marmosets of both sexes, with a mean body weight of 339 ± 9 (SEM) g, were used. Throughout the experimental period, they were maintained on their normal diet. Regional blood flows were measured using miniaturized, ultrasonic-pulsed Doppler flow probes, according to the method developed by Haywood et al. (1981) for rats. Doppler flow probes of 18, 21, and 24 gauge, respectively, were implanted on a renal artery (renal blood flow, RBF), the inferior mesenteric artery (mesenteric blood flow, MBF), and the distal aorta (hindquarter blood flow, HQBF). The marmosets were anaesthetized with alfatesin (Glaxo, 2 ml/kg i.m.), supplemented with diazepam (0.3 mg/kg i.p.) and atropine (0.15 mg/kg s.c.). They were then placedon a warming bed (American Hamilton, Aquamatic k module) maintained at 39°C. Throughout the operation care was taken to maintain sterile conditions. After a midline laparotomy had been performed the intestines were displaced to one side of the abdominal wall and kept moist with saline-soaked gauze covered with parafilm; then connective tissue was carefully removed from a 5–10 mm portion of one renal artery, the inferior mesenteric artery, and the distal aorta. The flow probes were then fixed into position. The wires from the implanted probes were led to a subcutaneous pocket at the base of the tail. Before the abdomen was closed, a dose of benzylpenicillin (300,000 IU/ml, 5 ml/kg i.p.) was given. The marmosets were allowed a period of one week to recover from the abdominal surgery. One day before a flow experiment, catheters (PP-10 with a 602-105 Dow Corning silastic tip) were implanted into a femoral artery and vein under anaesthesia induced by ketamine (25 mg/kg i.m.) supplemented with atropine (0.15 mg/kg s.c.). The arterial catheter was used for the measurement of mean blood pressure (BP) and heart rate (HR) and the collection of blood samples. The venous catheter was used for the injection of substances. The catheters and flow probe wires were exteriorized at the base of the tail and placed under a metal mesh band which was then bound to the tail with a strong tape. This protected the catheters and flow probe wires when the marmosets were returned to their cages. A period of at least 16 h was allowed after implantation of the catheters before a flow experiment was performed.

Experimental Procedure

The evening before an experiment the marmoset received an injection of furosemide (5 mg/kg i.m.) to stimulate renin release. On the day of the experiment the marmosets were placed into restraining tubes and the protective tape and metal band were removed from the tail. The arterial catheter was connected to a pressure transducer (Statham P 23 Db), and the wires from the flow probes to a pulsed Doppler flow meter (545c-3, Bioengineering Department of the University of Iowa). Blood flow, measured as the Doppler shift in kHz, was continuously recorded along with BP and HR (Hellige, Recomed 330-P). An equilibration period of 30 min–60 min was allowed before the administration of a test substance. The marmosets received an intravenous bolus injection (1 ml/kg) of one of the following: the converting enzyme inhibitor enalaprilat (2 mg/kg, $n = 6$), the renin inhibitor CGP 29 287 (1 mg/kg, $n = 6$), the renin-inhibitory monoclonal antibody R-3-36-16 (0.1 mg/kg, $n = 5$), or

vehicle (saline, 0.9%, $n = 7$). These doses of the renin inhibitors have been previously shown to induce complete inhibition of plasma renin activity. Most of the marmosets were used for 2 experiments, with a period of least 2 days between. They always received a different substance in the second experiment, and none of them received the antibody R-3-36-16 as the first substance. In some marmosets it was not possible to get adequate flow signals simultaneously in all 3 vascular beds.

Calculations and Statistics

All values given in the text and figures are means ± SEM. Since the Doppler shift is not a direct measurement of blood flow, data is expressed as percentage changes. The mean of 4 values taken during a 15 min equilibration period before injection of a substance (−15, −10, −5, 0 min) was taken as the baseline 100% value. Percentage changes were calculated as follows:

$$\text{Delta \% at time } x = \frac{\text{baseline value} - \text{value at time } x}{\text{baseline value}} \cdot 100$$

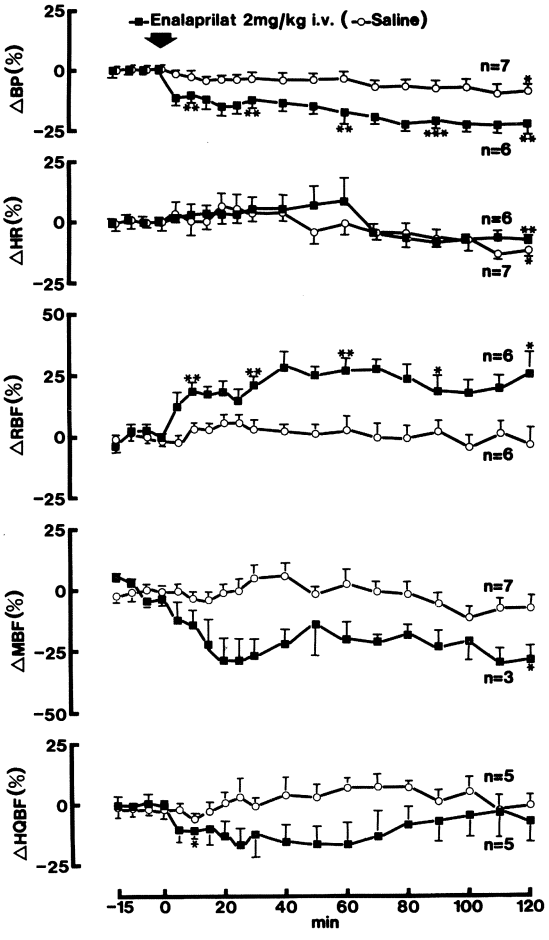

Fig. 1. Changes in blood pressure *(BP)*, heart rate *(HR)*, renal blood flow *(RBF)*, mesenteric blood flow *(MBF)*, and hindquarter blood flow *(HQBF)* after intravenous bolus injection of saline or of the converting enzyme inhibitor enalaprilat. Values are means ± SEM. Initial absolute values of BP and HR were 110 ± 4 mm Hg and 316 ± 21 beats/min for saline and 102 ± 7 mm Hg and 335 ± 16 beats/min for enalaprilat. The significance of changes compared to the initial baseline values is indicated at 10, 30, 60, 90, and 120 min only. *: $P < 0.05$, **: $P < 0.01$

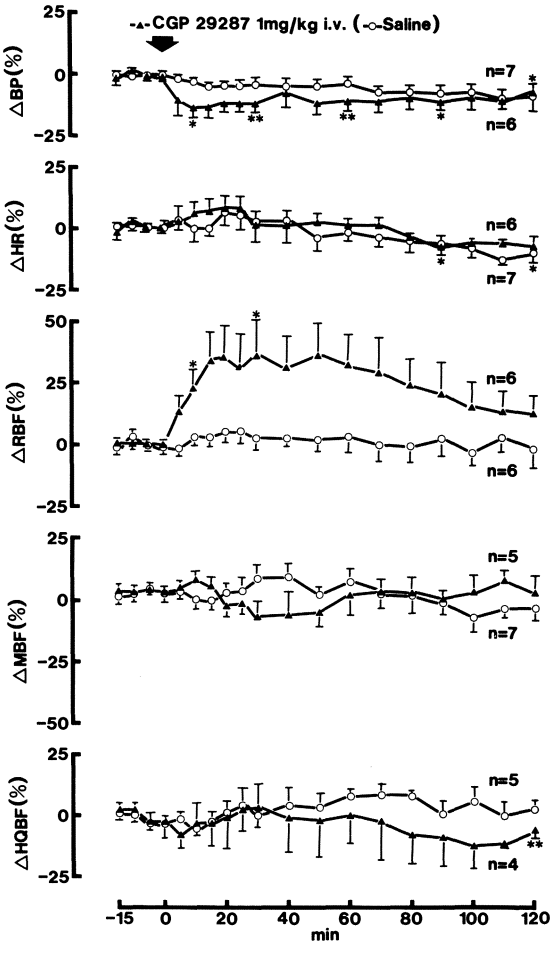

Fig. 2. Changes in blood pressure *(BP)*, heart rate *(HR)*, renal blood flow *(RBF)*, mesenteric blood flow *(MBF)*, and hindquarter blood flow *(HQBF)* after intravenous bolus injection of saline or of the renin inhibitor CGP 29287. Values are means ± SEM. Initial absolute values of BP and HR were 110 ± 4 mm Hg and 341 ± 19 beats/min for saline and 116 ± 8 mm Hg and 335 ± 16 beats/min for CGP 29287. The significance of changes compared to the initial baseline values is indicated at 10, 30, 60, 90, and 120 min only. *: $P<0.05$, **: $P<0.01$

Vascular resistance was calculated as follows:

$$\text{Resistance} = \frac{\text{mean arterial pressure (mm Hg)}}{\text{Doppler shift (kHz)}}$$

The significance of changes was estimated using paired Student's *t*-test.

Results

The converting enzyme inhibitor enalaprilat induced a rapid reduction in BP within 10 min after injection, which reached a maximum after 20 min (−16 ± 4 mm Hg, $P<$ 0.01) (Fig. 1). The fall in BP persisted for up to 2 h with a tendency for a further small progressive decrease after the initial response (−22 ± 4 mm Hg after 120 min, $P<$ 0.01). This later decrease probably reflects the spontaneous small progressive fall in BP seen in the control experiments (−10 ± 3 mm Hg after 120 min, $P<0.05$). De-

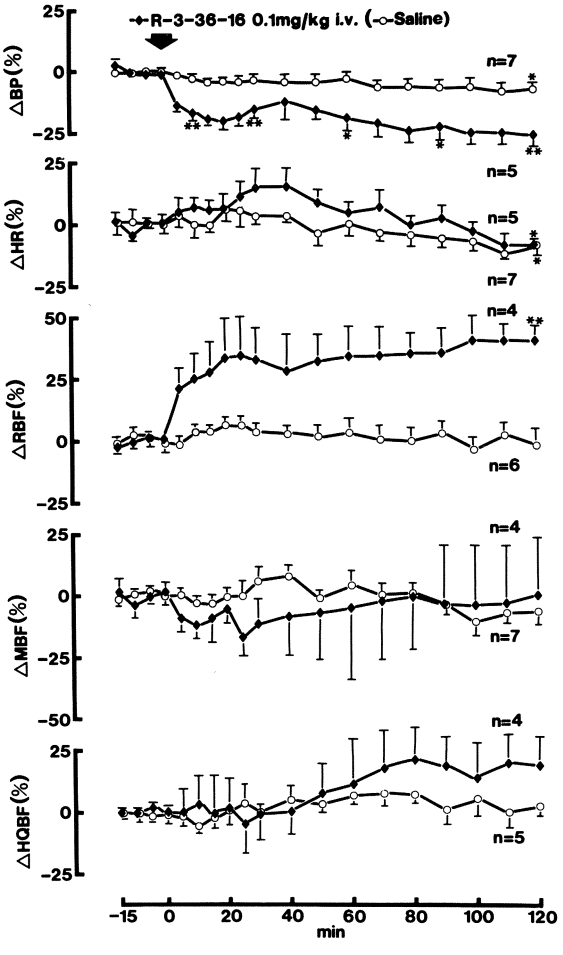

Fig. 3. Changes in blood pressure *(BP)*, heart rate *(HR)*, renal blood flow *(RBF)*, mesenteric blood flow *(MBF)*, and hindquarter blood flow *(HQBF)* after intravenous bolus injection of saline or the renin-inhibitory monoclonal antibody R-3-36-16. Values are means ± SEM. Initial absolute values of BP and HR were 110 ± 4 mm Hg and 324 ± 21 beats/min for saline and 106 ± 6 mm Hg and 335 ± 16 beats/min for R-3-36-16. The significance of changes compared to the initial baseline values is indicated at 10, 30, 60, 90, and 120 min only. *: $P<0.05$, **: $P<0.01$

spite the rapid fall in BP, there was no significant increase in HR. HR tended to decrease over the 2 h period in both the enalaprilat and the vehicle-treated marmosets (Fig. 1). RBF remained stable in control experiments, whereas it rapidly increased after injection of enalaprilat (Fig. 1). The maximum increase was observed after 40 min (27 ± 8%, $P<0.05$) and persisted for up to 2 h. MBF was also unchanged in control experiments (Fig. 1), but tended to decrease after enalaprilat. The maximum decrease developed within 20 min (−29 ± 9, n.s.) and persisted for 2 h. HQBF also tended to decrease after injection of enalaprilat (−17 ± 7 after 25 min, n.s.), but had recovered to values seen in the control experiments at the end of the experiment. HQBF was stable in the control experiments.

The renin inhibitor CGP 29287 induced a rapid fall in BP of a magnitude similar to that of enalaprilat (−16 ± 4 mm Hg after 10 min, $P<0.05$), but the response was of shorter duration (Fig. 2). BP returned to values seen in control experiments within 2 h after injection. CGP 29287 had no effect on HR (Fig. 2). RBF had significantly increased to a maximum of 36 ± 12% after 20 min ($P<0.05$) (Fig. 2) and began to re-

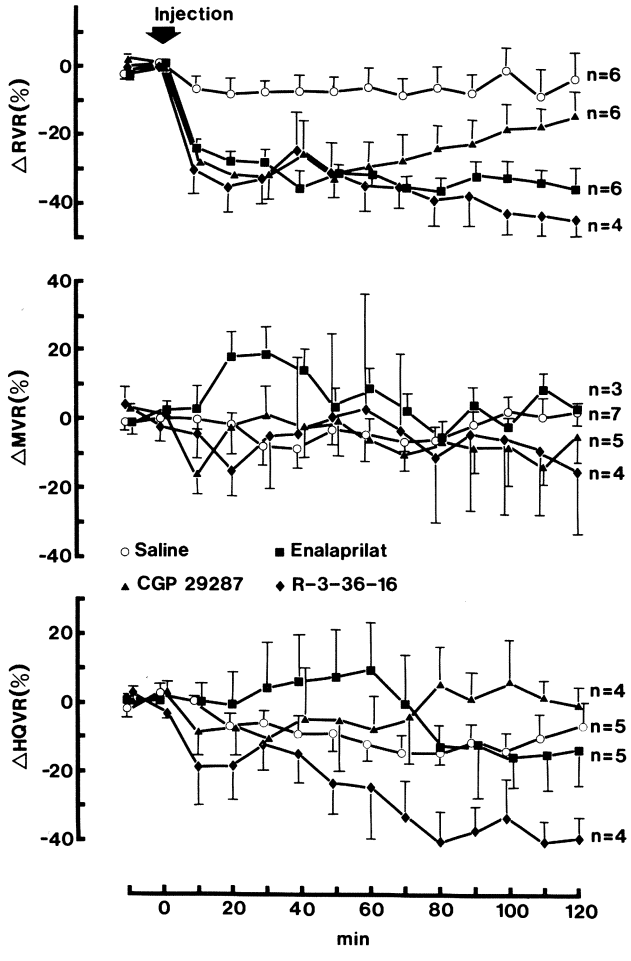

Fig. 4. Changes in renal *(RVR)*, mesenteric *(MVR)*, and hindquarter *(HQVR)* vascular resistances after intravenous bolus injection of saline (1 ml/kg), the converting enzyme inhibitor enalaprilat (2 mg/kg), the renin inhibitor CGP 29287 (1 mg/kg), or the renin inhibitory monoclonal antibody R-3-36-16 (0.1 mg/kg). Values are means ± SEM

turn to baseline values after 50 min. CGP 29287 had no consistent influence on MBF (Fig. 2). There was a tendency for HQBF to decrease in the second hour after injection of CGP 29287 (-11 ± 3 after 110 min, $P < 0.05$) (Fig. 2).

The renin-inhibitory monoclonal antibody R-3-36-16 also induced a rapid fall in BP (-20 ± 4 mm Hg after 20 min, $P < 0.01$) (Fig. 3). This effect persisted for 2 h, with a tendency for a further progress fall (-27 ± 4 mm Hg after 120 min, $P < 0.01$). HR was not changed by R-3-36-16 (Fig. 3). RBF increased rapidly ($34 \pm 16\%$ after 20 min, n.s.), and this effect persisted for 2 h, reaching a maximum after 100 min ($40 \pm 10\%$, $P < 0.05$) (Fig. 3). The initial increase in flow was not statistically significant, probably because of the small number of animals. There was a tendency for an initial decrease in MBF after injection of R-3-36-16 ($-17 \pm 7\%$ after 25 min, n.s.), whereas HQBF tended to increase over the second hour ($20 \pm 12\%$ after 100 min, n.s.) (Fig. 3).

Enalaprilat, CGP 29287, and R-3-36-16 all induced an initial decrease in renal vascular resistance (RVR), which was of similar magnitude ($-31 \pm 6\%$, $P < 0.001$; $-32 \pm 7\%$, $P < 0.01$; and $-33 \pm 7\%$, $P < 0.05$, respectively) (Fig. 4). RVR began to

recover 30 min after injection of CGP 29287, remained lowered after enalaprilat ($-37 \pm 5\%$, $P<0.001$), but continued to decrease for up to 2 h after R-3-36-16 ($-45 \pm 5\%$ after 2 h, $P<0.01$). RVR remained stable in control experiments. None of the inhibitors had a significant effect on mesenteric vascular resistance (MVR) (Fig. 4). Enalaprilat and CGP 29287 had no consistent effects on hindquarter vascular resistance (HQVR), whereas R-3-36-16 induced a progressive decrease ($-40 \pm 6\%$ after 110 min, $P<0.01$) (Fig. 4).

Discussion

In the present study the ultrasonic pulsed Doppler flow probe technique was applied for the measurement of regional blood flows in a small primate. After chronic implantation of the flow probes in conscious marmosets, it was possible to measure blood flow simultaneously in 3 different vascular beds. In previous experiments, we demonstrated the similarity between marmoset and human renin and the suitability of this primate for cardiovascular experiments with human-specific inhibitors of renin (Michel et al. 1984). In this study we used the Doppler flow technique to compare the renal vasodilatory effects of renin and converting enzyme inhibition.

The results of our experiments demonstrate that converting enzyme inhibitor enalaprilat induces a selective increase in RBF in normotensive marmosets after mild sodium and volume depletion. This is consistent with the findings of previous studies with converting enzyme inhibitors in rate, dogs, and man (Johnston 1984; Wong et al. 1981). The ANG II antagonist saralasin has also been reported to increase RBF (Navar and Rosivall 1984; Wong et al. 1981), but this response may be preceded by a fall in RBF (Arendhorst and Finn 1977) or completely masked because of the agonistic properties of the compound (Clappison et al. 1981; Wong et al. 1981; Zimmerman 1979). There is only one previous report on the effects of a renin-inhibitory agent (Dzau et al. 1983). In these preliminary experiments Fab fragments from a renin-inhibitory antiserum against canine renin appeared to induce a smaller increase in RBF in dogs than the converting enzyme inhibitor teprotide. However, in our study, 2 different types of renin inhibitor, a synthetic peptide and a monoclonal antibody, induced an increase in RBF of a magnitude simular to that induced by enalaprilat. The initial decrease in RVR was approximately 30% with all of the 3 inhibitors. The only difference between the inhibitors was in their duration of action. The reduction in BP and the increase in RBF persisted for up to 2 h after enalaprilat and R-3-36-16, but for less than 2 h after CGP 29287. To avoid any influence of blood sampling on the haemodynamic responses, plasma renin activity was not measured in this study. However, the duration of the effects of the renin inhibitors on BP and RBF correlates with the time course for the inhibition of plasma renin activity measured in previous experiments (Wood et al. 1985). The long duration of action of enalaprilat is in agreement with studies in other species (Kubo and Cody 1985). Since 2 different types of renin inhibitor produced a renal vasodilatory effect of a magnitude similar to that of a converting enzyme inhibitor, this effect appears to be entirely due to a reduction in the concentration of endogenous ANG II. The potential action of converting enzyme inhibitors on other vasoactive substances does not seem to contribute to the renal vasodilatory response observed in this primate model.

Our study was done in marmosets after a mild stimulation of the renin-angiotensin system by acute treatment with a diuretic. The magnitude of the increase in RBF would probably have been greater in more severely sodium-depleted marmosets and less after suppression of the renin-angiotensin system by a high salt diet, as has been observed with converting enzyme inhibitors in normotensive animals and man (Hollenberg et al. 1981; Wong and Zimmerman 1982).

The renal haemodynamic effects of a renin inhibitor have not as yet been evaluated in hypertensive animals. Although the renal response to converting enzyme inhibitors depends on the pretreatment value of plasma renin activity in normotensive animals and man, the response in hypertensive patients is greater than is predicted from plasma renin activity (Britton 1985; Hollenberg et al. 1981; Mimran 1983). Values of plasma renin activity many not always reflect the activity of the renin-angiotensin system in the kidneys. All of the components necessary to generate ANG I and ANG II are present in the kidney (Navar and Rosivall 1984), and selective intrarenal blockade of ANG II has been shown to increase RBF (Meggs and Hollenberg 1980). Thus, inhibition of intrarenally formed ANG II may be more important than inhibition of circulating ANG II.

The vasodilatory response to enalaprilat and the 2 renin inhibitors was relatively selective for the kidney. There were no consistent changes in MVR with any of these inhibitors. HQVR was not changed either by enalaprilat or CGP 29287. However, R-3-36-16 induced a slow progressive decrease in HQVR. Since the effect was slow in onset and only observed with the long acting antibody, it may indicate a reduction in tissue renin activity. Other studies have shown that the renin found in the blood vessel wall originating from the circulation, has a significant influence on vascular tone (Swales et al. 1983). The antibody has a long half-life in the plasma and a high binding capacity. Therefore, it may prevent the uptake of circulating renin. Thus, the initial response after the antibody may be resulting from inhibition of circulating renin, and the later response from a reduction in tissue renin activity.

The fall in RVR alone does not account for the fall in BP induced by the inhibitors. Vascular resistance was probably reduced in other vascular beds that were not measured in these experiments. In other studies converting enzyme inhibitors have been shown to increase blood flow to the heart, brain, liver, and kidney (Brunner et al. 1985; Johnston 1984).

Despite the rapid fall in BP, no reflex tachycardia was observed after any of the inhibitors. This agrees with experimental and clinical observations with converting enzyme inhibitors and is in contrast to the effects of other types of vasodilators, such as hydralazine or nifedipine. The absence of tachycardia may be a result of a reduction of 2 different actions of ANG II, an inhibition of vagal (Campell et al. 1985; Potter 1982) and a potentiation of sympathetic (Zimmerman et al. 1984) activity. The lack of reflex tachycardia may also be important for the chronic antihypertensive efficacy of blockers of the renin-angiotensin system.

References

Arendhorst WJ, Finn WF (1977) Renal hemodynamics in the rat before and during inhibition of angiotensin II. Am J Physiol 233:F290–F297

Britton KE (1985) Radioisotopic renal function studies in essential hypertension. Cardiology [Suppl 1] 72:22–29

Brunner HR, Nussberger J, Waeber B (1985) Effects of angiotensin converting enzyme inhibition: a clinical point of view. J Cardiovasc Pharmacol [Suppl 4] 7:S73–S81

Campell BC, Sturani A, Reid JL (1985) Evidence of parasympathetic activity of the angiotensin converting enzyme inhibitor, captopril, in normotensive man. Clin Sci 68:49–56

Clappison BH, Anderson WP, Johnston CI (1981) Renal hemodynamics and renal kinins after angiotensin converting enzyme inhibition. Kidney Int 20:615–620

Dzau VJ, Devine D, Mudgett-Hunter, Kopelman RI, Barger AC, Haber E (1983) Antibodies as specific inhibitors: studies with polyclonal and monoclonal antibodies and FAB fragments. Clin Exp Hypertension A5:1207–1220

Gerber JG, Nies AS, Friesinger GC, Gerkens JF, Branch RA, Oates JA (1978) The effect of PGI_2 on canine renal function and hemodynamics. Prostaglandins 16:519–528

Haywood JR, Shaffer RA, Fastenow C, Fink G, Brody MJ (1981) Regional blood flow measurement with pulsed Doppler flowmeter in conscious rat. Am J Physiol 241:H273–278

Hofbauer KG, Wood JM (1984) Inhibition of renin: recent developments. Contrib Nephrol 43:144–152

Hofbauer KG, Wood JM (1985) Inhibition of renin: recent immunological and pharmacological advances. TIPS 6:173–177

Hofbauer KG, Fuhrer W, Heusser Ch, Wood JM (1985) Comparison of different drug interference with the renin-angiotensin system. J Cardiovasc Pharmacol [Suppl 4] 7:S62–S68

Hofbauer KG, Wood JM, Gulati N, Heusser Ch, Ménard J (1985) Increased plasma renin during inhibition: studies with a novel immunoassay. Hypertension [Suppl 1] 7:61–65

Hollenberg NK, Meggs LG, Williams GH, Katz J, Garnic JD, Harrington DP (1981) Sodium intake and renal responses to captopril in normal man and in essential hypertension. Kidney Int 20:240–245

Johnston CI (1986) Angiotensin converting enzyme inhibitors. In: Doyle AE (ed) Handbook of hypertension, vol 5: Clinical pharmacology of antihypertensive drugs. Elsevier, Amsterdam, pp 272–311

Kubo SH, Cody RJ (1985) Clinical pharmacokinetics of the angiotensin converting enzyme inhibitors. Clin Pharmacokin 10:377–391

Lonigro AJ, Hagemann MH, Stephenson AH, Fry CL (1978) Inhibition of prostaglandin synthesis by indomethacin augments the renal vasodilator response to bradykinin in the anaesthetized dog. Circ Res 43:447–455

Marks ES, Bing RF, Thurston H, Swales JD (1980) Vasodepressor property of the converting enzyme inhibitor captopril (SQ 14225): the role of factors other than renin-angiotensin blockade in the rat. Clin Sci 58:1–6

McGiff JC, Terragno NA, Malik KU, Lonigro AJ (1972) Release of prostaglandin E-like substance from canine kidney by bradykinin. Circ Res 31:36–43

Meggs LG, Hollenberg NK (1980) Converting enzyme inhibition and the kidney. Hypertension 2:551–557

Michel JB, Wood J, Hofbauer K, Corvol P, Ménard J (1984) Blood pressure effects of renin inhibition by human renin antiserum in normotensive marmosets. Am J Physiol 246:F309–316

Mimran A (1983) Renal aspects of treatment by converting enzyme inhibitors in hypertension. Clin Exp Hypertension A5:1381–1394

Navar LG, Rosivall L (1984) Contribution of the renin-angiotensin system to the control of intrarenal hemodynamics. Kidney Int 25:857–868

Potter EK (1982) Angiotensin inhibits action of vagus nerve at the heart. Br J Pharmacol 75:9–11

Swales JO, Loudon M, Bing RF, Thurston H (1983) Renin in the arterial wall. Clin Exp Hypertension A5:1127–1136

Sweet CS, Blaine EH (1984) Angiotensin-converting enzyme inhibitors. In: van Zwieten PA (ed) Handbook of hypertension. Elsevier, Amsterdam, pp 343–363

Wong PC, Zimmerman BG (1982) Dependence of renal vasodilator effect of captopril on prevailing plasma renin level in the dog: influence of DOCA-salt treatment. Clin Sci 63:355–360

Wong PC, Zimmerman BG, Kraft E, Kounenis G, Friedman P (1981) Pharmacological evaluation in conscious dogs of factors involved in the renal vasodilator effect of captopril. J Pharmacol Exp Ther 219:646–650

Wood JM, Gulati N, Forgiarini P, Fuhrer W, Hofbauer KG (1985) Effects of a specific and long-acting renin inhibitor in the marmoset. Hypertension 7:797–803

Wood JM, Heusser C, Gulati N, Forgiarini P, Hofbauer KG (in press) Monoclonal antibodies against human renin: characterization in the marmoset. Hypertension

Zimmerman BG (1979) Blocking and agonistic actions of angiotensin antagonists in normotensive and hypertensive dogs. Cardiovasc Med 4:231–241

Zimmerman BG, Sybertz EJ, Wong PC (1984) Interaction between sympathetic and renin-angiotensin system. J Hypertension 2:581–587

The Influence of VIP on Ureteral and Renal Pelvis Motility

W. Blitz[1], B. Franzen[1], and J. Hannappel[1]

Introduction

Vasoactive Intestinal Peptide (VIP) was originally extracted from porcine small intestine by Said and Mutt (1970).

It was first known by its strong vasodilatory and hypotensive effects. Further experiments have revealed VIP to produce vascular dilatation (Blitz and Charbon 1983), secretory responses in pancreas (Blitz and Charbon 1985) and intestines (Krejs et al. 1978) smooth muscle relaxation in the trachea (Matsuzaki et al. 1980), digestive tract (Eklund et al. 1979) and the reproductive system (Larsen et al. 1981). The structure of VIP is identical in human, cow, pig and rat, and composed of 28 amino-acids (Wang et al. 1985).

Histochemical studies have demonstrated a widespread distribution of VIP in central and peripheral nervous system throughout the body (Larson et al. 1976). In the urinary tract VIP is present in nerve terminals located around vascular and non-vascular smooth muscle and beneath the epithelium (Polak and Bloom 1984). VIP-ergic nerves are supposed to be involved in non-cholinergic, non-adrenergic nerve-mediated relaxation of smooth muscle (Klarskov et al. 1984). The influence of VIP on urinary tract smooth muscle is not extensively investigated and the results seem contradictory. The aim of this study is to investigate the effect of VIP on the renal pelvis and ureteropelvic function of different species.

Material and Methods

Tissue strips were prepared from in toto removed kidneys and ureters (pigs and guinea pigs) and mounted in a thermostatically controlled organ bath (10 ml) treated with silicone and containing a modified Krebs solution of the following composition: Na^+ 137, K^+ 5.9, Ca^{2+} 2.5, Mg^{2+} 1.2, Cl^- 124, HCO_3^- 25, $H_2PO_4^-$ 1.2, glucose 11.5 mmol $\cdot L^{-1}$, equilibrated with 95% O_2 and 5% CO_2 at pH 7.4 and temperature 37°C.

To achieve a steady state the organ bath was flushed during 1 hour at a rate of 2 ml per min with Krebs solution. At the start of the experiments a solution of 50 10.5% human albumine in 0.9% NaCl was added to the organ bath as a control and subsequently VIP was added to the organ bath in increasing concentrations of 10^9–10^6 mol $\cdot L^{-1}$ at intervals of 8 min.

The mechanical activity of the strips was measured with isometric mechano-electrical transducers.

Student's *t*-test was used for statistical analysis.

[1]Department of Urology, Medical Faculty, RWTH Aachen, Pauwelsstr., D-5100 Aachen

Investigative Urology 2
Edited by G. H. Jacobi et al.

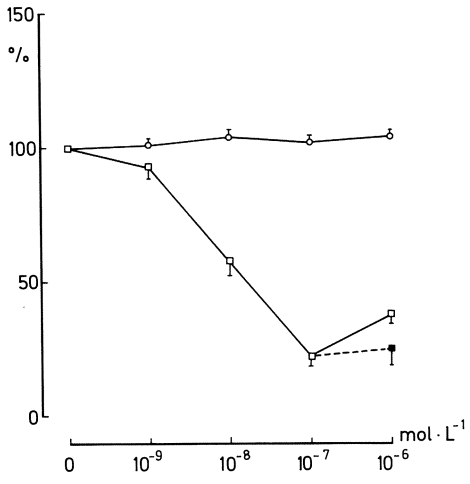

Fig. 1. Mean reduction of contraction frequency following increasing VIP doses in mol · L^{-1}. ○ Guinea-pig, ureteropelvic function ($n = 12$); □ pig, renal pelvis ($n = 21$); ■ pig, renal pelvis, single dosage of VIP 10^{-6} mol · L^{-1} ($n = 14$); I = standard error of the mean

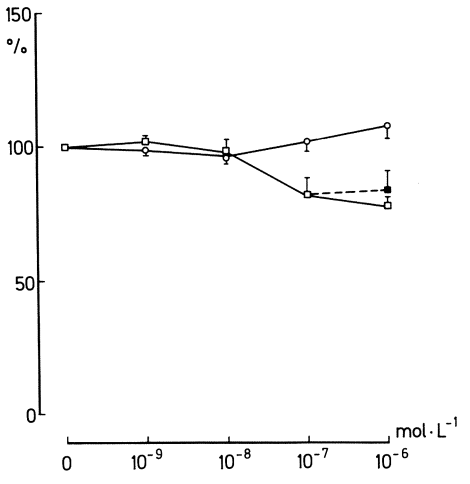

Fig. 2. Mean reduction of contraction amplitude following increasing VIP doses in mol · L^{-1}. ○ Guinea-pig, ureteropelvic function ($n = 12$); □ pig, renal pelvis ($n = 21$); ■ pig, renal pelvis, single dosage of VIP 10^{-6} mol · L^{-1} ($n = 11$); I = standard error of the mean

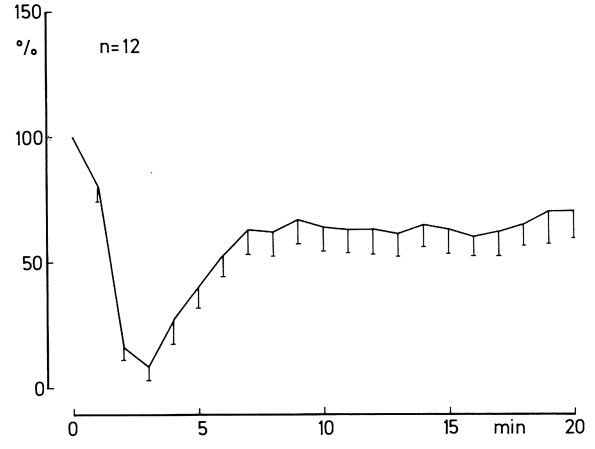

Fig. 3. Pig, renal pelvis. Time-course of contraction after a single dose of VIP $10^{-6} \cdot L^{-1}$ as % of initial value (amplitude × frequency); I = standard error of the mean

Results

VIP produced a marked dosage-dependant decrease of contraction frequency in the pig renal pelvis.

A maximum decrease of 78% was achieved at a concentration of 10^{-7} mol · L^{-1} (Fig. 1). A less notable reduction of contraction amplitude of 22% was observed at a concentration of 10^{-6} mol · L^{-1}.

No significant difference was noticed between dose-response curve and single dosage of 10^{-6} mol · L^{-1} (Fig. 2).

The tissue strips [renal pelvis] from guinea pigs showed no significant effect after addition of VIP at a maximal concentration of 10^{-6} mol · L^{-1}.

The time course analysis of the pig renal pelvis showed a strong inhibition at the start but later a lesser decrease of 40% of the maximal value (Fig. 3).

Discussion

The present experiments show a marked relaxation of the upper urinary tract smooth muscle. A tachyphylaxia was not observed. In accordance with another author (Finkbeiner 1983) no significant inhibition in guinea-pig renal pelvis contractions was observed although VIP-ergic nerves have been immunohistochemically proven in upper and lower urinary tract (Polak and Bloom 1984). Johns found on the contrary a weak contractile effect on the guinea pig bladder (Johns 1979). Other authors have demonstrated a similiar relaxation by VIP on tissue strips of ureter, detrusor, bladder base, urethra, Fallopian tube, uterus trachea, oesophagus, stomach, colon and gall bladder from various species (Larsen et al. 1981; Klarskov et al. 1984; Finkbeiner 1983; Walles et al. 1980; Botton et al. 1981; Fahrenkrug 1979). The VIP effect is probably exerted directly on the smooth muscle cell. Specific VIP-ergic receptors are likely to exist and specific binding sites for VIP have been proven on synaptic membranes from various organs. It seems most probable that the peptidergic nerve fibres (i.e., VIP, Substance P, Neurotensin and others) exert a modulatory role in the autonomic nervous control of the genito-urinary function and the VIP-ergic nerves comprise a major part with a relaxing effect.

However, how the peptidergic nervous control of the genito-urinary smooth muscle activity is integrated and coordinated remains to be elucidated.

References

Blitz W, Charbon GA (1983) Regional vascular influences of vasoactive intestinal polypeptide. Scand J Gastroenterol 18:755–763

Blitz W, Beijer HJM, Charbon GA (1985) Cholinergic and pancreatic actions of purified porcine and synthetic Vasoactive Intestinal Peptide (VIP). Arch Int Pharmacodyn Ther 277:66–76

Botton TB, Lang RJ, Ottesen B (1981) Mechanism of action of vasoactive intestinal polypeptide on myometrial smooth muscle of rabbic and guinea pig. J Physiol 318:41–45

Eklund S, Jodal M, Lundgren O, Sjöqvist A (1979) Effects of vasoactive intestinal peptide on blood flow motility and fluid transport in the gastrointestinal tract of the cat. Acta Physiol Scand 105:461–468

Fahrenkrug J (1979) Vasoactive intestinal polypeptide: measurement, distribution and putative neurotransmitter function. Digestion 19:149–169

Finkbeiner AE (1983) In vitro effects of vasoactive intestinal polypeptide on guinea pig urinary bladder. Urology 22:275–277

Johns A (1979) The effect of vasoactive intestinal polypeptide on the urinary bladder and taenia coli of the guinea pig. Can J Physiol Pharmacol 57:106–110

Klarskov P, Gerstenberg T, Hald T (1984) Vasoactive Intestinal Polypeptide influence on lower urinary tract smooth muscle from human pig. J Urol 131:1000–1004

Krejs GJ, Barkley RM, Read NW, Fordtran JS (1978) Intestinal secretion induced by vasoactive intestinal peptide. J Clin Invest 61:1337–1345

Larson LI, Fahrenkrug J, Schaffalitzky de Muckadell O, Sundler F, Hakansen R, Rehfeld JF (1976) Localization of VIP to central and peripheral neurons. Proc Natl Acad Sci USA 73–9:3197–3200

Larsen JJ, Ottesen O, Fahrenkrug J, Fahrenkrug L (1981) Vasoactive Intestinal Polypeptide [VIP] in the male genitourinary tract. Inv Urol 19:211–213

Matsuzaki Y, Hamasaki Y, Said SI (1980) Vasoactive Intestinal Peptide: a possible transmitter of non-adrenergic relaxation of guinea-pig airways. Science 210:1252–1253

Polak JM, Bloom SR (1984) Localization and measurement of VIP in the genitourinary system of man and animals. Peptides 5:225–230

Said SI, Mutt V (1970) Polypeptide with broad biological activity: isolation from small intestine. Science 169:1217–1218

Walles B, Häkanson R, Helm G, Ownan Ch, Chötery NO, Sundler F (1980) Relaxation of human femal genital sphincters by the neuropeptide vasoactive intestinal polypeptide. Am J Obstet Gynecol 138:337–442

Wang SC, Du BH, Eng J, Chang M, Hulmes JD, Pan Y, Yalow RS (1985) Purification of dog VIP from a single animal. Life Sci 37:979–983

Antidiuretic Action of Vasoactive Intestinal Peptide in the Canine Kidney

W. Blitz[1], H. J. M. Beijer[2], and G. A. Charbon[2]

Introduction

Vascoactive Intestinal Peptide [VIP] is a highly basic octacosapeptide (molecular weight 3809) originally extracted from porcine lung tissue by Said and Mutt (Said et al. 1968), but later isolated and purified from porcine upper intestine (Said and Mutt (1970). Immunhistochemical studies have revealed a widespread occurrence of VIP containing neurons and nerve fibers in the brain, the peripheral nerves, salivary glands, trachea, lung, upper and lower digestive tract, urogenital tract, and around peripheral blood vessels (Said et al. 1968; Said and Mutt 1970; Said and Rosenberg 1976; Lundberg et al. 1984; Polak and Bloom 1982; Larsson et al. 1976; Larsson 1977; Ottesen 1983; Hökfelt et al. 1978; Uddman et al. 1981). A broad spectrum of actions has been ascribed to VIP, of which the most important are vasodilation and hypotension (Said et al. 1968) relaxation of smooth muscle (Polak and Bloom 1982; Ottesen 1983), excretion of water and bicarbonate by the pancreas (Maklouf et al. 1978), intestinal secretion (Krejs et al. 1978) and release of insulin and glucagon (Schebalin et al. 1977). A recent study showed that VIP can stimulate renin relase and increase renal blood flow (Porter et al. 1982). The following experiments were conducted to investigate the effects of VIP on renal function in connection with hemodynamic responses.

Material and Methods

Adult dogs ($n = 9$) of either sex, weighing between 15 and 25 kg, were fasted 24 h before the start of the experiments, but were permitted free access to water. Anesthesia was induced with sodiumpentobarbital (30 mg/kg i.v.), supplemented hourly by 3 mg/kg beginning 2 h after introduction, but not during the intervals of VIP administration. After endotracheal intubation, ventilation (using a positive pressure respirator, Hospal 700) was maintained with a mixture of O_2 and N_2O ($O_2 : N_2O = 1 : 1$) and monitored by capnographic measurements of the expired CO_2, held at 4.5%. Body temperature was kept between 37°C and 38°C by a thermostatically controlled fluid-filled mattress. During the experiments the animals were sufficiently hydrated with saline infusions.

Preparation

Arterial pressure was measured in the abdominal aorta by an open-tip catheter inserted into a femoral artery and connected to a pressure transducer (Statham

[1]Department of Urology, Medical Faculty, RWTH Aachen, D-5100 Aachen
[2]Experimental Laboratory for Peripheral Circulation, University Hospital, NL-Utrecht

Investigative Urology 2
Edited by G. H. Jacobi et al.

P23Db). In each dog local blood flow through the left gastric artery, the superior mesenteric artery and the left renal artery was measured simultaneously by mounting in vivo calibrated pericascular flow sensors of suitable size and connecting them to a sine-wave electromagnetic flowmeter (Transflow 600, Skalar). To obtain mechanical zero flow, an occluding device was placed around the artery about 5 mm distal of the flow sensor. Heart rate was obtained from the R-peak of the ECG. In each ureter a polyethylene catheter (∅ 1.57 mm) was inserted and placed in the renal pelvis. Urine production was measured by means of a drop monitor (Treonic). Time interval between consecutive drops was measured electronically. Drop volume over time interval represents urine production rate. There was no delay in measuring changes of urine production: the volume entering the cannula equals the volume flowing out. After finishing the preparation steady state was achieved within 30 min after which VIP-administration was started.

Data Analysis

The ECG, pulsatile flow and pressure signals, and the urine production were recorded simultaneously on a polygraph (Schwarzer, physioscript 8000) and on magnetic tape (Ampex) for off-line analysis. The pulsatile flow and pressure signals were analog-digitally converted (sample rate = 200 points per s) by an on-line computer (PDP 11/04) and processed to obtain mean flow (ml/min) and mean pressure (mm Hg) values for every 3 s. The hemodynamic data are presented as conductances (the inverse of resistance), which were obtained by dividing mean flow in each artery by mean arterial pressure. Increased conductance signifies a reduction in the tone of arterioles (resistance vessels). The initial value of a variable was defined as the steady state value, observed before the first VIP administration. The maximum values of the vascular effect occurred within 30 s–45 s after injection of an effective dose of VIP. The lines connecting these maximum values represent the dose-response curves. The responses are expressed proportionally to the initial value. The sensitivity of a variable to VIP stimulation is expressed as D_{50}, i.e., the calculated dose at 50% of the maximal response. The data are averaged over the number of dogs. Differences between means were tested by the student *t*-test. The limit of significance was set at $P = 0.05$. Data are given as mean ± S.E.M.

Laboratory Analysis

Blood samples were collected at the beginning of the dose-response curve after 10 and 14 min. Urine samples were collected continously during the dose-response curve and until 10 min after the last VIP dose. In plasma and urine the concentrations of sodium, potassium, chloride, creatinine and the osmolality were measured. In urine the pH was estimated. Creatinine clearance, free H_2O clearance, sodium, potassium and chloride excretion were calculated.

Drugs

Synthetic VIP (Beckmann, California, USA) was injected into a brachial vein in doses doubling from 1 ng/kg to 1024 ng/kg at intervals of 1 min. VIP was dissolved in a 0.3 *M* potassium phosphate buffer (pH 7.4). Previous experiments have shown that

the diluting fluid at low pH and saline of similar volume and temperature were not vasoactive (Blitz and Charbon 1983). Dose response curves have many advantages over infusion, i.e., the total amount of a drug is much smaller, the exposure of the animal is shorter and thus it is less subject to deterioration (Charbon and Mark 1981). For several reasons a one minute interval between injections was chosen: 1. clearance through the liver is up to 100% in one circulation time (Kitamura et al. 1975); 2. half life of VIP is 1.4 minute (Mitchell et al. 1977); 3. previous experiments revealed a maximum vascular effect at about 30 s and this effect levelled off within one minute.

Table 1. Effects of VIP in anesthetized dogs

	Initial value blood flow (ml/min)	Maximum conductance change as % of initial value	Sensitivity D_{50} (ng/kg)
Left gastric a.	34 ± 6	+325 ± 60	734
Sup. mes. a.	338 ± 30	+17 ± 5	296
Left renal a.	203 ± 40	+27 ± 8	333
Arterial pressure	124 ± 10 mm Hg	−25 ± 9	744

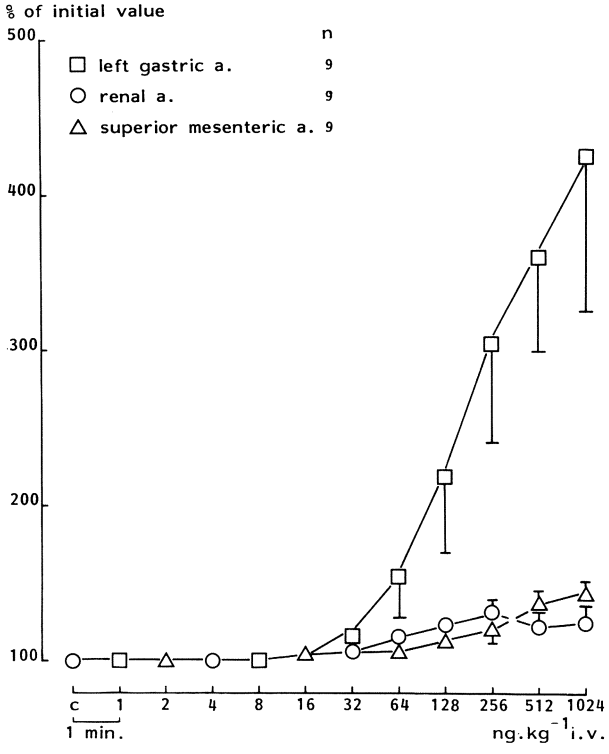

Fig. 1. Dose-response curves of conductanes (mean ± S.E.M. = standard error of the mean) induced by graded bolus injections of synthetic VIP in anesthetized dogs. S.E.M. indication has been omitted if smaller than symbol

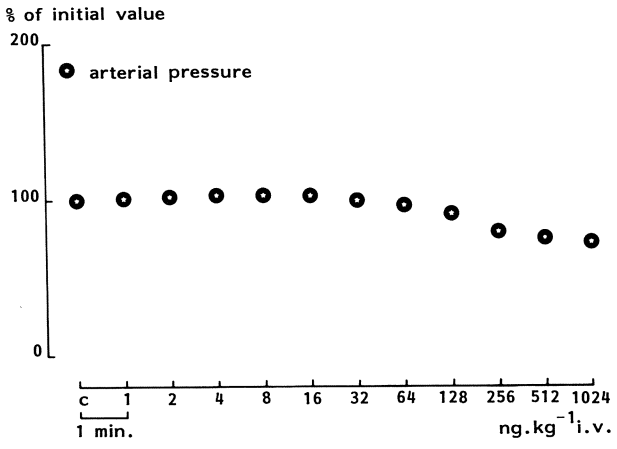

Fig. 2. Dose-response curves of arterial pressure (mean ± S.E.M. = standard error of the mean) induced by graded bolus injections of synthetic VIP in anesthetized dogs. S.E.M. indication has been omitted if smaller than symbol. $N = 9$

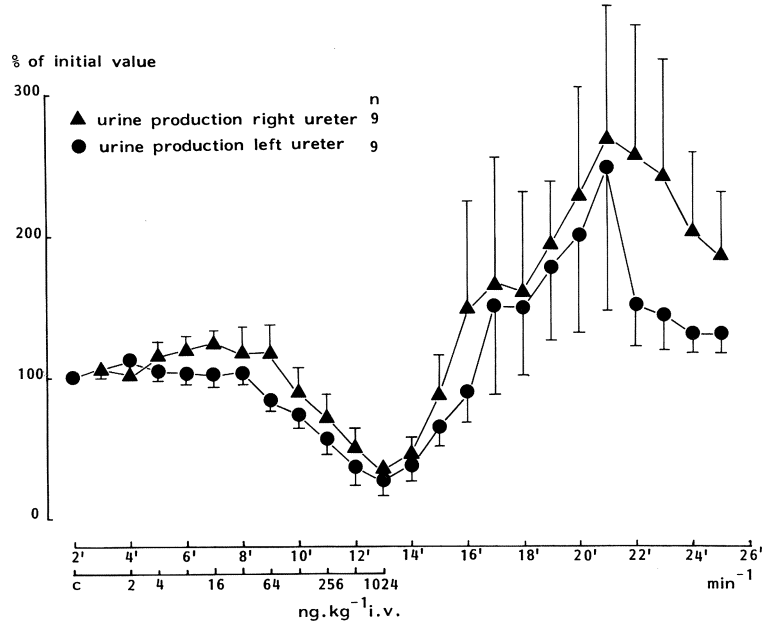

Fig. 3. Dose-response curves of urine production from left and right kidney (mean ± S.E.M. = standard error of the mean) induced by graded bolus injections of synthetic VIP in anesthetized dogs. S.E.M. indication has been omitted if smaller than symbol. On the abscissa is not only a time indication but also a dose indication

Results

The left gastric a., superior mesenteric a. and the left renal a. showed a conductance intrease of respectively 325%, 20% and 27% (Table 1). The arterial pressure exhibited a decrease of 25% (range from 124 to 90 mm Hg) (Figs. 1, 2).

A considerable reduction of urine production (−74% was observed in both kidneys at the maximum dose of 1024 ng/kg (Fig. 3, Table 2). No significant changes

Table 2. VIP administration

	Initial value (µl/min)	At dosis 128 (ng/kg)	At dosis 1024 (ng/kg)	Sensitivity D_{50} (ng/kg)	Maximal change as % of initial value
Urine production					
Right kidney	105 ± 6	92 ± 16	26 ± 5[a]	657	−74
Left kidney	136 ± 19	136 ± 13	39 ± 20[a]	491	−74
Free H_2O clearance					
Right kidney	−440 ± 72	−438 ± 74	−99 ± 23[a]		+76
Left kidney	−406 ± 52	−402 ± 61	−153 ± 41[a]		+52
Creatinine clearance					
Right kidney	−25 ± 1	20 ± 1[a]	5 ± 0.6[a]		−80
Left kidney	−30 ± 8	20 ± 2[a]	7 ± 1[a]		−67
Sodium excretion					
Right kidney	9.5 ± 3	6.7 ± 2	2.8 ± 1[a]	729	−75
Left kidney	14.0 ± 4	11.0 ± 5	2.3 ± 0.6[a]	461	−76
Potassium excretion					
Right kidney	17.4 ± 2	15.2 ± 3	5.6 ± 1[a]	760	−65
Left kidney	19.7 ± 3	15.4 ± 3	8.1 ± 2[a]	416	−68
Chloride excretion					
Right kidney	7.2 ± 2	4.7 ± 1.5	2.1 ± 1.0	731	−74
Left kidney	23.4 ± 8	37.1 ± 14	14.4 ± 5	232	−44
Filtered load					
Left & right kidney	3.4 ± 1	2.8 ± 1	0.8 ± 1		

[a] Significant change, $P \leqq 0.05$

occurred in the ion concentration or osmolality in plasma. No significant pH change in urine was observed. The free water clearance was notably increased in both kidneys to 76% and 52%, but creatine clearance was sharply reduced down to 20% and 23% respectively. Also sodium and potassium excretion showed a marked decrease in both kidneys of 75% and 76% respectively 65% and 68% at a maximum dosage of 1024 ng/kg.

Discussion

In this study a notable conductance increase was observed in the three measured blood vessels; the measured effects correspond with results in previous studies (Blitz and Charbon 1983). Although a decrease of 25% in arterial pressure occurred, the lowest pressure is still within the range of renal blood flow autoregulation (Porter et al. 1982; Abe et al. 1973). In the kidney the resting tone of the afferent arterioles is low and the blood flow per gram of tissue is high (20% of the cardiac output), thus

as a consequence of this low tone the fractional capacity to increase blood flow is lower than in other organs (Navar 1978). Therefore, the renal a. exhibited only a modest conductance increase compared to the marked conductance increase in the left gastric a. Increased renal blood flow [RBF] causes an increased glomerular infiltration rate [GFR], and this in turn enhances urine flow rate. No significant increase urine production was seen during the dose-response curves and at the highest dose there was a significant and marked fall in urine volume. So the enhanced urine flow must be compensated for by increased reabsorption in the proximal tubule. This confirms the results of Rosa et al. (Rosa et al. 1977) who found a direct action of VIP on the proximal tubule in the isolated perfused kidney. The initially increased GFR is presumably the result of an additional direct effect of VIP on mesangium cells and on the capillary permeability. No ADH-effects occurred as the electrolyte concentration and osmolality in plasma remained unchanged.

The increased urine secretion after conclusion of the VIP administration is most probably a physiological phenomenon (rebound) resulting from temporarily decreased urine production. Porter et al. (Porter et al. 1982) also found an increased renal blood flow (+27%) during a 15 min VIP infusion (33 ng/kg/min), an increased renin release, and on the contrary an increased urine volume probably resulting from measurement of rebound phenomenon. In these experiments no sequelae of increased renin release were observed as the duration of the dose-response curve is relatively short. Other authors (Dimaline et al. 1983) have demonstrated a decrease in effective renal plasma flow and glomerular filtration rate, but a slight increase in mean aterial pressure, owing to the employement of relatively low doses of VIP. Future investigations should perform intrarenal electrolyte measurements to assess the influence of VIP on changing ion-concentration. In summary VIP enhances renal hemodynamics and decreases urine flow, and could have a role in the regulation of renal blood flow and urine production.

References

Abe Y, Okahara T, Kishimoto T, Yamamoto K, Ueda J (1973) Relationship between intrarenal distribution of blood flow and renin secretion. Am J Physiol 225:F319–F323

Blitz W, Charbon GA (1983) Regional vascular influences of vasoactive intestinal polypeptide. Scand J Gastroenterol 18:755–763

Charbon GA, Mark vd F (1981) In: Granger DN, Bulkley GB (eds) Measurement of blood flow. Williams and Wilkins, Baltimore, pp 125–155

Dimaline R, Peart WS, Unwin RJ (1983) Effects of Vasoactive Intestinal Peptide (VIP) on renal function and plasma renin activity in the conscious rabbit. J Physiol (London) 344:379–388

Hökfelt T, Schultzberg M, Elde R, Nilsson G, Terenius L, Said SI, Goldstein M (1978) Peptide neurons in peripheral tissues including the urinary tract: Immunohistochemical studies. Acta Pharmacol Toxicol 43 (Suppl II):79–84

Kitamura S, Yoshida T, Said SI (1975) VIP inactivation in liver and potentiation in lung of anesthetized dogs. Proc Soc Exp Biol Med 148:25–29

Krejs GJ, Barkley RM, Read NW, Fordtran JS (1978) Intestinal secretion induced by vasoactive intestinal polypeptide. J Clin Invest 61:1337–1345

Larsson LI (1977) Occurrence of nerves containing VIP-immunoreactivity in the male genital tract. Life Sci 21:503–508

Larsson LI, Fahrenkrug J, Schaffalitzky de Muckadell O, Sundler F, Hakansen R, Rehfeld JF (1976) Localization of VIP to central and peripheral neurons. Proc Natl Acad Sci USA 73-9: 3197–3200

Lundberg JM, Fahrenkrug J, Hökfelt T, Martling CR, Larsson O, Tatemoto K, Anggard A (1984) Co-existence of peptide HI (PHI) and VIP in nerves regulating blood flow and bronchial smooth muscle tone in various mammals including man. Peptides 5:593–606

Makhlouf GM, Yau WM, Zfass AM, Said SI, Bodansky M (1978) Comparative effects of synthetic and natural VIP on pancreatic and biliary secretion and glucose and insulin blood levels in the dog. Scand J Gastroenterol 13:759–765

Mitchell SJ, Bloom SR, Modlin I (1977) Massive release of VIP after intestinal ischaemia. J Endocrinol 73:14p

Navar L (1978) Renal autoregulation: perspective from whole kidney and single nephron studies. Am J Physiol 234:F357–F370

Ottesen B (1983) VIP as a neurotransmitter in the female genital tract. Am J Obstet Gynecol 147-2: 208–224

Polak JM, Bloom SR (1982) Regulatory Peptides and neuron-specific enolase in the respiratory tract of man and other mammals. Exp Lung Res 3:313–328

Porter JP, Reid IA, Said SI, Ganong WF (1982) Stimulation of renin secretion by VIP. Am J Physiol 234:F306–F310

Rosa R, Stoff JS, Silva P, Epstein FH (1977) Tubular diuresis induced by VIP in the isolated perfused rat kidney. Clin Res 25:669a

Said SI, Mutt V (1970) Polypeptide with brood biological activity: Isolation from small intestine. Science 169:1217–1218

Said SI, Rosenberg RN (1976) Vasoactive Intestinal Polypeptide: Abundant immunoreactivity in neural cell lines and normal nervous tissue. Science 192:907–908

Said SI, Estep HL, Webster E, Kontos HA (1968) Potent vasodepressor substance in normal lung. J Clin Invest 47:85A–86A

Schebalin M, Said SI, Makhlouf GM (1977) Stimulation of Insulin and glucagon secretion by VIP. Am J Physiol 232–2:E197–E200

Uddman R, Alumets J, Edvinsson L, Hakanson R, Sundler F (1981) VIP nerve fibers around peripheral blood vessels. Acta Physiol Scand 112:65–70

Fetal Renal Effects of Intrauterine Diuretic Application in Wistar Rats

R. Seufert[1], D. Frohneberg[2], M. Hroport[3], and F. Casper[1]

Introduction

The application of placenta-permeable diuretics in the pregnant woman has been the subject of controversial discussion (Friedberg 1980; Souster and Emery 1980). Not only is the fetus endangered by potential placental ischaemia, natrium and potassium loss and possible dehydration in the mother (Friedberg 1980; Gant and Madden 1975), but also induced effects on fetal organ formation should be considered (Frohneberg and Hutschenreiter 1982; Seufert 1986). Depending on the site of action and placental permeability, fetal urine production can be increased (Wladimiroff 1975), thus leading to consequences for the morphological and functional embryogenesis of isolated nephron sections (Frohneberg 1985; Seufert 1986). Observations of ureteral and renal pelvic dilatation in congenital diabetes insipidus support this assumption (Hoffmann 1974).

Through the use of histromorphometric examination techniques and free-flow micropuncture, a more precise localization and characterization of the alterations can be achieved. By varying the duration of treatment, it should be possible to determine "sensitivity phases".

Material and Methods

The gravid mother animals of 140 Wistar rats were treated with 100 mg chlorthalidone and 40 mg Furosemide/kg at different stages of pregnancy and for different durations. 40 offspring were examined directly after birth, and 100 animals were examined at 6 weeks of age:

Group K	Untreated controls	35 animals
Group I	1st–21st day	35 animals
Group II	1st–10th day	35 animals
Group III	11th–21st day	35 animals

A free-flow micropuncture was performed at the age of 6 weeks in 5 male animals of each group (Fig. 1). 10 newborn rats (5 male/5 female) of each group were examined morphometrically after staining the kidneys with PAS (40×). We used the "Videoplan" morphometric computer system. The "growing cortex area" (Souster and Emery 1980) of the *infant* kidney – the outer part of the cortex, where undiffer-

[1]Departments of Obstetric and Gynecology, Johannes Gutenberg University, Medical School, D-6500 Mainz
[2]Department of Urology, University of Ulm, Medical School, D-7900 Ulm
[3]Hoechst AG, D-6000 Frankfurt/Main

Investigative Urology 2
Edited by G. H. Jacobi et al.

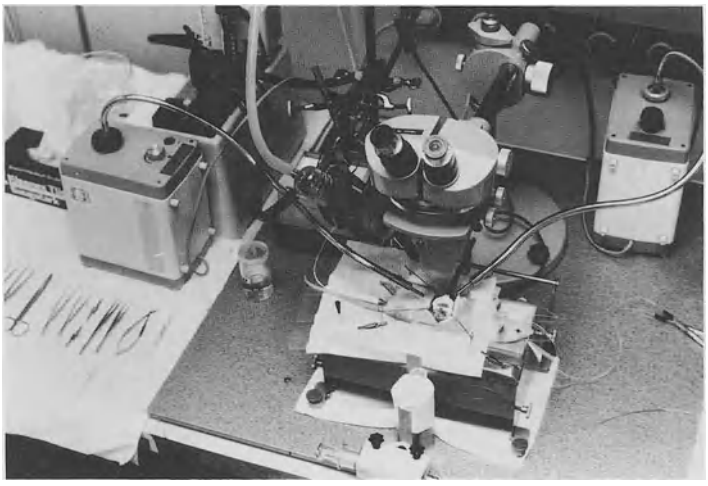

Fig. 1. Micropuncture work-bench

entiated tissue is localized and the percentage of immature glomeruli (which depends on endothelial and mesangial differentiation; Souster and Emery 1980) – were determined.

The remaining 20 animals (10 male/10 female) of each group were studied morphometrically at the age of 6 weeks using the "Videoplan" morphometric computer system (400 ×). After staining with PAS, the profile surfaces for glomeruli, proximal and distal tubules were examined as well as the ratio of the absolute number of nuclei to profile area in proximal and distal tubules. Treatment and sex effects were evaluated by the two-way variance test.

5 animals of each group were examined by electron microscopes and the serum renin activity in 15 rats of each group was determined.

Results

Newborn Animals

While the "cortex growing area" was measured at 5.1 mm^2 in group K, we found a significant increase in Group I up to 8.65 mm^2, Group II up to 6.41 mm^2, and in group III up to 7.30 mm^2.

Similarly, we found 51.4% immature glomeruli in group K, whereas all the treated groups increased significantly (Group I: 73.5%, Group II: 66.2%, Group III: 62.5%).

6-Week-Old Animals

In all treated groups, the profile size of the proximal tubules increased significantly (group K: 2007 mm, group I: 2272 mm, group II: 2294 mm, group III: 2184 mm). The profile size of the distal tubules showed no statistically significant treatment effect.

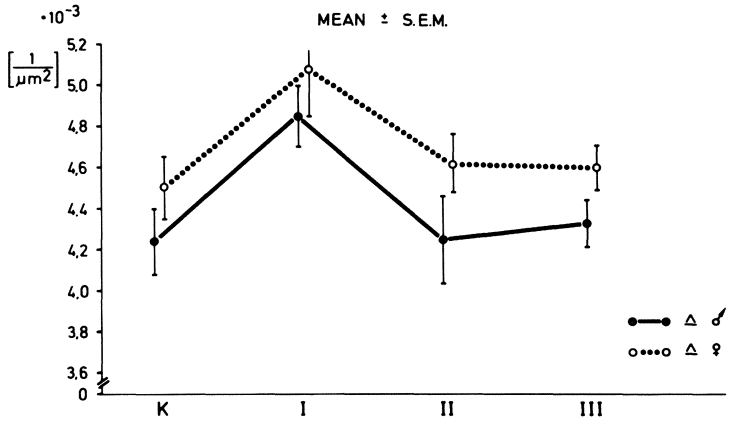

Fig. 2. Proximal tubulus; absolute number of nuclei/profile area

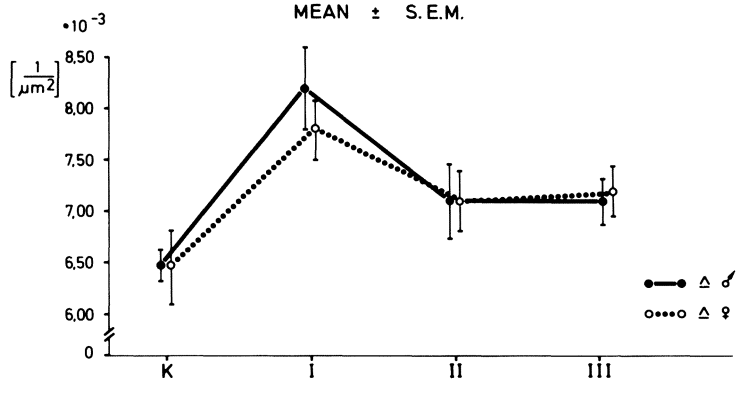

Fig. 3. Distal tubulus; absolute number of nuclei/profile area

A significant increase in the ratio of absolute number of nuclei to profile area was found in group I (13%, Fig. 2) for the proximal tubules and was 27% for the distal tubules (Fig. 3).

Only the male animals of group I showed a statistically significant reduction of glomerular area by 20%. Electron microscopy showed hypertrophy of the macula densa region only in group III, which was accompanied by significantly increased renin activity (100%, see Fig. 6). The singular nephrogenic glomerular filtration rate (SNGFR) showed a reduction of 38% in the surface nephrons of group II and of 26% in group I, whereas group III remained unchanged (Fig. 4). The total GFR of the kidney remained unchanged in all groups. Natrium resorption down to the end of the proximal tubulus was clearly reduced in group I (Fig. 5), while in the same group a marked potassium secretion in the collecting tubes – similar to the acute effect of diuretis – could be demonstrated.

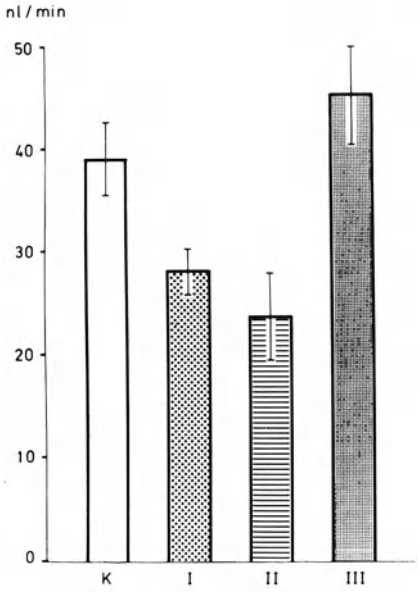

Fig. 4. SNGFR in proximal tubulus

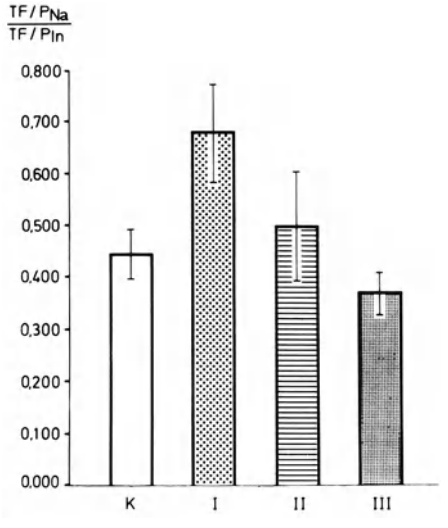

Fig. 5. Ratio $\frac{TF/P_{Na^+}}{TF/P_{JN}}$ at the end of the proximal tubulus

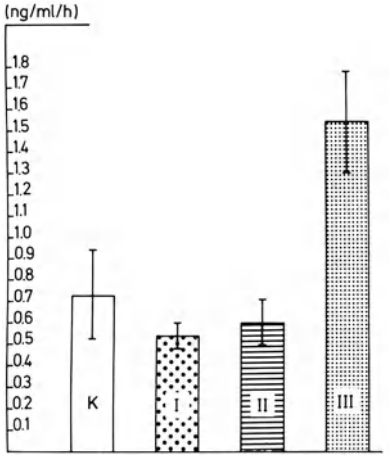

Fig. 6. Renin activities (M = 60)

Discussion

The treatment effects found showed no side preference and, with the exception of the glomenular changes, no sex correlation.

The increase of immature glomeruli and the increase of the "cortex growing area" in newborn rats must be interpreted as a disturbance of kidney maturity processes. The changes are more related to duration of diuretic treatment than to the stage of pregnancy in which it is administered.

The reduction in SNGFR in groups I and II as well as the reduced morphometric glomerular profile size in group I (males) with an unchanged total GFR suggests a compensational effect of the medullar nephrons. Marked effects on natrium and potassium transport could be demonstrated and showed compensation. Tubular changes are therefore more related to duration of diuretic treatment than to the stage of pregnancy in which it is administered.

The serum renin increase and hypertrophy of the macular densa found exclusively in group III must be viewed as an attempt at counter regulation by the more mature juxtaglomenular apparatus.

Toxic effects must be primarily considered as an aetiological explanation for the changes found, whereby secondary diuretic effects – such als electolyte and volume changes – cannot be ruled out. The primary changes in the fetus are modified by adaptation of the nephron during the 6-week growth period and are compensated.

The functional and morphological changes found do not, however, justify a general restriction of diuretics during pregnancy. Rather, a strict indication should be adhered to when prescribing diuretics to pregnant women, reserving them primarily for cases of lung edema and acute renal sufficiency.

References

Friedberg V(1980) Zur Therapie der Gestosen. Gynäkologe 13:67–73

Frohneberg D, Hutschenreiter G (1982) Der primäre Megaureter, ein tierexperimentelles Modell. 6. Symposium für experimentelle Urologie, Bonn

Frohneberg D (1985) Auswirkungen der forcierten intrauterinen Diuretikatherapie auf das Urogenitalsystem der Ratte. Habilitationsschrift, Ulm

Gant NF, Madden PK (1975) The metabolic clearance rate of dehydroisoandrosterone sulfate. Am J Obstet Gynecol 12:159

Hoffmann L (1974) Das Diabetes insipidus Syndrom und konsekutive Harnwegsveränderungen. Dtsch Ges Wesen 29:463

Käch O, Hochuli E (1981) Diuretika in der Schwangerschaft – Kontroverse oder Alternative. Schweiz Rundschau Med (Praxis) 70:2305–2311

Seufert R (1986) Hochdosierte Diuretika – Applikation während der Gravidität. Med. Inauguraldissertation, Mainz

Souster LD, Emery JC (1980) The size of renal glomeruli in fetuses and infants. J Anat 130:595–602

Wladimiroff JW (1975) Effect of furosemide on fetal urine production. Br J Obstet Gynecol 82:220–224

Morphometric Examination of the Dilated Rat Ureter

R. Nafe[1], D. Frohneberg[2], and R. Seufert[3]

Introduction

Dilatations of the ureter are known in rats with diabetes insipidus as well as after the administration of diuretics (Wladimiroff 1975). Nevertheless, similarities to congenital deformities, such as the primary megaureter, have not been established to date. It has not yet been determined whether in the fetus increased diuresis can lead to a functional overstrain of the transport capacity of the ureter and thus to mutations in the sense of a congenital megaurter. In addition to the direct influence of increased diuresis, teratogenic effects of the administered diuretics during pregnancy are possible. Furthermore, it should be determined whether the dilatation can be classified as an adaptive reaction owing to the increased volume load or as the decompensation of the transport capacity. Effects pertaining to treatment and sex must also play a role in these considerations. By means of this study it should be determined whether congenital deformities and the dilatation of the ureter can be experimentally reproduced in animals and whether the results allow an interpretation regarding the pathological mechanisms in the case of intrauterine increased diuresis.

Diuretics from different substance groups, when administered in combination, can increase the diuretic effect in a so-called summation effect (Heidenreich and Baumeister 1964). After oral administration of the Sulfonamide derivate Chlortalidon, the maximum effect occures after 6 h–8 h. In contrast, Furosemid is a fast-acting diuretic with a maximum effect after 30 min–60 min. The site of action of both substances is the ascending part of the Henle Loop. The combination of these diuretics was chosen in order to influence the fetus through diaplacental passage, in particular in regard to the urogenital system.

Histomorphometric examinations of ureter cross sections make the quantitative differentiation of the tissue components possible, whereby the effects of qualitative or semi-quantitative evaluations can be largely avoided. However, standardized preparation and measurement techniques are prerequisites for the use of statistical testing methods. Thus, when determining the circumferences of individual tissue layers, for example, the course of the ureter must be taken into consideration. Hyperplastic or hypertrophic changes of the musculature must be objectified by determining the absolute and relative number of leiomyocytes. For this series of experiments, a semi-automatic morphometric system was used which was expanded by a personally developed, problem-adapted software.

[1]Department of Urology, Johannes Gutenberg University, Medical School, Langenbeckstr. 1, D-6500 Mainz
[2]Department of Urology, University of Ulm, Medical School, Prittwitzstr. 43, D-7900 Ulm
[3]Departments of Obstetric and Gynecology, Johannes Gutenberg University, Medical School, D-6500 Mainz

Investigative Urology 2
Edited by G. H. Jacobi et al.

Material and Methods

41 Wistar rats (age: 4 months, body weight: 186 g–200 g) were used. During pregnancy they were treated by oral administration of a combination of Chlortalidon (100 mg/kg/day) and Furosemid (40 mg/kg/day) and divided into 4 groups:

Group 1 (10 rats):	The mother rats were treated from the 1st to the 21st day of pregnancy
Group 2 (11 rats):	Treatment from the 1st to the 10th day of pregnancy
Group 3 (11 rats):	Treatment from the 11th to the 21st day of pregnancy
Control group (9 rats):	No diuretics were administered.

All of the rats had free access to Altromin 1314 and Ringer's solution. After spontaneous birth, the infant rats remained with their mothers for 3 weeks. After 3 weeks, they were placed in seperate cages and had free access to Altromin 1314 and tab water. At the age of 42 days, one male and one female rat were randomly selected from every brood for morphometric examination:

Control: 18 rats (9 male, 9 female)
Group 1: 20 rats (10 male, 10 female)
Group 2: 22 rats (11 male, 11 female)
Group 3: 22 rats (11 male, 11 female)

After injection with Evipan and preparation of the abdominal wall, kidneys, and ureters, the entire specimen including the dorsal abdominal wall was fixed in 4% buffered formaline saline. The length of the ureter was then determined by projection onto millimeter paper. In order to avoid measurement errors caused by section angles other than 90°, every ureter was divided into 3 parts of equal length, which were embedded in paraffin.

Each of these 3 parts was again divided into 3 parts of equal length so that it was possible to make 9 equidistant cross sections from every ureter (Thickness: 4 µm, PAS staining).

For morphometric examination, we used the semi-automatic system "Videoplan" (manuf. Kontron). The light microscopic image was projected through a drawing tube onto a magnetic tablet, on which the contours of the histologic structures were traced with a cursor. An object micrometer was used for calibration. A special software was programmed in Microsoft-Basic. It is capable of detecting the average thickness of the entire ureter wall, muscularis, lamina propria, and urothelium by simply tracing the inner and outer circumferences of each tissue layer. The mathematical algorithms are described elsewhere (Nafe 1986). The parameters of the ureteral cross section were: outer circumference (boundary between the muscularis and the adventitia), average radius (from the center of the lumen to the outer circumference), relative thickness of the different tissue layers, and the relative number of smooth muscle cells (nuclei) in the muscularis area. A magnification of 260 times was used in order to detect the circumferences. The nuclei of the smooth muscle cells were counted in 3 different areas of the cross section, equidistant from each other (for example, at 4, 8 and 12 o'clock). A magnification of 600 times was used for this. An impulse was manually given for each nucleus, after which the area was traced with the cursor, and the computer printed out the relative number of nuclei for each section.

A statistical analysis was made using the two-way variance analysis in regard to the influence of the animal's sex, and the possible interaction between treatment and sex.

Results

The measurement error was calculated by determining the coefficient of variation of 10 measurements within the same cross section. This coefficient was 0.8%–1.2% for nucleus counting and 1.8%–3% for planimetry. The measurement error was thus lower than the standard deviations determined in the experimental animal groups. Compared to the detection of tissue layer thickness using the personally developed software, the procedure for measuring the thickness of slightly curved parts of the ureter wall with the commercial software leads to a systematic error (values increase

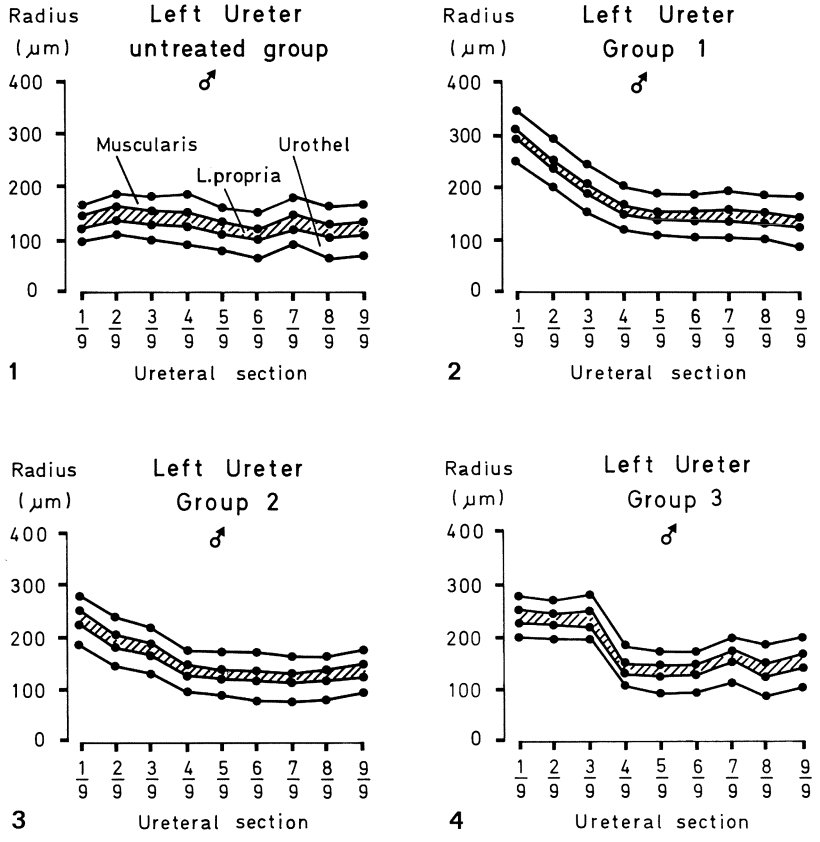

Figs. 1–4. Inner and outer radius of the ureter, thickness of muscularis, lamina propria, and urothel in every cross section (1/9 = near pyeloureteral junction, 9/9 = near vesicoureteral junction). Significant dilatation of the proximal ureter, especially in group 1. No alteration of the middle and distal ureter

by up to 15%). The error can be reduced by increasing the number of measurements in one section so that the average thickness is closer to that obtained with the personally developed software.

The body weight at birth and after 6 weeks did not vary significantly between the 4 groups. The weight of the female animals was significantly less than that of the male animals ($P<0.01$). Compared to the control animals, the length of the right ureters increased in all treated female groups ($P<0.01$), but there was no significant increase of the left ureters or the ureters in the treated male groups ($P<0.05$).

From 9 cross sections, the second, fifth, and eighth were evaluated statistically and are representative for the proximal, middle, and distal third of the ureter. The other sections were examined only for the graphic reconstruction (Figs. 1–4). There was a significant increase of the radius in the second cross section (near pyeloureteral junction). In group 1, the increase was approx. 50% on the right side and 70% on the left side ($P<0.05$). In the other groups, the increase was not as great but also significant. Compared to the control animals, only the lamina propria was thicker on both sides ($P<0.05$); the other tissue layers showed no alteration. No differences could be seen between the 4 groups with respect to the number of smooth muscle cell nuclei per muscularis area ($P<0.05$). Neither sex nor the side location had significant influence on the morphometric parameters.

In the fifth cross section (middle third), there was only a decrease in the relative thickness of the urothel on the right side ($P<0.05$), but no alteration of the submucosa or the radius as in the second section. The eighth cross section (near vesicoureteral junction) showed no significant differences at all. Thus, the only effect of treatment was a dilatation of the proximal ureter on both sides and tendential alterations of the thickness of the tissue layers in the proximal and middle third.

Discussion

The ureters of 82 rats whose mothers were treated with large doses of diuretics during pregnancy were examined. The only effect resulting directly from this treatment was the dilatation of the proximal ureters in all test groups. There was no hypertrophy or hyperplasia of the musculature and no differences in the morphometric data in regard to sex. Tendential differences in the thickness of individual wall layers could be established; however, no interpretation can be derived from this in regard to reactive alterations after forced intrauterine diuresis. There were no alterations resulting directly from this treatment in the middle and lower thirds of the ureter. Morphological similarities to the primary megaureter could not be established. In contrast to the megaureter, no false differentiation of the wall layers, no significant alteration of the muscularis, and a normal terminal segment were found. Supported by the morphometric examination results of the fetal kidneys (Seufert 1986), functional obstructions can also be ruled out in the infant animals.

In contrast to the diuretic Acetazolamid (Vickers 1972), no teratogenic effect could be detected from Chlortalidon or Furosemid to date. Deformities of the kidneys can arise through secondary hypokaliemia (Crocker 1973), which could not be detected in our specimens. It was determined with pregnant dogs that extreme hypokaliemia in the pregnant females has no significant effect on the electrolyte metabo-

lism of the fetuses, which can apparently be contributed to the regulative function of the placenta (Stewart and Welt 1961). Therefore, a direct or indirect teratogenic effect from the administered diuretics is improbable.

The administration of a diuretic during pregnancy causes increased diuresis in the fetus (Wladimiroff 1975). The mechanism of this effect, however, is still unclear. It is possible that a direct invasion by the diuretic of the renin-angiotensin-aldosterone mechanism plays a role (Soveri 1977). In the last trimester of pregnancy, the fetal kidney behaves similar to the adult kidney.

The dilatation of the proximal ureter section can thus best be interpreted as a functional adaptive reaction to the increased intrauterine diuresis, without pathogenicity for the urogenital tract. However, the persistence of the dilatation to the 42nd day p.p. could clearly indicate its irreversibility. Since there were no significant differences between the individual test groups in regard to their ureter morphology, the alterations seemed to depend more on the duration of treatment than on the time the diuretic was administered. Since the dilatation was only present in the proximal third, these findings are interpreted as a reaction of the fine mesenchymal periureteral tissue located at the border between the ureter bud and the metanephrogenic tissue.

Semi-automatic image analysis has become a standard testing procedure for histologic examinations from a scientific standpoint. Fully automatic systems are much more expensive and comparatively less suited for standard morphometric examinations. Commercial software and hardware can be used for large series studies with storage of a large data pool for the application of modern statistical testing methods, and in order to largly avoid subjectiv criteria in the histologic evaluation. Nevertheless, the use of commercial measurement programs does not satisfy several specific problem needs. The program designed for the morphometry of the ureter cross section makes the determination of additional parameters possible, including the average thicknesses of individual tissue layers. Further advantages of the program are the definition of the order of the individual measurements and their storage, which allows for continuous storage and display of the data, in contrast to the commercial software.

References

Crocker JF (1973) Human embryonic kidneys in organ culture: abnormalities of development induced by decreased potassium. Science 181:1178–1179

Heidenreich O, Baumeister L (1964) Über die additive Wirkung von chemisch und wirkungsmäßig unterschiedlichen Diuretika. Klin Wochenschr 42:1236–1240

Nafe R (1986) Entwicklung und Anwendungsmöglichkeiten morphometrischer Untersuchungstechniken an Organen des Urogenitalsystems. Dissertationsschrift, Mainz

Seufert R (1986) Hochdosierte Diuretikaapplikation während der Gravidität. Dissertationsschrift, Mainz

Soveri P (1977) Plasma renin activity in pregnant women with oedema treated with hydrochlorothiazide. Ann Clin Res 9:62–65

Stewart EL, Welt LG (1961) Protection of the fetus in experimental potassium depletion. Am J Physiol 200:824–826

Vickers TH (1972) Acetazolamide dysmelia in rats. Br J Exp Pathol 53:5–21

Wladimiroff JW (1975) Effect of furosemide on fetal urine production. Br J Obstet Gynaecol 82: 221–224

Subject Index

H.-J. Schneider, Giessen (Ed.)

Urolithiasis: Etiology, Diagnosis

1985. 168 figures, XIII, 428 pages.
(Handbook of Urology, Volume 17/1).
Hard cover DM 268,–
Reduced price for subscribers of the entire series:
Hard cover DM 248,–. ISBN 3-540-15582-1

Contents: *H.-J. Schneider:* Morphology of Urinary Tract Concretions. – *H.-J. Schneider:* Epidemiology of Urolithiasis. – *W. G. Robertson, M. Peacock:* Pathogenesis of Urolithiasis. – *W. Vahlensieck:* Diagnosis of Urinary Calculi. – References. – Subject Index.

H.-J. Schneider, Giessen (Ed.)

Urolithiasis: Therapy, Prevention

1986. 127 figures. XV, 355 pages.
(Handbook of Urology, Volume 17/2).
Hard cover DM 218,–
Reduced price for subscribers of the entire series:
Hard cover DM 198,–. ISBN 3-540-15789-1

Contents: *W. Lutzeyer, F. Hering:* Drug Therapy of Urinary Calculi and Prevention of Recurrence. – *D. Bach:* The Treatment of Ureteric Colic and Promotion of Spontaneous Passage. – *M. Marberger, W. Stackl:* Surgical Treatment of Renal Calculi. – *H.-J. Schneider:* Ischemia and Regional Hypothermia in Renal Stone Surgery. – *P. Alken:* Radial Nephrolithotomy Under Ultrasound and Doppler Probe Control. – *P. Alken:* Intraoperative Pyeloscopy. – *P. Alken:* Intraoperative Radiology. – *M. Marberger:* Percutaneous Manipulation of Renal Calculi. – *P. Alken:* The Instrumentation and Surgery of Ureteric Calculi. – *R. Hautmann:* Treatment of Bladder Stones. – *H.-J. Schneider:* Treatment of Urethral Stones. – *Ch. Chaussy, E. Schmiedt:* Extracorporeal Shock-Wave Lithotrips (ESWL) in the Treatment of Kidney and Ureter Stones. – *H.-J. Schneider:* Preventive Measure. – Subject Index.

W. Leistenschneider, R. Nagel, Berlin

Atlas of Prostatic Cytology

Techniques and Diagnosis

Foreword by G. Dhom

Translated from the German by R. Mills, D. Winter

1985. 325 color and black and white illustrations, 27 tables. X, 227 pages. Hard cover DM 220,–. ISBN 3-540-13954-0

Distribution rights for Japan: Igaku Shoin, Tokyo

This monograph fulfills the double mission of describing all tried and proven methods of cytological evaluation of the prostate known to date which are relevant for the clinic and independent practice, and of providing instruction in the basic techniques required for the application of this approach. The full potential of prostatic cytology is clearly and impressively demonstrated.
One of the book's decisive advantages is its comprehensive treatment of both primary diagnosis and, especially, of follow-up of the therapeutic success afforded by different forms of treating advanced, inoperable prostatic carcinoma with the aid of cytological methods. This is the first work to include all these aspects.
It is also the first time that the basic principles and results of DNA cytophotometry and a discussion of secondary tumors of the prostate have been published in this form.
Inflammatory diseases of the prostate gland (prostatitis), which have been accorded little space in previous publications, and the wide range of cytomorphological forms in which they are present, are discussed in detail. Each section of the book also contains new, standardized methods of classification. The distinguishing feature of the volume is its magnificent illustrations which are all of high informative value and almost all in color.

Springer-Verlag
Berlin Heidelberg New York
London Paris Tokyo

K. Korth, Freiburg

Percutaneous Surgery of Kidney Stones

Techniques and Tactics

Foreword by W. Mauermayer

1984. 65 figures, 3 color plates. X, 96 pages. Hard cover DM 88,–. ISBN 3-540-13572-3

The noted urologic surgeon K. Korth has drawn upon his experience with hundreds of percutaneous renal lithotomies to provide a uniquely comprehensive introduction to this important operative technique. He covers all aspects of the operation, including the equipment involved, selection and positioning of the patient, operative strategy and execution, as well as eventual pitfalls and how to avoid them. Each step is fully illustrated with line drawings, photographs, sonograms and x-ray photographs.

Dr. Korth devotes particular attention to the all-important placement of the percutaneous canal. The tactical considerations involved (size, shape and location of the stones) plus the tricks on which the success of the operation often depends are described for you in detail without unnecessary theoretical ballast. The author also outlines additional percutaneous kidney operations in the appendix, such as the lancing of subpelvic ureteral structures, resection of papillary tumors, and intrarenal marsupialization of renal cysts. Clear, concise, authoritative – **Percutaneous Surgery of Kidney Stones** is your guide to a surgical technique whose efficacy has been proved over and over again.

Springer-Verlag
Berlin Heidelberg New York
London Paris Tokyo

W. Mauermayer, Munich

Transurethral Surgery

With contributions by K. Fastenmeier, G. Flachenecker, R. Hartung, W. Schütz

Translated from the German by A. Fiennes

Foreword by W. E. Goodwin

1983. 240 figures, 14 color plates. XXIX, 473 pages. Hard cover DM 420,– ISBN 3-540-11869-1

"Surgical techniques are described in a number of steps . . . this enables even a novice to understand the various procedures. (Dr. Mauermayer) also describes many tried and proven 'clinical secrets,' which are illustrated by means of numerous outstanding drawings. A number of excellent color illustrations at the end of the book demonstrate his impressive cystoscopic photography."

Journal of Urology

W. Lutzeyer, J. Hannappel, Aachen (Eds.)

Urodynamics

Upper and Lower Urinary Tract II

1985. 243 figures, 22 tables. XI, 343 pages. Hard cover DM 168,–. ISBN 3-540-15357-8

Contents: Workshop on Upper Urinary Tract Urodynamics: Myogenic Control for the Upper Tract. Hydrodynamics and Mechanics of the Upper Tract. – Upper and Lower Urinary Tract Urodynamics – Reviewing the Aachen 1971 Meeting: Lower Tract Urodynamics. Upper Tract Urodynamics. – Subject Index.

This volume reviews the essential results of clinical and research urodynamics during the past 12 years. It is based on a follow-up meeting held to review the development since the historical 1971 Aachen meeting. Speakers who had lectured in 1971 or who had made significant contributions to urodynamics critically examine the validity of previous statements and the clinical applicability of their findings. This follow-up review is preceded by reports from a special workshop on mycogenic control, hydrodynamics and mechanics of the upper urinary tract.